



HAL
open science

Ventilation strategies for improving the indoor environment quality in vehicles

Paul Alexandru Danca

► **To cite this version:**

Paul Alexandru Danca. Ventilation strategies for improving the indoor environment quality in vehicles. Fluid mechanics [physics.class-ph]. Université de Rennes; Universitatea tehnică de construcții București, 2018. English. NNT : 2018REN1S089 . tel-02131572

HAL Id: tel-02131572

<https://theses.hal.science/tel-02131572>

Submitted on 16 May 2019

HAL is a multi-disciplinary open access archive for the deposit and dissemination of scientific research documents, whether they are published or not. The documents may come from teaching and research institutions in France or abroad, or from public or private research centers.

L'archive ouverte pluridisciplinaire **HAL**, est destinée au dépôt et à la diffusion de documents scientifiques de niveau recherche, publiés ou non, émanant des établissements d'enseignement et de recherche français ou étrangers, des laboratoires publics ou privés.

THESE DE DOCTORAT DE

L'UNIVERSITE DE RENNES 1
COMUE UNIVERSITE BRETAGNE LOIRE

ECOLE DOCTORALE N° 602
Sciences pour l'Ingénieur
Spécialité : Mécanique des Milieux Fluides

Par

Paul Alexandru DANCA

Stratégies de ventilation pour l'amélioration de la qualité de l'environnement intérieur dans les véhicules

Thèse présentée et soutenue à Bucarest, le 18/12/2018

Unité de recherche : EA 3913 - Laboratoire de Génie Civil et Génie Mécanique

Thèse N° : **(10)**

Rapporteurs avant soutenance :

Walter Bosschaerts	Professeur, Ecole Royale Militaire de Bruxelles, Belgique
Chadi Maalouf	Maître de conférences, Université de Reims, France

Composition du Jury :

Walter Bosschaerts	Professeur, Ecole Royale Militaire de Bruxelles, Belgique
Chadi Maalouf	Maître de conférences, Université de Reims, France
Loretta Batali	Professeur, Université Technique Constructions de Bucarest, Roumanie
Laurent Serres	Maître de conférences, Université de Rennes 1, France
Amina Meslem	Professeur, Université de Rennes 1, France
Ilinca Nastase	Maître de conférences, Université, Technique, Constructions de Bucarest, Roumanie

DOCTORAL THESIS

Cotutelle between:

TECHNICAL UNIVERSITY OF CIVIL
ENGINEERING OF BUCHAREST
Building Services Engineering Faculty
CAMBI Research Center

UNIVERSITY RENNES 1
Civil and Mechanical Engineering
Laboratory

VENTILATION STRATEGIES FOR IMPROVING THE INDOOR ENVIRONMENT QUALITY IN VEHICLES

Author: Eng. Paul-Alexandru DANCĂ

Jury:

Thesis supervisors:

Mrs. A. MESLEM	Professor at University of Rennes 1, Rennes, France
Mrs. I. NASTASE	Associate Professor at Technical University of Civil Engineering, Bucharest, Romania

Rapporteurs:

Mr. Walter BOSSCHAERTS	Professor, Royal Military Academy, Brussels, Belgium
Mr. Chadi MAALOUF	Associate Professor at University of Reims, France

Jury members:

Mrs. Loretta BATALI	Professor at Technical University of Civil Engineering, Bucharest, Romania
Mr. Laurent SERRES	Associate Professor at University of Rennes 1, Rennes, France

Abstract

Prediction of comfortable thermal conditions inside a vehicle cabin is still a challenge due to the transient behavior of this environment. Understanding flow patterns is still difficult nowadays for researchers due to the complexity of the interior cabin geometry and of the ventilation system (flow rate, location and geometry of the air diffusers). To this challenge is added the fact that the non-homogeneity of the temperature distributions of the surfaces affects directly the air flow patterns through the occurring convective effects. In the same time the flow patterns and their effect on the thermal sensation of the users are not completely understood by car designers and manufacturers or by the users themselves. Indeed, because of the thermal gradients and of the presence of the driver and of the passengers the global flow trajectory might substantially differ from the direction imposed by the guiding vanes of the air diffusers. This is related on one hand to these previously mentioned convective effects but might be also an intrinsic characteristic of the air diffusers themselves. Their design and the fan characteristics are not taken into consideration by the manufacturers at the conception of the air conditioning system/ They could be a serious source of noise with impact on passenger's state of comfort. The currently available standard intended for the evaluation of vehicle thermal environment, EN ISO 14505, propose models extensively used for buildings, which do not seem to be entirely adapted for the vehicular space. Unlike the indoor environment from buildings, the vehicular cabin climate is dominated by thermal transient conditions: the strongly non-uniform temperature distributions, both in air and on the surfaces, associated with the high localized air speeds that might be accompanied by low frequency fluctuations or other turbulent behavior when an automatically controlled air conditioning system is present, the relatively higher levels of relative humidity compared to the buildings, the solar radiation intensity, and the radiative heat exchange from the interior surfaces, the angles of incidence of the solar radiation etc. Added to all these parameters, arise the physiological differences between the passengers in terms of age, sex, state of health for instance. The psychological component represents in this case even a greater supplementary challenge knowing that drivers' concentration could be associated with different thermal sensations between different subjects or compared to other passengers. In the absence of the evaluation models adapted to this environment, the available literature is dispersed around those papers dealing with environmental conditions inside the vehicle that might affect the human thermal comfort and those concerning the human's response and perception of its interaction with the environment.

In this context, we decided to orient the research work in this thesis around the complex problematic of cabin thermal environment and its effect on driver's and passenger's thermal state. Thermal comfort has been widely studied in build environments, while thermal comfort in vehicles is a relatively new subject, with fairly few extensive studies that are exploring all possibilities of investigation in this direction.

The thesis presents numerical and experimental studies of the effects of an improved set of dashboard air diffusers over passengers' thermal comfort. The general objectives of the doctoral research project could be summarized as following: **to deepen the knowledge and to understand thermal phenomena that occur in cabin thermal environment; to develop an advanced thermal manikin able to evaluate cabin thermal comfort** knowing that thermal manikins are the most proper measurement tool in the case of non-uniform and transient environments; **to develop and validate a complex numerical model in order to get insight into the complex phenomena previously evoked.** These three general objectives were intended to sustain the main goal of the doctoral research that is: **improvement of thermal sensation of vehicle occupants, by implementation of innovative air diffusers.** To this end we oriented our research towards diffusers with a special geometry that allows flow control mechanisms resulting in the improvement of mixing between air supply by the ventilation system and the ambient air in the cabin.

During the complex quest represented by the doctoral project we could have the opportunity to become familiar to the intricate thermal phenomena governing the thermal comfort in general, to analyze the real role played by transient environment parameters (such as radiant temperature of surfaces, air velocity pulsation, local air turbulence for instance) air flow turbulence in perceiving thermal comfort and in its estimation.

During all this quest we tried to stay on a line that would ultimately allow to respond to a set of fundamental questions, namely: *To what extent this kind of parameters can affect the perceiving of comfort, and also the consequences of an "incomplete" assessment proposed by the existing evaluation models? How is, in this context, affected the ventilation and air conditioning design due to the use of current models for pre-evaluating a good functioning of the HVAC systems – in particular for vehicles - and an acceptable environment for their users?*

Résumé

La prédiction des conditions thermiques confortables à l'intérieur d'une cabine de véhicule reste un défi en raison du comportement transitoire de cet environnement. Le développement des modèles d'écoulement reste toujours une préoccupation pour les chercheurs en raison de la géométrie complexe de la cabine et de la complexité du système de ventilation (débit, emplacement et géométrie des diffuseurs d'air). De plus, la non-uniformité thermique des surfaces affecte directement la distribution du flux d'air par le biais des effets convectifs. Les modèles d'écoulement et leur effet sur la sensation thermique ne sont pas complètement pris en compte par les fabricants des systèmes CVC ou par les utilisateurs, étant donné que la trajectoire d'écoulement peut différer considérablement de la direction imposée par les aubes directrices des diffuseurs d'air. Ceci est lié d'une part à ces effets convectifs mentionnés précédemment, mais pourrait également être une caractéristique intrinsèque du diffuseur lui-même. Les constructeurs ne tiennent pas toujours compte de la conception des diffuseurs d'air et des caractéristiques des ventilateurs lors de la conception du système de climatisation – représentant des sources de bruit importantes ayant une incidence sur le confort du passager. La norme actuellement disponible destinée à l'évaluation de l'environnement thermique du véhicule, EN ISO 14505, propose des modèles d'évaluation des bâtiments, qui ne répondent pas aux exigences de l'évaluation de l'environnement cabine. Contrairement à l'environnement intérieur des bâtiments, le climat de la cabine de véhicule est dominé par des conditions transitoires thermiques: environnement thermique fortement non uniforme associé aux vitesses élevées de l'air localisé qui pourraient fluctuer si nous sommes en présence d'un système de climatisation à contrôle automatique, des niveaux plus élevés d'humidité relative, le flux de chaleur solaire et le flux de chaleur radiatif des surfaces intérieures, l'intensité solaire et sa diffusion sur les différents types de matériaux et niches de surface de la cabine, les angles d'incidence du rayonnement solaire, etc. à tous ces paramètres découlent les différences physiologiques entre les passagers en termes d'âge, de sexe, d'état de santé par exemple. La composante psychologique représente dans ce cas un défi supplémentaire encore plus grand, sachant que la concentration des conducteurs peut être associée à des sensations thermiques différentes entre les différents sujets ou par rapport aux autres passagers. En l'absence de modèles d'évaluation adaptés à cet environnement, la littérature disponible est dispersée autour des articles traitant des conditions environnementales dans le véhicule susceptible d'affecter le confort thermique de l'homme ainsi que de celles concernant la réaction de l'homme et la

perception de son interaction avec l'environnement.

Dans ce contexte, nous avons décidé d'orienter le sujet de la thèse autour de la problématique complexe de l'environnement thermique de la cabine et de ses effets sur l'état thermique du conducteur et du passager. Le confort thermique a été largement étudié dans le bâtiment, alors que le confort thermique dans les véhicules est un sujet relativement nouveau, avec peu d'études qui y sont dédiées. Le manuscrit présente des études numériques et expérimentales des effets de différentes grilles passives sur le confort thermique des passagers. Ainsi, les objectifs généraux du projet de recherche doctorale pourraient être résumés comme suit: approfondir les connaissances et comprendre les phénomènes thermiques qui se produisent dans l'environnement thermique de la cabine; développer un mannequin thermique avancé capable d'évaluer le confort thermique de la cabine, sachant que les mannequins thermiques sont l'outil de mesure le plus approprié dans les environnements non uniformes et transitoires; développer et valider un modèle numérique complexe afin de mieux comprendre les phénomènes complexes précédemment évoqués. Ces trois objectifs généraux visent à soutenir l'objectif principal de la recherche doctorale, à savoir: l'amélioration de la sensation thermique des occupants du véhicule, par la mise en œuvre de diffuseurs d'air innovants. À cette fin, nous avons orienté nos recherches vers des diffuseurs à géométrie spéciale permettant des mécanismes de contrôle du débit et permettant d'améliorer le mélange entre l'alimentation en air par le système de ventilation et l'air ambiant dans la cabine.

Au cours de la quête complexe représentée par le projet de doctorat, nous pourrions avoir l'opportunité de nous familiariser avec les phénomènes thermiques complexes régissant le confort thermique en général, afin d'analyser le rôle réel joué par les paramètres d'environnement transitoires, la turbulence de l'air local par exemple, la turbulence du flux d'air dans la perception du confort thermique et dans son estimation.

Pendant toute cette quête, nous avons essayé de rester sur une ligne qui permettrait finalement de répondre à un ensemble de questions fondamentales, à savoir: *dans quelle mesure ce type de paramètres peut affecter la perception du confort, ainsi que les conséquences d'une évaluation "incomplète" proposée par les modèles existants? Dans ce contexte, comment la conception de la ventilation et de la climatisation est-elle affectée par l'utilisation des modèles actuels pour pré-évaluer le bon fonctionnement des systèmes CVC - en particulier pour les véhicules – et un environnement acceptable pour ses utilisateurs?*

Rezumat

Predicția valorilor parametrilor confortului termic din interiorul habitaculului este o provocare datorită comportamentului tranzitoriu al acestui mediu. Înțelegerea modelelor curgerilor din habitacul este chiar și în zilele noastre relativ dificilă, în primul rând datorită geometriei complexe a habitaculului cât și complexității sistemului de ventilație al acestuia (debitul, poziția și geometria difuzoarelor de aer). În plus, neuniformitatea termică a suprafețelor influențează în mod direct distribuția fluxului de aer prin fenomenele convective ce apar. Studiul curgerilor de aer și efectul acestora asupra senzației termice nu sunt luate în considerare complet de producătorii de autovehicule, cu toate că traiectoria curgerilor poate diferi substanțial de direcția impusă de lamelele de ghidare ale difuzoarelor de aer. Acest lucru este datorat, pe de o parte, efectelor convective menționate mai sus, dar ar putea fi, de asemenea, datorat concepției difuzorului de aer în sine. Designul difuzoarelor de aer și caracteristicile ventilatorului de introducere a aerului nu sunt armonizate și optimizate de către producători atunci când se proiectează sistemul de aer condiționat. Atât difuzoarele cât și ventilatorul reprezintă o sursă de zgomot care afectează starea de confort a pasagerului. Standardul disponibil în prezent pentru evaluarea confortului termic în vehicule, EN ISO 14505, propune modele de evaluare a clădirilor care nu îndeplinesc cerințele pentru evaluarea mediului în habitacul. Spre deosebire de mediul interior din clădiri, climatul din cabina autovehiculelor este dominat de condiții tranzitorii: neuniformitatea și variația puternică în timp a temperaturilor din aer și de pe suprafețe, asociată cu vitezele mari ale aerului din anumite zone, turbulența aerului, fluctuații ale debitului de aer dacă suntem în prezența unui sistem de climatizare automat, niveluri mai ridicate ale umidității relative, radiația solară și fluxul de căldură radiant de pe suprafețele interioare, etc. La toți acești parametri se adaugă diferențele fiziologice dintre pasageri în ceea ce privește vârsta, sexul și starea de sănătate. Componenta psihologică reprezintă în acest caz o provocare suplimentară, știind că atenția șoferilor ar putea fi corelată cu diferitele senzații termice. În absența modelelor de evaluare adaptate acestui mediu, studiile din literatura sunt concentrate în jurul acelor lucrări care se referă la condițiile de mediu din interiorul vehiculului care ar putea afecta confortul termic uman precum și cele referitoare la răspunsul și percepția omului asupra interacțiunii acestuia cu mediul.

Am decis să aprofundez în cadrul tezei de doctorat această problemă complexă atât din punct de vedere al caracterizării fenomenelor curgerilor de aer și de transfer de căldură ce apar în interiorul habitaculului cât și influența acestora asupra senzației termice a șoferului.

Confortul termic reprezintă o problemă studiată pe scară largă în spațiul construit, în timp ce în domeniul autovehiculelor, acesta este un subiect nou, de actualitate, pentru care în literatură este disponibil un număr relativ redus de studii numerice și experimentale care să propună o metodologie completă de evaluare și care să trateze explicit acest subiect.

Teza de doctorat propune o abordare numerică și experimentală a efectelor generate de un set de grile de aer îmbunătățite asupra confortului termic al pasagerilor. Obiectivele generale ale proiectului de cercetare doctorală pot fi rezumate după cum urmează: aprofundarea cunoștințelor și înțelegerea fenomenelor termice ce apar în habitacul; dezvoltarea unui manechin termic avansat capabil să evalueze nivelul de confort termic resimțit în cabină, știind că manechinele termice sunt instrumentul de măsurare cel mai potrivit a fi folosite în cazul ambianțelor termice neomogene caracterizate de fenomene tranzitorii; dezvoltarea și validarea unui model numeric complex pentru a obține o perspectivă asupra fenomenelor menționate anterior. Aceste trei obiective generale au fost menite să susțină scopul principal al cercetării doctorale, și anume: îmbunătățirea senzației termice a ocupanților autovehiculelor prin implementarea difuzoarelor inovative de aer. În acest scop, ne-am orientat cercetarea către difuzoare cu o geometrie specială ce se încadrează într-o categorie de metode de control al curgerilor numite metode de control pasiv. Scopul acestor metode este de a obține îmbunătățirea amestecului dintre aerul introdus și aerul ambiant din habitacul.

În cadrul acestui studiu am încercat să ating o direcție care să furnizeze în cele din urmă un răspuns la un set de întrebări fundamentale, și anume: *În ce măsură acest parametru studiat în mod obișnuit pot afecta percepția asupra gradului de confort și, de asemenea, care sunt consecințele unei evaluări "incomplete" propuse de modelele de evaluare existente? Cum influențează, în acest context, proiectarea sistemului de ventilație și climatizare utilizarea schemelor uzuale de distribuție a aerului - în special în cazul autovehiculelor - și cum putem contribui la asigurarea unei ambianțe acceptabile pentru ocupanții acestora?*

Acknowledgement

Teza de doctorat reprezintă o lucrare științifică prezentată de un candidat pentru obținerea titlului de doctor în științe [DEX, 2009]. Este o definiție abstractă, dar reală. Doar susținerea tezei este efectuată de o singură persoană; aceasta obține un titlu de care se va bucura toată viața. La elaborarea unei teze de doctorat de cele mai multe ori sunt implicate mai multe persoane și care îi oferă doctorandului unui cadru adecvat și necesar desfășurării activității de cercetare, dar mai ales o îndrumare științifică de calitate. Cred că aici și acum este momentul și am prilejul să le mulțumesc tuturor celor care cu atâta pasiune și drag m-au sprijinit și ajutat pe parcursul acestor ani de studiu.

În primul rând precizez că mă simt norocos că doamna conf. univ. dr. ing. Ilinca Nastase și doamna prof. univ. dr. ing. Amina Meslem au ales să fie îndrumătorii mei în realizarea acestei teze de doctorat. Le datorez recunoștință și le adresez mii de mulțumiri atât pentru încrederea, pentru profesionalismul și pentru calitatea științifică oferită, dar mai ales pentru răbdarea și înțelegerea cu care m-au tratat de-a lungul acestei perioade.

Mulțumesc d-lui conf.univ dr. ing. Florin Bode și d-lui ing. Tiberiu Horobeț pentru răbdarea și suportul acordat în realizarea modelului numeric. Implicarea lor directă și sfaturile prețioase primite m-au ajutat la elaborarea unui model numeric complex de habitacul.

În mod deosebit le mulțumesc pentru sinceritate, disponibilitate și sugestiile acordate, dar mai ales suportul moral și fizic în reușita mea, doamnei șef lucr. dr. ing. Cristiana Croitoru, d-lui conf. dr. ing Mihnea Sandu și domnului asist. univ. dr. ing. Angel Dogeanu care împreună cu domnul conf. univ. dr. ing. Florin Bode și comisia de îndrumare au constituit ”motorul” de dezvoltare a acestei teze. Aceștia m-au sprijinit și încurajat în fiecare moment dificil și alături ei am beneficiat de un cadru ambiental foarte plăcut.

Calde mulțumiri adresez colegilor mei Laurentiu Tăcutu, Stefan Simionescu, și fratelui meu Cătălin Dancă pentru ajutorul acordat în realizarea sesiunilor experimentale de măsuratori.

Adresez, în egală măsură, mulțumiri d-lui conf. univ. dr. ing. Costin Ioan Coșoiu, colegilor și prietenilor din Departamentul de Hidraulică și Protecția Mediului – Facultatea de Hidrotehnică, pentru răbdarea cu care m-au învățat să operez sistemul de măsura LDV 3D și suportul acordat în construcția noilor grile de ventilare.

Tot pe această cale doresc să le mulțumesc colegilor din cadrul INCAS, dar mai ales domnilor cercetători dr. mat Ioan Ursu, dr. ing. Dragoș Daniel Ion-Guta, ing. Mircea Dan ca și

tuturor celor de la Secția de Mecatronică, pentru disponibilitate și ajutorul acordat în realizare manechinului avansat de evaluare a confortului termic.

Respectul și mulțumirile mele se îndreaptă și către distinșii referenți domnul prof. dr. ing. Walter Bosschaerts (Royal Military Academy, Brussels, Belgium), domnului conf. dr. ing. Chadi Maalouf (Université de Reims, Reims, France). Sincere mulțumiri adresez și domnilor conf. dr. ing. Tiberiu Catalina, conf. dr. ing. Laurent Serres membrii ai comisiei de îndrumare și pentru timpul acordat analizei acesteia. De asemenea mulțumesc doamnei prof. univ. dr. ing. Rodica Frunzucă director departament STHPA și domnului prof. univ. dr. ing. Christophe Lanos director IUT Rennes - pentru disponibilitatea și sprijinul lor în realizarea demersurilor administrative.

Mulțumesc Școlii Doctorale pentru sprijinul financiar și moral acordat în formarea mea ca cercetător, pe tot parcursul celor trei ani de studiu. Mulțumesc colegilor din Facultatea de Inginerie a Instalațiilor în cadrul căreia îmi desfășor activitatea, pentru atmosfera de colegialitate și prietenie, fiind unul din factorii care m-au ajutat să duc la bun sfârșit această lucrare.

Cele mai importante contribuții morale au venit din partea soției, îi mulțumesc și îi sunt recunoscător pentru înțelegeres, răbdarea și afecțiunea cu care m-a încurajat în fiecare moment dificil. Membriilor familiei mele și prietenilor le sunt recunoscător că au fost alături de mine și m-au sprijinit din toate punctele de vedere în această perioadă.

Ce travail a été appuyé par la région Bretagne pour l'Allocation de recherche doctorale (ARED)

This work was supported by the grant of the Romanian space agency ROSA, QUEST - Advanced air diffusion system of the crew quarters for the ISS and deep space habitation systems, STAR-CDI-C3-2016-577

TABLE OF CONTENT

Table of content	16
General Introduction	18
Chapter 1 – State of the art	25
A. General theory of thermal comfort– history, problems.....	25
B. Vehicles – particular aspects.....	28
C. How is evaluated thermal comfort in vehicles cabins today?	30
D. Fanger’s models and other heat balance models and indexes.....	31
E. Current standards for thermal comfort assessment in vehicles.....	34
F. Nodal physiological models.....	40
G. Psychological component integration	44
H. Synthesis of experimental evaluation of the vehicle environment in the current literature	46
I. Numerical models for prediction and evaluation of comfort in vehicles.....	54
J. Passive control strategies for mixing ventilation and possible application to vehicles	66
K. Discussions and conclusions of the first chapter.....	71
Chapter 2 – Building and advanced thermal manikin.....	75
A. Short history of thermal manikins.....	75
B. Development of our thermal manikin	80
C. Architecture of Suzy	87
D. Innovative control model based on a neuro-fuzzy control law	91
E. The user interface.....	96
F. Testing the thermal manikin	99
G. Calibration of the thermal manikin	108
Chapter 3 – EXPERIMENTAL SET-UP.....	114
A. Measurement principles and employed instruments	114
B. Experimental set-ups and measurement protocols.....	135
Chapter 4 – Numerical model	161
A. Numerical modeling: limitations for thermal comfort domain	161
B. First simplified model of the car cabin	171
C. Final, complex model of car cabin with enhanced boundary conditions and human body	182
Chapter 5 – results and discussion	205

A. Numerical results obtained using the complex model with realistic boundary conditions and virtual manikins.....	205
B. Experimental results obtained from the third experimental campaign	227
C. Discussion of the results	241
Chapter 6 – PERSONAL CONTRIBUTIONS	246
CHAPTER 7 – CONCLUSIONS AND PERSPECTIVES.....	251
References.....	261

GENERAL INTRODUCTION

Designers from the automotive industry started to be concerned on comfortable mobility only in the last decades with the lowering of production costs and with the increased safety of vehicles. Furthermore, their approach was extensively based on methods used in the research field of building systems. Certainly, achieving thermal comfort for occupants of the spaces from buildings independently of the outdoor conditions, sometimes for extreme set points and without any concern regarding the environment, has been the preoccupation of the Heating Ventilation and Air Conditioning (HVAC) design engineers and developers of building services for more than fifty years. On the other hand, the thermal comfort of vehicular occupants and globally the Indoor Environment Quality (IEQ) gained more importance mostly since the time that people spend in vehicles (private or public transport) has grown substantially. Researchers focused their attention in direction of thermal comfort of car passengers in the last decades due to increasing of both public and private numbers of cars. Occupant's thermal comfort in the vehicular cabin is also gaining more importance due to the increasing of the distance between home and workplace [1] with direct impact on the amount of time that people spend in vehicles [2]. The distance between the home and the workplace increased due to the diversity of activities and hence to the job diversity. During each trip, thermal comfort must to be ensured for a good psychological and physical state of the passengers. Certainly, comfortable vehicular climate control in many cases not only help to reduce driver's stress but also guarantee good visibility by avoiding the fogging phenomenon, and thus contributing to a safer driving. In addition, today's demand for more efficient vehicular energy exploitation has led to an increased interest in investigating and analyzing the system and the design requirements [3, 4].

An environment that is not comfortable can affect both the physical and the psychological state of a person and may be essentially unhealthy. In the case of the driver and of the passengers a comfortable thermal environment may ease a sensation of fatigue and could improve their mood thus contributing to the safety of driving. An example is given in the study of Tsutsumi et al. [5], which shows that a cabin environment which is not comfortable could affect drivers performance and level of tiredness. In another study proposed by Danen et al. [6] it has been found that the driver performance has been affected by the extreme conditions (both hot and cold) of the vehicular space. This way it can be observed, that a moderate thermal environment of the vehicle cabin is important not only for the state of comfort of the driver and of the passengers but also for their safety. In the same time, the present concerns towards the environment impose us preserving

energy resources [7]. This way it has been a challenge in the past decade to obtain high performance systems and to try to achieve in the same time a good quality of all artificially controlled environments. The need to reduce the heat or cold loads that enter in cabins has become an important criteria from the earliest design stages, in order to obtain reduced energy consumption. A quantitative example is given in [8] where it has been shown that in United States alone approximately 26 billion liters of fuel are consumed annually for cooling vehicle passenger compartments.

The cost related to the air conditioning of the cabin could be improved through the initial design of the HVAC systems. Some of the previous studies of the team from UTCB [9, 10] put in evidence the fact that usually employed air distribution schemes are not necessarily optimized in order to comply with two inseparable objectives: thermal comfort and energy efficiency. These two objectives were for a long time considered as being somehow in contradiction. This is due on one hand to the non-efficient diffusion of the treated (cooled or heated) air and on the other hand to the non-optimized flow of the discharging devices (diffusers, grilles, blowers,...etc). In the same time the schemes of air distribution in enclosures, that are commonly used in design purposes, propose simplified models of the airflow patterns that are not entirely adapted to the real conditions inside the spaces of the buildings or of the vehicles. A possible response to these issues is found in the adaptation of the theory and its associated models. These adaptations should take into account if possible a larger number of aspects related to human thermal comfort. All these considerations are advanced of course, in the context of the present developments of both experimental and numerical resources that allow the researchers to use advanced methods and instruments.

Thermal comfort is usually defined as the state of a person that would express a feeling of wellbeing regarding the thermal conditions in an occupied space. But, for the same environment, different individuals can provide different feedback regarding their thermal sensation. This difficulty is directly related to the presence of the two inseparable human components: the physical and the mental condition. Nevertheless, it is the tangible interest of engineering applications that motivated a continuous exploration of quantitative models for estimating, predicting or classifying the state of thermal comfort in occupied spaces. The great majority of these trials are focusing on the physiological component. Most of them are relying on the assumption that the state of thermal comfort is related to a constant body-core temperature, around 36.7°C, without a serious intervention of the thermo-regulatory mechanisms which are important when the body produces for instance too much heat. In this case the heat must be evacuated so that the central body temperature remains constant. Fanger [11] showed that "the human thermo-

regulatory system is quite efficient and tends primarily to ensure thermal equilibrium without an explicit effort and then adjust their reaction to external stimuli". It is currently accepted that a thermal environment is thermally comfortable when 80% to 90% of its occupants do not display thermal dissatisfaction [1-4].

The understanding of the flow patterns is still a challenge for the today's researchers. This is a result of the combination of extremely complex factor as: the geometry of the vehicular space, the intricate flows generated by the ventilation system, the flowrate control system, the locations of the air diffusers [8]. Added to this, the non-uniform distribution of the temperatures on the interior surfaces impacts the air flows distribution through the convective effects. The global flow patterns from the cabin and their impact on the thermal comfort level of the users are not completely take into account by the designers and the manufactures of the vehicles. It is the same paradigm or even worse on as in the case of the buildings. The trajectories of the flows might directly be modified by these other convective flows, such as the trajectory which was originally imposed by the guiding vanes of the air diffuser might be different than the real one. This aspect might be related to the previously mentioned convective effects but also could be related to the non-optimization of the air diffuser itself. The design of these air diffusers and the fan characteristics are not taken into consideration by the manufacturers when coonceiving the air conditioning system, even they could represent a serious source of noise [12] with impact on passenger's state of mind.

The currently available standard developed for the assessment of vehicle thermal environment, EN ISO 14505/1-3 [13-15], propose models that are derived from the field of buildings. They do not meet the demands for vehicular ambient evaluation. Unlike the indoor environment from buildings, the vehicular cabin climate is dominated by transient conditions: the strongly non-uniform thermal environment correlated with the localized high values of the air speeds that might also fluctuate if we are in the presence of an automatically controlled air conditioning system, the higher levels of relative humidity, the solar heat flux, and the radiative heat flux from the interior surfaces, the solar intensity and its scattering over the different material types and surface niches in the cabin, the angles of incidence of the solar radiation etc. [5-6]. Added to all these parameters arise the physiological differences between the passengers in terms of age, sex, state of health for instance. The psychological component represents in this case even a greater supplementary challenge knowing that drivers' concentration could be associated with different thermal sensations between different subjects or compared to other passengers [7]. In the absence of evaluation models adapted to this environment, the available literature is dispersed

around those papers dealing with environmental conditions inside the vehicle that might affect the human thermal comfort and those concerning the human's response and perception of its interaction with the environment. The available literature is equally divided within experimental and numerical approaches. Due to complexity of this environment and due to un-adapted models of evaluation from standards, this process experimental and numerical is divided in three subcategories of studies. The first category is represented by studies that deal with the idea of thermal environment assessment without considering any comfort assessment. The second subcategory includes those studies where thermal comfort assessment models proposed by standards are used. The third subcategory covers the articles using or proposing new thermal comfort assessment methods.

Objectives of the thesis

Starting with the previous idea of a real need of developing models for the human body for studying IEQ in vehicles and after a survey of the specialized literature we identified several problems:

- (1) There is a lack of knowledge regarding consequences of using the existing, non-adapted, comfort models for vehicular cabins.
- (2) Few studies regarding the influence on ventilation strategies on thermal comfort and on the passengers' behavior are available.
- (3) Studies focused on improving HVAC system strategies of control are rarely connected with thermal comfort studies.

In this context, we decided to orient the subject of the thesis around the complex problematic of cabin thermal environment and its effect on driver's and passenger's thermal state. Thermal comfort has been widely studied in build environments, while thermal comfort in vehicles is a relatively new subject, there have been relatively few studies. In the manuscript are presented numerical and experimental studies of the effects of different passive grills over passengers' thermal comfort. Thus, the general objectives of the doctoral research project could be summarized as following:

- (1) The first general objective of this thesis was **to deepen the knowledge and to understand thermal phenomena that occur in cabin thermal environment.**
- (2) The second general objective of this doctoral study was **to develop an advanced thermal manikin able to evaluate cabin thermal comfort** knowing that thermal manikins are the most proper measurement tool in the case of non-uniform and transient environments.
- (3) The third general objective was **to develop and validate a complex numerical model**

in order to get insight into the complex phenomena previously evoked.

These three general objectives were intended to sustain the main goal of the doctoral research that is: **improvement of thermal sensation of vehicle occupants, by implementation of innovative air diffusers.** To this end we oriented our research towards diffusers with a special geometry that allows flow control mechanisms resulting in the improvement of mixing between air supply by the ventilation system and the ambient air in the cabin.

During the complex quest represented by the doctoral project we could have the opportunity to become familiar to the intricate thermal phenomena governing the thermal comfort in general, to analyze the real role played by transient environment parameters (such as radiant temperature of surfaces, air velocity pulsation, local air turbulence for instance) air flow turbulence in perceiving thermal comfort and in its estimation.

During all this quest we tried to stay on a line that would ultimately allow to respond to a set of fundamental questions, namely: *To what extent this kind of parameters can affect the perceiving of comfort, and also the consequences of an "incomplete" assessment proposed by the existing evaluation models? How is in this context affected the ventilation and air conditioning design due to the use of current models for pre-evaluating a good functioning of the HVAC systems – in particular for vehicles - and an acceptable environment for their users?*

Structure of the thesis

This manuscript is divided in five chapters each representing a distinct phase of the doctoral research process.

In the first part, the thesis is organized around the study of current research, mainly aiming two directions: methods, models and indicators for (1) prediction of vehicular thermal comfort and (2) numerical simulation techniques for airflows inside confined enclosures such as the car cabin. Thus Chapter 1, offers an overview of the main concepts and results of numerous studies from literature for numerical and experimental research in the field of thermal comfort. This chapter is the summary of our initial search of landmarks in the literature that allowed us to get directions in our study and to choose a specific numerical and experimental validation, based on the existing results and on the available means. The first chapter is a bibliographical one, proposing an extensive and exhaustive introduction in the thermal comfort research field with focus on cabin thermal environment.

The second chapter is dedicated to the design and development of an advanced thermal manikin with 79 independent zones and neuro-fuzzy control. The concept and the development are

presented step by step as well as the preliminary tests of this prototype. I was directly involved in designing and manufacturing of this particular thermal manikin that was conceived and developed with the help of the Systems and Mechatronics department from the National Institute of Research Aerospace Elie Carafoli (INCAS) from Bucharest.

Besides the thermal manikin, several protocols and measurement techniques are used in the experimental part of the study. This way, the third chapter is dedicated in a first part to the measuring principles of all used measuring instruments and in a second part to the three main experimental set-ups used during the entire study.

In the introduction of the fourth chapter we propose to pass briefly through some current developments related to Computational Fluid Dynamics applied to air distribution in occupied spaces and thermal comfort in general. In the bibliographical chapter we put in evidence several numerical studies that we found to be relevant for our subject. Still, the great majority of these studies lacks details and explanations of modeling choices, this way we decided to rely on the knowledge gained in the much more studied field of air distribution and thermal comfort in buildings. In the following parts of the chapter we present the steps employed in our numerical approach. In a first time, a simple car-cabin numerical model was designed and in our quest of methods of calibration of the correct boundary conditions, we used temperature and air flow measurements in a real car-cabin. In a second time, a complex numerical model has been developed. This model includes a passenger with anatomic shape and takes into consideration two types of air diffusers: one which is the reference – the classic air grilles that were originally designed in the cabin and one innovative set of air diffusers that we wanted to test. The validation of the chosen approach for introducing the effect of the flows generated by the two types of diffusers is also presented in this chapter.

With the previously elaborated complex numerical models we can proceed in the fifth chapter to our final quest, namely: finding which is the influence of the inlet conditions determined by the two types of air diffusers this way, we wanted to check first what is happening with the global distribution of the flow inside the cabin in non-isothermal conditions. Next, we wanted to gain a deeper perspective in the thermal comfort aspects. To this end we compared thermal indexes from the numerical data with the measured values of the parameters characterizing the thermal environment from the car such as described in the experimental set-up from Chapter 3.

We finish this last chapter dedicated to our study with a comparison between the numerical study and the experimental results obtained in the real car cabin from measurements and from the subjective studies.

Chapter 6 is dedicated to a synthesis of the personal contributions to the state of the art in the field, chapter that is mandatory according to the Romanian guidelines for elaborating the PhD manuscript.

Chapter 7 presents the general conclusions of our study and the short and long term perspectives.

CHAPTER 1 – STATE OF THE ART

This chapter presents a synthesis of theoretical aspects concerning thermal comfort, vehicle environments and other related environmental factors, which have a major effect on the vehicular space mainly aiming two directions: methods, models and indicators for the prediction of indoor thermal comfort and numerical simulation techniques for the turbulent flows used for the study of air flow in the cabin environment. This chapter represents the summary of our initial extensive search of milestones in the existing literature. It allowed us to set the main directions for our research and to define specific numerical and experimental validation based on the existing data and on the available methods.

A. *General theory of thermal comfort– history, problems*

Human perception induced by thermal stimulation includes two states of mind: *thermal sensation* and *thermal comfort* [16]. While thermal sensation could be described as a subjective response associated with the temperature information of external objects or of the environment which is explored by warm and cold receptors in the skin, thermal comfort is commonly considered as a combination of the subjective sensation and the objective interaction with the environment [17]. This distinction is common in neuro-physiology sciences, but it is not usual in the field of indoor environment quality. In our field, usually the thermal sensation is a measure of the state of the thermal comfort level.

The most found interpretation and definition of **thermal comfort** is the one that is explaining it as the state of a person that would express a feeling of wellbeing regarding the thermal conditions in an occupied space. Notwithstanding, “*the thermal comfort is a term difficult to define and an universal definition of its meaning is almost impossible to obtain*” if we quote from the famous book of Slater [18], "Human Comfort". Starting with any trial itself of a definition for the concept of thermal comfort, it is obvious that in the same formulation we will have terms as “feeling” or “mental state” and “conditions” or “physical parameters”. If we want to go further and search for a quantitative way of defining thermal comfort, this turns out to be a difficult task. This difficulty is directly related to the presence of the two inseparable human components reflecting the physical and mental condition. The physical part of the problem is intricate itself given the complex physiological mechanisms governing the human body and its thermo-regulatory system. The psychological component comes to raise the difficulty of the problem at an unsolvable level through analytical equations in an engineering approach. Nevertheless, it is the

tangible interest of engineering applications that motivated a never-ending quest of quantitative models for estimating, predicting or classifying the state of thermal comfort in occupied spaces. Almost all these attempts are focusing on the physiological component of the thermo-regulation. Most of these trials started with the hypothesis that the state of thermal comfort might be ensured only when the heat produced in excess by the human body through its metabolic sources has the possibility to be dissipated in the close environment of the body. In this case, an intervention of the thermo-regulatory system would be infinitesimal, characterizing this state of the body as thermo-neutrality. This is why it is universally accepted today that an environment would be considered comfortable from the thermal point of view, when 80-90% of people from that environment would not be thermally dissatisfied [13-15, 19]. However, Humphreys and Hancock [49] showed that a state of thermal equilibrium does not necessarily correspond to a desired or preferred thermal sensation. As an example, we should cite the case when it is hot outdoor and people would prefer a cooler condition over the neutrally-thermal requirements, or the case when outdoor is very cold and people would prefer a warmer condition than the neutrally-thermal ones. This is the concept of **thermal alliesthesia** which defines the dependence between the internal state of the organism and thermal perception (hot or cold stimuli).

Historically, one could distinguish between the three main directions in the philosophy of “thinking” the thermal comfort. This way, a **first category** of concepts is represented by all models that are based on energy balance equations. Even if they are called “physiological”, these models propose relationships between physical parameters that may affect thermal sensation of the human body. These physical parameters are connected with the thermo-regulatory system via some physiological parameters for which empirically established values are commonly agreed in the literature, such as the metabolic rate, the work rate, the surface of an average person, etc. [11]. Given the difficulty of evaluating these constants and the limited computing resources in the twentieth century, a full analysis of the heat balance was not an option for engineering applications particularly before the seventies. Most of these models are heat-stress models with simplified representations of the environmental stress, as opposed to models of physiological response to the climate. The most well-known and **widely accepted is Fanger’s “Comfort Equation”** and the associated indexes called "Predicted Mean Vote" and "Predicted Percentage of Dissatisfied" [11]. Fanger’s models represent a predicted vote of thermal sensation using some parameters defining the thermal environment being analyzed and empirical equation that describe the heat exchange between the human body and the environment. These models were obtained from a long term study involving laboratory controlled steady-state conditions on human subjects.

The second category of concepts is represented by the so called “psychological” models, the adaptive approach being the most popular. If the previously cited models promoted the idea of relationships between physical parameters and physiological constants, the adaptive models represent a first attempt to integrate the mental component. The principle behind the adaptive models is to add to the previous balance equations some confidence intervals expressing the elasticity of the human acceptability of indoor thermal conditions versus its adaptability of outdoor conditions. The most known approaches were proposed by **Nicol and Humphreys [20]** and by **De Dear and Brager [21]**. Nevertheless, other influences of psychological nature, such as emotions, stress, concentration, cultural features, etc., were never addressed, most likely given the complexity of such studies.

The third category of concepts is represented by the nodal thermo-physiological models that were intended to put in the same balance equation, the heat and mass production of the human body and its transfer with the environment at a local level. The idea being to provide the local skin temperature variation as a result of simulated physiological reactions, thus giving possibility of simulating transient capabilities of adaptation of the human regulatory system to the external stimuli. A first **nodal model “Pierce two-node model”** was proposed by **Gagge et al.** in [22]. This model is considering the modification of the temperature of the central core of body inherently of the skin. Thermo-regulatory processes (sweating, increased blood flow, shivering) are defined in terms of thermal signals from the core, the skin and “the mean body”, for moderate activity levels and uniform ambiances.

It was Haldane [23], at the beginning of the twentieth century, among the first researchers to address the issue of thermal comfort. He suggested that the wet-bulb temperature could be used as an index to evaluate discomfort due to the heat stress of working people in high temperature industrial environments. Since that, in literature there were proposed a large number of indices for thermal comfort with application to the built environment. These indices were generally only a combination of thermodynamic parameters of the air. They might be considered as precursors of the first category models that are based on energy balance equations. One of these indices which was proposed in the late twenties, is the Effective Temperature (ET) [24] based on three parameters: the air temperature, the relative humidity and the air speed. Later, the metabolic rate and the thermal resistance of the clothes (clothing) was integrated in the same way as Fanger did previously, by Gagge [25] in an index Effective Temperature (ET*) and in its corresponding Effective Temperature Scale (SET*), This indices are based in the same way as the PMV, on the thermal equilibrium of the human body. The SET* index is including the two node model [25],

and is described in the American standard of the [26].

In the seventies, Fanger [11] proposed a first comprehensive study taking into account different parameters including physical activity and clothing, as well as environmental characteristics (air temperature, mean radiant temperature, air speed and air humidity) resulting in PMV and PPD indices. An exhaustive presentation of all models and associated indices based on energy balance equations, for thermal comfort or heat stress assessment, from a historical point of view, is given in [27]. We will not discuss them further with the exception of the models proposed by Fanger which were first adopted by ISO 7730 [28] in 1984, and are used even nowadays. These indices were also adopted in the first part of ISO 14505 standard [15], designated for evaluation of thermal environments in vehicles even if they are applicable only within certain limits of variation of aforementioned parameters, i.e., to environments with very low thermal stress levels.

The main characteristic of all the previously reviewed models is that they were intended to be used for buildings, which means that the temporal scale of the considered phenomena could let us assume that all the parameters are on a quasi-steady state. In the same time, even for buildings one could not say that real steady-state conditions are present, since there are a lot of interactions between the building itself, the occupants, the heating system, the set-points of the HVAC system, etc. In the case of new air distribution schemes like the displacement or the personalized ventilation, the transitory and non-uniform characteristics are even more amplified.

B. Vehicles – particular aspects

Unlike buildings' indoor environment, the vehicular ambient is dominated by thermal transient conditions: the strongly non-uniform thermal environment associated with the high values of the air speeds of localized flows (in contradiction with the diffuse air movement from the buildings) with high turbulence or low frequency fluctuations - if an automatically controlled air conditioning system is present, the solar heat flux and the intensity of the solar radiation, the radiative flux occurring from the in-cabin surfaces, the angles of incidence of the solar radiation on the wind shield, and the much higher levels of relative humidity compared to the buildings, etc. [7, 9][29].

This way, one first particular aspect is represented by the high values of the air velocity compared to other occupied enclosures. This leads to the high localized air velocities that might highly fluctuate if we are in the presence of an automatically controlled air conditioning system [30, 31].

A second aspect is related to the interior surfaces materials and temperatures which have a

direct impact on the mean radiant temperature. Surface temperatures are mostly influenced by solar radiation. Beside this, in the case of direct solar radiation which touch human body that was found that the thermal state changes and this is the third solar radiation this is also in the most of the cases the cause of interior temperature non-uniformity. Air temperature inside the car can reach 72 °C in summer with an outdoor temperature of 34°C and a solar radiation of around 800 W/m² according to Grundstein et al.[32]. In such situations, the heater and air conditioner cannot easily control the vehicle compartment thermal environment.

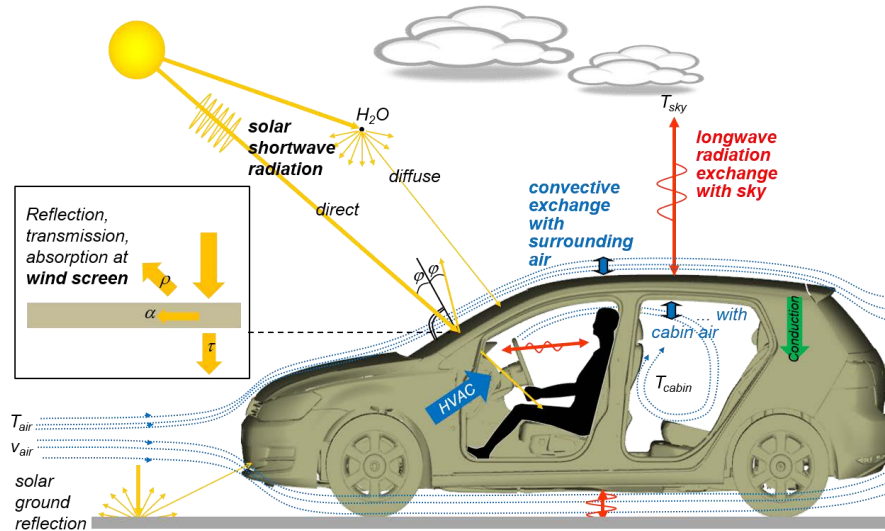


Figure 1: Various environmental conditions acting on the thermal environment of a car cabin with passengers [29]

Added to all these parameters are the physiological differences between the passengers in terms of age, sex, state of health, cultural differences that would result in various clothing approaches for instance. The psychological component represents in this case even a greater supplementary challenge knowing that drivers' concentration could be associated with a thermal sensations depending on each subject or in comparison to other passengers [33]. Undeniably, the driver will come across situations that impose requirements over and above those represented by other routine operations. He must perceive a potential hazard becoming consciously aware of it, and then diagnose it. If a response is demanded, the driver must then carry out the required action. Owing to the mental processing involved, each of these encounters takes time, even in those cases where no obvious response is made. In most driving situations events are spaced sufficiently and there is adequate time available. In others they come thick and fast, placing the driver under some stress and increasing the possibility of error [34]. In this context, a direct connection between drivers' thermal sensation and his focus on the driving tasks could be established in the literature [35, 36]. All these parameters are linked with unknown dependencies [37].

c. How is evaluated thermal comfort in vehicles cabins today?

A large number of research studies are addressing the subject of thermal comfort related to the in-cabin environment. If we would like to sort them around the models proposed by the three historically directions previously presented, we would be somehow in difficulty. The available literature is dispersed around those papers dealing with: A - the observation of environmental conditions inside the vehicle that might affect the human thermal comfort and B. - those concerning the human's response and perception of its interaction with the environment.

The main standardized methods for prediction or assessment of thermal comfort in vehicles ISO 14505 [13-15] are related to methods *from the first category* and we will discuss them in the first part of this chapter.

Regarding *the second category*, the integration of the *psychological component* into thermal comfort evaluation is performed through other ways that it was done in the past for buildings, usually relying on behavioral and neuro cognitive experimental methods related to drivers' safety mainly, by acquiring physiological signals using medical techniques like the electroencephalogram and the electrocardiogram [33].

As for *the third category*, there are a certain number of studies dedicated to the use of the *nodal physiological models*. Typically, these studies are numerical and might be related to experimental validation via the use of thermal manikins.

The great majority of the papers is neither applying the previously discussed thermal comfort models nor applying the standardized methods. Usually authors try to investigate the influence of one physical parameters (air velocity, solar radiation, relative humidity) into the in-cabin conditions, in a quest of knowledge regarding the phenomena around the interactions between the human body and its environment. The available literature is equally divided within experimental and numerical approaches.

Several good review articles are available in the literature [37-41], but each of them is not offering a structured synthesis of all the knowledge that has been proposed up to date with focus on the three categories of concepts mentioned earlier. Sometimes the authors are using confusing terms mixing the physiological and psychological components [37, 42]. In this chapter we wanted in particular to give clear definitions of the three components involved in this problematic which are: the physical environmental parameters, the physiological characteristics of the human body and the psychological inherent component that has to have an important underestimated weight in our opinion. Moreover, we felt that a discussion of the principal standards that are used in this

specific field should also be proposed.

D. Fanger's indexes and other heat balance models

As shown in [11], Professor Ole Fanger was convinced that only a trans-disciplinary approach between thermodynamics, physiology, psychophysics, ergonomics, meteorology, architecture and clothing engineering, can lead to satisfactory results regarding the prediction or assessment of thermal comfort of inhabitants. His vast research work had as an objective to predict the conditions necessary for the choice of the optimal parameters defining the indoor thermal environments. Professor Fanger's studies were based on the main hypothesis for a comfortable thermal sensation the human body must to be in a state of equilibrium from a thermodynamic point of view. This way the heat produced, consumed and transferred to the surrounding environment would be in balance. All the studies initiated by Fanger and many other investigations inspired by them used real human subjects wearing standardized clothing, performing standardized activities in strictly controlled laboratory environment.

In this framework, the most important parameters that could play a role into the thermal comfort state were analyzed. They were introduced in an equation representing the thermal balance of the human body taking in consideration all heat transferred with the environment through conduction convection and radiation, perspiration and respiration. The result was an index, namely, the PMV (Predicted Mean Vote) [11], which is in accordance with the seven-point thermal sensation scale:

$$PMV = (0.303e^{0.303} + 0.028) \{ (M - W) - 3.05[5.73 - 0.007(M - W) - p_a] - 0.42[(M - W) - 58.15] - 0.0173M(5.87 - p_a) - 0.0014M(34 - t_a) - 3,96 \cdot 10^{-8} f_{cl} [(t_{cl} + 273)^4 - (t_{mr} + 273)^4] - f_{cl} h_c (t_{cl} - t_a) \} \quad (1)$$

Where:

$$t_{cl} = 35.7 - 0.0275(M - W) - I_{cl} \{ (M - W) - 3.05[5.73 - 0.007(M - W) - p_a] - 0.42[(M - W) - 58.15] - 0.0173M(5.87 - p_a) - 0.0014M(34 - t_a) \} \quad (2)$$

And:

M : metabolic heat rate (W/m^2);

W : activity level (W/m^2);

t_{cl} : temperature at clothes level ($^{\circ}C$);

p_a : water vapor pressure (Pa);

t_a : air temperature ($^{\circ}C$);

I_{cl} : thermal insulation of clothes (Clo);

f_{cl} : clothing factor;
 t_{mr} : mean radiant temperature ($^{\circ}\text{C}$);
 h_c : convective heat transfer ($\text{W}/\text{m}^2 \text{K}$);

As explained by this theory, when the equilibrium equation which is represented by the PMV model is satisfied, there is no increase or decrease of the central core temperature, which means no accumulation of the heat is in the body [11]. The heat which is generated by the human body is thus exchanged with its environment.

Another index, Predicted Percentage of Dissatisfied (PPD) was proposed in the association with the PMV and it is indicating the percentage of the occupants that would express a state of thermal discomfort. The index is expressed in percentage, thus for 10% of the PPD, the associated values of the PMV are comprised between -0,5 and 0,5. When the body is supposed to be in thermal neutrality i.e. for $\text{PMV} = 0$, the predicted percentage of the dissatisfied is however equal to 5%, thus at least 5% of an analyzed space would be supposed to be in thermal discomfort. The mathematical expression of PPD index:

$$\text{PPD} = 100 - 95 \exp[-(0.03353 \text{PMV}^4 + 0.2179 \text{PMV}^2)] \quad (3)$$

It is important to note that Fanger's models were derived from normal indoor clothing, in regular indoor climate, for low to moderate activity levels. This way, the PPD is expressed via a single equation that is based on the hypothesis that the mean skin temperature values and the sweating are related to the state that is somehow close to the thermal comfort state [11]. This assumption reposes on the nature of the experiments that have been performed, based on human subjects, and resulting in the previous indexes that are empirical.

A short time later after the initial series of studies concluded by Professor Fanger, it was shown in [43] by Fanger and Pedersen that the velocity fluctuations, especially at certain frequencies, have direct impact on the sensation of the thermal discomfort. In [44] Fanger and Christensen put in evidence that the local turbulence intensity was also playing a role in the thermal discomfort sensation. Both studies used human subjects as previously. A new index called "Draught Rate" (D.R.) was proposed, allowing to display which are the problem zones in an enclosure in case of bad distribution of air. D.R. is an index depending on several parameters: air speed, air temperature, local air speed turbulence intensity value.

$$\text{DR} = (34 - t_a) \times (v_a - 0.05)^{0.62} \times (0.37 \cdot \text{Tu} \cdot v_a + 3.14) \quad (4)$$

Where:

t_a - mean air temperature (°C);

v_a - mean air speed (as measured with an omnidirectional probe)(m/s);

T_u - air turbulence intensity (%);

The previously presented models proposed by Fanger and his team have been used for more than 40 years. The great majority of their investigations were related to the steady-state conditions. They are the most employed models used in the current practice for indoor environment assessment [45]. *They are the basis of two international standards – European and American [46, 47] used for evaluating thermal comfort characteristics for all type of occupied enclosures, despite to the fact that they were originally intended to be applied to buildings.*

Fanger’s model was preceded with almost five decades by the concept of “*Effective Temperature*” (ET) [24] based on three parameters: the air temperature, the relative humidity and the air speed. Afterwards, a metabolic constant and the thermal resistance of the clothes (a constant which is also called clothing) was introduced in a model, in the same way as Fanger did previously, by Gagge in a corrected index called “*corrected Effective Temperature*” (ET*) and in its corresponding “*Effective Temperature Scale*”: (SET*). Both SET* and ET* are defined as the PMV, on the heat balance of the human body. SET* is integrating the two-node model [25], and is also proposed in the text of the American standard ASHRAE [26]. We have to observe here the following idea: *like for the Predicted Percentage of Dissatisfied, the SET* and the ET* indices are the equivalent characteristics of a type of fictive environments, with fixed parameters taken into consideration as derived from some empirical models.*

Also, earlier than Fanger’s studies, Koestel and Tuve [48] investigated the role played by the air motion on comfort. They defined **draft** as “*any local feeling of coolness or warmth of a region of the body skin due to both air speed and air temperature, at humidity and radiation of constant values*”. They proposed an index called *Effective Draft Temperature* (EDT) [49] which takes into consideration the local value of the difference between the local air temperature and the desired value of the set-point and the local difference between the value of local air speed and a desired value of 0,5 m/s. This model was based on a relation proposed by Rydberg and Norback [50] and Straub et al. [51]:

$$EDT = (T_i - T_{a\text{mean}}) - 8(v_{ai} - 0.15) \quad (5)$$

Where:

T_i : local air temperature (°K);

T_{amean} : mean air temperature of the room (°K);

v_{ai} : local air speed (as measured with the omnidirectional probe) (m/s);

The scale of values resulting from evaluation of the EDT index ranges between 1.1 K and -1.7K. The value of 1.1K is corresponding to a sensation of warm and -1.7K is corresponding to a sensation of cold. The authors indicate that in order to consider an environment as comfortable, a limit of 80% of the points considerate for the evaluation should fall within these values [49, 52]. The level of activity considerate in this care was corresponding to sedentary. The percentage of points respecting the other conditions from the total number of points used for assessment represents the *Air Diffusion Performance Index* (ADPI).

Another thermal comfort model, combining the EDT index with the Fiala model concept [53-56] is the *Universal Thermal Climate Index* (UTCI). This new model, was used in a number of recent papers [56-58]. The index itself was derived conceptually as an equivalent temperature: for any combination of air temperature, air velocity, radiation, and humidity, UTCI is defined as the isothermal air temperature (corresponding to the same value of the mean radiant temperature) of the reference condition that would draw out the same dynamic response of the physiological model.

E. *Current standards for thermal comfort assessment in vehicles*

The EN ISO 14505 standard “Evaluation of thermal environments in vehicles” is composed by three parts: 1. Principles and methods for assessment of thermal stress; 2. Determination of equivalent temperature; 3. Evaluation of thermal comfort using human subjects[13-15].

EN ISO 14505 Part 1[15] deals primarily with recommendations for whole body thermal effects assessment: thermal comfort understood as thermal neutrality, but also situations of heat or cold stress. The heat stress is dangerous since it puts a physiological strain on the driver that cannot be tolerated and might eventually evolve into heat injuries. For the heat stress, the 14505-1 standard is referring to recommendations that are given in ISO 7243[49] or ISO 7933[59]. Contact with hot surfaces is recommended to be assessed using ISO 13732-3[60]. However, due to the presence of considerable asymmetric climatic conditions, special care needs to be taken to assure a representative measure of the total climate in the vehicle, which seem in real exploitation conditions quite difficult to achieve.

On the other hand, when the heating system fails, or is insufficient under cold climatic conditions, there is a progressive risk of whole-body cooling as well as local cooling of body parts. Initially, discomfort arises, but with time and further cooling more pronounced physiological strain and, eventually, cold injuries can occur. Recommendations for assessment of

cold stress are given in ISO 11079 [61]. A very strong local coolness sensation may be introduced by the presence of local cooling may arise from the cold areas, such as windows, or from a cold seat. Recommendations for the evaluation of the discomfort caused by the contact with cold surfaces are given in ISO 13732-3 [60]. The assessment in both cases is based on the evaluation of whole body effects and whole body heat balance using heat stress indexes that were previously introduced for industrial environments[62, 63].

In terms of thermal comfort, it refers mainly to already existing international standard ISO 7730 [28], its defined purpose being to evaluate the actual thermal environment the driver or the passenger is exposed to, with the precaution that this thermal environment *would be moderate*. The PMV and PPD indexes are recalled for the evaluation of whole-body comfort assessment based on calculations using the measurements of air temperature, mean radiant temperature, humidity and air velocity, as well as estimations of metabolic rate and clothing thermal insulation. In these cases, the value of PMV is assumed to indicate the level of thermal neutrality assumed to be perceived by drivers for the conditions under examination. We have to note here, once again, that current conditions in real vehicles are far from the limits imposed to these parameters via ISO 7730 [28].

EN ISO14505 Part 2 [64] deals with the definition of the concept of *equivalent temperature* and the detailed evaluation of local climatic conditions in vehicles. The equivalent temperature index is presented in both standards ASHRAE and ISO. It is called *operative temperature* in the standard ASHRAE 55 [47]. Several methods are proposed and described for the measurement of t_{eq} in EN ISO14505 Part 2[64]. This part of the standard is intended to be used for comfort assessment or for testing the performance of the vehicle's HVAC-system. For this second purpose, the environmental conditions need to be carefully defined to allow for in-factory comparisons of different systems or for consumer assessment of the performance of different vehicles.

The concept of **equivalent temperature** (Figure 2), is explained in the American ANSI/ASHRAE standard. The definition that is given states that the equivalent temperature “represents the uniform temperature of an imaginary black enclosure in which an occupant would exchange the same amount of heat by radiation plus convection as in the actual non-uniform environment” [47]. At fixed values of the air speed, relative humidity, level of activity (metabolic rate), thermal clothing resistance, a diagram with comfort zones may be determinate, showing the range of the operative temperature that could be found acceptable. *It does not account for heat exchange by evaporation*. Once sweating is required for maintenance of heat balance, the t_{eq} is not anymore a true representative of the thermal stress, although it may serve as an indicator of

deviation from thermal neutrality [65].

The equivalent and the operative temperature are using the same relation when the values of air speed are less than 0,1 m/s. In this case, the operative temperature or the equivalent temperature might be expressed as an average between the values of the air temperature and the radiant mean temperature weighted using the heat transfer coefficients (convection and radiation) between the occupant and the environment [47]. When the air speed values are larger than 0,1 m/s, the relation for the calculation of the equivalent temperature is:

$$t_{eq} = 0.55 \cdot t_a + 0.45 \cdot t_{mr} + \frac{0.24 - 0.75\sqrt{v_a}}{1 + I_{cl}} (36.5 - t_a) \quad (6)$$

Where:

t_a : temperature of the air (°C);

v_a : air speed (as measured with the omnidirectional probe) (m/s);

I_{cl} : clothing thermal insulation (Clo);

t_{mr} : mean radiant temperature (°C);

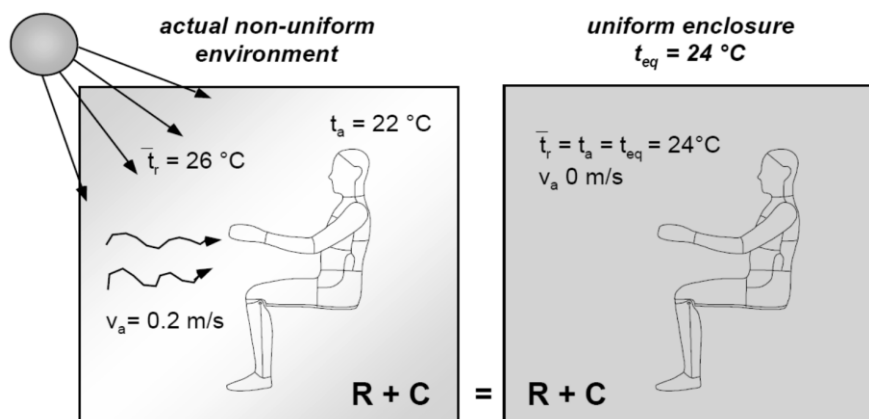


Figure 2: Illustration of the definition of equivalent temperature [66]

Apart the operative temperature, as a single global value resulting from the previous relation, it can be observed that several other concepts of equivalent temperatures are discussed by the standards such as: - the *directional equivalent temperature* – characterizing the heat transfer in the space defined by the region in a front of a virtual infinite plane. This quantity is described as a normal vector to a plane passing through the measurement point. It has a magnitude and a direction; the *omni-directional equivalent temperature* that can be defined either for the whole body, either for a body part is measured with an ellipsoid sensor; the *whole body equivalent*

temperature is the standardized quantity and is defined in the relation to the whole human body; and the *local equivalent temperature* related to only one body part or to a number of different body parts.

The determination of the above mentioned equivalent temperatures might be operated using different sensors such as described in EN ISO 14505/2 [64], like hot films, ellipsoid sensors or thermal manikins. The method using thermal manikin is explained distinctively in the standard and it is explained that it is intended for real asymmetrical ambient and will be described later, in detail in this manuscript.

The current definitions of t_{eq} from EN ISO 14505/2 [64] as well as the associated comfort zones diagrams are based on the work of Nilsson et al. [67-70], mainly on Nilsson's thesis [66].

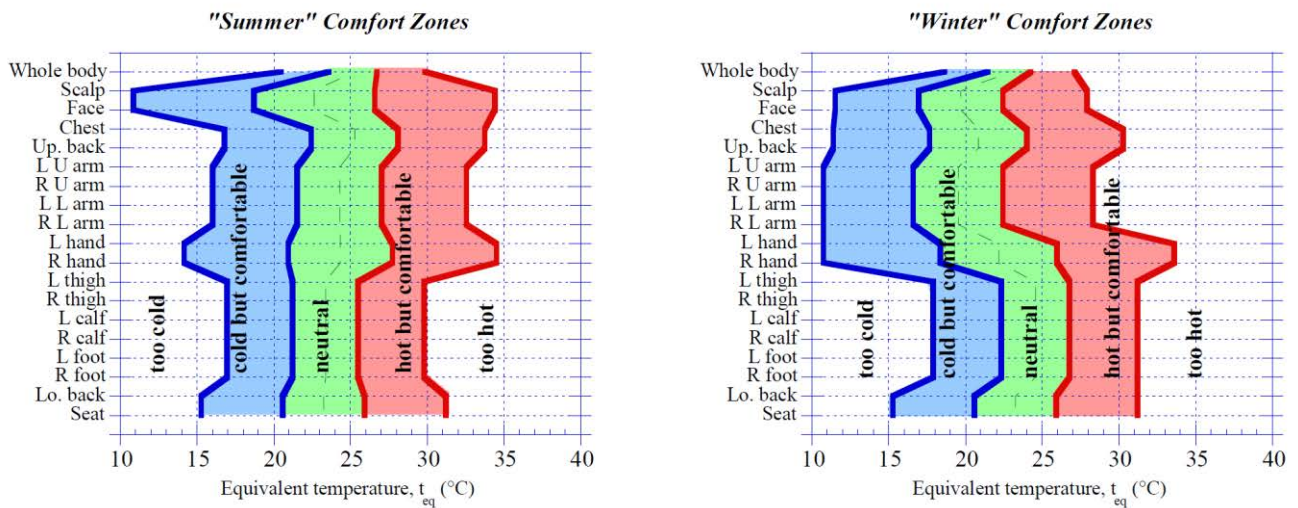


Figure 3: Proposed evaluation scheme for measured t_{eq} values in terms of anticipated subjective perception of conditions by driver or passenger [64, 66]

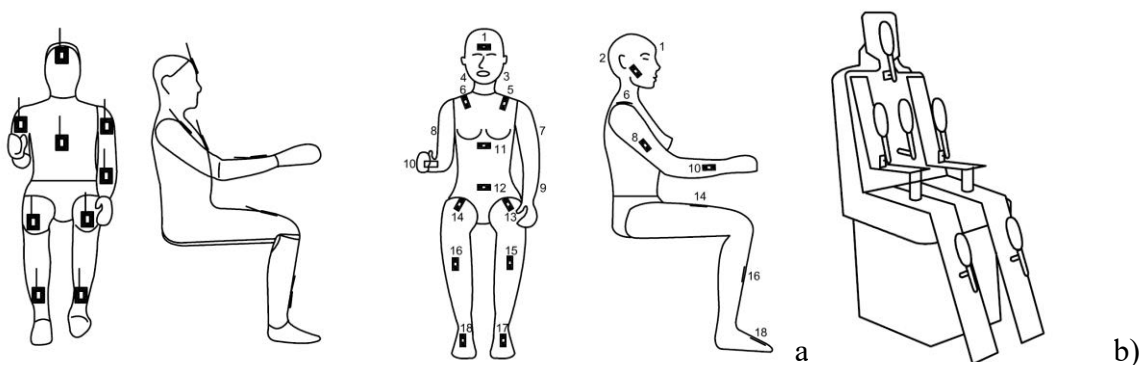


Figure 4: Examples of set-up for the measurement of t_{eq} as proposed in EN ISO 14505/2 [64] using several, discrete heated sensors mounted on a human-shaped dummy or a real person (a) or ellipsoid sensors mounted on a rig simulating a human body (b)

In Figure 3 are presented the comfort zones for the evaluation scheme for measured t_{eq} values

in terms of meaning subjective perception of conditions by driver or passenger as proposed by EN ISO 14505/2 [64]. Summer conditions are considered for the situation where the vehicle's HVAC-system is used in cooling mode. Persons are assumed to wear light clothing of 0,6 clo [0,09 (m² K)/W]. For winter conditions vehicle's HVAC-system is used in heating mode and persons are assumed to wear clothing of 1,0 clo [0,155 (m² K)/W].

However, the true t_{eq} cannot be measured directly but several methods are available for approximate determination of it. Depending on the method that is used, the t_{eq} needs specific definitions. This way, the *directional equivalent temperature* characterizing the heat transfers in the space defined by the region in a front of a virtual infinite plane. This quantity is described as a normal vector to a plane passing through the measurement point. It has a magnitude and a direction; the *omni-directional equivalent temperature* that can be defined either for the whole body, either for a body part is measured with an ellipsoid sensor; the *whole-body equivalent temperature* is the standardized quantity and is defined in the relation to the whole human body. The local equivalent temperature or the *segmental equivalent temperature* is related to a number either one single body part, being based on the measurements for one zone or for more zones of a human-shaped heated sensor, at the full scale of the human body. All these equivalent temperatures are possible to estimate through the use of several types of sensors as described in the EN ISO 14505/2 either using hot-film sensors, either using ellipsoid sensors [64]. Some examples of set-up from the standard are given in Figure 4. The segmental equivalent temperature is usually determined with a multi-segmented thermal manikin being (Figure 5) adapted for asymmetrical environments such as vehicles is also described in EN ISO 14505/2 [64]. A thermal manikin is associated with the local heat balance of defined zones. Different manikins will not necessarily give the same t_{eq} value for the same climatic conditions. The reason is that differences in construction and number of zones create body segments of different size, geometry and position. A given segment on one manikin can be composed of several minor segments, and cover a slightly different area, as a consequence, it is exposed to minor different climatic conditions.

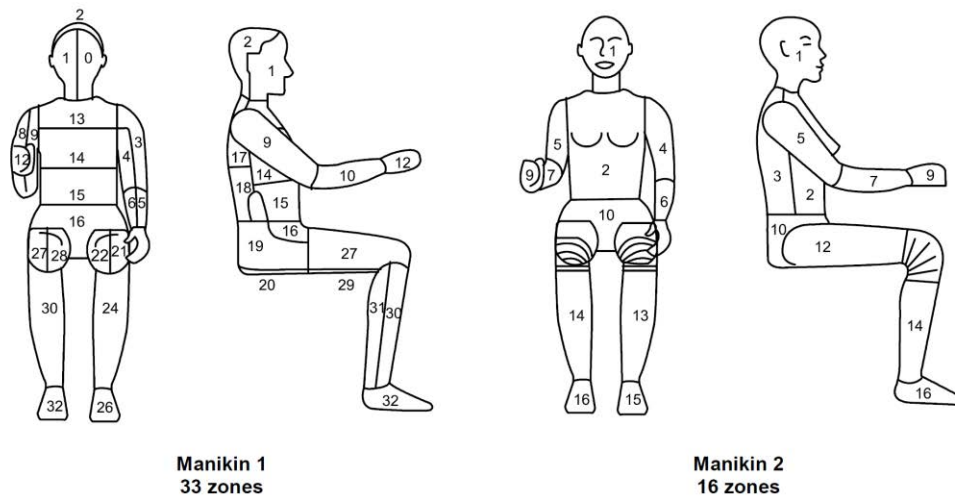


Figure 5: Schematic pictures of two versions of manikins proposed in EN ISO 14505/2 [64]

ISO14505 Part 3 [13] deals with a direct method for evaluating thermal comfort level in vehicles using human subjects. The evaluation index is called Thermal Sensation Vote (TSV). This method is called “subjective” approach because it records and quantifies responses from human subjects about their thermal sensation in an environment. The same seven points scale values, from “very warm” to “very cold” is used like in the case of PMV index. The questionnaires that are used are standardized by ISO 14505/3 in order to obtain a controlled and a representative sample of responses. The method does not have any limitations concerning the vehicle type. It offers only general principles that could be applied for both development and evaluation. ISO 14505 is presumed to be usable for all the categories of vehicles that include: cars, trucks, buses, passengers train compartments, aircraft cabins, ships compartments submarine habitation spaces, similar spaces on craft vehicles such as crews’ compartments. The method of assumed to be applicable to all the situations where people are confined in cabins wherever they are exposed or not to outside conditions. For example, in the particular case of drivers of exposed cabin or motorcycle riders, it is clear that the weather conditions will dominate the responses, but the method still proposes the same principles of assessment.

Subjective methods quantify the response of people to an environment using subjective scales. Such scales are derived via statistical methods from psychological responses of large samples of subjects. These responses are relevant to the physiological phenomena of interest such as the thermal sensation in contact with a specific environment. Thus, it is important to know the properties of the scales in order to correctly interpret the results. Scales of thermal sensation (hot or cold), preference, comfort and stickiness are often used in thermal comfort assessment. The main advantages of subjective methods are that they are relatively simple to put in practice and are

directly related to the psychological phenomenon. An important disadvantage is that responses itself may interfere with what they are measuring. It is recommended that ISO 10551 [71] should be used for guidance on the construction of subjective scales.

F. Nodal physiological models

The thermo-physiological model consists typically of a virtual representation of the human body as a combination of multi-layered cylinders and spheres with properties corresponding to tissues (so-called *passive system*) and a set of algorithms simulating human thermo-physiological responses such as shivering, sweating and vaso-constriction or vaso-dilation (so-called *active system*). The main principle of the human thermoregulation system is to maintain the internal body-core temperature at a value being situated around 37 °C while staying in a dynamic thermal equilibrium with the surrounding environment. This implies that the heat produced by the body is balanced by the heat dissipated in the ambient and the heat stored in the body. A simple relation for the body heat balance can be written as:

$$M - W = E + R + C + K + S \quad (7)$$

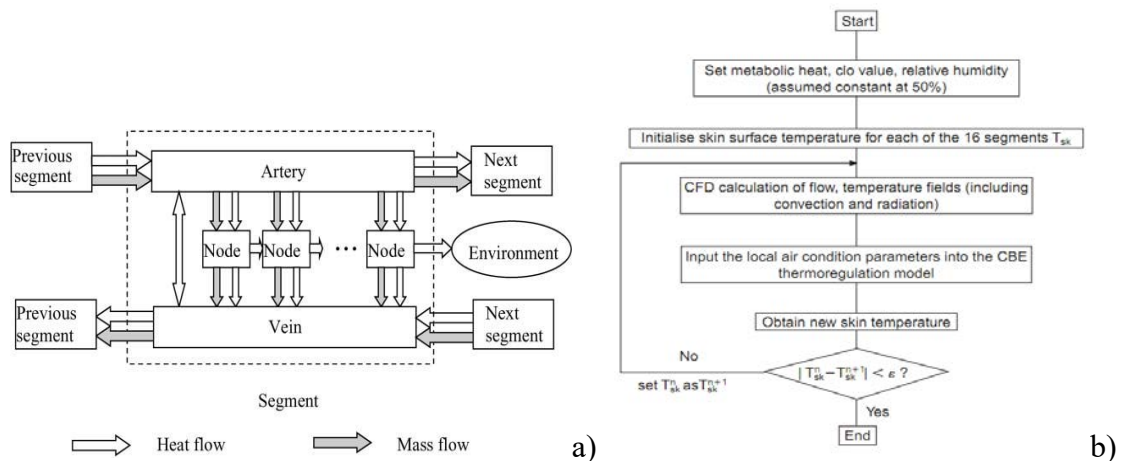
where M is the metabolic rate of the body, W is mechanical work, E, R, C, K are body rates of heat exchange via evaporation, radiation, convection and conduction, respectively, and S is rate of heat storage in the body, all terms in (W/m²).

The role of the thermo-physiological model is to provide a reliable prediction of the human thermo-regulatory response under both steady-state and transient conditions. Typically, the thermo-physiological models allow a multi-parametric input of the boundary conditions such as: ambient and radiant temperatures, air velocity, relative humidity, and short and long wave radiant heat load. Based on these parameters the sum of conductive, convective and radiative heat exchange through the clothing is calculated and balanced with the metabolic heat production to obtain a resultant skin temperature.

Close to PMV/PPD models, the nodal thermo-physiological models were intended to put in the same equilibrium equation, the heat and mass production of the human body and its transfer with the environment. As an alternative of correlating the empirical thermal sensation scale with the heat transfer, they give the local skin temperature variation as a result of simulated physiological reactions. The principal difference with the PMV/PPD concepts consists in their capability of simulating the transient ability of response of the human thermo-regulation system to the stimuli

from the surrounding environment. The numbers of nodes are corresponding to the number of parameters taken in account. The physiological reaction of the human body that are characterizing the thermo-regulatory processes are in this case defined as the adaptive feature of the human body to different conditions at which it is exposed. This is occurring though the variation of the heat fluxes (the shivering for the instance is increasing an increased metabolic rate, the sweating leads trough the high evaporation to an increased flux rate, the vaso-constriction leads to lower convection and radiation heat fluxes). Givoni and Goldman [72] proposed in the early seventies an empirical relation intended to predict the central core temperature. Their concept was defining a couple between determinate body core temperature and its corresponding core temperature. This couple could be calculated as a function the parameters defining the thermal state of a person: metabolic rate, clothing, environment. The idea being that to unified biological relations which could be developed in order to adequately predict the response represented by the skin temperature starting from the body core temperature. An example of first model is the one of Gagge et al. [22]. In this example the human body is considered to be composed by two layers: the body core and the skin. The model considers the variation of the skin temperature as a function of the core temperature both being weighted by the percentage of each of them.

The thermo-regulatory processes are in this case represented by signals of the specific temperature of the core, skin and body in the case of low to moderate activity levels and in the case of homogenous temperatures.



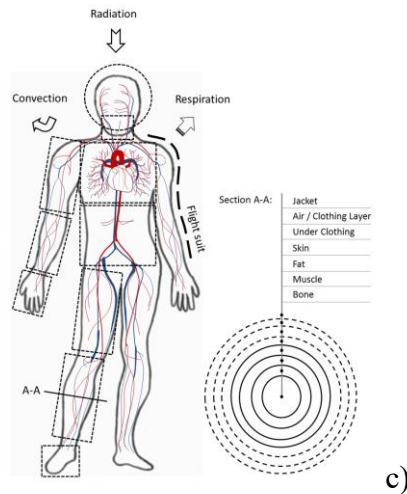


Figure 6: a) Berkeley model [73], b) coupling between the Berkeley model and CFD [74], c) nodal model of an aircraft pilot [75]

Another nodal model that can be discussed is the KSU model developed at Kansas State University [76]. This model is like the Gagge model but, the index resulted is a thermal sensation that is calculated in different way for warm or cold environments. A more elaborated multi-nodal model was proposed in the seventies just at the same period as Fanger's studies. This is Stolwijk's 25-node model [77], was used in the aerospace applications field, where non-uniform conditions had to be evaluated. The six-part distribution of this model gives more dynamicity allowing the estimation of the thermal sensation for each of those parts. The ambient environment is supposed as previously to be in steady-state condition however this model was the starting point of a suite of more adaptive thermo-regulatory models. A representative one is IESD – Fiala thermo-regulation model [54, 55], which also involves a controlled passive system and an active controlling system as previously explained. The model was validated with experimental studies, in both transient and steady state conditions, and displayed a good agreement with experimental data. Another model based on the Stolwijk model is proposed by Tanabe et al. [78] was published in 2002. The model has sixteen body segments corresponding to the thermal manikin, each divided in four layers: the core, the muscle, the fat and the skin. A 65th node is the represents central blood segment, which exchanges heat with all other nodes via the blood flow. The heat transfer coefficients and the thermal resistance of the clothing insulation were deduced from the thermal manikin experiments.

The Berkeley Model [73] is perhaps the most famous. It has an unlimited number of segments that represent some environmental and physiological input conditions and which are called phases. One phase contains information on the following parameters: metabolic rate, duration of the exposure, physiological constants, thermal resistance and permeability to the moisture of the

clothing, the temperature of the air, the radiant mean temperature the conduction coefficients of the surfaces of contact. These phases are time intervals where environmental conditions are constant in time or their variation is linearly time dependent. These way, very short nonlinear transient parameters could be approximated by linear variations of the same parameters. The physiological constants may take different values. The basic element of this model is an object called “node”. Multiple nodes from a higher level are which is called “segment”. These objects are organized in a tree-like structure. A segment has also a “blood” object with its sublevels an “artery” and a “vein”. The human body in then reproduced by several segments that are interconnected using the blood. The heat transfer occurs trough conduction between each node and trough convection via the blood.

In [79] are presented five stages in using the Berkeley model for prediction of a local thermal sensation. These are: the definition of the human body geometry, or its import; the meshing of the geometry; the definition of each characteristics of the biological material (fat, muscle, bones...); defining the boundary conditions; the resolution of the heat transfer equilibrium equations using a finite-difference method. Another famous model that allows to simulate the adaptation of the human body, is the Stolwijk's multi-node model [80]. It includes a distinctive layer corresponding to the clothes, which is in fact a multi-layer system. The clothing model takes into consideration the absorption of water vapor in the textile fibers. Different textile materials can be simulated. The specificity of Stolwijk's model is related to its capability to simulate the sweat accumulation into the skin surface.

It should be observed that the nodal thermo-physiological models have not yet been prescribed by any of the international standards as methods for evaluating the local and overall thermal sensations.

The characteristics like the shape, the size, the metabolic-rate, the clothing-level or the activity-level have an important role on the estimated thermal perception of the ambient of the human body [81]. In this case, the most appropriate assessment method should be a numerical instrument allowing a Computational Fluid Dynamics model to be coupled with a thermo-regulatory model (see Figure 2b). We consider that, the thermo-regulatory Berkeley model [82] which takes into account the interactions between the local body parts and the whole body thermal sensation is the most appropriate model to be used in the real situations of the environments from the buildings and vehicles. The available thermal comfort models that address the asymmetry environments require further development and improvement. For example, the Fiala [54] model appears to address transient conditions while the Berkeley model [85] focuses on the cooling

effects in warm environments. Also, it is foreseen that in the long term, applied robust prediction of heat transfer between the human body and environment can be obtained with CFD methods. The idea is to have the possibility of inserting back the human body thermal regulation model directly this type of results in order to obtain a much more accurate approximation of the thermal sensation and the level of comfort of the different body segments.

g. Psychological component integration

Modeling the comfort response itself is the goal in using heat balance models. Indeed, all of the rational models make the inherent assumption that there is some predictable comfort response for a given physiological state of the body. Still, it is not clear if there is such a relationship and how it could be expressed in a universal, applicable way. The state of comfort is inherently a psychological response, not a physiological response and we should expect many nonphysical factors to affect the perceptions of comfort which has to be also very much dependent on expectations. Generally the integration of the psychological component into the thermal comfort evaluation in the case of vehicles is performed through other ways that it was done in the past for buildings, usually relying on behavioral and neuro-cognitive experimental methods related to drivers' safety mainly, by acquiring physiological signals using medical techniques like the electroencephalogram and the electrocardiogram [17, 33, 83].

During the past several years, the thermal sensation and thermal comfort research have attracted a lot of interest in the field of not only building and industrial design but also of neurophysiology. Understanding the intimate neuro-mechanisms of thermal comfort would be beneficial to all fields including advanced indoor environment control or design of efficient products like wearable devices. The functional activities of brain detected by neuro-imagery and electrophysiological tools could be used to evaluate the human thermal comfort during various thermal environments. Kanosue et al. [84] used functional MRI (magnetic resonance imaging) to detect the pattern of regional brain activity during whole body cooling. Their results revealed the increased MRI activation in the bilateral amygdale during the cold discomfort condition. With positron emission tomography, Farrell et al. [85] have determined the independent relationship between the changes of regional cerebral blood flow in the posterior part of the cingulated cortex and the ratings of the hedonic dimension of thermal sensation during whole body warming and cooling. Electroencephalograph (EEG) has also been used to investigate the cerebral response to thermal stimulation. The global relative powers in EEG alpha and beta bands were found to be sensitive to human thermal sensation of ambient temperatures[86]. Most of these neuro-

physiological studies were conducted on whole body thermal stimulation, and their results provided us more neuro-physiological evidences about the process of thermal sensation and thermal comfort in peripheral and central nervous system. The relative importance of surface regions or ambient temperatures for human local thermal comfort has been examined by the skin temperature [17, 87]. Previous EEG studies investigated the electrophysiological responses to pain cold water [88] or non-painful warm/cold water [89] on non-dominant hand. The experimental data demonstrated the different patterns of EEG power spectra [88, 89] or the different topographical distribution of cortical sources associated with the different local thermal stimuli. However, in all these studies, the thermal stimuli were all water based and the effect of ambient temperature has not been considered EEG studies.

We observe at this point that there is no consensus between the existent theories and models as how comfort should be connected to the psychological variables or even which are the variables. It is still unknown whether there are some neuro-physiological responses corresponding to the possible influence factors (e.g. stimulus mode and ambient temperature) during the local thermal stimulation.

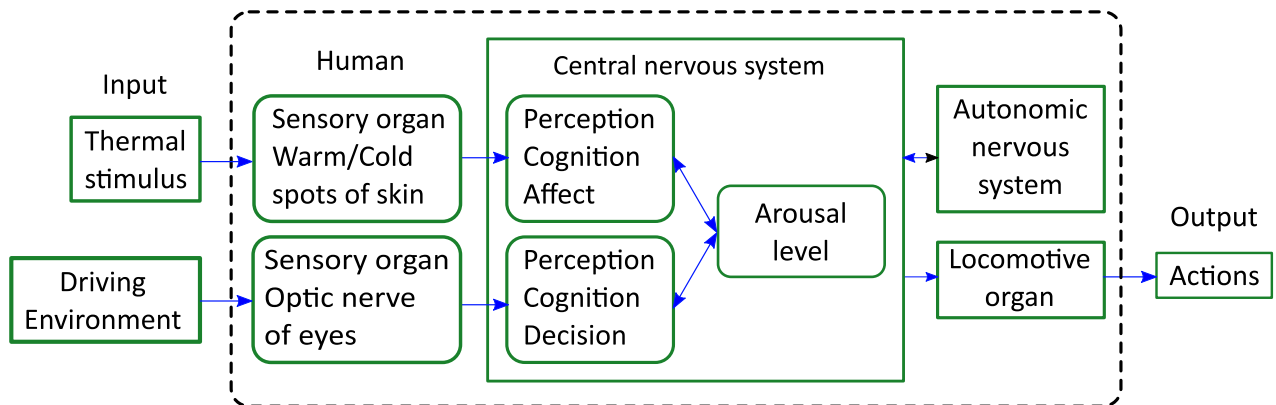


Figure 7: Flow of the physiological responses [83]

A representation of the flow of the physiological responses to simultaneous stimuli related to driving and to the thermal environment could be schematized like in Figure 7. Thermal stimulation is transmitted from the skin to the central nervous system affecting the thermal sensation and the comfort sensation, and a change in comfort sensation affects the autonomic nervous system and the response is performed through the locomotory organ. In addition, the driving environment is transmitted from the optic nerves of eyes to the central nervous system and then is transmitted to the locomotory organs to perform the driving tasks after passing through the information processing (perception, recognition, and judgement) in the central nervous system.

And it is thought that the performing of the driving tasks also affects the autonomic nerves system as mental workload.

H. Synthesis of experimental evaluation of the vehicle environment in the current literature

Physical parameters observation

The above presented standards are either difficult to interpret, either impossible to apply, either use expensive approaches. There are many papers dealing with the observation of the environmental conditions inside the vehicle that might affect the human thermal comfort and those concerning the human's response and perception of its interaction with the environment. Part of them stops only on the study of the effect of a certain parameter (the air temperature and the mean radiant, the relative humidity, the solar radiation including the effect of the glass transmittance, the outdoor temperature, etc.) on the thermal environment of the vehicle without considering any thermal comfort assessment using comfort models. Others are addressing the combined effect of several parameters from those mentioned above, and sometimes correlations with the air quality are also addressed via the recordings of the CO₂ concentration.

Ambient temperature is considered to be affected by the solar load, ventilation system load, human body load, and external temperature. External parameters have a strong influence upon the environmental parameters. As example the air temperature in a car cabin could reach as high as 70°C during the summer for an outside temperature of 34°C and a value of the solar radiation intensity higher than 800W/m² [32]. During the winter, when outdoor, the temperature is very low, the passengers will be confronted with the same temperature inside vehicle when they will get in the car, if the car is parked outside.

The available literature is displaying a few studies that discuss and address the use of the thermography for the evaluation and assessment of the thermal conditions inside the car cabin. This technique is a contactless method that is suitable for the characterization of the interior surfaces or even for the dynamic monitoring of the skin temperatures over the passengers' bodies. In [90] are described the approaches involving different IR sensors for the automotive climate analysis. Additionally, the same authors, are proposing a method allowing the direct IR measurement of the air temperature using a thin layer of polyethylene film. In the study of Korukçu et al.[91] it has been used a thermographic camera to measure the temperature of the interior surfaces such as the dash-board but also the temperature distribution on the human skin of the face of the driver. The measurements were performed during cooling and heating trials. The

measurements from the IR camera were compared with both spatial and temporal evolutions from a network of thermocouples and a good agreement has been found.

High air velocities are common in vehicles and can vary over the body surface. They are caused either by open windows during driving or by the HVAC-system. The result in both cases normally is a local cooling of the affected parts of the body. Measurements of air velocities should be done in representative spots representing areas exposed and weighted according to their percentage of the total body surface. In most cases, this value will be less than 20 %, as large parts of the body are protected by the seat. Understanding the flow pattern is still a challenge due to the complex interior geometry and the layout of the ventilation system. The pattern is influenced by several parameters, namely location and geometry of vents, flow rate, and geometry and shape of the air diffusers [92], also high shell temperature boundary of a vehicle directly affects the temperature distribution of the interior flow [93].

Air velocity measurements usually are made in the same points as the temperature and also close to the discharge diffusers. As measurement tools in literature are used omni-directional probes for punctual measurement and some complex systems for field measurements. With the second air velocity measurement technique can be monitored particles displacement on three axes. Velocity field measurements are rarely seen in the literature, because insertion of the measurement equipment in car cabin is a problem. One of the solutions of this problem is cutting some parts of the car. It is possible to create a car cabin from a transparent material, but in this case the geometry and thermal insulation is not the same as in the real case.

The car air-conditioning system generates a complicated transient non-isothermal three-dimensional turbulent flow pattern inside the cabin. In some cases it was found that jet direction differs substantially from the direction that was set by the vanes [94]. Also, for a good understanding of thermal sensation is necessary to know velocity profiles and airflow from all the grills. Results from some studies show that the actual jet direction differs substantially from the direction that was set by the vanes [94]. In the case of automat HVAC systems, is necessary as input only desired temperature, and depending on the internal temperature, it will change introduced air proprieties and ventilation strategies. Thereby air distribution in summer is focused on passengers' upper body (76 %) and windshield (20 %). Rest of the air leaks to the other vents insignificantly. Winter and spring / fall cases are foot well oriented (ca 40 %), the rest of the air is used to heat up the windows and improve passengers thermal comfort [95].

These two physical factors are used also in validation of numerical studies.

The third essential parameter is **solar radiation**. This is a new factor introduced in the

thermal comfort and is considered as a strongly influenced factor especially in the summer time. Solar radiation affects the most: ambient temperature, mean radiant temperature (through overheating the dashboard and seats), and when it falls on the human body could produce a high local overheating. This overheating has a major influence on the thermal sensation of the body. The evaluation of effect of solar radiation is conducted by exposing the vehicle at different solar radiation intensities, while variations of the environmental parameters are followed in the passenger compartment: using a thermal manikin, either asking human subjects to complete a questionnaire regarding thermal sensation. If direct solar radiation is present, the local temperature on the manikin's surface raises leading to local discomfort on some parts of human body, also a non-uniform environment is created. The vast majority of the studies that have focused on the analysis of the solar radiation effect were realized in laboratory conditions. They all show a link between the thermal environment and the thermal sensation influenced by the solar radiation. The final effect depends upon factors such as glazing area, insulation of compartment walls, size of compartment, and surface color of vehicle. Most important is the direct radiation that hits the driver through the glass, as large quantities of heat can be absorbed locally by clothing and underlying skin. The radiated area can be small when the sun is at the zenith, or large, in modern vehicles with large front windows when the sun stands lower. Radiation effects can be estimated on the basis of shielded and unshielded globe temperature measurements or by measurements of the radiant flux. Measurements should be weighted according to their percentage of the total body surface. In most cases the radiated area will be less than 20 %.

Compared to buildings, vehicles have much larger glazing surfaces, the effect of the sun's radiation is felt more strongly through and rapidly the local warming produced where the sunlight is "falling". In a car parked under the sun, the air temperature can easily reach 70° C and as a consequence seats, boards driving wheel are heated [96]. The thermal diffusivity and emissivity of these elements influences the time to attain the global comfort air temperature and inherently influences the distributions of the velocity and temperature fields [45, 46]. Most studies do not consider the thermal inertia of the elements inside the car. The main solution to reduce solar radiation studied by some researchers is the installation of anti-solar films on glazed surfaces, the insulating of some countries prohibits the installation of foils and objects that can obstruct the visibility of the glazing on the glazed surfaces. To balance the injected heating or cooling loads exchanged with the surrounding environment but also for achieving temperature and velocity values considered as comfortable in the shortest possible time some researchers have focused on modifying the air distribution system. As a consequence, they observed the effects of different

ventilation system configurations on the environment of the vehicle cabin.

A small proportion of the studies assessing the thermal environment in cars is focused on the **effects of relative humidity** [97, 98], average radiation temperature and other factors specific to this environment. The water vapor pressure in general is uniform all over the vehicle compartment. Accordingly, a single measure should be sufficient for the assessment. It is expected, though, that radiated areas and areas with high convection allow more evaporative heat exchange. This effect is difficult to determine. It is recommended that the effect be neglected, as it works on the positive side (reduces heat stress).

High humidity level might be specific to the in cabin environment. The influence of relative humidity high levels on the perception of the thermal sensation (60% – 90%) for a range of 20–26 °C has been investigated by Fountain et al. in [99]. The study was performed considering sedentary activity level. The effect of relative humidity was discussed in [99] without any distinction from other parameters such as the dry bulb temperature for instance. In [79] Alahmer et al. presented the effects of relative humidity variation on the cabin environment from the thermal comfort assessment perspective but also from the subjective assessment of the thermal sensation perspective. This analysis has been performed using thermodynamics and psychometrics coupled to the simulations based on the Berkeley model [98]. The authors are known for proposing a practice implementation of their findings in a controller system that uses the evaporative cooling principle [100]. It has been shown in their studies that the control of relative humidity along with the control of the dry bulb temperature could improve the air conditioning efficiency by reducing the removed thermal load while enhancing the thermal sensation of the passengers [100].

Experimental studies using standardized methods

The first results using the concept proposed by Nilsson's thesis [66] were also a part of an European Project named EQUIV, carried out by a consortium integrating vehicle manufacturers and universities [101], the objective being to propose a basis for EN ISO 14505/2 [64] standard. The main conclusion that emerges from the analysis of the various papers published by that research group [66-70, 101] about the measurement of the equivalent temperature is that the authors felt the need to introduce some variations on the concept in order to put up the differences resulting from the nature of the measuring procedure. The four different definitions that appear in the standard: global equivalent temperature, segmental equivalent temperature, directional equivalent temperature and omni-directional equivalent temperature are all based upon the dry

heat losses of the human body, or a part of it. Differences appear in the way the balance equations are formulated. In the global equivalent temperature the whole human body is considered. In the segmental equivalent temperature only a part of the body is analyzed. The directional equivalent temperature refers to the vector normal to the infinitesimal plane in each measuring point, being the thermal balance established between the point and the semi-hemisphere in front of it, while the omni-directional equivalent temperature is considered to be related to the whole body or a segment, but is measured by an omni-directional device.

Different methods are used to measure these different equivalent temperatures, besides the use of individual sensors dedicated to all the intervenient variables, e. g. thermal comfort meters with heated sensor, local discomfort meters, plane surface sensors and thermal mannequins. These last are considered as the reference method with which other methods are compared. Significant differences were found in the values of equivalent temperatures arising from different methods in tests performed in uniform environments inside a climatic chamber, which are attributed to different characteristics of the measuring devices, such as size, geometry, posture, number and type of sensors, control method, etc.

EN ISO 14505/2 [64] standard has been published quite late, in 2006. There are but a few articles using standardized methods for evaluating thermal comfort and even less that are combining air distribution strategies with thermal comfort.

In his thesis Nilsson proposed three types of methods for assessing the comfort level in vehicles spaces. A first category of methods employed human subjects – based on the TSV, a PPD was also evaluated and an adaptive model implemented. A second category employed manikin measurements, with two slightly different manikins, both in the seated position. The manikin surface was divided in independently controlled segments. Each zone of the manikin was covered with resistive wires, introduced in a hard-plastic shell. On the surface the temperature sensors were placed. The principle of control for the thermal manikin was based on maintaining the surface temperatures constant at 34°C. The necessary electrical power was recorded for each zone. The authors acquired heat loss measurements as a function of different factors such as air temperature, air speed, radiation and clothing. In another study published by Bohm et al. [102] before EN ISO 14505/2 [64] a good correlation between the equivalent temperature measured with a thermal mannequin and the subjective evaluation of humans subjected to the influence of a flow inside a car cabin model was found.

In the more recent paper of Martinho et al. [103] maps of the equivalent temperature in the zone occupied by a person seated in a car cabin have been determined by two different methods.

In the first empirical equation derived by Madsen et al. [14] has been used, in which the values of the environmental physical parameters measured within the car cabin mockup, without the presence of the thermal mannequin, are introduced for different conditions generated by the HVAC system. In the second the measurements taken using a real-scale thermal mannequin, divided into 16 body sections, for the same conditions as in the first method. A comparison is made between the equivalent temperatures measured by the two methods. The main idea was to analyze the possibility of replacing the analysis performed by thermal mannequins in time consuming experiments by calculations done with physical values characterizing the flow field in the space surrounding the passenger. Tests were carried out on a life-size laboratory model of a car cabin, constructed with a simplified geometry, for different conditions: with and without the presence of a thermal mannequin, with different values of air velocity and temperature and with different regulation of the air inlets. The values of equivalent temperature were determined for each one of the various parts of the body, by two distinct forms: from the measurements performed by the thermal mannequin and from the physical parameters of the airflow, air velocity and temperature. The mapping of these flow parameters inside the cabin was done through a scanning process carried out with a traversing mechanism with eight low-velocity thermal anemometer probes, controlled from the exterior of the car cabin. Thus, using the values measured in plans in the neighborhood of the different parts of the thermal mannequin, the equivalent temperature profiles were computed during tests carried out without the presence of the thermal mannequin.

The scientific research reality, shows nowadays, only rare solitary set-ups to assess the thermal comfort in vehicles using the equivalent temperatures experimentally. These are either very expensive or suitable for punctual measurements only. However, data acquisition at different locations in the interior space of a vehicle is highly desired, generating the need for cost-effective and precise measurement equipment that are intended to allow access to the local distribution of the equivalent temperatures especially for the ventilation systems where important thermal gradients are present, allowing to evaluate the heat impact of real passengers as well. This is the motivation of developing thermal manikins in our research group and thus one of the most important objectives of the thesis was consisted by the development of the thermal manikin Suzi that is presented in the following chapter.

Recently thermal dummies that are simulating passengers of the German Aerospace Center have been turned into very low cost thermal comfort manikins [104]. To ensure the measurement of equivalent temperatures for several body parts, the obtained thermal manikins are calibrated in

a climatic chamber. Then, the surface temperature of the manikin is measured using a high-definition thermographic camera. This method offers the possibility to calculate local equivalent temperatures at a spatial resolution of 10 cm and with a precision of ± 0.5 °C.

Experimental studies based on the physiological and psychological components quantification

As it is difficult to really separate the physiological and psychological components in the literature a series of studies are combining the collection of all sorts of biometric signals with thermal sensation or the state of thermal comfort.

Lee et al. [105] conducted studies to analyze the concentration while paying attention to something, by measuring the brain wave signals of occupants at different inside temperatures, and to understand the effects of floor temperature on body relaxation. Kum et al. [106] carried out studies to measure the brain wave signals and electrocardiograms of the occupants at different indoor temperatures, and to evaluate thermal comfort of humans at various levels of the difference between outdoor and indoor temperatures in summer. Kim et al. [107] evaluated thermal comfort during sleep in summer using physiological signals and average skin temperature. Kim et al. [108] also studied the method of evaluation of comfort using brain wave signals at the frontal lobe and parietal lobe.

Kang and Song [109] evaluated the thermal sensation and physical characteristics of an air-conditioning system that applies fluctuation characteristics similar to those of natural wind, by measuring skin temperature. Lan et al. [110] reported thermal comfort levels during sleep for different air temperatures using mean skin temperature and the responses to subjective thermal comfort questionnaires. Liu et al. [111] investigated the variations in the average temperature of the human skin and surface in stable and unstable thermal environments. Nguyen et al. [112] developed a correlation for an adaptive thermal comfort model for a hot and humid climate like the one in South East Asia using the responses to a subjective thermal comfort questionnaire. Choi et al. [96] reported that the optimal cabin temperature was 23°C based on measurement of psychological and physiological signals of the driver, and suggested a comfort index and an evaluation model.

In the previous studies on thermal comfort of the driver in the vehicle, Yao et al. [113] performed an experimental study on physiological responses and thermal comfort at various cabin temperatures. Seo et al. [114] reported that cooling between the legs took the longest time, so it was more effective to locate the vent exit at the top area. They reported that air-blowing at the

center of the top side was effective in maintaining thermal comfort continuously. Kobayashi et al. [115] reported that having the air flow direction toward the chest was the most effective method among various air flow directions while cooling the vehicle. In the same time, Alahmer et al. [100] conducted the analysis on the effect of relative humidity (RH) control in the cabin to achieve thermal comfort in a short time, and reported that the subject felt comfortable with an increase in RH in the cooling condition, and with a decrease in RH in the heating condition. Marcos et al. [17] were proposed and validated a simplified and dynamic thermal model for the cabin of a vehicle. Liu et al. [18] were performed study on occupants' behavioral adaptation in workplaces with non-central heating and cooling systems and Yang et al. [19] observed and examined the discrepancies between the PMV in an air-conditioned environment through a laboratory study. Gilani et al. [20] carried out study to bridge the gap between actual mean vote and PMV by considering the individual the blood pressure as physiological parameters in the PMV model.

Even though much research work on the bio-signals generated by human body have been actively conducted in the world, most of these studies are associated with bioelectrical signal changes under only comfortable temperature ranges. There are no studies on bioelectrical signal changes in the human body when there is a change from a temperature that causes discomfort to a comfortable temperature range. Moreover, it is found that there are hardly any studies on thermal comfort with the consideration of cabin and vent exit temperatures simultaneously during the temperature variations. The variations in comfort and concentration with changes in cabin temperature during driving for a long time are not found in open literature. In the recent study of [83], the brain wave and pulse wave signals of subjects were measured and analyzed when the temperature is changed from a level that causes discomfort to a comfortable temperature range, with full load in the cooling and heating modes in a car cabin. The result of this study can be applied as the basic data in algorithms for the design of a future human machine interface and smart indoor air-conditioning system in vehicles.

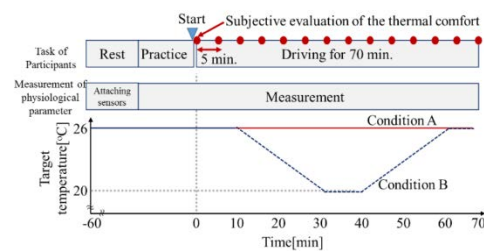
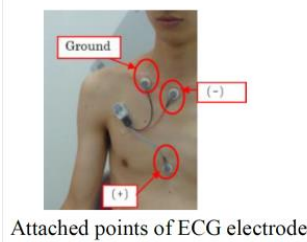
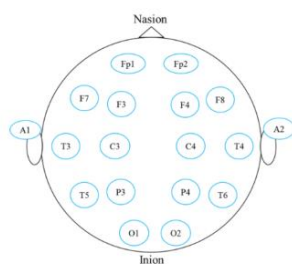


Figure 8: Experimental set-up in [83]: a) attached points of EEG electrodes, b) attached points of ECG electrodes, c) experimental protocol and thermal conditions

1. Numerical models for prediction and evaluation of comfort in vehicles

If we take a look to the numerical studies involving virtual human bodies, it was in 1996, that Murakami et al. [116] introduced a human model in CFD study, being interested in the dynamic effect of air flow around the body. This model was called by the authors "computational thermal manikin" used to predict thermal comfort. The article describes the development of a virtual thermal manikin, being analyzed in a first phase the convective heat transfer between body and air flow, using a CFD code. The novelty of this study came from the analysis of convective transfer, analysis difficult to realize experimentally to human body skin. The virtual manikin used in this study is detached from other CFD studies by the curved shape that looks like the human body. CFD calculations using virtual thermal manikins (VTM), with simple geometries involving low computing resources, but an anthropomorphic geometry can lead to more accurate results. VTM differ in size, posture and geometric complexity. In general, we meet VTM's closest in size to adult human body, with heights between 1.65 and 1.90 m and areas between 1.6 m² and 1.8 m². Depending on the study, three positions are used: lying, sitting and standing. The level of geometry details of a human virtual body depends on the computing resources available and the purpose of the numerical simulations involving an VTM. Dunnett [117] used a cylinder with elliptical section to simulate a person and Niwa et al. [118] simulates a seated body by a heated cube. To simulate a person standing, it was used a parallelepiped of the same height for flow field visualizations [119] and thermal comfort indexes determination [120] which describes the atmosphere around it. Other researchers have used three dimensional rectangular shape to model airflow around a seated [121] or standing person [122-125]. Lightly complex geometries of the human body could be obtained using specialized CAD software or through laser scanning that is used for other purposes.

Modeling vehicular air flows and thermal environment

The first category of numerical studies includes those dealing with the qualification of passenger compartment environment without using thermal comfort assessment models. In the corresponding articles are analyzed the effect of different changes imposed over the vehicle thermal environment, relative to a reference case. The most considered parameters in these studies are: ventilation strategies [126-129], external physical factors [93, 96, 130-132] and the number of

passengers in the vehicle [133, 134].

The number of passengers in the cabin influence flow and temperature distributions, due to bodies' generated heat loads. Zhang's studies [133, 134] were specially focused on that effect. The main information concerning this study is given in

Table 1. The simulation has been carried out using the commercial software FLUENT. The vehicular cabin is modeled in 0.6 million tetrahedral elements. The standard k- ϵ turbulent model with a wall function was used for in cabin air flow simulation. Imposed surface heat flux is determined via Newton's law. For the reference case heat dissipation from passengers' bodies was 116W, and from the driver body was 176W. Temperature of outside air was 43°C, in cabin air temperature was 60°C and solar radiation was imposed like a heat flux on the cabin surface. For the inlet air temperature user-defined function (UDF) was developed, to simulate the same variation like in the experimental study, air velocity was not specified. The reference case was validated with a experimental study carried out in the environment test room. The same simulation was repeated by varying the number of people (driver and passengers) in the cabin from 0 to 4. The authors' consideration is that for the thermal comfort achievement, the compartment temperature should be within the range 24–29°C and the local air velocity should not be larger than 0.5 m/s. The main conclusion is that the more persons are in the vehicle the more air temperature rise, due to the heat load from the human bodies, while the air velocity slightly decreases. The decrease in air velocity is not explained by the authors. In our opinion, this is due to impingement of ventilation jet on the occupants, which decelerates the flow at the vicinity of the occupant's' bodies. In all cases, the air velocity rises in some points beyond the limit of 0.5 m/s. The temperature range exceeds the top limit of 29 °C, and the most critical situation was with 4 persons in the cabin.

The authors recommend, if there are 3 or 2 persons in the cabin that the passengers should stay on the back seats where air temperature and air velocity levels are near the considered comfortable limits. Maintaining the same conditions as in the reference case with 4 persons in the vehicle, the solar radiation intensity was decreased from 1635 to 400 W. The results show that the average temperature of the compartment reduces by around 5 °C, which corresponds to a decrease by about 50 % in cooling energy consumption. Hence, solar radiation level has a great effect in the in cabin thermal environment.

Kilic [126] was interested in the effect produced by different ventilation strategies on the rapidity of temperature (air and surfaces temperature) decreasing and air flow distribution in the car cabin. STAR-CD software coupled with heat transfer equations was used as solver. The

calculation domain is composed by 0.9 million elements with triangular shape on surfaces and hexahedron shape in volume region. RNG k- ϵ model was used for modeling the turbulent flow of transient cool down process. In the vehicle a model of virtual manikin with temperatures of 33°C and 33.7°C for body clothed parts respectively for unclothed body parts was introduced. Convective heat transfer coefficient at outside of the cabin was set as 15 W/m² K and initial environmental temperature 41 °C. The inlet air temperature has been set transient to reproduce experimental condition. Three ventilation strategies with uniform velocity profiles were tested. For this strategies, dash board and defrost grills air velocity was varying: case I – console type, introduced air velocity 2.5 m/s; case II – dash board air diffusers velocity 1.5 m/s defrost 1.2 m/s; case III - console grills velocity 2 m/s defrost 0.6 m/s . This study numerical study was not validated. The most uniform temperature and air velocity fields were found during the first case, moreover also with this ventilation strategy the lowest ambient uniform temperature was achieved after 30 min. Comparing the results of the 3 strategies, we conclude also that in the case of console type grills (case I), the faster temperature decrease and the most uniform temperature and velocity distributions were obtained. The authors do not explain the results found. In our opinion utilization of the console type grills lead to a better mixing between injected air with cabin air, while the air introduced through defrost grills is less mixed with de cabin air because it is turned to the windscreen.

For this best strategy of ventilation, other authors [127] proposed the use of an innovative dynamic air vents system, which consist in an active control of flow direction using automatic and periodic changes of air vent vanes inclination. To simulate flow directions changing a UDF function was compiled. The numerical simulation was performed with the commercial software FLUENT. The calculation domain consists in a dynamic mesh structure with 12 million tetrahedral elements. The initial test conditions are: outside ambient temperature 35°C, in cabin temperature 65°C, discharge grills mass flow rate of 0.1426 kg/s and 8°C temperature. To achieve thermal comfort state author's consideration is that temperature should be between 20° C and 22° C, relative humidity should be about 50% and air velocity should be between 0.5 to 0.8 m/s. The results show that after 30 min of cooling period, with baseline steady vents the average velocity of 0.62 m/s while with dynamic air vents a rise of 0.27 m/s. In term of temperature is observed with a drop of 3°C of mean air temperature in the dynamic vents type. The dynamic air vents system increase the uniformity of temperature and velocity distributions in the cabin, and reduces by 25% the time of achieving thermal stability due to improvement of the mixing between the injected air and the cabin air.

Numerical studies in which the effect of the solar radiation over the cabin environment is followed are more complex, because solar radiations change not only environmental characteristics but also the thermal perception of passengers in contact with. In the other hand, in the summer case, in a parked car, easily a high air temperature is reached [93, 96]. Also high temperatures are present on the surfaces exposed to direct solar radiation. Thereby on the dashboard, chairs, roof, parcel shell surfaces high temperature values were found. The temperature and thermal inertia must be taken in to account because they influence the cooling process and temperature and air distribution in the cabin [96, 131, 132]. From these numerical studies was found that these surface temperatures decreased more slowly than the others because a constant persists during cooling process. Jonsson [96] proposes, to insert solid cells inside the car part exposed to direct solar radiation to obtain more precise results.

Srisilpsophon [135] studied the effect of different anti-solar glass film on the heat transfer and mean radiant temperature in a vehicle cabin. Initial in-cabin in the driver position was 25 °C, outside temperature 30 °C and the solar insolation was considered to be 25 MJ/m². The solar radiation was not simulated but included in the heat fluxes passing through the wall of the vehicle who take in account the convective heat transfer from outside air to the wall, the heat conduction through the wall. In the vehicle cabin the convection and the radiation heat transfer were calculated. The heat transfer entering the cabin walls and their surface temperatures was estimated using equations proposed by Stoecker [136]. Numerical study reveals that the solar load could be reduced by about 14, 18 and 20%, for 40, 60 and 80% solar cut-off anti-solar films, respectively, compared with that without the film, also at higher outside air temperatures (more than 30°C), the darker film shows an advantage over the lighter one in terms of MRT reduction.

Predicting thermal comfort through numerical studies

Numerical studies from a second category are aiming to include also a method to evaluate the human thermal comfort. The most considered papers in these studies are presented in Table 2. One of the most used standardized assessment model, is the well-known Fanger's model [11]. This model was used by Chien [93] – to evaluate thermal comfort in a vehicle cabin under effect of the air conditioned, in the summer time. Computational domain consisted in non-staggered grid system of 0.05 million points. STAR-CD software was used as heat transfer equation solver. The chosen turbulence model is k-ε. For this study only dashboard grills was used, with a total flow rate 430mc/h and the initial temperature in the passenger compartment was set to be 60°C, radiation was not considered and different heat fluxes was imputed on the cabins walls. The PMV

index was calculated at 60 s, 300 s, 600 s and 1200 s for head, chest, knee and foot. As results it was found different predicted thermal state for the body parts: 2 (warm) for head, chest and more than 3 (hot) for the foot region after 60 second. After 1200 s PMV index values were reduced with around 0.5, but a difference about 1 unit was found between upper part of the body (head and chest) comparing with the lower part of the body (knee and foot). This high PMV difference is due to low air velocity values in the foot and knee region.

Another study where are used standardized thermal comfort models is the one of Moon [137]. The author evaluated the effect of the solar radiation over the thermal comfort using PMV and equivalent temperature. FLUENT commercial solver and k- ϵ standard turbulence model were used. For the radiative heat transfer surface-to-surface model was used, calculation domain consisting in 3.51 million elements, with triangular shape on the surface and tetrahedral shape in volume region compose computational domain. As a boundary a discharge flow rate value of 0.12 m³/s for each air vent, for direct solar irradiation value of 875 W/m² and initial temperatures are 50 °C in passenger compartment and 30 °C outside temperature were imposed. The results of this study show differences between PMV and t_{eq} indexes in both with and without solar radiation. Then PMV predict a comfortable state (-0.49), while t_{eq} predict a cold but uncomfortable state (18.7) after 30 min of cooling without solar radiation and in the case of solar radiation consideration PMV grows with 0.5 while t_{eq} with 2°C. Also, in this study authors studied the effect of reduction of inlets flow rate with 20% and 40%, considering as initial the other conditions. Was found differences between these 2 indexes, at the low flow rate a most uncomfortable value was found in PMV case, while t_{eq} evaluate the thermal environment as comfortable. The authors do not explain the results. In our opinion these differences are due to the fact that PMV is a global index and is unadapted to this transient and non-uniform environment.

Ozeki [138] evaluated the effect spectral proprieties on glasses over the thermal comfort using t_{eq} index. Equivalent temperature values were determinate with a multi-nodal virtual thermal manikin. The authors didn't specify the simulation solver used. Calculation domain consists in 0.1 million elements. Imposed boundary condition are: direct solar radiation value 637 W/m², outside temperature 33°C, inlet air temperature 10°C and 350 m³/h inlets flow. The simulated cases are with solar radiation and without it; with infrared solar lamp and without it. Simulation results show different t_{eq} values for different body parts for all the cases. The passenger chest was exposed to direct solar radiation and t_{eq} value higher with 3°C which is considered by the authors to be a 1 rank difference in TSV. While with simulated radiation from infrared solar lamp chest t_{eq} difference was 4.2 °C which is considered by the authors to be a 1.4 rank difference in TSV. Solar

reduction glass can reduce the difference between the segmental maximum and minimum equivalent temperature in the whole body for both radiation sources, which leads to increased comfort of car occupants.

Another article Han's article [139] used a virtual manikin to evaluate effect of solar radiation, different air velocities, different relative humidities and different air temperatures over the EHT (Equivalent Homogenous Temperature) index. Fluent + VTCE codes were used to simulate and evaluate physical parameters behavior and thermal comfort. Initial conditions considered: direct solar radiation 750 W/m^2 , diffused solar intensity of 100 W/m^2 ; in cabin temperature 60°C and relative humidity 50%. Comparing EHT values, a high local thermal discomfort is showed at the chest and left arm level when the solar radiation was considered. Comparing the calculated PMV index with EHT a small difference was found between them, EHT index shows a comfortable state while PMV index slightly cool Slightly Cool thermal state. The authors specified that the effect of relative humidity in the cabin was less sensitive to PMV values comparing with EHT values. Although no information is given concerning inlet conditions of ventilation system, the authors report a large effect of air velocity on EHT in the regions of head, arm, and hand. Numerical model was validated with experimental data provided UC Berkeley segmented thermal manikin.

Considering that the standardized evaluation models are not adapted to this vehicle environment some of research work is focused in development in new assessment models. Turnow [140] used Fiala [56] model to investigate effect of three different vent modes (defrost, panel and foot mode) over the human body. Fiala solver has been dynamically coupled with numerical flow solvers in OpenFOAM, calculation domain consist in 12.1 cells and $k-\omega$ -SST in combination with wall function turbulence model was imposed. The outside temperature was set at 30°C , the introduced air temperature was 15°C , a heat flux of 50 W/m^2 was imposed on the thermal manikin surface. Regarding ventilation strategies, different inlet flow rate was imposed as follow: $0.0283 \text{ m}^3/\text{s}$ for defrost mode, $0.04 \text{ m}^3/\text{s}$ for panel mode and for foot mode $0.0283 \text{ m}^3/\text{s}$. From this numerical study, on the driver place was found the follow results: a slightly warm to warm sensation for defrost ventilation strategy because the flow is directed along the windshield and car top to the rear window of the car; slightly cool thermal sensation for panel ventilation strategy because jet flow from the outer panel-vent nozzles is directed on the driver's thorax, slightly warm thermal sensation for foot ventilation strategy because the flow streams are decelerated in the foot well and minor ventilation by forced convection near the top was observed.

Going further, a different arrangement of the discharge grill, also improves the ventilation system

efficiency and balance the temperature and velocity distribution over the passenger compartment leading to a better thermal comfort. Konstantinov [128] studied the effect of 4 air vents configuration on the thermal sensation of a FIALA-Manikin model, with the values provided by the manikin Zhang local comfort index (ZLC) and Zhang local sensation index (ZSI) [141, 142] was determinate. The computations have been performed by coupling flow simulations conducted with the Computational Fluid Dynamics (CFD) code OpenFOAM with simulations of the heat transport within the passengers using the finite-element code THESEUS-FE, calculation domain consist in a hybrid mesh counting 10 million cells. The $k-\omega$ /SST turbulence model was used to solve the heat and mass transfer equations. In the cabin are placed 4 persons, and inlet air temperature 13.6 °C overall inlet volume flux of 0.028 m³/s were imputed, ventilation strategy used are: conventional reference case (console type grills REF), trickle inlet ceiling (TI), cabin displacement ventilation (inlets under seats TI), hybrid case (combination of ceiling and under seats inlets HYB). The most balanced air velocity was found using combination case (HYB) in the same time with the lowest mean cabin temperature, because in this case was considerate 2 type of inlets, some installed in the ceiling and some under the seats. By comparing the thermal comfort of the passengers and the heat removal efficiency obtained for different car cabin ventilation cases it was found that all alternative ventilation scenarios lead to better comfort indices than the conventional REF case with more homogeneous air flow within the cabin.

Ahirrao [129] used the Berkeley model to evaluate different vents shape effect on the thermal comfort. FLUENT & RADTHERM software was used to simulate thermal transfer between outside and inside compartment and inside compartment and thermal manikin. The vehicular cabin is modeled in 10 million non-structured elements. The standard $k-\epsilon$ model with standard wall function was used for in cabin air flow simulation. At the beginning of cool down process, in cabin temperature was 45°C, manikin temperature 37°C and temperature 8°C and 7.8 m/s at the inlet was imposed. The outlet vent shapes were: square, circular, elliptical, circle side and square center. This study reveals that for same opening area circular shape of vents gives best performance in vehicle cabin cooling and thereby thermal comfort of manikin, these results are not explained by the authors.

A comparison between Fanger model and Berkeley model results is made by Alahmer [98]. RADTHERM solver package was used as heat transfer equation. In the article there was no mention about the turbulent model and mesh used. The initial virtual manikin temperature was 32.8°C. Both models show that in the winter season, a low value of relative humidity produce a more comfortable thermal sensation after 30 min. In the summer time, the higher value of RH,

results in more comfortable state according to the Berkeley after 30 min while for PMV/PPD the comfort state is achieved when the RH value is around 40%. From the literature it was put in evidence that people may express a comfortable opinion within an elastic interval of the relative humidity values (20% - 70%) as long as the operative temperature stays within the region which is called the comfort zone [11, 143].

Finally, the authors present a numerical model of a virtual manikin (MANIKIN 3) with 18 zones. The model was elaborated using CFX and STAR-CD environments. The National Renewable Energy Laboratory (NREL) proposes a package of tools allowing to predict human thermal sensation in non-uniform and transient thermal environment. They consist of a finite elements model of human thermo-physiological mechanism, a thermal manikin with 150 individual zones of skin and a so called “psychological model” that allows to predict the global thermal comfort in relation to the local thermal sensation. The thermal manikin is highly sophisticated, each segment comprises heating, temperature sensors and a system of simulating sweating [135]. It has high density of sensors with a fast response and a feedback control developed loop that allows to continuous adjustment of the transient thermal environment. A similar approach is presented in [136] by Rugh and Bharathan, who built a thermal manikin with 120 segments (individually controlled zone of the anatomic reproduction of the human body). The manikin was intended for non-homogeneous transient environments and was thus coupled with a nodal model. The model received as inputs the heat losses data from the manikin and then predicted the thermal sensation and the thermal comfort level. The coupling between thermal manikin and nodal models has been realized through the comparison with other models and seems to be good agreement with the human subjects studies excepted for the same body parts such as the head and the feet. , a package that consists of three main tools that allows to predict the human thermal comfort in non-uniform transient thermal environments. Mahmoud et al. [137] developed a three dimensional representation of two different manikins to study the influence of the different shapes on the flow patterns, the temperature distribution, the equivalent temperature, and the comfort assessment by using PMV and PPD thermal indices [137]. Other researchers proposed thermal manikins’ modeling using only virtual thermal manikins as the work by Curran et al. [138] They presented two scenarios: one using air temperature and the other using equivalent temperature for a homogenous space. Two virtual thermal manikins placed in a simulated aircraft cabin; with one used to determine the equivalent temperature and the other used to predict human thermal comfort [138].

Table 1 : Numerical studies of in cabin environment – first category

Reference	Vehicle	Comfort evaluation model	Solver	Simulation model	Pressure-velocity coupling	Buoyancy	Solar radiation model	Radiation	Process	Mesh (millions)	Boundary conditions
Zhang et al. 2009 [133, 134]	Volkswagen Passat 1.8L	Thermal environment assessment	FLUENT	k- ϵ standard + wall function	SIMPLE	Not available	Introduced in surface heat flux and is determined via Newton's law	Introduced through surface heat flux	Steady and transient cooldown	0.06 tetrahedral elements	Air velocity and temperature, Convective and radiative heat transfer between the compartment envelope and ambient
Jonsson 2007 [96]	Volvo S80	Thermal environment assessment	FLUENT	k- ϵ standard	PISO	Boussinesq	Solar ray tracing algorithm	S2S	Transient and steady cooldown	2.6 tetrahedral elements	Air velocity and temperature, 3 different thermal boundary conditions were used: CONVECTIVE, HEAT FLUX, COUPLED; Convective and radiative heat transfer between the compartment envelope and ambient
Kiliç et al. 2012 [126]	Fiat Albea 1.6l	Thermal environment assessment	STAR-CD	RNG κ - ϵ coupled with heat transfer equations	SIMPLE	Not available	Not applicable	S2S	Transient cooldown	0.9 triangular elements on the surface and tetrahedral in volume region	Air velocity, incompressible airflow; Convective heat transfer between the compartment envelope and ambient and human body. Convective heat transfer coefficient at outside of the cabin
Varad et al. 2012 [127]	Not available	Thermal environment assessment	FLUENT	Not available	Not available	Not available	Not considered	Not available	Not available	dynamic mesh, 12 elements, tetrahedral	Mass flowrates and convective thermal transfer
Kader et al. 2012	Samsung SM3	Thermal environment	Scryu Tetra	k- ϵ standard	Not available	Not available	Not considered	Governing equations	Transient cooling	0.65 elements,	Air velocity and temperature; incompressible fluid; Convective and

[144]			assessment	(SC/T)							tetrahedral	radiative heat transfer between the compartment envelope and ambient; radiation heat transfer is considered through the windshield and other glasses
Sevilgen et al. 2013	Fiat Albea	1.6l	Thermal environment assessment	Finite volume FLUENT	RNG k-ε	SIMPLE	Not available	Solar ray tracing algorithm	S2S	Transient cooling	0.9 triangular elements on the surface and tetrahedral in volume region	Air velocity and temperature, Convective and radiative heat transfer between the compartment envelope and ambient and human body.
[132]												

Table 2 Numerical studies of in cabin environment – second category

Reference	Vehicle	Comfort evaluation model	Solver	Simulation model	Pressure-velocity coupling	Buoyancy	Solar radiation model	Radiation	Process	Mesh (million)	Boundary conditions
Nilsson 2003 [145]	Not available	PMV/PP D and t_{eq}	CFX software	RNG k- ϵ	Not available	Not available	Not specified	Not available	Cooldown	tetrahedron elements	Adiabatic ceiling, wall and floor conditions were assumed. The discretization method used is based on the Finite Volume approach, heat flow on the manikin surface was imposed
Nilsson et al. 2007 [69]	Not available	PMV/PP D and t_{eq}	STAR-CD	Not available	Not available	Not available	Not available	Not available	Cooldown	Not available	This zero-equation model uses a constant to express the turbulent viscosity; This does not require the solution of any additional differential equations beyond the Navier–Stokes equations
Myoung et al. 2014 [146]	Generic car cabin	PMV/PP D	FLUENT	k- ϵ standard	SIMPLE	Not available	Not available	S2S	Transient and steady cooldown	1.6 elements, geometry not available	Air flow rate and temperature, vehicle speed, Convective and radiative heat transfer between the compartment envelope and ambient. Windows transmissivity
Moon et al. 2016 [137]	A typical medium-sized passenger car	PMV/PP D and t_{eq}	FLUENT	k- ϵ standard	Not available	Governing equations	spectral radiation discrete ordinates model (SDOM)	S2S	Transient cooldown	3.51 triangular elements, on the surface and tetrahedral in volume region	Air velocity, atmospheric pressure and temperature at AC outlets; conduction, convection, and radiation heat transfer; transmittance and reflectance
Neacsu et al. 2016 [147]	Not available	PMV/PP D; DTS	FLUENT & THESEU	Not available	Not available	Not available	Not available	Not available	Transient cooldown	Not available	Air velocity and temperature, Convective and radiative heat transfer between the compartment envelope and ambient and human

J. Passive control strategies for mixing ventilation and possible application to vehicles

The main purpose of ventilation systems is to satisfy the need for thermal comfort and air quality for the occupants along with reduced energy consumption. These three criteria must be considered in the design of a mixing ventilation system as they are fundamental to the thermal environment and energy performance. A high induction level is desired in these systems because it allows an optimal mixing of the ventilating jet with the ambient air such as the occupants would be satisfied in terms of thermal comfort and air quality. Following an innovative idea developed at the French University of La Rochelle, in the LaSIE laboratory, and pursued at Technical University of Civil Engineering of Bucharest, and at the University of Rennes, the one of introducing lobed geometries passive control for improving air diffusion in buildings and vehicles, several studies regarding different configurations were conducted [9, 148-163]. Under low or moderate Reynolds numbers, such as the particular HVAC conditions, the analysis of the elementary lobed jets showed that the lobed shape introduces a transverse shear in the lobe troughs, leading to a breakdown of the Kelvin-Helmholtz structures into “ring segments” [158-160, 163]. Streamwise structures continuously develop in the lobe troughs, at the resulting discontinuity regions, and control the lobed jet self-induction [158]. The inclination angle of the lobes in the case of the nozzle [152], increases the shear and organizes the vorticity into some particular large scale structures. These large scale structures appear to be perfectly correlated to the transverse shear. This way an intensification of the mixing is associated to the conservation of the induction benefit in the far field of the lobed jet (Figure 9). An innovative concept for optimized air diffusion in buildings which is using what is called a passive method of induction and which consists in the introducing of air jet through lobed grille diffusers was also proposed and developed at the UTCB [10]. It was shown that the jet flows issued from innovative air diffusers in the form of rectangular grilles with lobed ailerons are characterized by higher mixing. The study was performed at the scale of a room. Lobed ailerons jets were compared to reference jets from classical rectangular air diffusion grilles with straight ailerons [161]. Other studies concerning perforated panels with lobed orifices shown that such devices inducts twice more ambient air in average than the circular perforated panels when the orifices spacing is $S= 2.7De$ (De is the equivalent diameter based on the exit area of the elementary orifice) [157, 158].

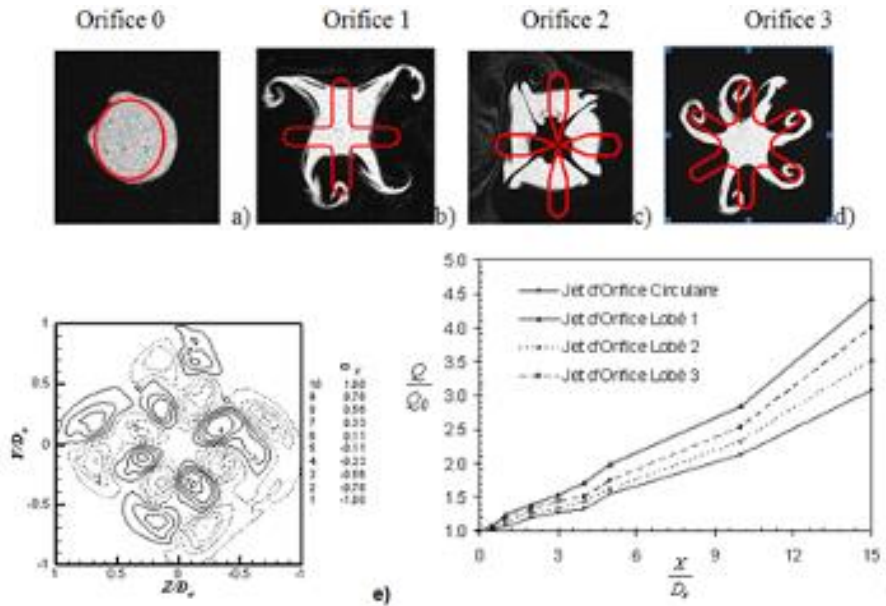


Figure 9: a – d) Different shapes of lobed orifices used for passive control, e) streamwise vorticity field in the near exit region of the orifice 2, f) axial volumetric flow rates evolution of the corresponding jet flows [9]

In the studies of Nastase et al [161, 164] are presented detailed analyses of the phenomena governing the induction mechanism in air diffusers with lobed ailerons. We will present a synthesis in this paragraph since these studies inspired us to develop innovative diffusers for automotive application. In their investigations, the authors wanted to apply the previous findings for the lobed forced mixers and for the lobed jet flows in order to improve geometry of ailerons of the existent commercial grilles used for air diffusion in buildings. They analyzed flows from two air diffusers, one with straight ailerons and the other one with lobed ailerons. The two studied diffusers considered are respectively a commercial one, with straight ailerons (Figure 10a) and a prototype of a new innovative grille, having lobed or lobed ailerons (Figure 10c). Vortex dynamics in the near region of the exit of the flows, was visualized for two elementary slits, one with straight ailerons (Figure 10b) and another with lobed ailerons (Figure 10c). All the studied diffusers (grilles and slits) were made through rapid prototyping.

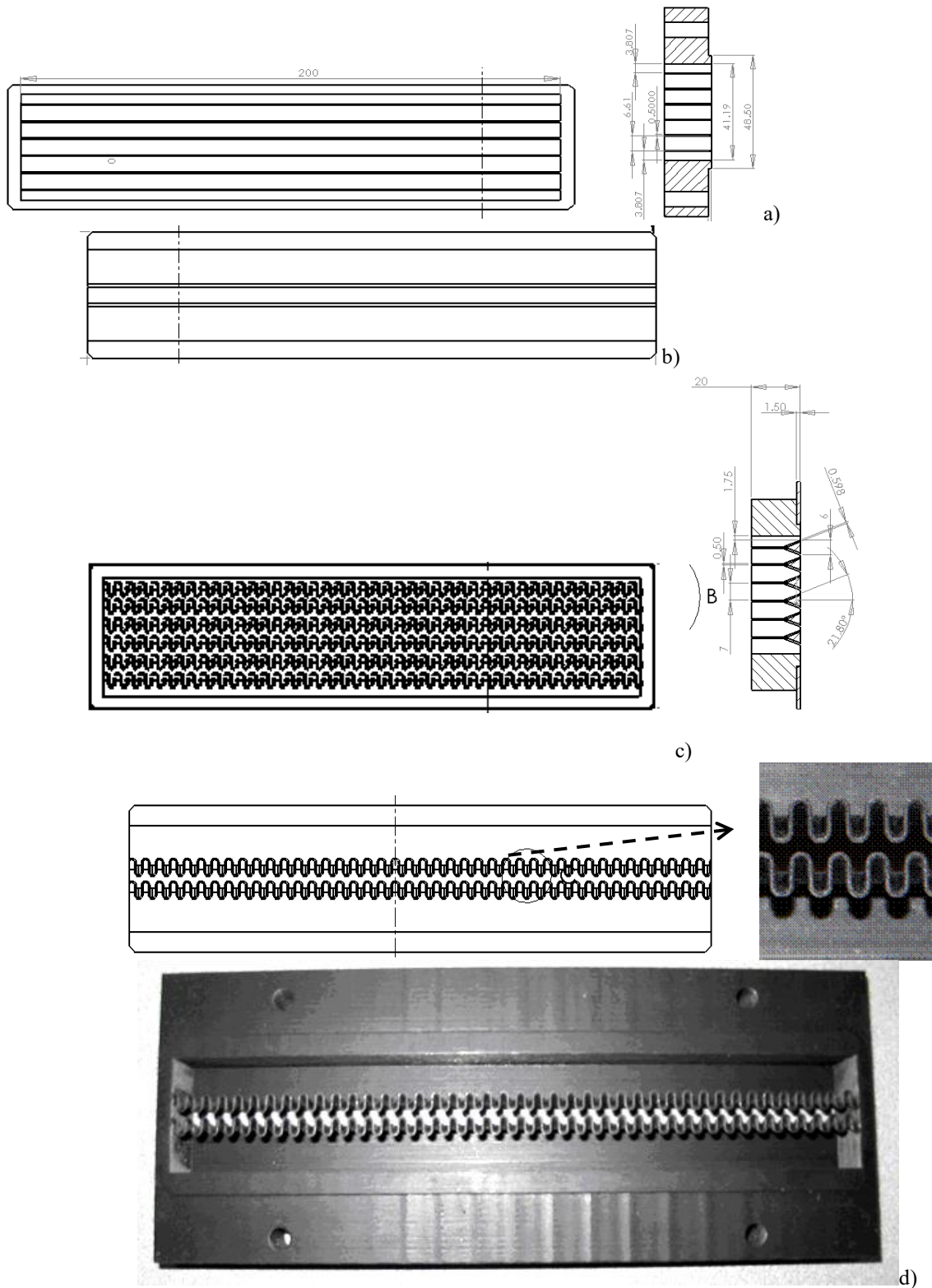


Figure 10: Air diffusers and slits from [161, 164]: a) straight ailerons grille, b) straight ailerons slit, c) lobed ailerons grille, d) lobed ailerons slit

Authors showed that the lobed air diffusers are performing better in terms of mixing and induction as displayed in Figure 11a where are represented the streamwise evolution of the

volumetric flow rates for the two studied diffusers. These flow rates were obtained from the integration of the streamwise velocity profiles obtained in the median plane of the flows by the width of the grilles. As in the case of the throw of the lobed perforated panel flow from a previous study [157] the lobed grille jet throw is not reduced despite it's higher induction. The results presented in Figure 11 provide valuable information, giving an indication on the entrainment and the throw improvement by the lobed grille.

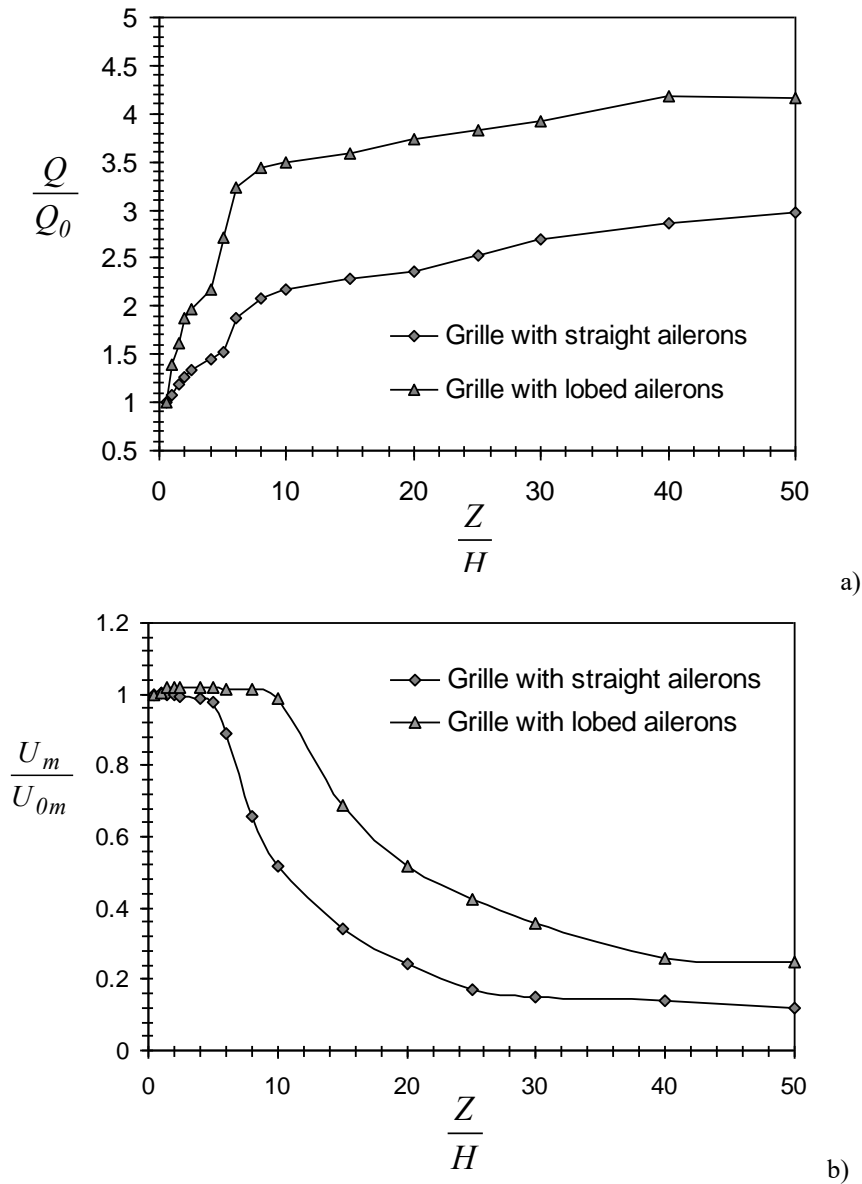


Figure 11: a) Axial evaluation of the normalized volumetric flow rates, b) Decays of the maximum velocities along the axis [161, 164]

In order to understand the phenomena which are governing this important capability of mixing and entrainment, the authors performed high speed visualizations of the transverse planes, in the near region of the two flows generated by one elementary straight slit and one

elementary lobed slit. This choice was made due to the image quality problems induced by the seeding of the mixing flows several parallel jets. In Figure 12 are presented images of the two elementary flows at different axial distance from $X=0.3h$ to $X=3.5h$.

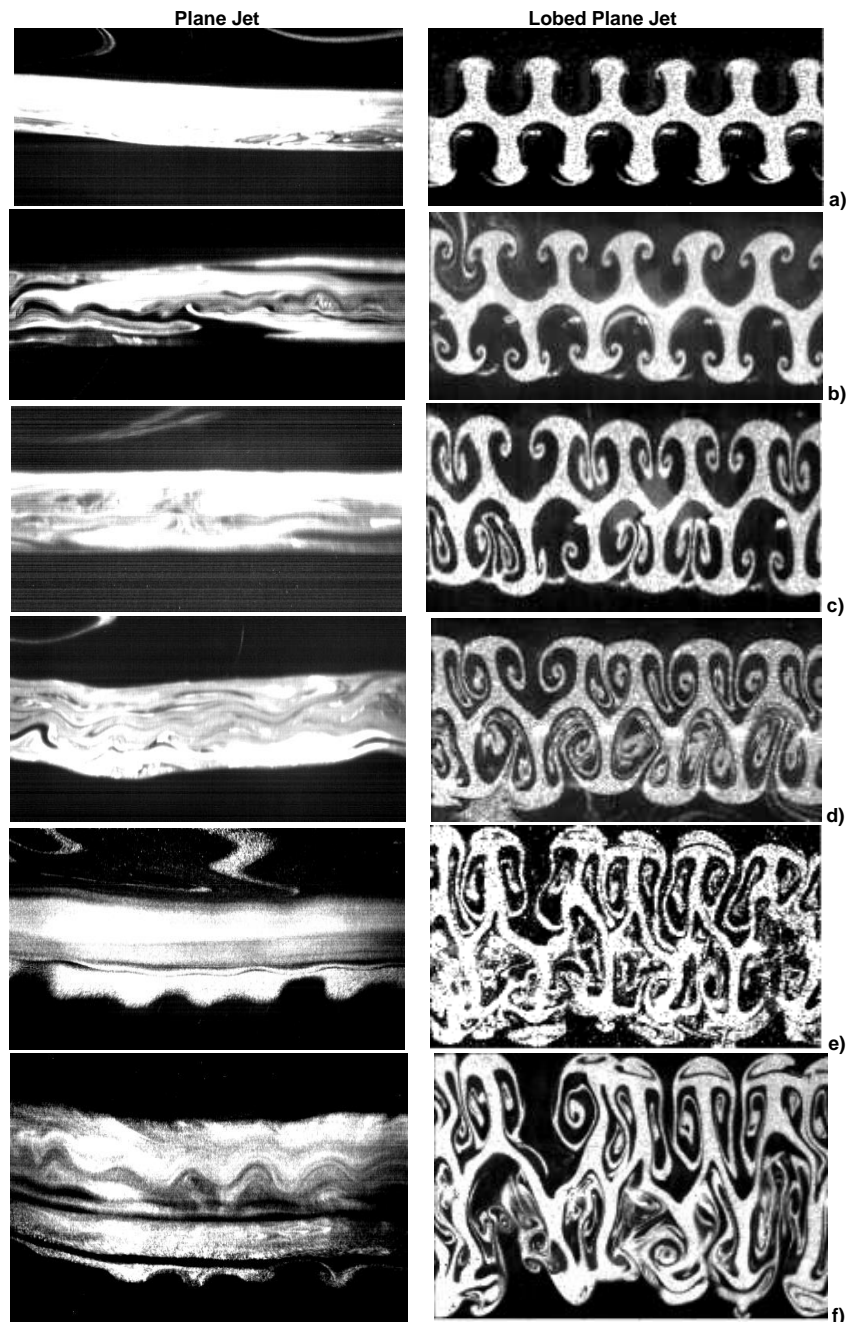


Figure 12: Visualizations in the transversal planes of flows produced by used the elementary slits: a) $X/h=0,3$; b) $X/h=0,6$; c) $X/h=1,2$; d) $X/h=1,5$; e) $X/h=3,0$; f) $X/h=6,0$ [161, 164]

As expected, and in a similar manner to the lobed jet flows investigated in previous studies [9, 151, 158, 165], the lobed slit flow is characterized by the appearance of organized large scale streamwise instabilities that are transforming in vortical structures. The small instabilities that

are observable in the proximity of the initial plane, close to the diffuser, plane grow in intensity and turn themselves into large scale streamwise vortices further downstream. As for the flow generated by the slit with straight ailerons, only small secondary structures appear much later than in the lobed flow and they do not display any particular coherence being located randomly (Figure 12). For the slit having lobed ailerons, no primary-like structures (i.e. Kelvin-Helmholtz vortical structures) were visible. In the case of the jet from the plane slit, the horizontal marks that are observable in Figure 12 g and h may represent such primary structures. In the light of the previous studies [158] this might be an explanation for the observed entrainment performance of the lobed grille, knowing that the presence of Kelvin-Helmholtz vortices does not favor mixing and entrainment.

During all the studies of research teams of Professors Meslem and Nastase, the quest for high performance geometries the practical issue of esthetical concerns arisen [10, 155, 157, 160, 166-169]. Architectural considerations revealed that the lobed orifice geometry is preferred to the nozzle geometry giving the possibility of easily replacing the circular or linear shape in perforated grilles or panels. In the same time orifices are interesting only if their dimensions stay relatively reduced, so the perforated panels are the only possibility of integrating them which is limiting their applications. A good compromise for our vehicular application is represented by the previous lobed ailerons and this kind of air diffusers are presented later in the third Chapter.

K. Discussions and conclusions of the first chapter

Modeling the comfort response itself is the final goal when using heat balance models. Indeed, all of the rational models make the inherent assumption that there is some predictable comfort response for a given physiological state of the body. Still, it is not clear if there is such a relationship and how it could be expressed in a universal, applicable way. The state of comfort is inherently a psychological response, not a physiological response and we should expect many nonphysical factors to affect comfort perceptions (e.g. expectations). *We observe at this point that no consensus and no unity between the existent theories and models as how comfort should be connected to the psychological variables or even which are the variables.* It is still unknown whether there are some neuro-physiological responses corresponding to the possible influence factors (e.g. stimulus mode and ambient temperature) during the local thermal stimulation.

Although the adaptive thermal comfort concept has been discussed only for buildings, in our opinion a viable direction for taking into account the psychological component in the case of the thermal state assessment in vehicles and would be to orient some studies towards this

direction. In the adaptive thermal comfort approach, there are not such parameters as *set point* as the comfort level of the occupants is acknowledge to be elastic and adaptive at the expectations of the occupants themselves, which was expressed in the following manner: “*changing the conditions to accord with comfort and changing comfort temperature to accord with the prevailing conditions*” [170]. In the case of the buildings, the adaptive comfort approach display the advantage of widening the range of acceptable comfort temperature, makeing it possible to obtain more energy savings in buildings designed using this approach than those design using Fanger’s approach. However, in the long term, various authors classified this approach to be unsustainable. Some results from adopting the adaptive approach to the design of a number of buildings have shown that some green buildings are quite uncomfortable [171]. In fact, Nicol and Humphreys [170] have warned that “*a low energy standard which increases discomfort may be no more sustainable than one which encourages energy use*” because of the adaptive principle that “*occupants may well use energy to alleviate their discomfort*”.

The subjectivity in the interpretations of the personal thermal experience from a very complex interaction between the occupants and their environment has been the focus of a great deal of study and provides the theoretical foundation to the adaptive approach for thermal comfort [53]. As shown by Nicol and Humphreys [172], „*the adaptive method, unlike the heat-exchange method, does not require knowledge of the clothing insulation and the metabolic rate in order to establish the temperature required for thermal comfort. Rather it is a behavioral approach, and rests on the observation that people in daily life are not passive in relation to their environment, but tend to make themselves comfortable, given time and opportunity. They do this by making adjustments (adaptations) to their clothing, activity and posture, as well as to their thermal environment.*” The fundamental principle of adaptive thermal comfort is that: “*If a change that occurs induces discomfort, the occupants’ body reacts to restore comfort.*” [172].

The thermal temperature is a result of the interaction between occupants and the building. Either the occupants have to adapt to the environment either to adapt the environment to meet their needs, so they feel less discomfort.

In this equation, there are three varying and unsteady variables that are interacting together: the climate, the vehicle and the time. The internal loads in the cabin are much more added depending on the climate conditions than in the case of a building. The second variable is the cabin itself, especially the features and the level of ergonomics that it offers to its users. The third variable is the time scale at which the human activity in this case is measured and which is much inconstant from a short trajectory ride to a long trip.

Even if in this study we didn't have the time to extend our researches to the adaptive approach, our belief is that a future perspective of study in the field of thermal comfort studies dedicated to vehicles is to combine the quest for a new comfort equation adapted to these enclosures, taking into account the rapid climate changes and physical and psychological adaptation of the human occupants. This is crucial in our opinion given that all presented evaluation methods based on environmental physical parameter measurement cannot capture the inherent mental capabilities of humans.

Nevertheless, *the importance of the thermal manikins and of the concept of equivalent temperature cannot be denied*. However the afore presented standardized methods are either difficult to interpret, either impossible to apply, either expensive to realize. There are few articles in the literature using standardized methods for evaluating thermal comfort and even less combining air distribution strategies with thermal comfort.

On the other hand, there are many papers dealing with the observation of the environmental conditions inside the vehicle that might affect the human thermal comfort and those concerning the human's response and perception of its interaction with the environment. Part of them stop only on the study of the effect of a certain parameter (the air temperature and the mean radiant, the relative humidity, the solar radiation including the effect of the glass transmittance, the outdoor temperature, etc.) on the thermal environment of the vehicle without considering any thermal comfort assessment using comfort models. Different protocols are used to measure these different equivalent temperatures, therefore a set of individual sensors dedicated to all the intervenient variables, e. g. thermal comfort meters with heated sensor, local discomfort meters, plane surface sensors and thermal mannequins. The latter are considered as the reference with which other methods are compared. Significant differences were found in the values of equivalent temperatures arising from different methods in tests performed in uniform environments inside a climatic chamber, which are attributed to different characteristics of the measuring devices, such as size, geometry, posture, number and type of sensors, control method, etc. The scientific research reality, shows nowadays, only rare solitary set-ups to assess the thermal comfort in vehicles using the equivalent temperatures experimentally. These are either very expensive or suitable for punctual measurements only. However, data acquisition at different locations in the interior space of a vehicle is highly desired, generating the need for cost-effective and accurate measurement equipment that are intended local equivalent temperature measurement in the case where large thermal gradients occur in the presence of the ventilation systems are considered, and that are also used to simulate the heat release by real

passengers as well. *This is the motivation of developing thermal manikins in our research group and as a consequence of the most important objectives of the thesis consist of the development of the thermal manikin (presented in the following chapter).*

No studies combining passive induction control via the conception of air diffusers were found in the literature. The proposal of some innovative designs of air vents for the present studies was based on the previous findings of the French and Romanian research teams where the doctoral project was developed. The following parts of the manuscript are dealing with the development of an innovative thermal manikin and of new concepts of air diffusers. The approach is based upon both an experimental and a numerical approach.

CHAPTER 2 – BUILDING AND ADVANCED THERMAL MANIKIN

A. Short history of thermal manikins

A thermal manikin is a human model tool designed for testing thermal environments without inherent known inconveniences for human subjects [173-175]. The main use of thermal manikins can be encountered in the automotive industry [69, 176, 177], indoor environment [74, 178, 179], outdoor environment [180, 181], military [182] and textile research [183]. Thermal manikins have a long history, being used for more than 70 years. At the beginning they were used for testing clothes for soldiers at the US Army [182]. The shape and heating system were very simple at that stage. Nowadays, due to technological and material advance, the shape and complexity of the thermal manikins increased and is approaching the complexity of the human body. The number of independently controlled zones has increased from a single zone corresponding to the entire surface up to 120 individually controlled zones [184]. The materials used for developing thermal manikins have diversified, from copper to advanced composite plastic and carbon fiber to skin like silicone [185]. Most of them are conceived to simulate the human body and the associated dry heat exchange with environment. Others are more or less complex measurement devices for assessing thermal environment quality by simulating the human body thermal regulatory mechanisms and measuring its heat loss towards its environment [182]. The most advanced of them can also simulate body sweating and heat exchange through evaporation [37, 182, 184, 186].

During the time, various materials were employed in the manufacturing and developing of thermal manikins. This evolution arrived to the use of plastic or aluminum in order to ensure users safety. Because a stand-alone thermal manikin is constrained to limited experimental situations, there were made models with articulations that allowed the exploitation of various positions of the human body was also proposed. The mobile articulations have led to flexible thermal manikins, being able to simulate the human body in motion. Most of these models were intended and being used to test clothing thermal characteristics in the textile industry.

Thermal mannequins began to be increasingly widely used, they are constantly improving, reaching to act as "human", integrated with a system of breathing or even perspiration on the skin.

Manikins used in advanced thermal comfort studies are expensive and delicate instruments as well, but also have many advantages, such as accurate simulation of human body, measurements of the heat transfer, methods for measuring the thermal resistance of clothing,

fast, repeatable and accurate response etc. An efficient thermal manikin can measure the heat transfer through convection, radiation and conduction all over the surface, whether it receives or releases heat. Depending on the number of measurement zones (called also segments), the spatial resolution of the thermal manikin may increase. Some of the newest models are foreseen with more than 100 individual segments. A thermal manikin may be the subject to long-term tests, repeatable, under extreme or even dangerous conditions for a real human, in an environment that could subjectively distort the results. Manikins can have any distribution of temperature on the skin surface or could be controlled for a fixed the heat release (nature and intensity). They can be used in different environments and the results thus can be interpreted in terms of thermal comfort or in thermal stress. They can use for the assessment of IEQ of the air systems, of the clothing resistance and also of the air quality if a respiration circuit is coupled. This could lead also to new ways of study of IAQ in different environments [187, 188].

A thermal manikin called „Walter” [189] was improved with a heating circuit and sweating circuit, using textile moisture with the help of specially designed pumps allowing to control the heat released through evaporation. Thermal Observation Manikin, or TOM [177], was designed to measure heat fluxes from the in terms of exposure to heat sources in the vehicular ambient. Some of these manikins incorporate a thermo-physiological model that is coupled to the thermal or heat flux sensors and electrical power sources controller. This in allowing to obtain a direct response in the form of thermal vote. In the automotive field, the increasing interest regarding the climate comfort evaluation has led to new developments of manikins [176] ADAM (ADvanced Automotive Manikin) is a manikin having 126 independent segments manufactured from a composite material. All the segments can be independently controlled in temperature distribution, sweating simulation and released heat fluxes. The manikin has also a breathing circuit and it can be controlled wireless or via data transmission cables.

Concerning the shape of the manikin, Topp et al. [190, 191] show that in a room, the air flow and temperature distribution are influenced by the geometric shape of the manikin. It is recommended a more detailed study when near occupants. Over the past decade, there has been a growing interest in developing new measurement methodologies for existing devices [176, 183, 185, 192] to simulate adequately human thermal behavior. Various attempts have been undertaken to mimic the human thermal response more realistically. For example, constant heating power resulting in uniform heat flux allows simulation of different workloads and metabolic heat production [193]. Models using non-uniform surface temperatures over the body, such as cooler hands and feet [194] allowing imitation of local vasomotor responses, and

uniform surface temperature dynamically changing dependent on the heat loss over time (so-called comfort mode) are used for the simulation of transient response in the narrow range of close-to-comfortable conditions [195].

Table 1: Thermal manikins' history after [196]

<i>Name</i>	<i>Components</i>	<i>Material</i>	<i>Posture</i>	<i>Country/year</i>
SAM	1 segment	copper	Upright	USA 1942
ALMAKIN	11 segments	aluminum	Upright	Great Britain 1964
CEPAT400	1 segment	aluminum	Upright	France 1972
HENRIK2	16 segments	plastic	Upright /Seated	Denmark 1973
CHARLIE	16 segments	plastic	Upright /Seated	Germany 1978
SIBMAN	16 segments	plastic	Upright /Seated	Sweden 1980
VOLTMAN	19 segments	plastic	Upright /Seated	Sweden 1982
ASSMAN	36 segments	plastic	Upright /Seated	Sweden 1983
TORE	19 segments	plastic	Upright /Seated	Sweden 1984
CLOUSSEAU	7 segments	plastic	Upright /Seated	Sweden 1987
COPELIUS	Sweating manikin	plastic	Upright /Seated	Finland 1988
NILLE	Female manikin	plastic	Upright /Seated	Denmark 1989
HEATMAN	36 segments	plastic	Upright /Seated	Sweden 1991
WALTER	Sweating manikin	textile	Upright /Seated	Hong Kong 1991
HEATMAN	36 segments	plastic	Upright /Seated	France 1995
NILLE	Breathing manikin	plastic	Upright /Seated	Denmark 1996

As discussed previously, in the last decade the thermal comfort component in the automotive industry gained more interest from the car manufacturers. The thermal conditions encountered in vehicle cabins are mostly transient and non-uniform, which results in dynamic changes of passengers' physiological response and of their thermal comfort assessment. The heat exchange between the human body and its surroundings results from direct contact with internal surfaces of the vehicle, such as seat, steering wheel, from radiation with other surrounding surfaces and from the air distribution system. In hot conditions, the heat gains from solar radiation need to be counterbalanced by a cold flow of air, which might also be incorporated into the seats. In cold conditions, warm air is supplied to the compartment and some additional thermal load might be delivered by heated seats [35, 197, 198] and elements of the cockpit e.g. heated wheel [199]. Therefore, the temperature difference between various elements inside the vehicle, the airflow and surrounding surfaces is often important, leading to highly heterogeneous and dynamically changing conditions overtime. On the other hand, the clothing of the occupants is usually dependent on the diurnal and seasonal changes of the outdoor conditions and the user might change it during the trip.

The thermal resistance and the moisture permeability of the clothes play an important part in the perception of the thermal environment, acting in the same time as a barrier for both the heat loss from the human body and for the undesired draught effect of the air conditioning systems. Finally, the automotive industry aims development of energy efficient air conditioning systems, especially focusing on the vehicles powered by electric batteries [200, 201]. This approach demands smart, effective and localized solutions for thermal comfort in the compartment at the lowest possible energy expenditure.

To determine the effect of such temporally and spatially heterogeneous conditions on the human thermal perception, often, human subject tests are performed [79, 202-204]. Since the vast majority of tests takes place in actual driving and weather conditions outdoors, it is difficult to ensure identical exposure parameters for all human subjects, which in practice is translated by a single person non-quantitative but qualitative outcome. In a majority of cases, the complete information about the thermal state of the human body is not recorded (only few locations of the skin temperature measurement and discrete number of thermal perception questionnaires during highly transient exposure [79, 205]). On the other hand, the use of thermal manikins allows the integral analysis of skin temperature on all body segments (limited by the number of manikin body segments) but does not provide other important physiological parameters, i.e. core temperature, sweat rates or thermal perception ratings. The use of adaptive manikins in

automotive industry is, therefore, a valuable opportunity to obtain a complete assessment of the physiological response of the human body evaluating an average-person continuous response in one-time exposure for both the thermo-physiological and perception response. Both physiological and thermal comfort models need to be more reliable in transient and non-uniform scenarios, as these are frequently occurring in vehicles compartments [36, 41].

The first adaptive manikin developed for vehicular studies was the Advanced Automotive Manikin [63–65]. This adaptive manikin has been tested both in steady-state and transient conditions, as well as in a study of ventilated car seat [66]. The measurements performed with a ventilated seat showed potential of a 7% power reduction for air conditioning purposes in hot conditions [206]. Another adaptive manikin consisting of a Newton manikin coupled the Manikin PC2 has been also applied in a car study [207]. The results from the adaptive manikin showed good agreement with human subject data concerning skin temperature. In addition, the trends in thermal sensation and comfort were well reproduced.

Relationship between the heat loss from the manikin and the thermal sensation of human subjects exposed to the same conditions, the equivalent temperature method has been widely used for the evaluation of moderate environmental conditions [195, 208]. Thermal manikins have proved to be powerful tools to assess the indoor environmental quality [29,30], the spread of airborne particles [31–33] and also to calculate the human environment heat transfer coefficients used in numerical simulations of indoor spaces [209]. Modern thermal manikins have provided opportunities to study the simulation of breathing or walking [31, 210] which are both influencing the air flow parameters in indoor spaces.

Given the advantages of thermal manikins develop an advanced thermal manikin to be used as a tool to evaluate the vehicle environment. This manikin, familiarly called Suzi, is one among the five prototypes of thermal manikins conceived at the Building Services Engineering Faculty (CAMBI Research Center) at the Technical University of Civil Engineering of Bucharest and manufactured with the help of the National Institute of Aerospace Research Elie Carafoli. This prototype has complex anatomic shape, with 79 independent active zones, 395 temperature sensors and its own in-house software for data acquisition and control of the body zone's surface temperature. In this chapter we are presented all the stages that have been put in practice during the development of our advanced thermal manikin prototype with neuro-fuzzy control. The construction of all the parts of the manikin and the validation strategy are also presented.

B. Development of our thermal manikin

The thermal manikin was designed for both seated and standing postures. The size of the manikin is defined by the standard skin surface of a human of 1.8m² [178, 196]. The base structure of the manikin is made of polyvinyl and uses a medical manikin with the typical weight of a female human body. The surface of the manikin has been covered with a 5mm insulation layer (Figure 13b and c).



Figure 13: Different stages of making the hardware part of the thermal manikin: a) designing patrons for the heating element disposal, b) and c) designing the heating insulation under the thermal patches, d) inserting the heating elements, e) developing the electrical circuits

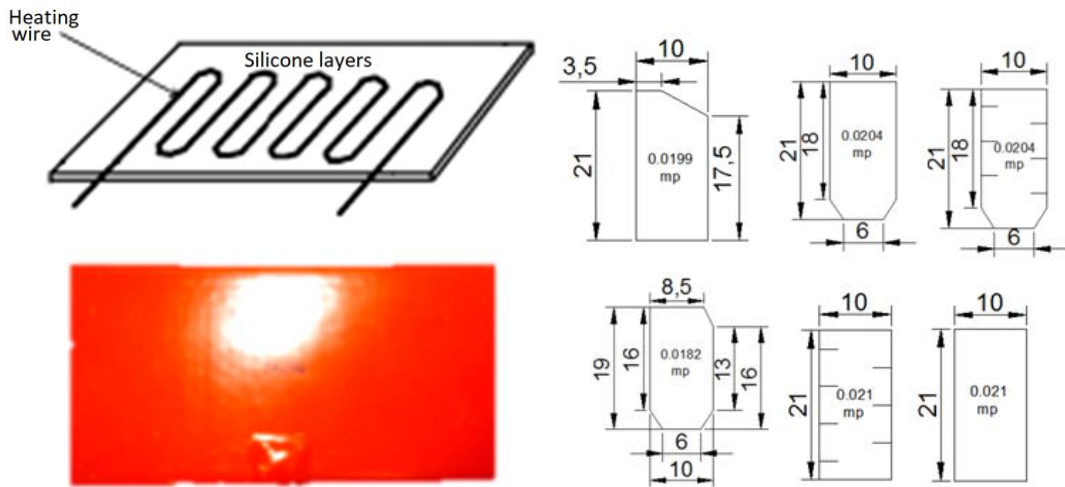


Figure 14:a) finished thermal manikin in lying position, b) testing the upper and the bottom body parts

A medical manikin made of polyvinyl is used as a support, on which surface was glued a thermal-insulation elastomeric membrane (Figure 14). The function of this 5mm insulation membrane is to prevent the heat transfer to the manikin interior.

The heating system chosen for this prototype consist, in four geometries elementary flexible patches (Figure 15), manufactured by the Keenovo Company. These are made of a thin layer of silicone (1,5 mm) that includes a heating circuit made of nickel chrome heating wire (Figure 15a.) having good electrical isolator proprieties and in the same time is a good thermal conductor. Geometries of the used heating silicone are presented in Figure 15b. Several solutions of were tested but the heating silicone patches were found to provide the best uniformity of the temperature distribution. In Figure 17 are compared the surface temperature distributions of a silicone patch with one of the human skin on the hand of a human subject. It can be observed

that the temperature distributions of the manikin arm are reasonably similar as the human arm.



a) Heating element embedded in silicon b).Different geometries of the heating elements

Figure 15: Base heating elements geometry

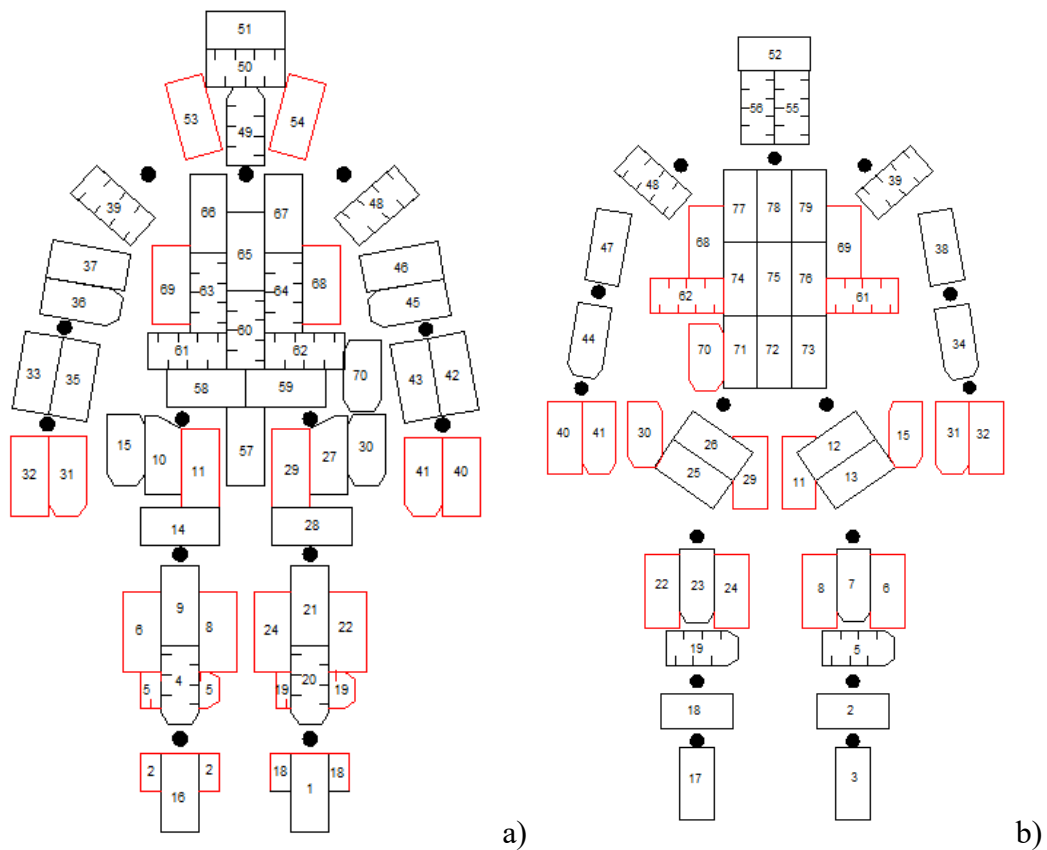


Figure 16: Distribution of the heating elements on the individually anatomic zones controlled (red patches are corresponding to the other side of the manikin): a) front view, b) back view

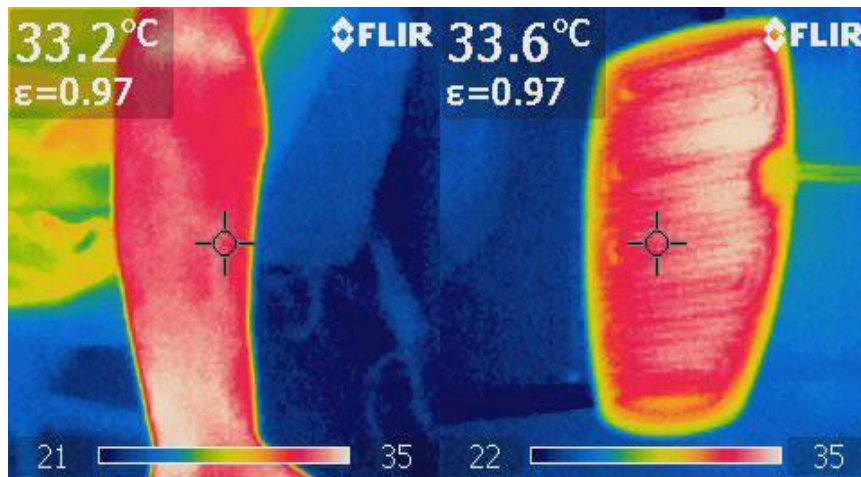


Figure 17: Comparison between the temperature distribution of a heating element and the skin of a person[211]

The heaters elements are flexible following the anatomic shape of the body. The heating film patches were placed on the insulation layer on the polyvinyl base using adhesive duct tape. Every heating patch position was selected to cover as much as possible from the entire dummy surface, without overlapping them. The heating elements distribution is presented in Figure 16 on the front and back of the manikin. After covering a body zone, the electrical connections and the circuits were created. Each electrical connection was tested for safety reasons. The electrical wires were embedded inside the manikin and there were fitted inside the manikin to ensure that the thermal load of the film mounted over the wires will not influence the cables stability. Each patch was carefully characterized using the thermostatic bath to determine the function of the electric circuit resistance variation with the temperature in order to implement necessary correction in the control algorithm.

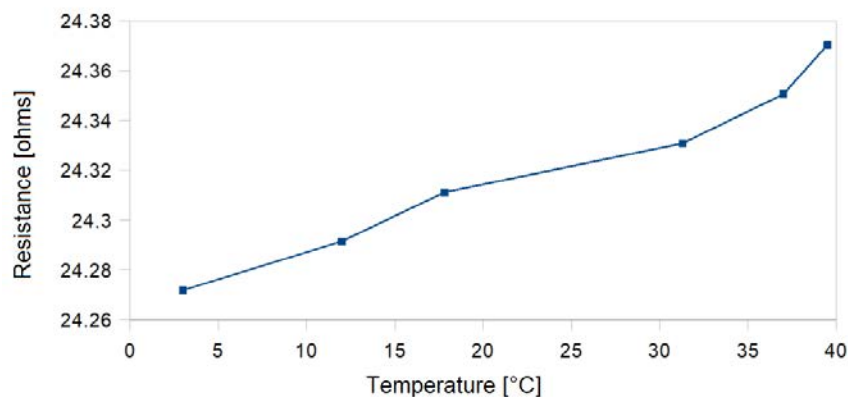


Figure 18: Variation of the electrical circuit of an elementary patch (type 1) with the global temperature of the patch (thermostatic bath essays)

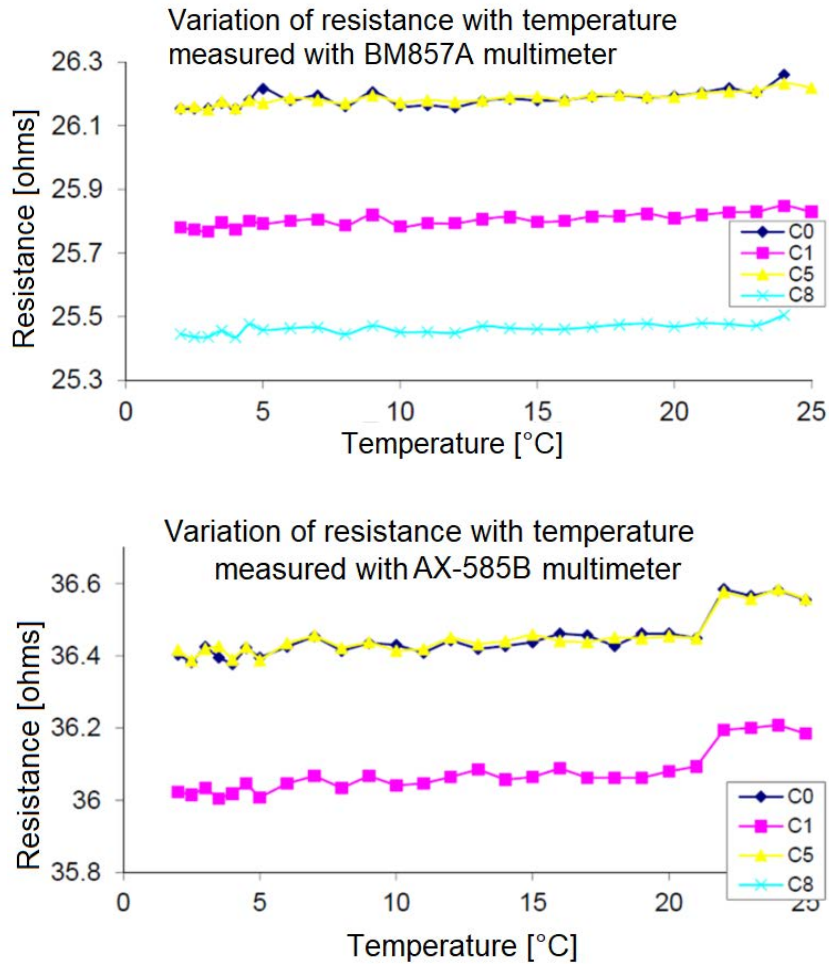


Figure 19: Variation of the electrical circuit of several connected patches with the global temperature of the patch (thermostatic bath essays)

Five digital temperature sensors are glued on each heating element to control the temperature. The sensors are TSic T501 model and there were manufactured by IST. The heat-conducting paste was applied to the temperature sensors to improve the contact and the heat transfer.



Figure 20: Photographs of Tsic T501 temperature sensors as disposed on the patches

Given the constructive form of the heating elements (put in evidence using an IR camera in Figure 21), a risk of wrong temperature measurement could appear if the temperature sensor is not in a proper place. Therefore, each sensor position has been established using a thermal vision

camera Flir E40. The mean temperature value of the five sensors and of the patch is the same. The thermographs of heating elements and some sensors positions are shown on the images below.

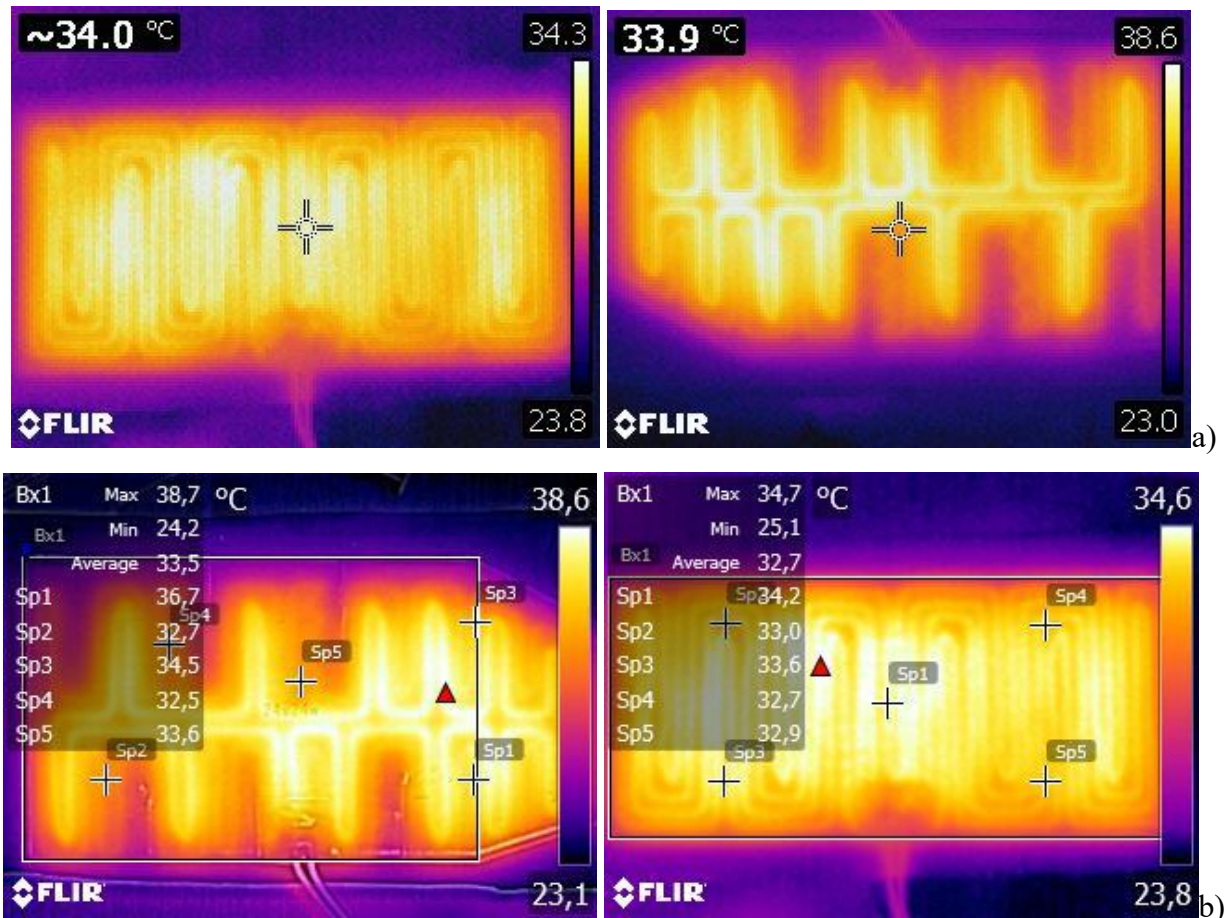


Figure 21: a) thermographs of heating elements; b) thermal sensors position (+)



Figure 22: a) TSic T501 sensors used for the measurement and control part of the thermal manikin, b) thermostatic water bath Lauda Eco with immersion thermostat Lauda Eco Silver – The photographs are from the archive of our team during the numerous campaigns of calibrations of the TSic sensors that were also used at another prototype from [215]

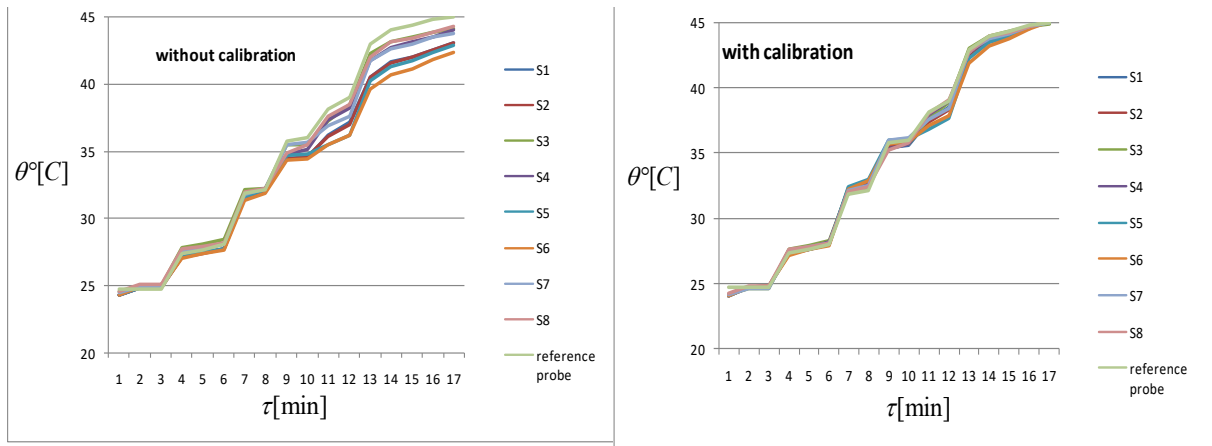


Figure 23: Response at thermal solicitations over time of TSic TO92 sensors: a) without calibration, b) with calibration

Every sensor was carefully tested. The calibration process has been conducted using a thermostatic water bath with immersion thermostat Lauda Eco Silver (Figure 22). The response at thermal solicitations over time for eight of these sensors calibrated and non-calibrated is shown on Figure 22. Because a non-uniform temperature of the manikin surface had to be avoided [212], the entire manikin surface was covered with adhesive aluminum foil to ensure a better temperature uniformity through conduction heat transfer (Figure 14). The entire manikin surface was covered with a transparent adhesive film to facilitate further investigations with a thermal (IR) camera. We have also performed tests concerning the distribution of the surface temperature of every manikin zone in order to validate the heating part of the manikin prototype.

As mentioned before, the thermal manikin has a female anatomical shape. The surface of the manikin is divided in 79 zones as presented in Figure 16. For each zone the temperature can be measured and separately controlled. The red zones are lateral zones while the black points represent joints points (figure 16).

The electrical connections and circuits were created after the body surface had been covered. Every electrical connection has been tested for the safety reasons. The electrical wires were embedded inside the manikin. We have selected special electrical wires that works at temperatures above 7°C to ensure that the thermal load of the film mounted over the wires does not influence the cable stability. During a first test, without any control of the circuits, the temperature of each zone has been stabilized at 45°C while the room temperature was stable at 24°C. This is a rather an encouraging result offering a wide range to control the temperature of each zone and the possibility to simulate different cases of body heat release.

c. Architecture of thermal manikin

The thermostatic manikin system consists of 16 regions divided in 79 circuits. Each region is covered by several heating elements (each has 24 Ohms constant resistance) to warm the surface. Each heating element is covered, as mentioned before, by 5 analog temperature sensors (TSic 501 – Figure 20). These sensors are providing the signal of temperature that is being are used by the control system to maintain a constant setpoint for the manikin surface. The 395 temperature acquisition channels are providing data that is collected by the multiplexer interface (Figure 26). It helps miniaturizing of the electronic system, by reducing the space occupied by wires, thus being able to fit inside the manikin. All the control part is using the FPGA (Field Programmable Gate Array) technology (Figure 24).

Appeared for the first time at the mid of the 80's. The father of FPGA was Ross Freeman (Xilinx). FPGA is semi-conductor based integrated circuits that use logical elements and I/O (Input/Output) blocks. The main advantage of FPGA is that it can be configured by the user and can be implemented in advanced digital automation systems.

FPGA allows for the design of the hardware architecture providing the advantage of the flexibility of the programming language used for implementation of the software solution. This approach provides, a flexibility also in the design of the control concept in relation to the CPUs because the hardware architecture of the system is not imposing a particular platform.

The architecture of the system hardware was designed by the Mechatronics Department of the National Institute of Aerospace Research and developed with the team from UTCB. **I was actively involved in this prototype development, being detached at INCAS for a period of three months.** The solution proposed is composed of two systems provided by NI based on the FPGA. In comparison to the first solution taken into consideration (the use of the microcontrollers) this solution represent an evolution in terms of high data collection capacity (up to 400chanells, filters, signal, bias, etc.), being able to generate appropriate signals for all 80 channels represented in software implementation of the NI (as presented in Figure 26). Another advantage is the possibility to use sequential/parallel calculations for signal generation for all 80 channels (time modulation PWM for transistor MOS gates activation in accordance to the output of the neuro-fuzzy controller. The control algorithms for the 80 channels are transposed in software for the sequential section of the NI boards (as presented in Figure 27 the RIO systems are having the sequential/parallel computing units implemented.

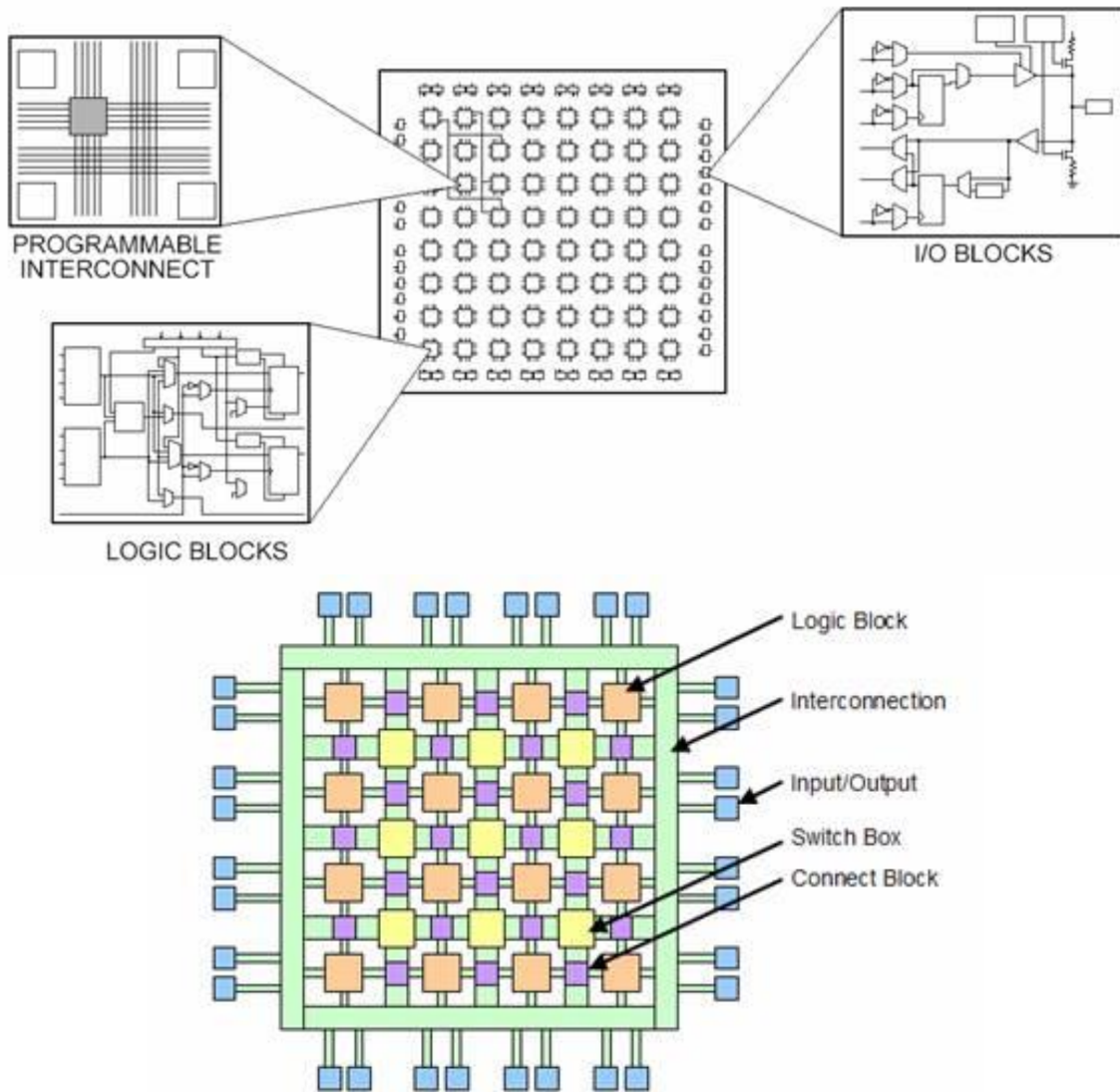


Figure 24: Standard structure of a FPGA system (cRIO www.ni.com)

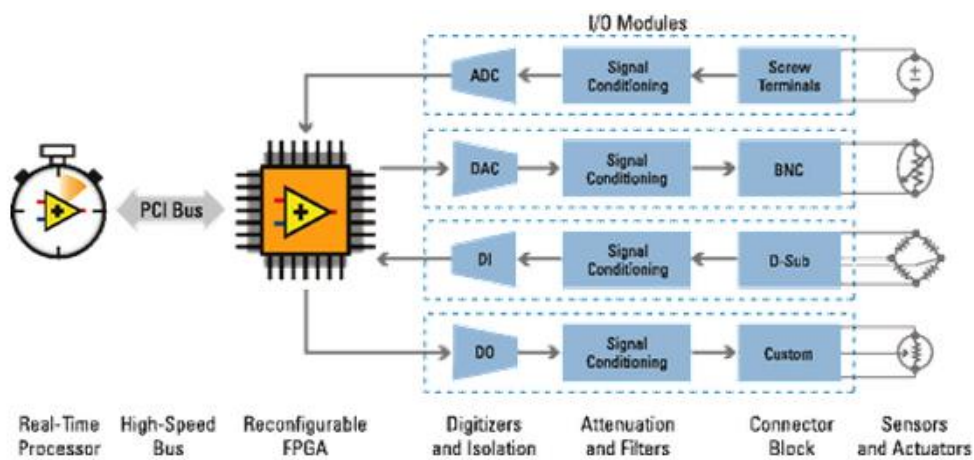


Figure 25: Typical architecture of a NI system based on FPGA (cRIO www.ni.com)

The architecture of the new system is presented in Figure 28. We have used for this project two development NI boards (myRIO si sbRIO). Each of the two boards are provided with a sequential computing unit (x86) and a matrix computing unit (FPGA). A multiplexing interface was developed based on HEF 4067B circuits in order to interconnect the boards with the temperature transducers. We have developed an interface based on SN7407 circuits to control and sent commands to MOS transistors used for the execution system.

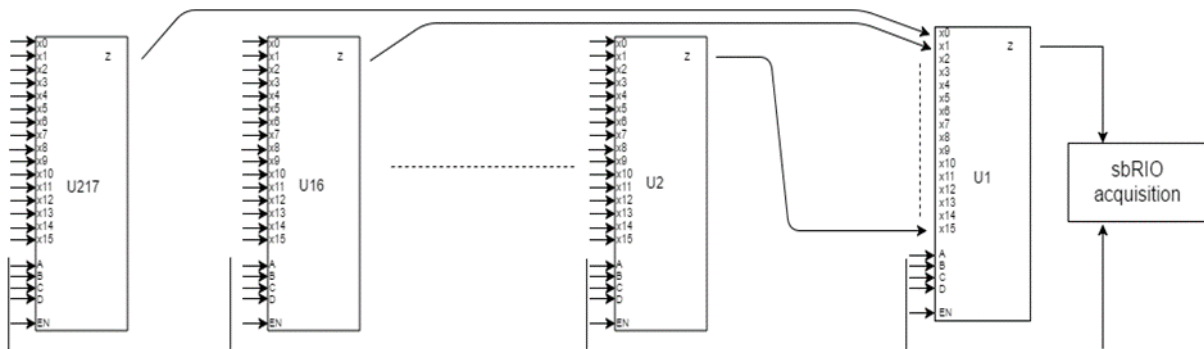


Figure 26: Multiplexer simplified circuit diagram [213]

The basic architecture of the manikin system is presented in Figures 27 and 28. The FPGA software on the sbRIO 9636 board allows the acquisition of the signal that is coming from the multiplexer interface which, instead of requesting one input at a time, collects all the inputs and separates them by shifting the register in the temperature data memory. The software from myRIO 1900's FPGA creates the PWM pulse used to control the patch surface on. Both NI boards is implemented real-time software, the acquisition device also processes the data to obtain reliable mean temperature of every patch using a fault detection and isolation algorithm, while the heating control devices, using the data processed by the acquisition board, generate a robust and adequate response using the neuro-fuzzy controller. The real-time hardware and software can run independently from the computer user interface, with the limitation of maintaining the last (or default) requested set point of temperature.

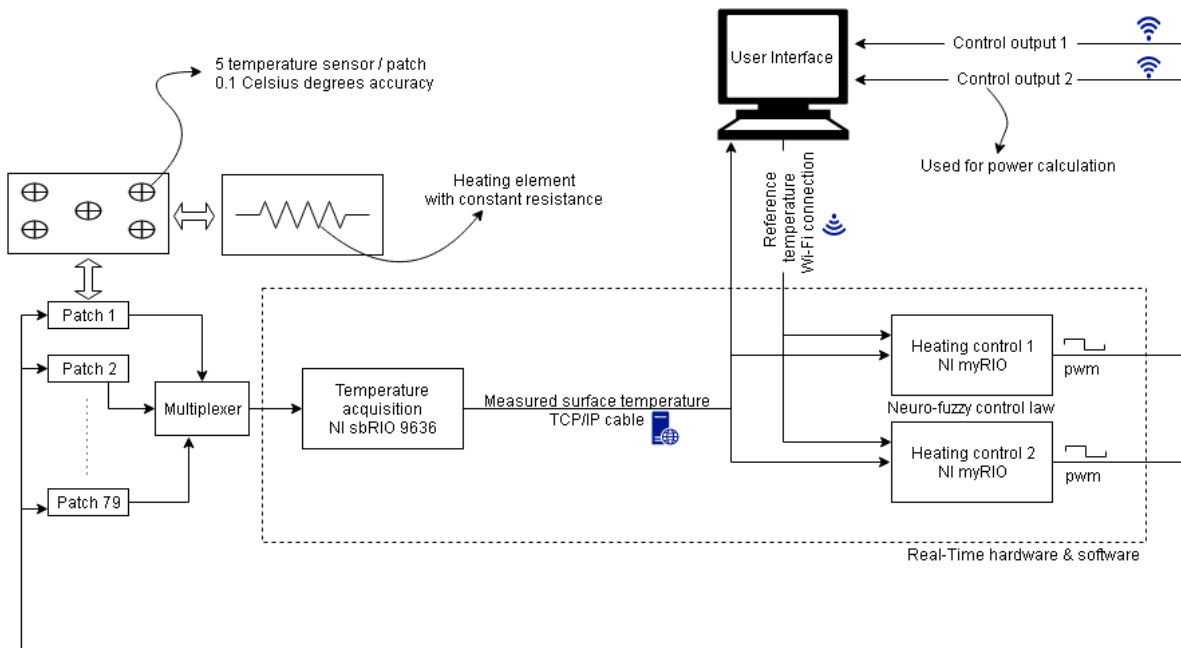


Figure 27: Basic architecture of manikin system [220]

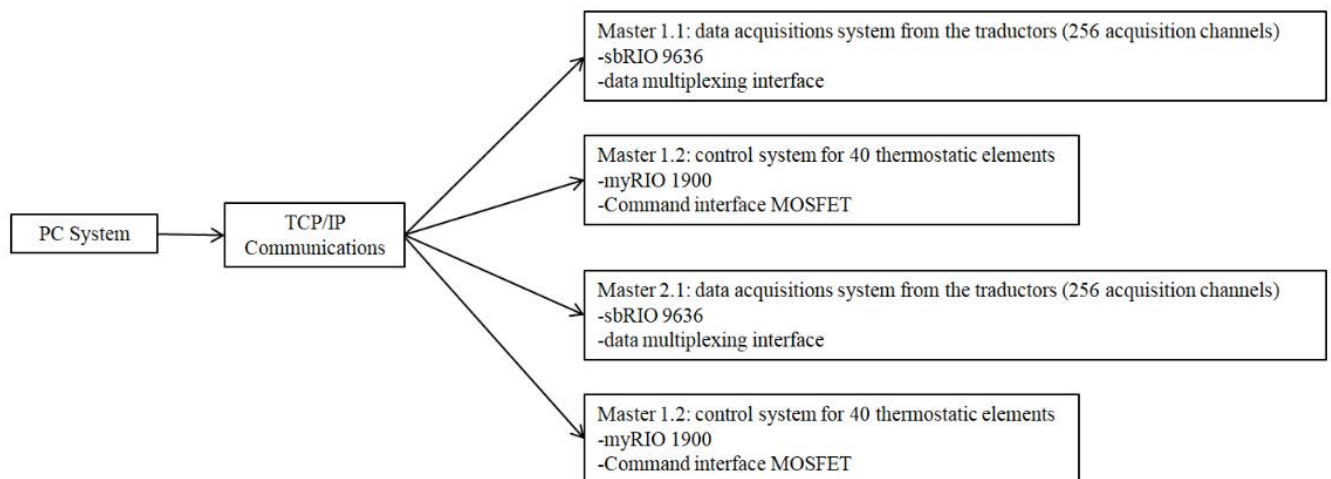


Figure 28: Thermostatic system architecture [220]

The software of the thermal manikin allows the user to upload set points for several testing situations, to change the set point on each anatomical zone independently, to monitor the behavior of the temperature data and the system controller. The user can also view the equivalent temperature value displayed graphically as well as the average power consumption for each region. The necessity of processing a high amount of information (395 acquisition channels and signal filtering) and generating proper signals for 79 command channels, as well as the strict

timing, provided by the NI boards Real-Time processor and required for the control of electronic circuits (multiplexer and MOS driver interface), allow to conclude that this technology is the best solution for the manikin system. The control algorithm for the command channels was converted into software for the sequent calculus unit of the NI boards.




<p>Main power supply used for the heating patches – PS1 Power supply Mean Well RSP-2400-24 24V/100A 2400W</p>	
<p>Power supply used for myRIO boards (temperature controller) – PS2 TENMA 72010500, 2Ch, 30V, 3A, Adjustable</p>	
<p>Power supply used for sbRIO boards (temperature acquisitions) – PS3 Axiomet AX-3003D-3</p>	

Figure 29: Power supplies used for the manikin

D. Innovative control model based on a neuro-fuzzy control law

The diagram used for the control of one channel is shown in Figure 31. PWM (pulse width modulation) is a well-known technique to produce analog signal, using digital devices that output a square signal by switching on and off the output port.

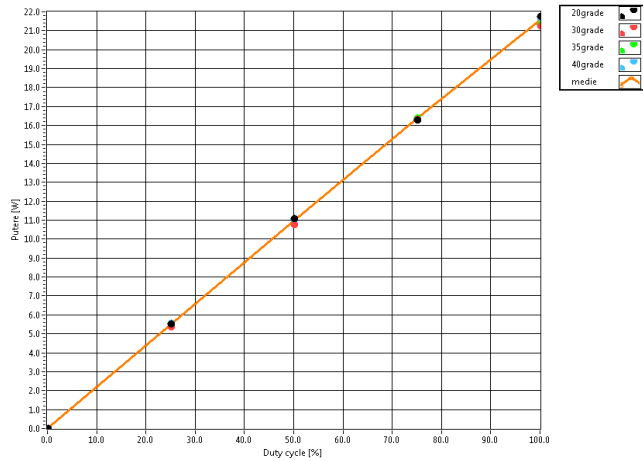


Figure 30: Power variation as function of Pulse With Modulation duty-cycle

When the on/off period of the signal is modified, a voltage between 0 and 24V (the maximum value of the voltage recommended for the patches) can be simulated. Since myRIO 1900 boards can output only 3.3V in Digital I/O (DIO) ports, it has been added an interface allowing to convert 3.3V Transistor - Transistor Logic(TTL) signal to 5V Complementary Metal Oxide Semiconductor (CMOS) signal needed by the transistors to open and close the 24V supply circuit according to the PWM (Pulse With Modulation) control generated by the neuro-fuzzy controller.

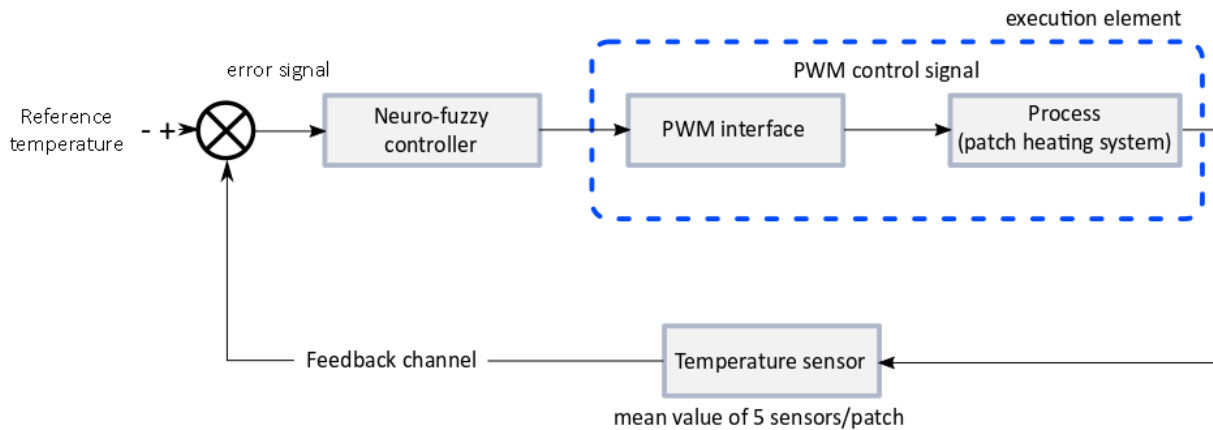


Figure 31: Control system diagram for one control channel

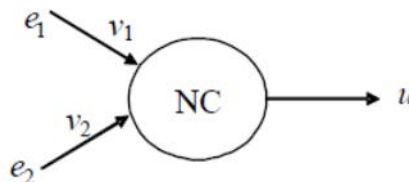


Figure 32: Schema of elementary perceptron [214]

The approach of using artificial intelligence for control problems concerns in principle an input-output behavioral philosophy of solution. The neuro-fuzzy control strategy adopted for the temperature control of the system was proposed by dr. Ioan Ursu from INCAS. It is composed of two components: a neuro-control and a fuzzy logic control supervising the neuro-control to counteract the saturation [221].

As neuro-control, a mono-layer perceptron is used (Figure 31) as described by the following

$$\text{relation: } u = u_n = v_1 y_1 + v_2 y_2 =: v_1 (T_{ref} - T) + v_2 \dot{T} \quad (8)$$

where T_{ref} is reference temperature input and T is the measured temperature. The input is u_n and the output is $y = (y_1, y_2)$.

The performance of the system is evaluated by the *cost function*, a criterion based on the difference between the first input y_1 – tracking error –, the second input component y_2 and the control u :

$$J = \frac{1}{2n} \sum_{i=1}^n (q_1 y_1^2(i) + y_2^2(i) + q_2 u_n^2(i)) := \frac{1}{2n} \sum_{i=1}^n J(i) \quad (9)$$

The weighting vector $v = [v_1 \ v_2]^T$ is updated by the *gradient descent* learning method allowing to reduce the cost J . Consequently, the update is given by the expression:

$$v(n+1) = v(n) + \Delta v(n), \Delta v(n) := -\mathbf{diag}(\delta_1, \delta_2) \frac{\partial J}{\partial v(n)} = \mathbf{diag}(\delta_1, \delta_2) \sum_{i=n-N}^n \left(\frac{\partial J(i)}{\partial y(i)} \frac{\partial y(i)}{\partial u(i)} + \frac{\partial J(i)}{\partial u(i)} \right) \frac{\partial u(i)}{\partial v(i)} \quad (10)$$

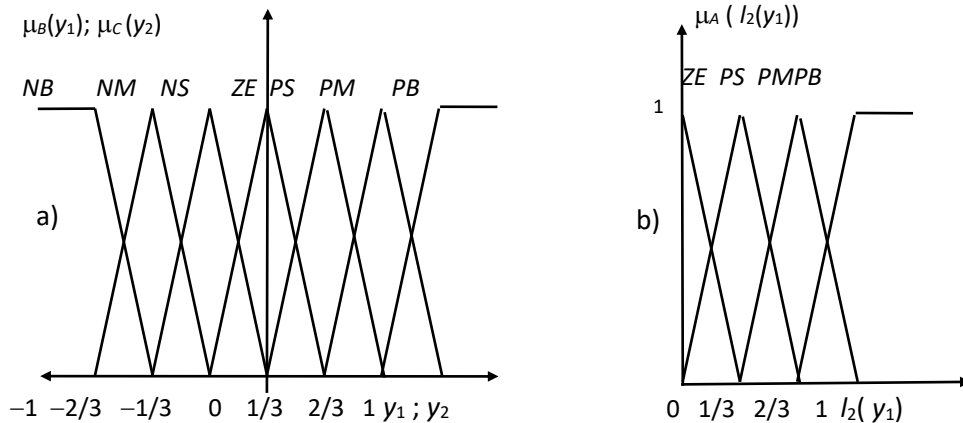


Figure 33: Membership functions for: a) scaled input variables y_1, y_2 and b) $l_2(y_1)$ [221]

where the matrix $\mathit{diag}(\delta_1, \delta_2)$ introduces the learning scale vector, $\Delta v(n)$ is the weight vector update and N represents a back memory (of N time steps). The derivatives in (10) require input-output information about the system. The derivative $\partial y(i)/\partial u(i)$ is approximated in real time by the relationship:

$$(y(i) - y(i-1))/(u(i) - u(i-1)) \quad (11)$$

In order to avoid a risk of neuro-control saturation and to achieve the goal of strengthening the learning system, a Fuzzy Supervised Neuro-control (FSNC) was proposed in [215]. FSNC shifts to a *Mamdani type fuzzy logic* control when the neuro-control saturates. Moreover, the three components of the fuzzy control: fuzzyfier, fuzzy reasoning, and defuzzyfier, are briefly explained. In this case, the *fuzzyfier* component converts the input crisp signals :

$$l_2(y_{1k}) := \sqrt{\sum_{j=k-2}^k y_{1j}^2}, \quad y_{1k}, y_{2k}, k=1, 2, \dots \quad (12)$$

into their relevant fuzzy variables (or membership functions) with the following set of linguistic terms: zero (ZE), positive or negative small (PS, NS), positive or negative medium (PM, NM), positive or negative big (PB, NB) (triangular and singleton type membership functions are chosen - see Figure 33). l_2 is a norm giving, over a sliding window of three samples, the maximum variation of the tracking error. Introducing the crisp signal in the fuzzifier will result in a reduction of fuzzy control switches due to the effects of spurious noise signals.

The strategy of fuzzy principle demonstrates the idea of a (direct) proportion between the error signal y_l and the required fuzzy control f . Therefore, the fuzzy reasoning engine sums several $n = 4 \times 7 \times 7$ IF..., THEN... rules, that is the number of the elements of the Cartesian product $A \times B \times C$, $A = (\text{ZE}; \text{PS}; \text{PM}; \text{PB})$, $B = C = (\text{NB}; \text{NM}; \text{NS}; \text{ZE}; \text{PS}; \text{PM}; \text{PB})$. These sets are associated with the sets of linguistic terms chosen to define the membership functions for the fuzzy variables $l_2(y_1)$, y_1 and, respectively, y_2 . Consequently, the succession of the n rules is the following: 1) IF $l_2(y_1)$ is ZE and y_2 is PB and y_1 is PB, THEN u_f is PB; 2) IF $l_2(y_1)$ is ZE and y_2 is PB and y_1 is PM, THEN u_f is PM; ... 7) IF $l_2(y_1)$ is ZE and y_2 is PB and y_1 is NB, THEN u_f is NB; 8) IF $l_2(y_1)$ is ZE and y_2 is PM and y_1 is PB, THEN u_f is PB; ... 196) IF $l_2(y_1)$ is PB and y_2 is NB and y_1 is NB, THEN u_f is NB. If we consider τ to be the discrete sampling time, and the three scaled input crisp variables $l_2(y_{1k})$, y_{1k} and y_{2k} , at each time step $t_k = k\tau$ ($k = 1, 2, \dots$). The ordinates corresponding in Figure 33 to each of the three crisp variables, a number of $M \leq 2^3$ combinations of three ordinates must be

investigated. Then, a number of M IF..., THEN... rules will operate in the form:

$$\text{IF } y_{1k} \text{ is } B_i \text{ and } y_{2k} \text{ is } C_i \text{ and } l_2(y_{1k}) \text{ is } A_i, \text{ THEN } u_{fk} \text{ is } D_i, i=1,2,\dots,M \quad (13)$$

(A_i, B_i, C_i, D_i are linguistic terms belonging to the groups A, B, C, D and $D = B = C$). The *defuzzifier* concerns just the transforming of these rules into a relationship providing the output control variable u_f . Each rule of defines a fuzzy set $A_i \times B_i \times C_i \times D_i$ in the input-output Cartesian product space $R_+ \times R^3$, whose membership function can be defined as:

$$\mu_{u_i} = \min[\mu_{B_i}(y_{1k}), \mu_{C_i}(y_{2k}), \mu_{A_i}(l_2(y_{1k})), \mu_{D_i}(u)], i=1, \dots, M, (k=1, 2, \dots) \quad (14)$$

The singleton-type membership function $\mu_{D_i}(u)$ of control variable has been preferred in this case, $\mu_{D_i}(u)$ being replaced by u_i^0 , the singleton abscissa. Therefore, using the singleton fuzzifier for u_f , the center-average type defuzzifier, and the min inference, the M IF..., THEN... rules can be transformed, at each time step $k\tau$, into a relation providing the crisp control u_f [216].

$$u_f = \frac{\sum_{i=1}^M \mu_{u_i} u_i^0}{\sum_{i=1}^M \mu_{u_i}} \quad (15)$$

The Fuzzy Supervised Neuro-control functions as fuzzy logic control u_f when neuro-control u_n saturates, or l_2 the norm of the tracking of the error y_1 increases. In the case of fuzzy control operating, the fuzzy neuro-control u_n is simultaneously updated for a real acting fuzzy control u_f . For a precise and accurate controlled process tracking, fuzzy logic switches on neuro-control whenever readapted neuro-control u_n is not saturated and the scaled norm $l_2(y_1)$ is smaller than a fixed value $l_{2,\min}$. At the time t_s , when the swapping from fuzzy logic control to neuro-control occurs, the readjusted weighting vector v_r will be derived by considering a scale factor u_f/u_n [216].

$$v_{1r} = (u_f - v_2 y_2) u_f / (u_n y_1), v_{2r} = v_2 u_f / u_n \quad (16)$$

This model of control was brought to the proof in various numerical simulations [214, 217, 218]. In accordance to a large number of simulation studies, performed by dr. Ursu and his team, it is proved that the nonconventional neuro-fuzzy control, improves the transient dynamics, compared to a proportional control, mainly in the case of sinusoidal references: thus, a better

tracking, meaning smaller attenuation and dephasing, are achieved.

E. The user interface

The LabVIEW platform was used to develop the programs that allow to communicate with the controller and the interface of the neuro-fuzzy system. Labview interface is allowing to set manikin surface temperature, sampling rate, activation and deactivation of one zone and coupling of the 79 elementary circuits in several larger regions if wanted. We chose to respect the 16 zones recommended by EN ISO 14505-2[14] (see Figure 37) but any other combination is possible. In the left side of the Figure 37 there are presented instantaneous temperatures and power consumption of each zone and on the right there are drawn the 16 areas of manikin with the equivalent temperatures measured on each area. The blue color of the left leg reveals a thermal discomfort. On the lower part on the left manikin's leg there was subjected to increased ventilation from a nearby mounted room ventilator.

The performance of the control system in maintaining the set point temperature within the $\pm 0.1^\circ\text{C}$ required error for the temperatures imposed on each region similar with the human surface temperature is presented in Figure 34.

As it was already explained in the first chapter the equivalent temperature represents a quantitative assessment of the conditions for the physical heat balance. The base of principle of the determination of the equivalent temperature is to measure the total heat flow of one or more zones, each with a specific measured surface temperature similar to that of a human body. The power consumption under steady-state conditions is a measure of the convective, radiative and conductive heat losses. Measurements and control are possible through the LabVIEW software interface. Typically, the quantity measured for each zone is the power consumption or heat loss and the surface temperature. The direct measurement of heat loss/power consumption and mean temperature of surface region eliminates the need for determining the other components. By normalization to a climate according the definition of equivalent temperature, the heat loss can be converted to an equivalent temperature.

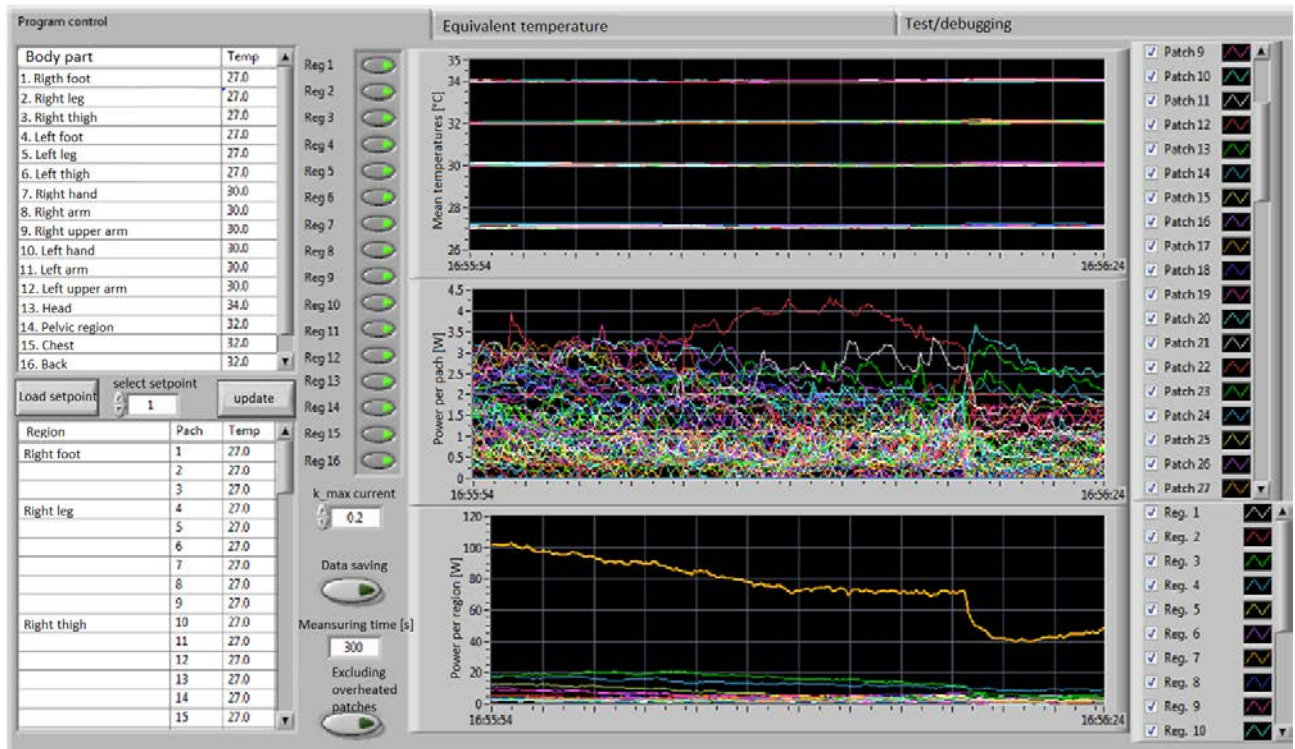


Figure 34: User interface to monitor temperature of manikin surface and control output energy consumption

Region	Preconfigured set point [°C]	
	1	2
1. Right foot	27	34
2. Right leg	27	34
3. Right thigh	27	34
4. Left foot	27	34
5. Left leg	27	34
6. Left thigh	27	34
7. Right hand	30	34
8. Right arm	30	34
9. Right upper arm	30	34
10. Left hand	30	34
11. Left arm	30	34
12. Left upper arm	30	34
13. Head	34	34
14. Pelvic region	32	34
15. Chest	32	34
16. Back	32	34

Figure 35: Preconfigured set-points that are available under the user interface (anatomic distribution and constant distribution of temperature)

The 79 patches divided in 16 regions according to ISO thermal manikin standard

Regiune	Temp
1 Laba picior dreapta	27.0
2 Tibie picior drept	27.0
3 Coapta picior drept	27.0
4 Laba picior stang	27.0
5 Tibie picior stang	27.0
6 Coapta picior stang	27.0
7 Palma dreapta	30.0
8 Antebrat dreapta	30.0
9 Brat dreapta	30.0
10 Palma stanga	30.0
11 Antebrat stanga	30.0
12 Brat stanga	30.0
13 Cap	34.0
14 Bazin	32.0
15 Trunchi fata	32.0
16 Trunchi spate	32.0

Possibility to set individual temperatures on each region

The changes that the user makes in the upper table DO NOT TAKE EFFECT unless the ACTUALIZARE button is pressed

Set points described in the table on next page
To change between set points, press "UP" or "DOWN" on increment button

Load set point Select setpoint: 1 Actualizare

Regiune	Patch	Temp
Laba picior dreapta	1	27.0
	2	27.0
	3	27.0
Tibie picior drept	4	27.0
	5	27.0
	6	27.0
Coapsa picior drept	7	27.0
	8	27.0
	9	27.0
	10	27.0
	11	27.0
	12	27.0
	13	27.0
	14	27.0
	15	27.0

Here it can be seen the patch distribution for each region, but more important, the temp. set point can be adjusted for each patch individually.

Every change that is made in the lower table TAKES EFFECT IMMEDIATELY on the temperature controller and manikin surface will follow the respective set point

Figure 36: User interface to control the set points of the regions or of the individual patches – the language of the user interface can be either English, either Romanian

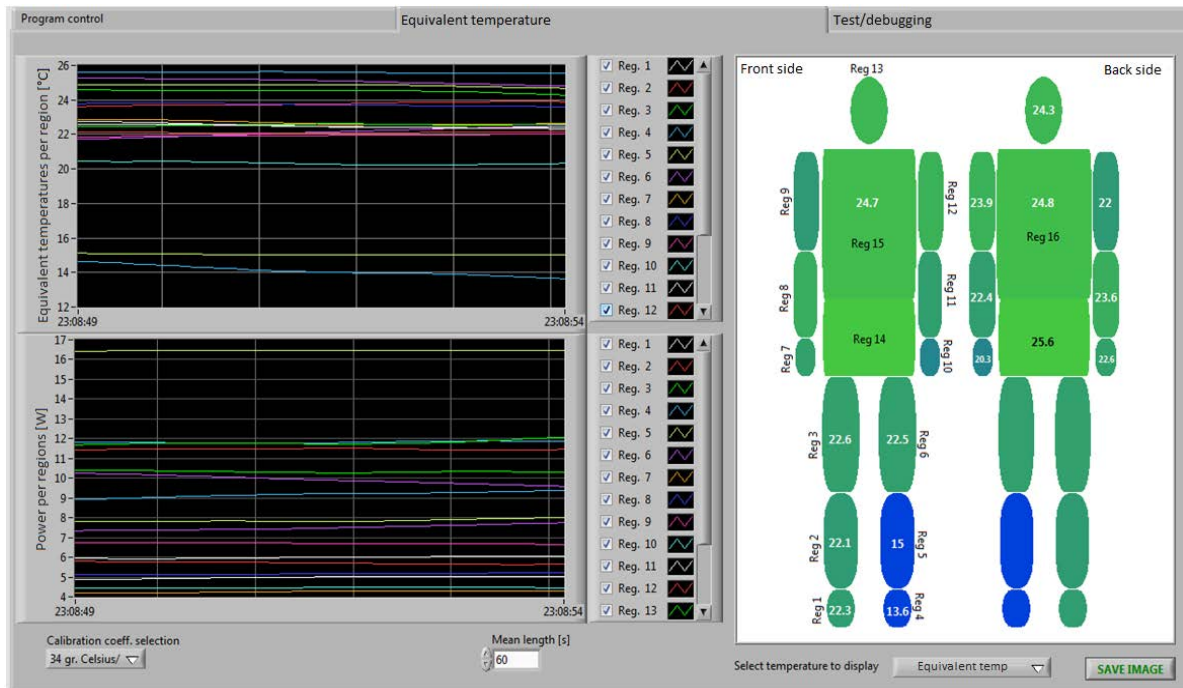


Figure 37: User interface to monitor equivalent temperature

F. Testing the thermal manikin

In order, to check the functionality of the control system, a single patch has been tested both in stationary and transitory conditions. We have also tested the response of the system in terms of temperature variation up and down from 30 °C to 40°C using a step of 1°C (Figure 40). Figure 40 shows in white color the desired temperature and in red the drowned real surface temperature variation. The desired temperature value is higher, the time needed to reach steady condition is longer. When the desired temperature value is increased, the controlling system injects continuously electrical power in order to heat the surface until desired temperature is reached. The time needed to obtain this temperature depends on the desired value and on the environmental conditions. In these test cases the surface attends the desired temperature and the control system works in stationary regime after a time interval of about 3 minutes (see Figure 40).

A simple sensitivity test was done by opening a door and allowing external air to come into the room. Once the stationary regime is settled the door was open such the incoming air disturb the patch temperature. The system response can be observed in the Figure 41 below. The fast response of the regulation system and his high sensitivity are demonstrated after the preliminary tests on the single patch. These results show that the control algorithm might be implemented on

manikin exposed to fast transient thermal environments as in a vehicle. There is also a great dependency between the perturbation intensity and the response of the regulation system.

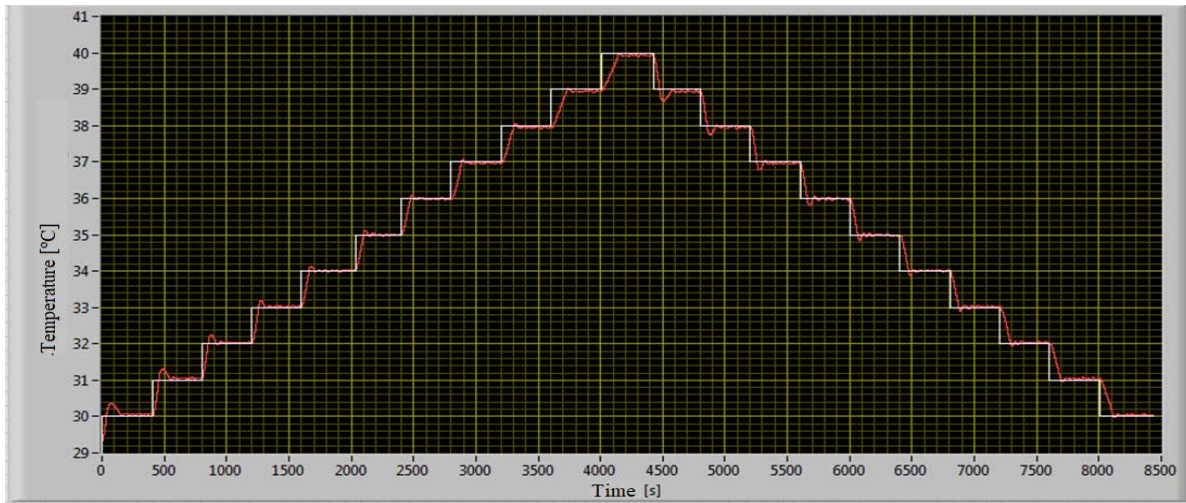


Figure 38: Temperature variation from 30°C to 40°C and vice versa with a step of 1°C

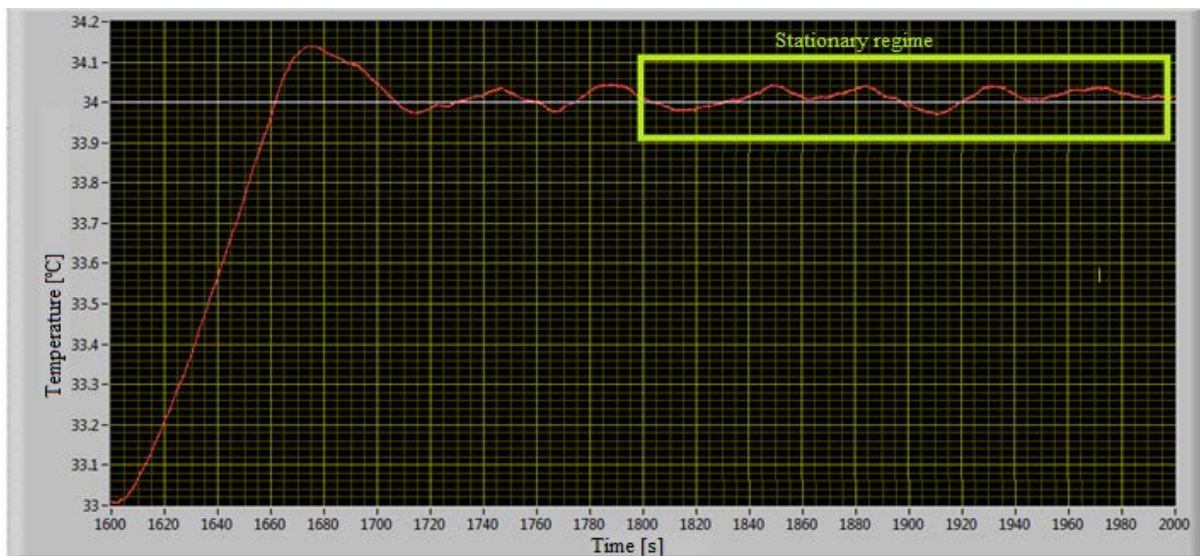


Figure 39: Temperature variation in transitory and stationary regime

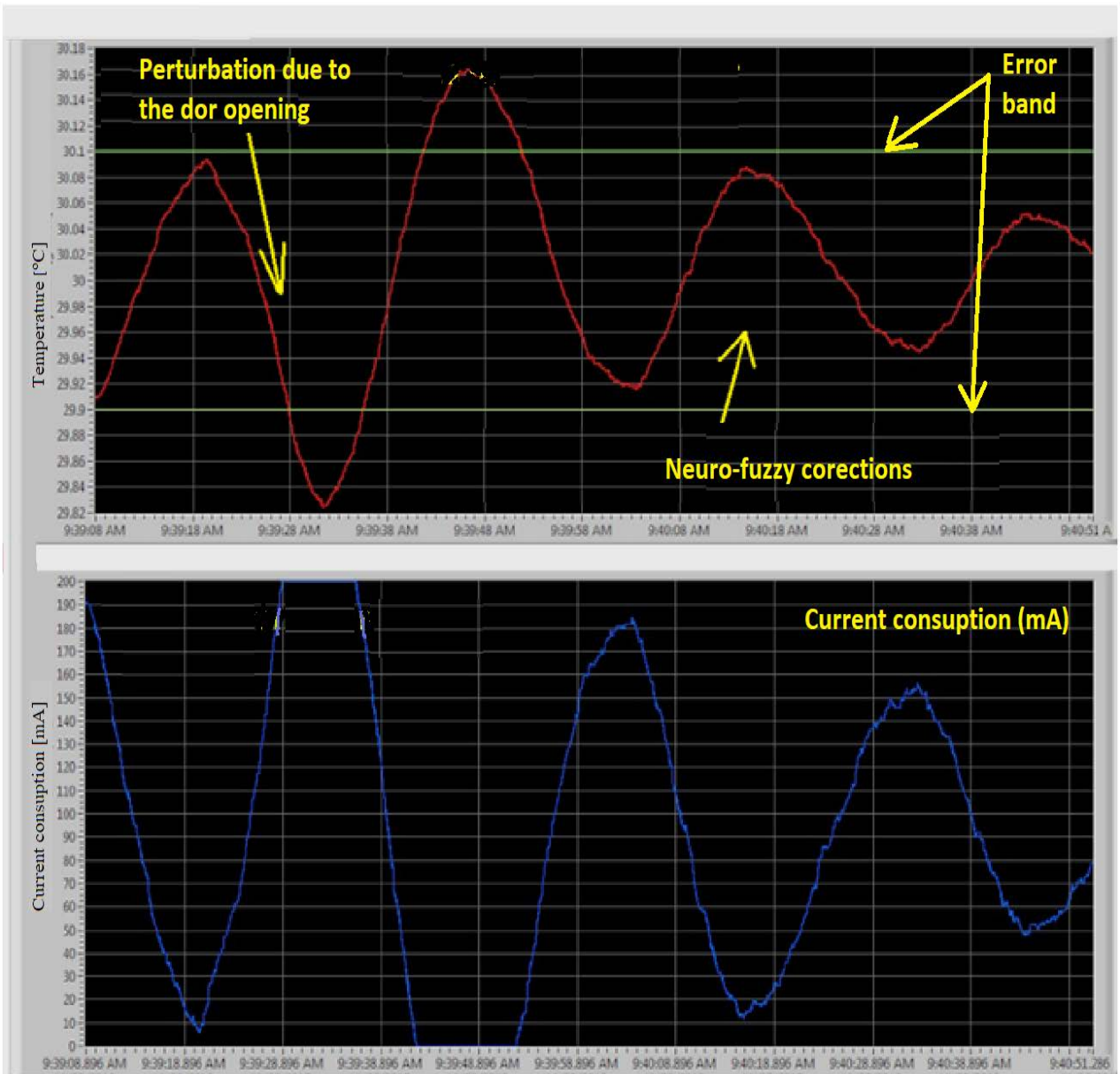


Figure 40: Regulatory system response in transitory regime



Figure 41: Experimental setup and temperature distribution for upper part of the manikin

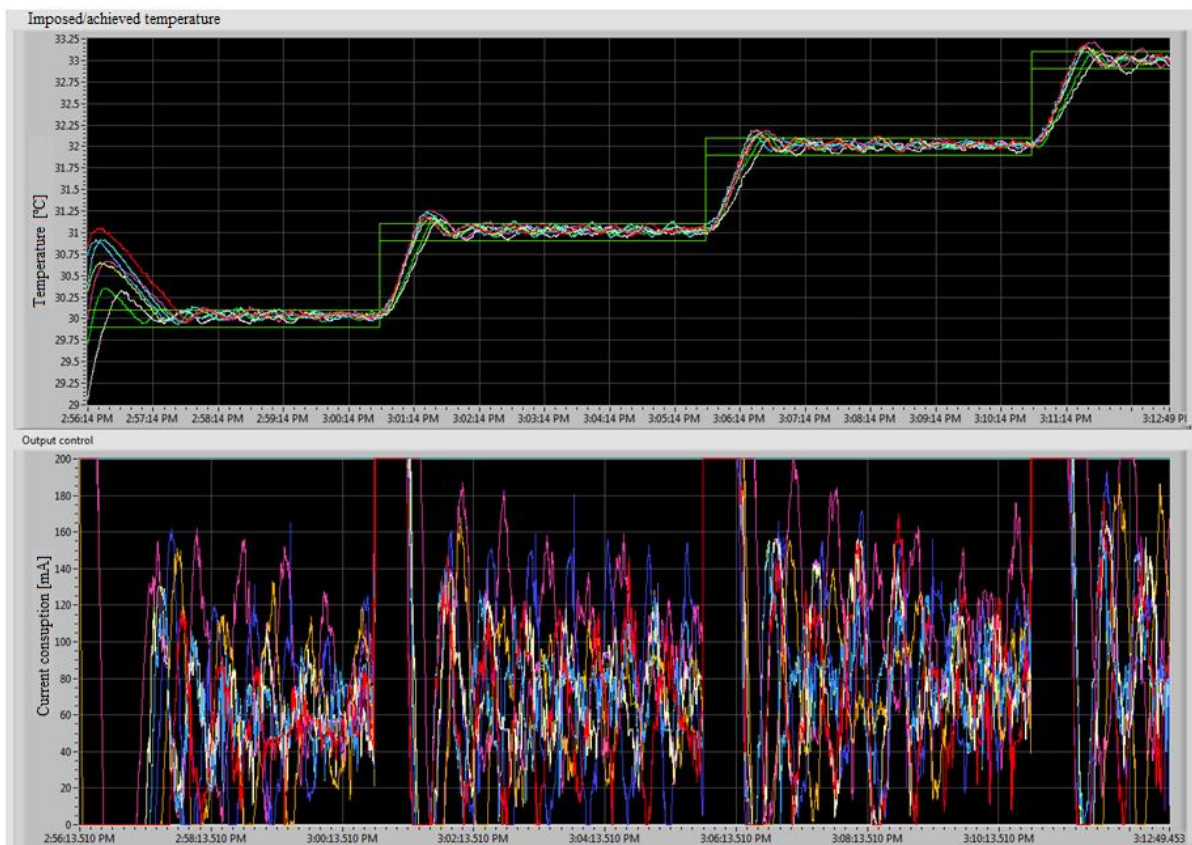


Figure 42: Regulatory system response in transitory regime for head and chest zones

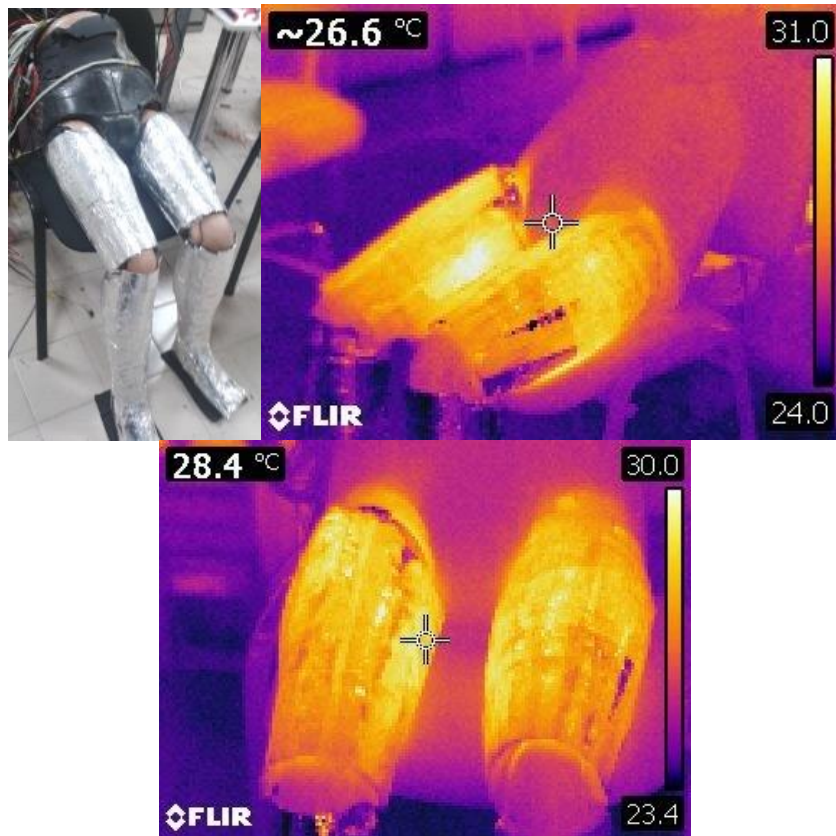


Figure 43: Images with the lower part of the manikin during the tests

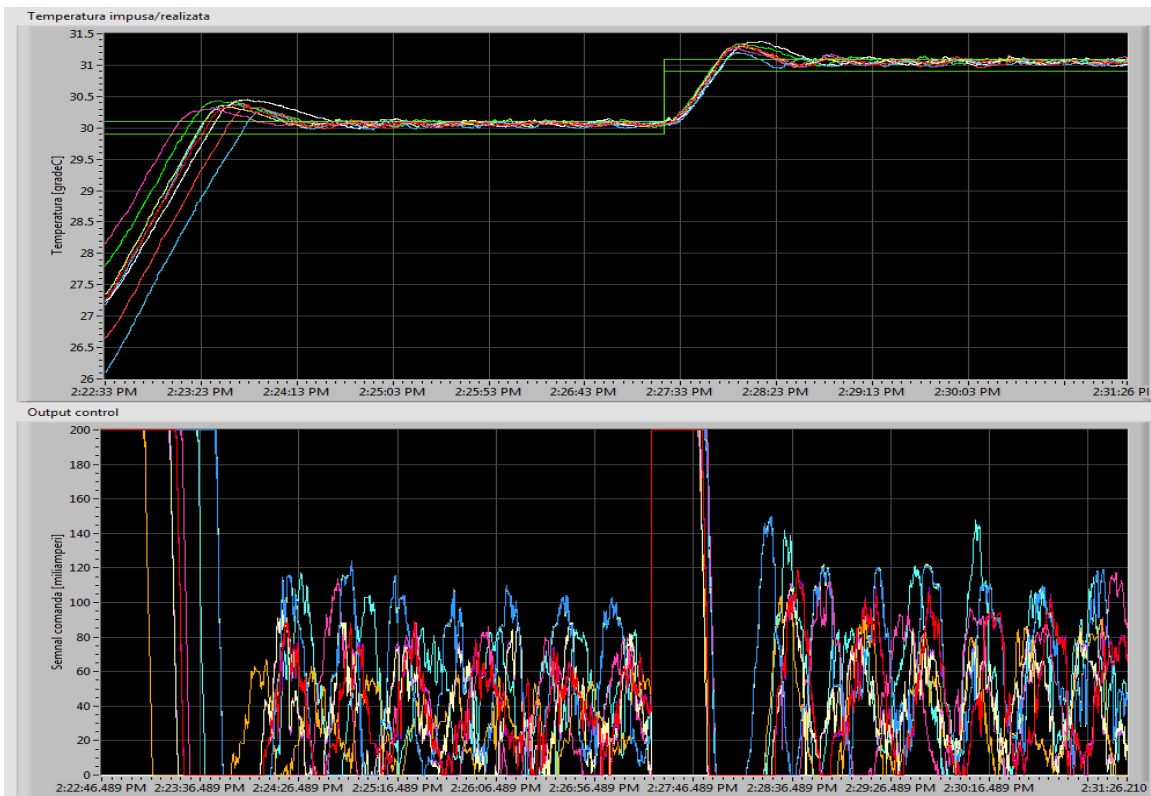


Figure 44: Response of the lower part of the manikin to the step changing temperature – increasing the electrical power

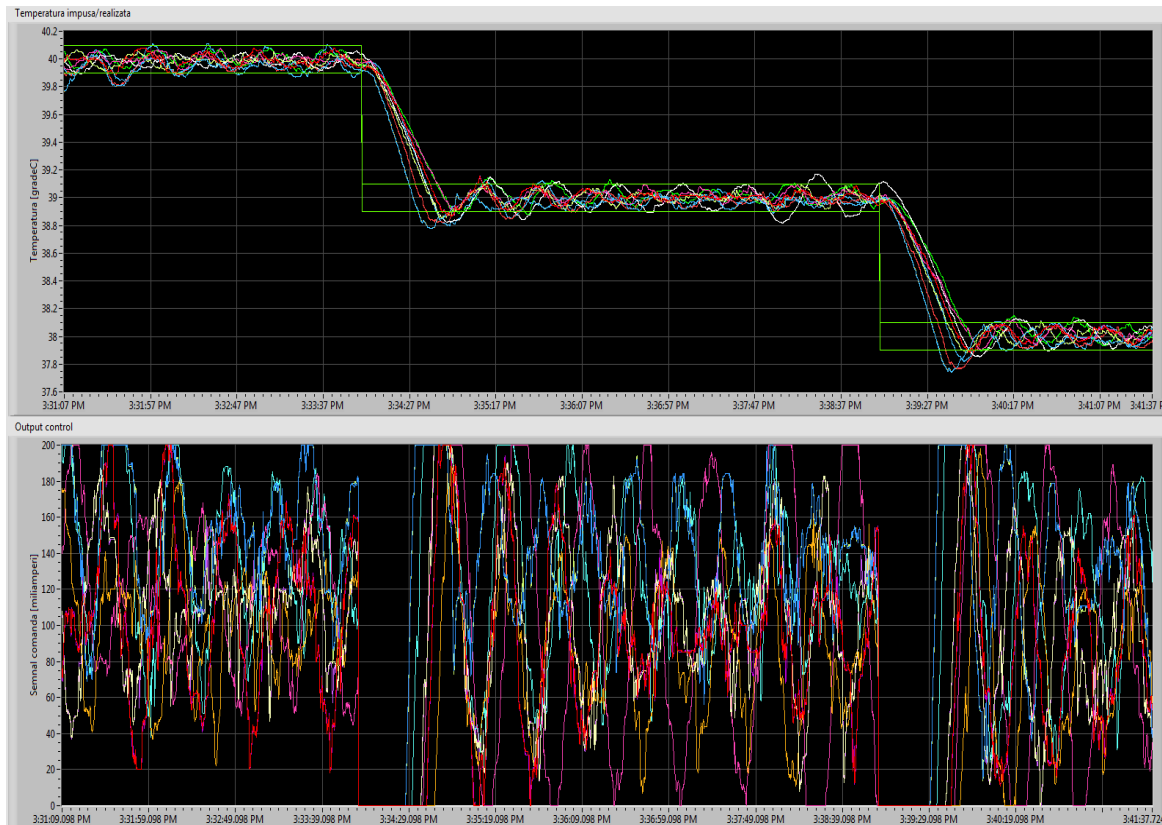


Figure 45: Response of the lower part of the manikin to the step changing temperature – decreasing the electrical power

Next, the control model was implemented upon each part of the manikin: the upper part (trunk and head), inferior limbs (foots, legs and thighs) and on superior limbs (arm, forearm and hand). A test was performed to verify correct functionality of each manikin zone and to verify the common response of multiple heating elements composing these zones. In Figure 41 is represented upper part of the manikin, during the test. Results on changing desired temperature with 1°C are displayed in Figure 42. Manikin inferior limbs were tested in the same way as the trunk, in Figure 43 are presented some images during the test, and in Figure 45 temperature variation with a step change of 1°C of the desired temperature.

In order to verify control the system applicability using a computer cooling fan, air was blown on arm and forearm of the manikin, with 4 different velocity speeds. This test was made at 22 °C ambient temperature. Imposed manikin temperature was 33 °C. Experimental setup is presented Figure 46. At the distance of 10 cm from the manikin was placed a hot wire anemometer. Using this anemometer the air velocity near the manikin was measured. It helps to

have an idea about the magnitude of the perturbation. The characteristics of the anemometer are: range $0.1 \div 25$ m/s; accuracy 5%; resolution 0.01 m/s.

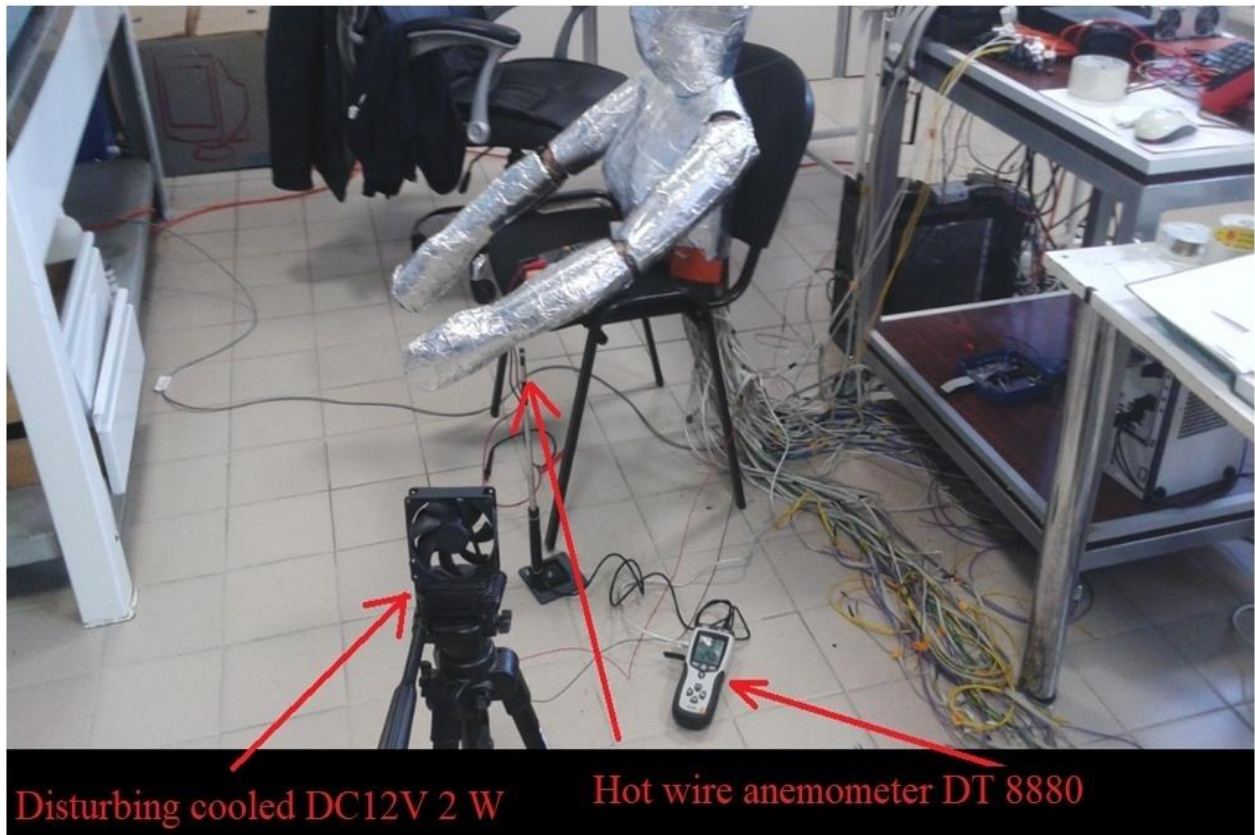


Figure 46: Testing manikin response for different air speed, using a computer cooler - experimental setup

The regulation system achieved steady condition and surface temperature of 33°C before each test at different cooler speed. In Figures 48-51 there are highlighted the temperature and the power injected variations for air velocities values of 0.2, 0.3, 0.55 and 0.8 m/s. This perturbation has been maintained for 3 minutes. The yellow color indicates the areas under the influence of the computer cooler. The most exposed area was the forearm zone as the airflow from the cooler was orientated in this zone.

The value of 0,2 m/s of air velocity didn't have a significant effect. The surface temperature fluctuation did not exceed the limit of $\pm 0.1^{\circ}\text{C}$. With a rising air velocity near the manikin, the control system intervention is illustrated in Figures 47-50 . As a consequence of imposing a velocity value of 0,8 m/s, the current injected is almost for all test period at the maximum level. The desired temperature is restored after about 1 minute after the introduction of the perturbation and has remained at the inferior acceptability limit of 32.9°C (see Figure 50).

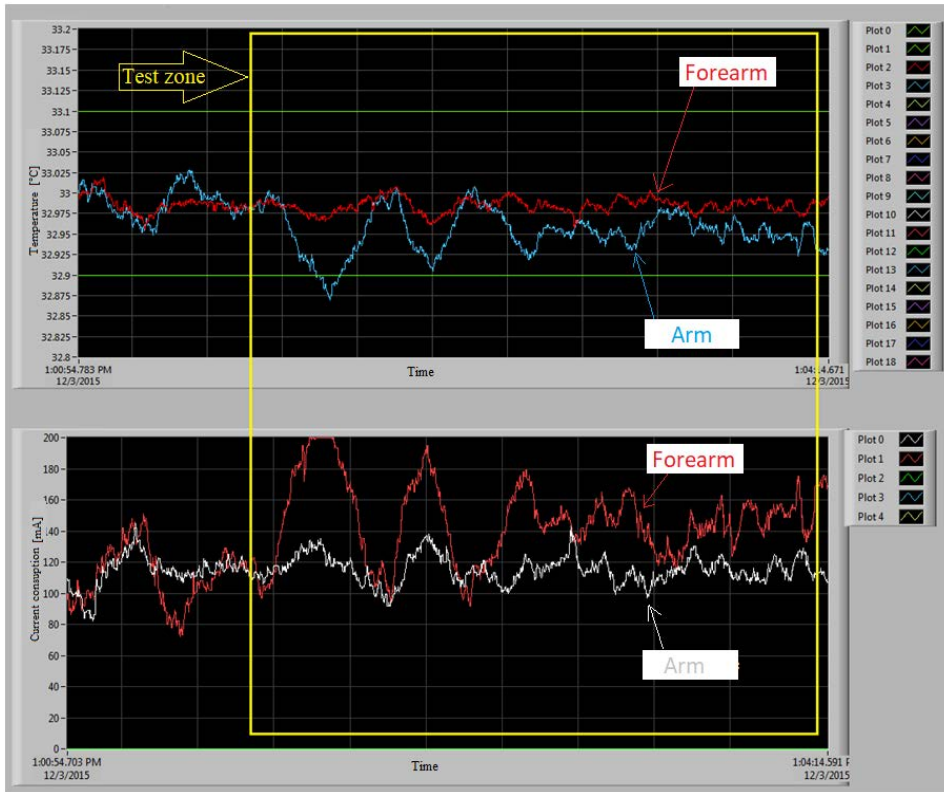


Figure 47: Regulatory system response for velocity of 0.2 m/s

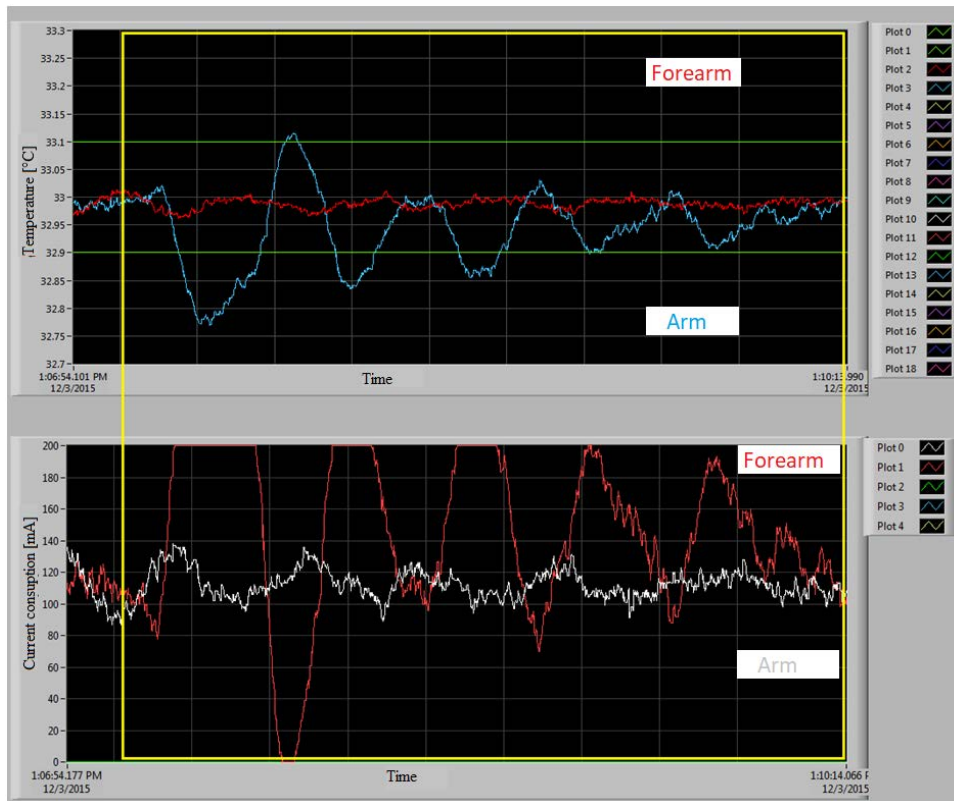


Figure 48: Regulatory system response for velocity of 0.3 m/s

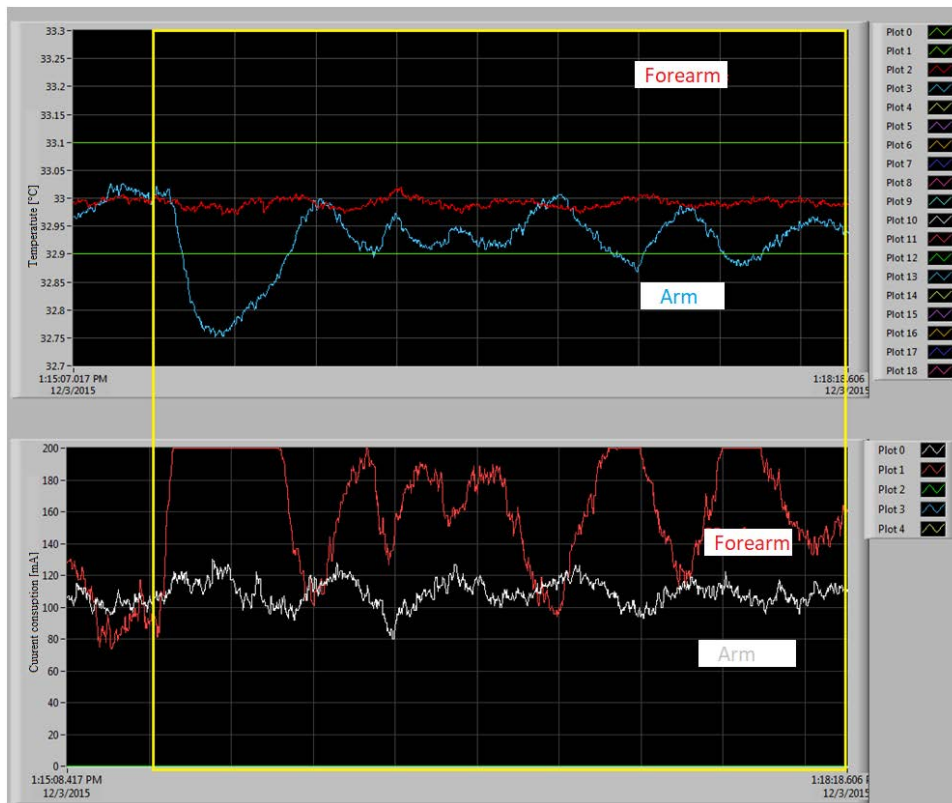


Figure 49: Regulatory system response for velocity of 0.55 m/s

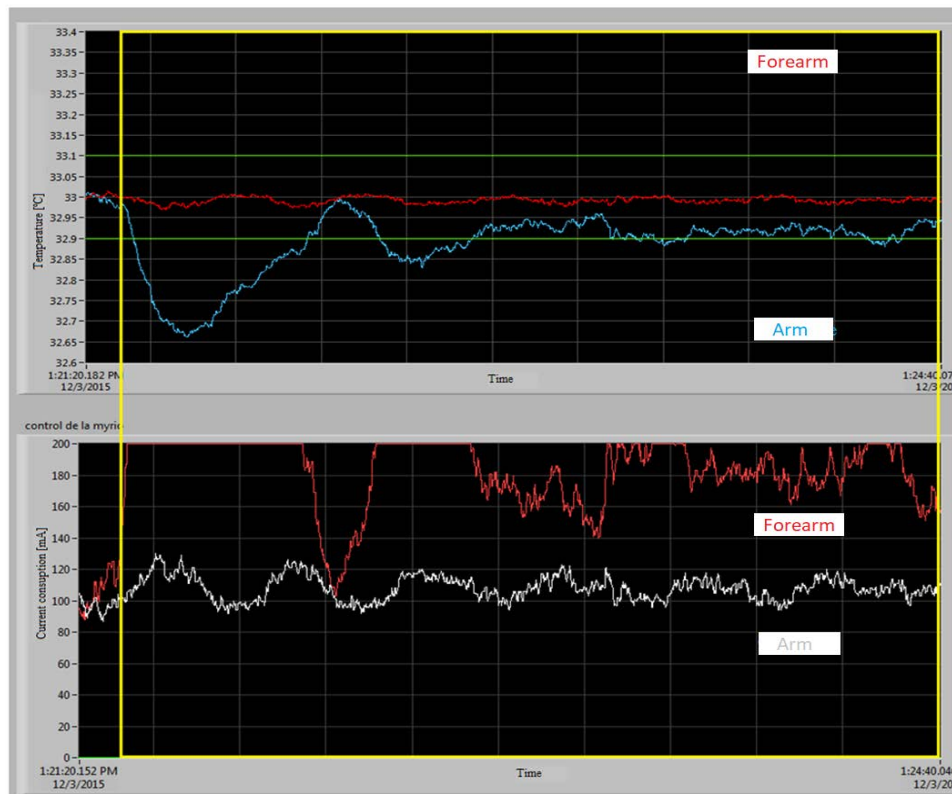


Figure 50: Regulatory system response for velocity of 0.8 m/s

g. Calibration of the thermal manikin

The thermal manikin was calibrated in a climatic chamber in order to find the relationship between surrounding temperature and heat loss. The nude thermal manikin was placed in the climatic chamber at UTCB. The climatic chamber (3.6m by 3.6m by 2.5m) has active walls and an advanced ventilation system, allowing several ventilation strategies. Air is supplied from the surface of a perforated ceiling. The air temperature inside the cell and the surface temperatures of the walls were measured with PT100 sensors which are connected to a data acquisition logger. Used sensors were calibrated in an interval corresponding from 0°C to 34°C, their precision being of 0.2°C. On each wall, a sensor was placed while six sensors were placed on the height of the room to have a gradient temperature.

Table 3: Heat transfer coefficients for uniform temperature distribution with 34°C in seating position

Segment	anatomic temperature distribution		uniform temperature distribution	
	h_c [W/m ² K]	h_r [W/m ² K]	h_c [W/m ² K]	h_r [W/m ² K]
Head	4.74	4.47	4.68	4.58
Torso	4.76	4.53	3.06	2.41
Right thigh	4.16	3.32	4.16	3.88
Right tibia	3.06	2.11	5.12	5.49
Right foot	4.68	4.37	2.91	2.22
Right forearm	6.86	5.73	4.69	3.59
Right arm	4.64	4.28	4.96	4.94
Right hand	4.96	4.92	6.87	7.49
Left hand	4.96	4.92	4.64	4.52
Left arm	4.62	4.23	4.96	4.95
Left forearm	6.83	5.66	6.83	6.44
Left thigh	4.69	4.38	4.62	4.49
Left tibia	2.91	2.83	4.74	5.32
Left foot	5.12	5.23	4.64	4.52
Back	5.87	6.75	4.76	4.69
Pelvis	4.64	4.29	5.87	5.02

The values heat transfer coefficients with this thermal manikin are quite close to results from the literature. In

Table 4 are presented some typical values of convective heat transfer coefficients from literature.

Table 4: Convective heat transfer coefficients from literature with various anatomic distributions of the temperature

Author	de Dear et al. 1997 [223]		Quintela et al. 2004 [224]		Virgilio et al. 2012 [225]	Oliveira et al. 2014 [226]	C. Croitoru	Fojtlin et al. 2017[227]	
Body part/position	Seated	Standing	Seated	Standing	Standing	Standing	Standing	Seated	Standing
h_{conv} [W/m ² °C]									
Left foot	4.2	5.1	4.4	4.6	4.6	4.4	2.5	6.0	6.4
Right foot	4.2	5.1	4.5	4.6	4.7	4.4	2.5	6.3	7.2
Left leg	4.0	4.1	3.5	3.7	3.3	3.4	2.5	4.6	4.7
Right leg	4.0	4.1	3.8	3.8	3.5	3.9	2.5	4.6	4.4
Left thigh	3.7	4.1	3.7	4.0	3.7	3.9	2.5	4.4	3.9
Right thigh	3.7	4.1	3.5	3.8	3.9	3.9	2.5	4.3	4.2
Pelvic region	2.8	3.4	2.8	2.6	2.6	2.8	-	4.4	3.3
Head	3.7	3.6	4.3	5.0	4.5	4.3	2.7	3.2	3.3
Left hand	4.5	4.1	4.9	5.1	4.1	5.3	2.5	-	-
Right hand	4.5	4.1	4.3	4.6	4.2	4.1	2.4	-	-
Left arm	3.8	3.7	4.1	4.1	3.6	3.7	2.5	4.1	3.8
Right arm	3.8	3.7	4.1	3.9	3.8	3.6	2.4	4.0	3.6
Left upper arm	3.4	2.9	3.0	3.6	3.1	3.2	2.5	4.2	3.9
Right upper arm	3.4	2.9	2.7	3.5	3.3	3.4	2.4	3.9	4.0
Chest	3.0	3.0	2.3	2.5	2.2	2.3	2.3	4.1	3.0
Back	2.6	2.9	2.2	2.0	2.6	2.8	2.3	4.3	3.2
Whole body	3.3	3.4	3.3	3.5	3.3	3.5	-	-	-

During the calibration the air temperature value was the same as the mean radiant temperature value of 24°C. A first calibration was performed with the nude manikin at an uniform surface temperature of 34°C and it was exposed in seating position in the center of the climatic cell from CAMBI research center at UTCB. A second one was performed for the anatomic distribution of temperature. No vertical temperature difference was observed in the chamber. The relative humidity was monitored and we found a variation of the values at around 50 % RH. Mean air velocity was measured as 0.1 m/s using an omnidirectional air velocity sensor (that will be described later in the following chapter). The heat losses and skin temperatures of the 16 parts of the body were measured.

Allocation of temperature

according to region:

Legs - 27°C

Arms - 30°C

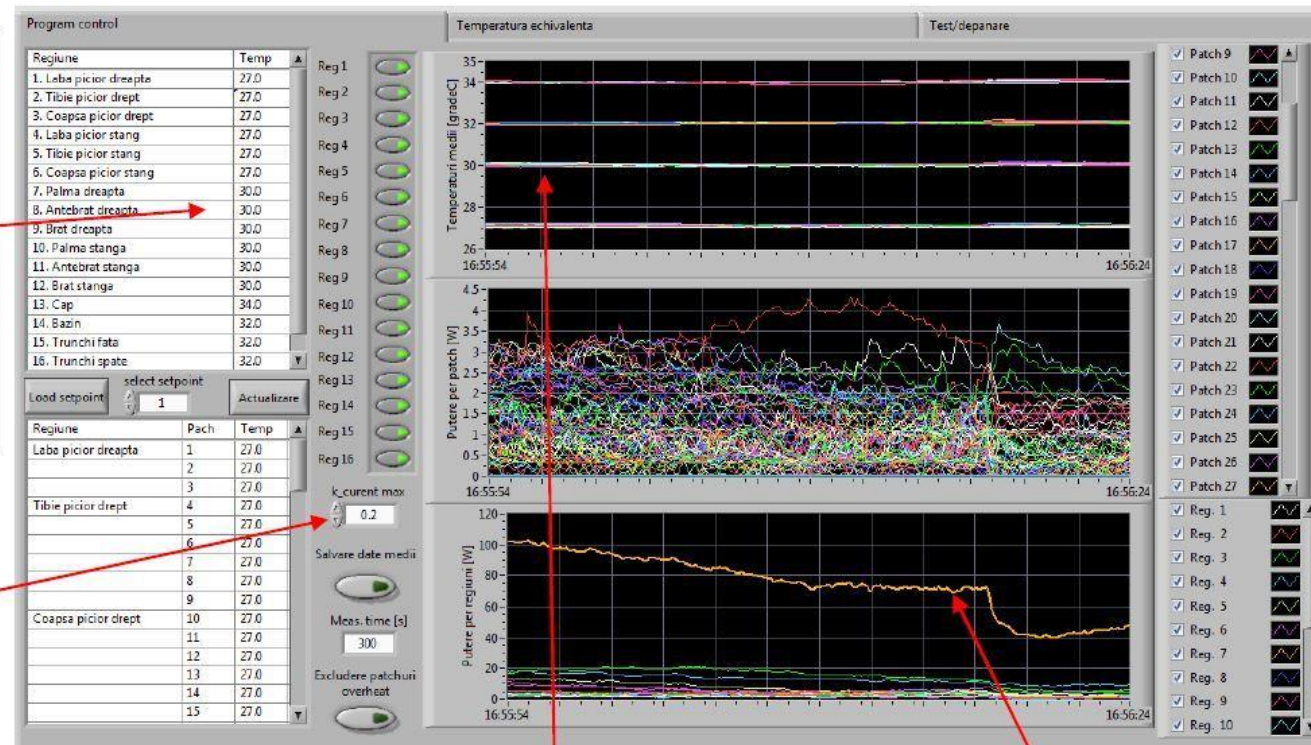
Front/back body and hip - 32°C

Head - 34°C

Thermal chamber at 24°C

Note 1: notice the maximum current of 0.2A. To avoid high overshoot do not increase this value greater than 0.3A.

Observation: the manikin's total power consumption should not exceed 380W with a current limitation of 0.2A (while the temperature is in transitory state from one set point to another), or 1700W with the maximum current of 0.9A.



Note 2: the bandwidth of the steady state that the surface temperature reaches around the set point is $\pm 0.1^\circ\text{C}$

Note 3: the overall average consumption of the entire manikin is around 80-100W when the surface temperature reaches steady stable state

Figure 51: Typical response after calibration for the Case 1 – anatomic temperature distribution

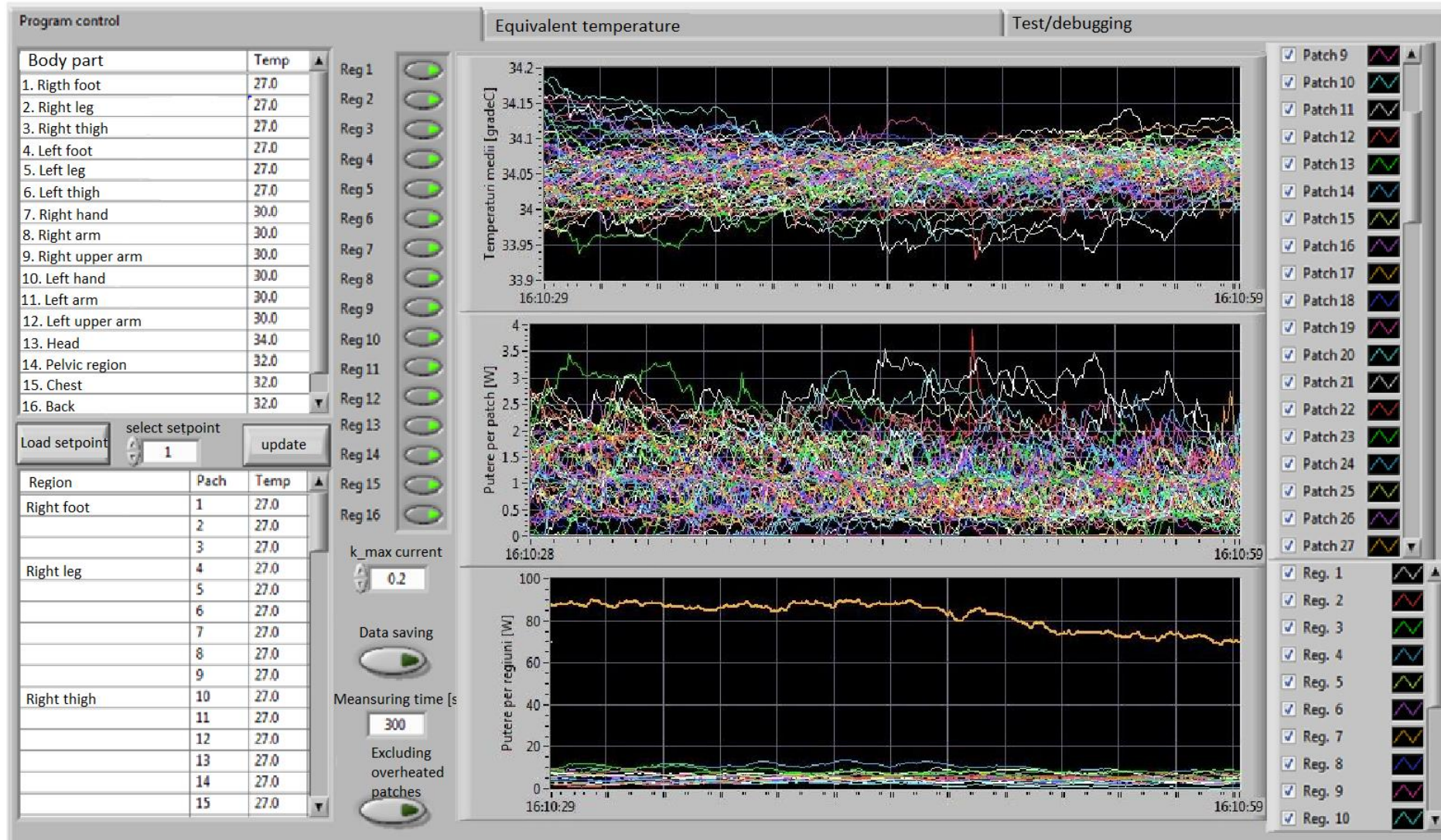


Figure 52: Typical response after calibration for the Case 2 – constant temperature distribution

CHAPTER 3 – EXPERIMENTAL SET-UP

In this chapter will be first presented the measuring principles of all used measuring instruments and in a second time a description the three main experimental set-ups is given.

A. Measurement principles and employed instruments

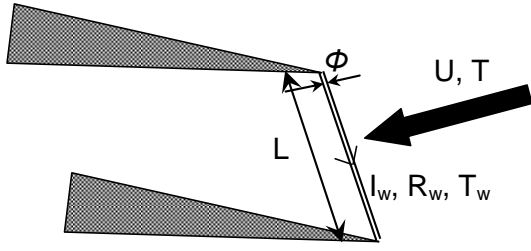
a) Air speed and velocity measurements

Air velocity measurements were performed mainly by two distinctive methods. For in cabin measurements the intrusive hot film anemometry was used. We employed both directional handheld anemometers and omnidirectional hot film probe for the air speed determination. For the characterization of elementary air flows used as boundary condition in the numerical model (as explained later), and for validation and calibration of the numerical model we used Laser Doppler Anemometry which is an optical non-intrusive measurement method.

➤ **Hot wire anemometers**

The hot-wire (hot film) anemometer, is a traditionally used to measure the instantaneous velocities of fluid flows. The method is based on the dependence of the sensor's heat transfer on the fluid velocity.

The sensor in the hot-wire anemometer is a thin metal wire (see Figure 53) or a film deposited on a quartz substrate, made of a material with a high temperature coefficient of resistance such as tungsten, platinum, platinum-rhodium, and platinum-iridium. Unlike non-intrusive optical measurement techniques, e. g. Doppler Laser Anemometry and Particle Image Velocimetry, Hot Wire Anemometry is an intrusive diagnostic method. In fact, with appropriate sensors and acquisition chains, Hot Wire Anemometry allows the resolution of the finest time scales of turbulent flows, which makes it essential to overcome some lack of information inherent in the use of other techniques. Its operating principle is based on the heat exchange between a very fine wire stretched between two pins and traversed by an electric current I and a speed flow U and temperature T (see Figure 53).



L – length of the wire ;
 Φ – diameter of the wire ;
 I_w –intensity of the electrical current;
 E_w – voltage at the wire ;
 R_w – nominal resistance of the wire
 at T_w ;
 U – flow velocity ;
 T- flow temperature

Figure 53 : Measurement principle of the hot wire

At the thermal equilibrium of the wire which represents one of the branches of a Wheatstone bridge, the electric power is equal to the losses mainly due to the forced convection of coefficient h:

$$Q = I^2 R_w = \frac{E_w^2}{R_w} = (T_w - T)\pi h \phi L \quad (17)$$

The voltage of the wire E_w is given by :

$$E_w^2 = R_w (T_w - T)\pi h \phi L \quad (18)$$

For constant wire and ambient temperatures, the wire tension is related to the fluid velocity by a simple relationship proposed by L.V. King in 1914 :

$$E_w^2 = A + BU^n ; \quad (19)$$

with : $n = 0.5$.

A and B are constants obtained by calibration of the sensor.

In practice, the hot wire anemometer can operate in two modes, Constant Current Anemometer (CCA) or Constant Temperature Anemometer (CTA). In the latter mode commonly used (Figure 54), the temperature of the wire is kept constant by the variation of the intensity of the current running through the wire. Thus, the imbalance of the bridge by the variation of the speed of the flow U is compensated by a servo system which keeps the temperature of the wire constant. The variation of the bridge voltage represents an indication of the heat flux exchanged and thus allows a direct measurement of the speed. The advantage of this technique is the improvement of the wire transfer function which becomes independent of its inertia, the bridge response being the limiting factor of the frequency response.

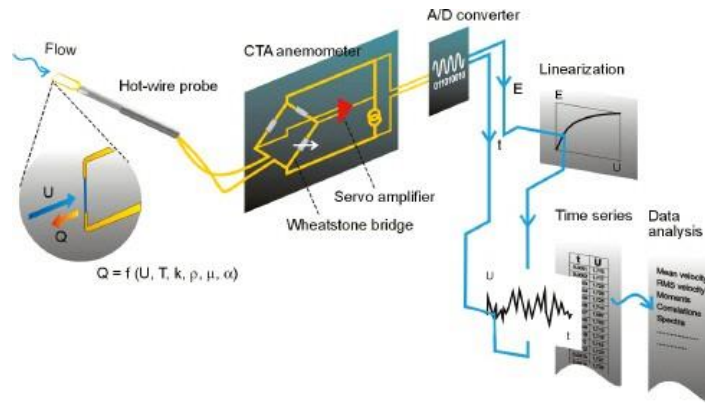


Figure 54 : Diagram of the operating principle of the acquisition chain for hot wire measurements, according to DANTEC



Range

0 to 9,999 ft/min (0 to 50 m/s)
0 to 200°F (-18 to 93°C)

Accuracy

±3% of reading or ±3 ft/min
(±0.015 m/s), whichever is greater
±0.5°F (±0.3°C)

Resolution

1 ft/min (0.01 m/s)
0.1°F (0.1°C)

Probe Dimensions

Length 40 in. (101.6 cm)
Tip dia. 0.28 in. (7.0 mm)
Base dia. 0.51 in. (13.0 mm)

a)



Velocity range	0.05-5 m/s, indicates up to 10 m/s
Accuracy	0-1 m/s: ± 2% OR* ± 0.02 m/s 1-5 m/s: ± 5% OR* 5-10 m/s: ±10% OR*
Time constant	< 0.1 s
Frequency response (90%)	2 Hz
Acceptance angle - relative to probe axis	0-1 m/s : ±160° 1-5 m/s: +50° to +130°
Temp. reading range	-20°C to +80°C
Accuracy at velocities above 0.1 m/s, radiation excluded	0°C to +45°C: ± 0.2K -20°C to +60°C: ± 0.3K +60°C to 80°C: ± 0.5K

b)

Figure 55: Hot film velocity probes used in this study: a) TSI Thermo-anemometer Straight Probe 960 and 9565 data logger, b) Dantec omnidirectional probe

During the experimental campaigns, air velocity was measured with two types of hot film anemometers. The first is a thermo-anemometer Straight Probe 960 connected to TSI 9565 data logger. The second is an omnidirectional probe included in a Comfort Sense equipment see Figure 73.

The Dantec omnidirectional 54T33 probe that we used has the great advantage that can be employed with the ComfortSense system that we will describe later on, but can be also integrated in a flexible measurement chain (Figure 56) allowing for example detailed calibration. The velocity sensor consists of two quartz spheres 3 mm in diameter, coated with a thin film of nickel and covered by a quartz layer. One of the spheres is kept at a constant over temperature relative to the other and the energy needed for maintaining this over-temperature is measured.

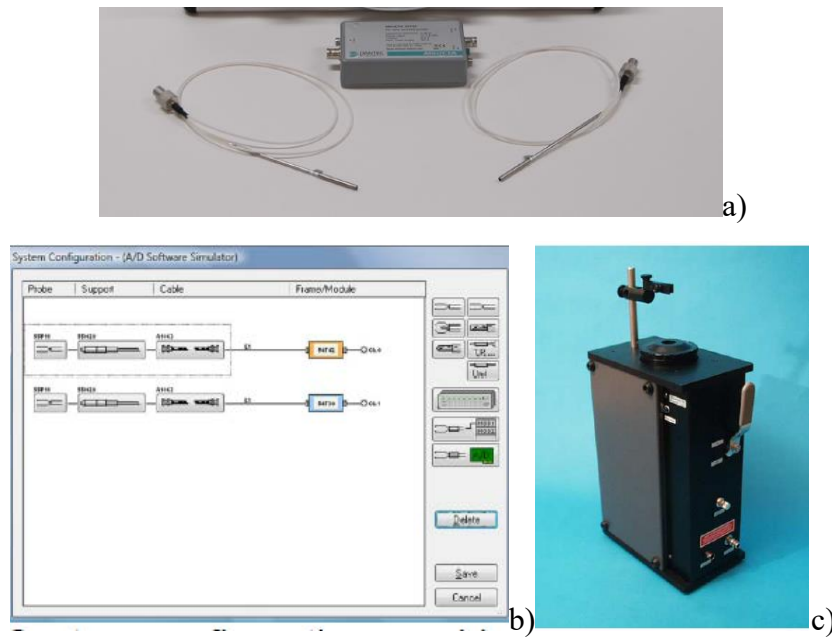


Figure 56: a) Dantec MiniCTA anemometer; b) graphical interface from StreamWare software allowing the configuration of the measurement chain; c) manual calibrator employed in our studies

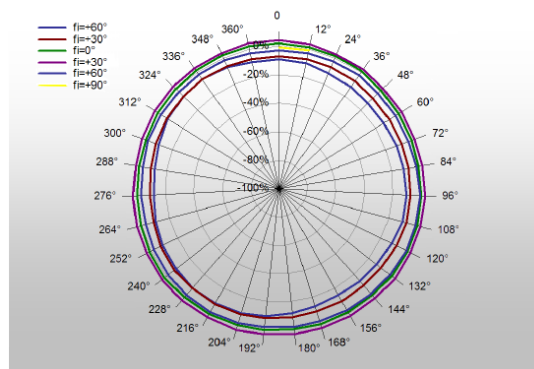


Figure 57: Typical directional characteristics for the omnidirectional 54T33 probe

We used the probe in both configurations. Both probes (TSI thermal anemometer and Dantec omnidirectional probe) were carefully verified during the experimental campaigns using the manual calibrator (Figure 56 c) in order to check their measurement accuracy.

➤ Laser Doppler Anemometry

This non-intrusive measurement technique uses the principle of the Doppler effect applied to fine non-weighty particles introduced into the flow. A laser source emits a coherent light that is separated into two beams by a prism (see Figure 58). After being focused by a lens, the two rays intercept each other and create interferences forming a network of alternating bright and dark fringes defining the measurement volume (Figure 58).

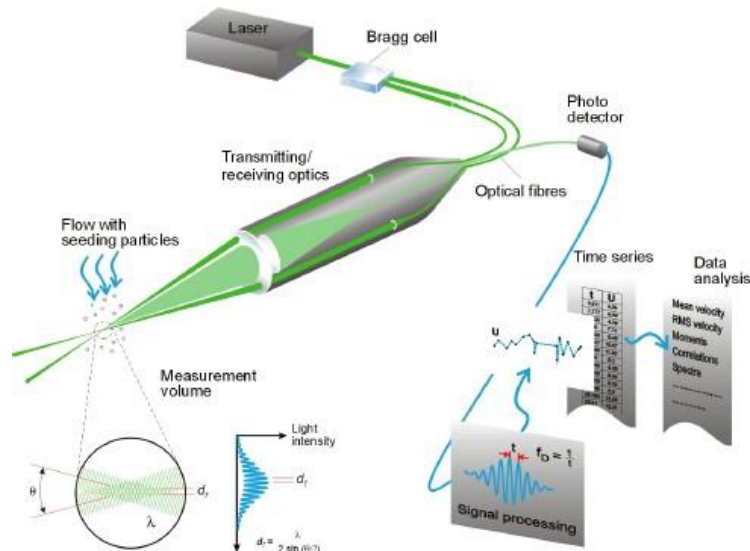


Figure 58 : Diagram of Doppler Laser Anemometry according to DANTEC

When a particle passes through the system of interference fringes, it diffuses by Doppler effect light in all directions. Part of this is recovered backscattered by a photomultiplier. The diffusion signal, associated with the wavelength λ of the fringe network, has a characteristic frequency f_{doppler} directly proportional to the velocity of the particle U and to the angle Θ formed by the two laser beams. This frequency is given by the relation:

$$\frac{2 \cdot U \sin(\theta / 2)}{\lambda} = f_{\text{doppler}} \quad (20)$$

In this relatively simple principle, the knowledge of λ and Θ on the one hand and the measurement of f_{doppler} on the other hand give access to the velocity vector of the particle whose meaning is ignored. In order to remove this ambiguity, we create a network of mobile interfrances so that the relative velocities of the particles always have the same sign (creation of a false zero in the frequency scale). This is achieved by implementing, in the measurement chain, an opto-acoustic system called a Bragg cell (see Figure 58), whose electronics are low noise and

provides up to 40MHz of offset. By introducing this scrolling of the fringes, a frequency f_{bragg} is added to all the Doppler frequencies and the signal collected by the photomultiplier becomes:

$$f_{PM} = \frac{2 \cdot U \sin(\theta / 2)}{\lambda} = f_{bragg} + f_{doppler} \quad (21)$$

In order to carry out a precise measurement, it is necessary to take care of the interference system and to ensure the homogeneity of the seeding. To achieve a powerful fringe system, it is necessary that the intensities of the two interfering beams, the "braggged" and the "non-braggged", are equal, that the shape of the beams is "Gaussian" and that the two beams cross each other. a perfect ellipse (Figure 59).

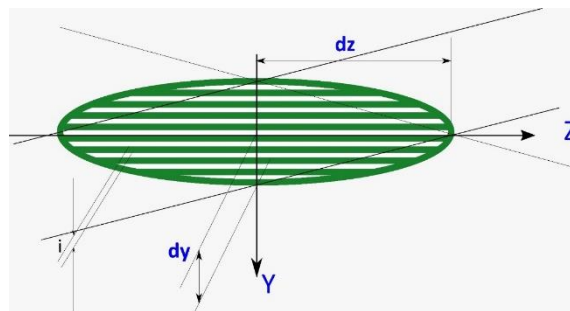


Figure 59 : Measurement volume formed at the intersection of the beams

The LDV system available at the Technical University of Civil Engineering of Bucharest, was a combination of a Flow Lite system with 1 component HeNe laser, and a 2D FiberFlow Ar-Ion. Both systems are from Dantec Dynamics (Figure 61). With this combination it was possible to measure all three components of the velocity. The three YAG solid sources emit beams of 200mW, at different wavelengths 488nm, 532nm and 561nm. These are connected to a Burst Spectrum Analyzer BSA Processor F/P 600 series.

The BSA (Burst Spectrum Analyzer) perceives the signals emitted by the particles through a certain frequency band. Thus, it functions as a bandpass filter whose terminals are set by the user. Once the bandwidth is determined, the acquisitions can be made optimal by adjusting the gain and the high voltage applied to the photomultiplier. Another important parameter that can be checked during measurement is the recording duration during which the BSA processes the information received. This time laps must be greater than the average residence time of a particle in the measurement volume, in order to avoid splitting the signal of the same particle into several distinct signals. An estimate of this passage time is achieved by the visualization of the signal on an integrated oscilloscope. The two Doppler frequencies relating to

two speed components are recorded and transferred to a computer connected to the BSA. Using a software adapted (BSA Flow Software) is carried out the conversion of the Doppler signals into velocities.

We used the BSA in "coincidence" mode. For this mode the acquisition of two channels is simultaneous, giving access to the Reynolds stress components $u'v'$, $u'w'$ or $v'w'$.

Tableau 1: Characteristics of the optical measurement system

Focal distance of the lens f		370mm		
Wave length λ		561nm	514.5nm	488nm
Angle θ		7.29°	7.29°	7.29°
Interfringe i		5.30 μ m	5.08 μ m	5.31 μ m
Beam diameter		2.20mm	2.20mm	2.20mm
Measurement volume dimensions	dX	0.12mm	0.11mm	0.10mm
	dY	0.12mm	0.11mm	0.10mm
	dZ	2.27mm	2.18mm	2.27mm
Number of fringes N_{fr}		19	21	22

This particular point represents one of the major problems of measurement by optical techniques such as Doppler Laser Anemometry and Particle Image Velocimetry. Indeed, unlike other techniques (hot wire, Pitot tube etc ...), the material support of the measurement consists of non-weighty fine particles driven by the flow and passing through the measurement volume. Special attention must therefore be paid to seeding the flow so as to reduce the errors induced by an asymmetry of their distribution. In addition, they must be small enough that they can reliably translate the movement of the fluid that carries them. Finally, another important point is related to the light scattering properties.

By using the evolution equations of a spherical particle in a viscous flow [219], we can deduce the characteristic response time τ_p at a sudden acceleration of the fluid. Theoretically, the sedimentation rate can be expressed from the Stokes drag law for spherical particles:

$$U_g = d_p^2 \frac{\rho_p - \rho}{18\mu} g \quad (22)$$

With g the gravitational acceleration, μ the dynamic viscosity of the fluid, d_p the diameter of the particle, ρ_p the density of the particles and ρ the density of the surrounding fluid. By analogy it is possible to derive an estimate for the velocity delay of the particle in a continuously accelerated fluid:

$$U_p - U_f = d_p^2 \frac{\rho_p - \rho}{18\mu} a \quad (23)$$

where a is the acceleration of the fluid, U_p the velocity of the particle and U_f the velocity of the fluid.

The velocity of the particle typically follows an exponential law if the density of the particle is greater than the density of the fluid:

$$U_p(t) = U_f [1 - e^{-\frac{t}{\tau}}] \quad (24)$$

where τ_p is the relaxation time expressed by the relation: $\tau_p = \frac{\rho_p d_p^2}{18\mu}$ (25)

Thus, for a type of surrounding fluid and for a given particle density, decreasing the size of the particles makes it possible to improve the relaxation time and therefore the monitoring of the fluid movement.

In the case of LDA measurements it is further recommended that a choice of particles having a diameter smaller than the interfringe i be used to eliminate any ambiguity related to the detection of the passage of particles in the measurement volume [220]. The diffusion of the particles depends on the ratio of the refractive index of the particles to the surrounding medium, the size of the particles which must be sufficiently large, the orientation and the shape of the particles. The choice of particle size is therefore a compromise allowing a low relaxation time and a sufficient diffusion of light. This is all the more true as the speed of the flow is great.

The distribution of particles in the flow is also an important factor. As shown by Kähler et al. [221], one of the essential problems of optical measurement techniques, is associated with the reproducibility of the generation of these particles. Indeed, the pressure, the liquid level and the fouling of the orifices of the atomizer have an effect on the size of the particles generated and on their spatial distribution at the outlet of the apparatus. This can lead to measurement errors, especially in strongly three dimensional flows [222].

For the measurements presented here, we chose for tracer olive oil that was atomized using a Flow Tracker 700 PR generator from Dantec using compressed air at a maximum pressure of 2bar. The analysis of the particle size distribution, which we carried out using a Grimm 1.108 optical counter (Figure 60), shows that their size is variable. However, 50% of particles have a diameter of between 1 and 2 μm . In addition, 91% have a diameter smaller than the interfringe i of the green and blue beams of the LDA system used. Measurements are thus more precise since the noise related to the ambiguities of visibility of the particles is reduced and a more efficient

detection of the Doppler frequencies by the BSA follows [220]. In order to avoid too much variation of this distribution, we have made sure to reload the atomizer very regularly to maintain a relatively constant oil level.

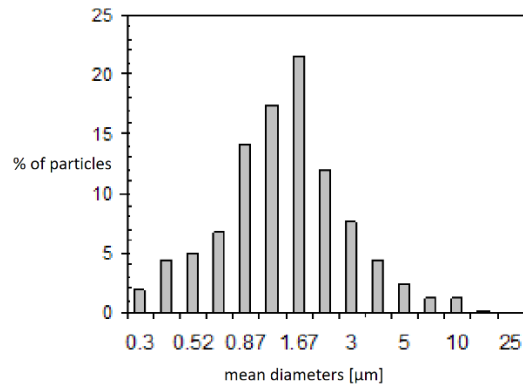


Figure 60 : Histogram of the repartition of oil particles from the same atomiser as the one used in this study [9]

Since we wanted to use the LDV system in 3D configuration we had to superpose the measurements volume of the 2D Fiber Flow system and of the 1D Flow Lite system. This procedure consists in aligning the probes, such that the beam intersection for the three components to be approximatively in the same “point.” Using a pinhole device (Figure 63), the probe position was fine changed in order to align the intersection points. The pinhole has an opening just large enough that the focused beam can pass through. Fine adjustment of the superposition of the measurement volumes was made using a power meter connected to a photodiode placed behind the pinhole, thus maximizing quantitatively the power of light passing through the pinhole for each beam.

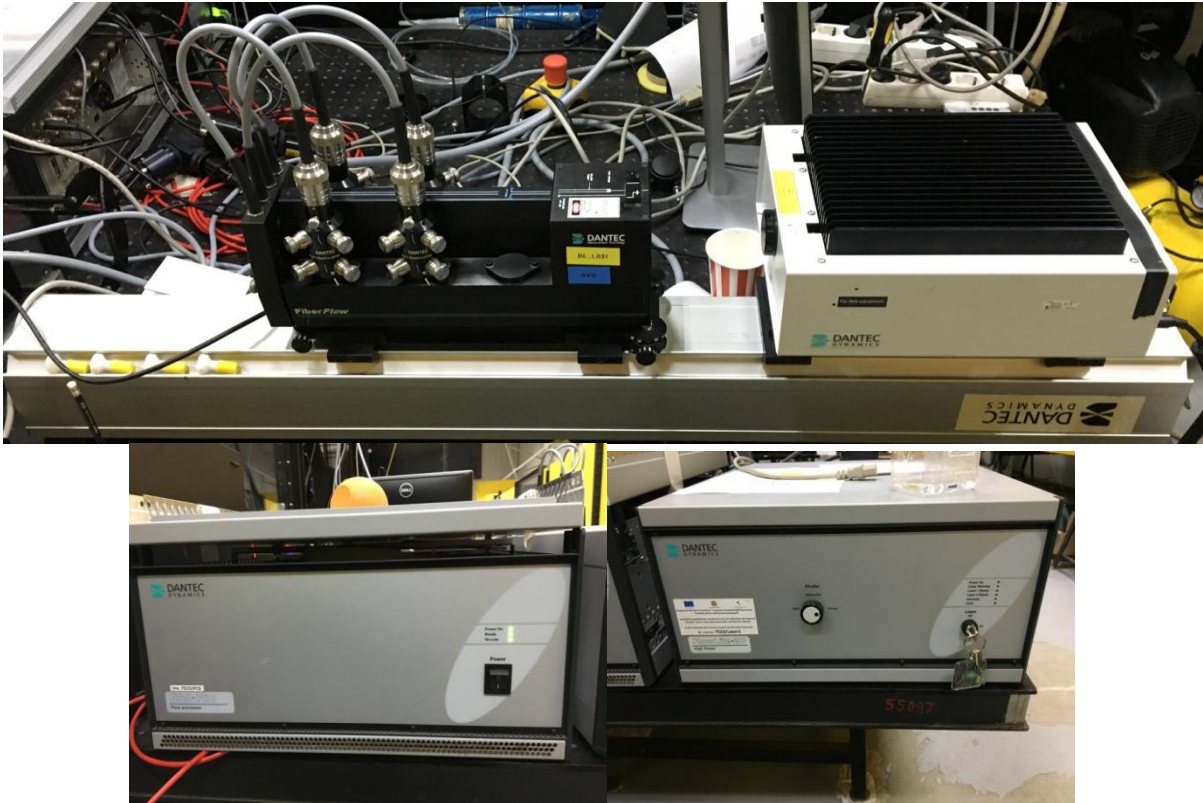
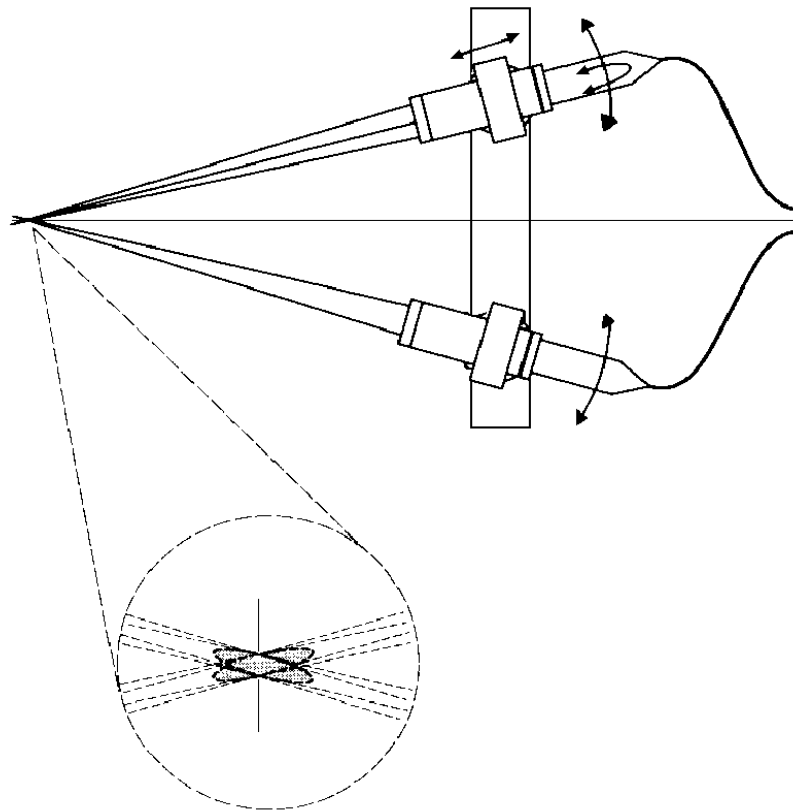


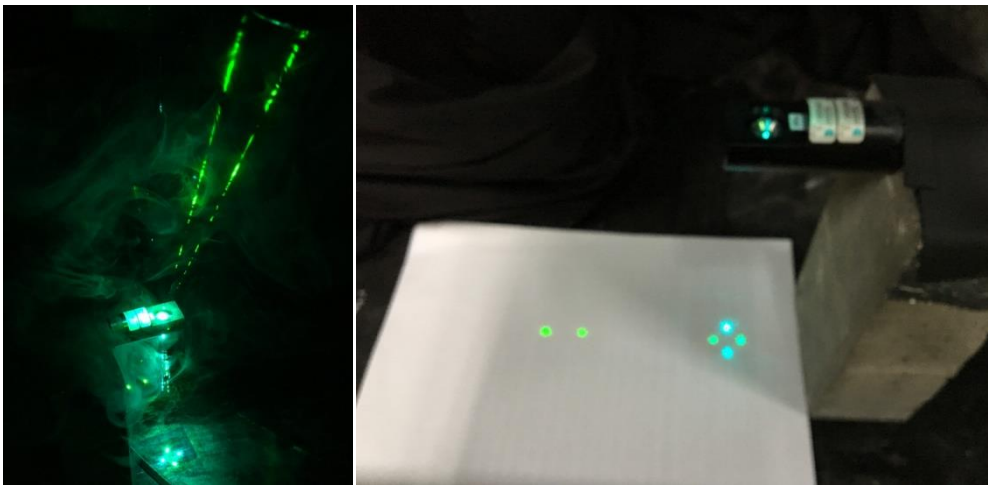
Figure 61: 3D-LDA system used in this study



Figure 62: 3D traverse system used in this study



a)



b)

Figure 63: a) Probe volume alignment principle for LDV 3D measurements, b) Laser beams passing through the pinhole

b) *Temperature measurements*

➤ **Thermocouples**

Since no special considerations are put upon the temperature measurement, we have decided to use common. They were installed to record air temperature variation as well as various surface temperatures inside the studied vehicle.

A thermocouple consists of two wire legs made from different metals. The wire legs are welded together at one end, creating a junction. This junction is where the temperature is measured. Temperature measurement by the thermocouple is based on the Seebeck effect, in other words, a conductor generates a voltage when subjected to a temperature change. The measurement of this voltage requires the use of a second conductive material generating a different voltage for the same temperature variation. When the junction experiences a change in temperature, a voltage is created. The voltage can then be interpreted using a calibration curve to calculate the temperature (Figure 64).

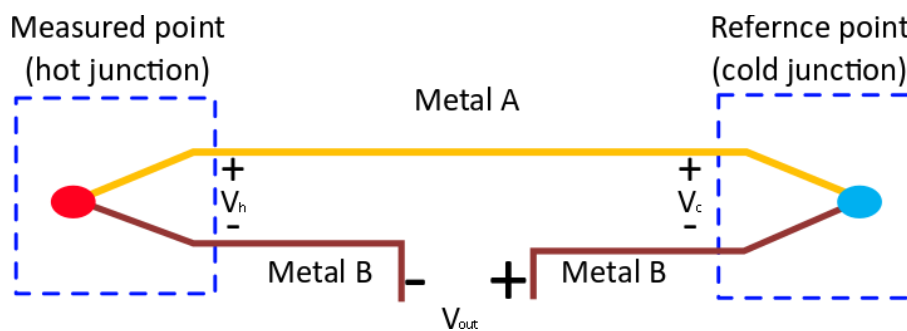


Figure 64: Measurement principle of the thermocouple

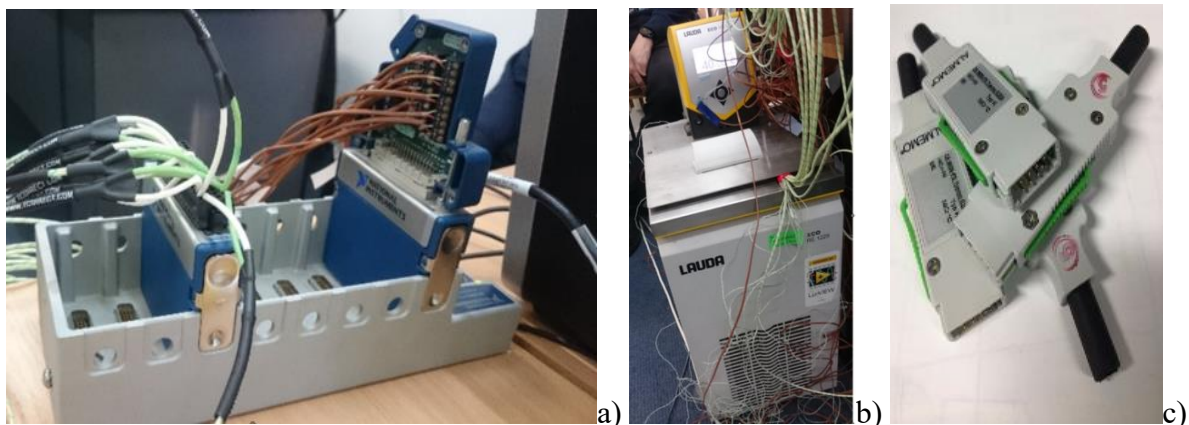
NiCr-Ni thermowire T 190-2



Accuracy: NiCr-Ni class 2*
 Insulation : PVC (wires and sheath)
 Operating temp.: -10°C to +105°C
 Wire diameter: 0.5 mm
 External diameter: approx. 2.2 x 3.4 mm

NiCr-Ni thermowire per meter with PVC insulation **Order no. LT01902**
 NiCr-Ni thermowire sensor, welded tip, with ALMEMO® connector 1.5 m long **Order no. FTA3902**
 ALMEMO® connector 5 m long **Order no. FTA3902L05**

Figure 65: Characteristics of Almemo K- type thermocouple T 190 – 2



Operative range	The temperature depends on the sensor type.
	Humidity 5 to 98 % RH
Measuring ranges	Temperature -20 to +80 °C
	Accuracy ±0.3 K at 23°C±5K
	±0.4 K at 10 to 40°C
	±1.3 K at -20 to 80 °C
	Reproducibility: typ. ± 0.1K
	Humidity 5 to 98 % RH
	Accuracy ±1.8 % RH at 23 °C ±5K, 20 to 90 % RH
	±2.3%RH at 23°C±5K, 10..<20%RH
	Hysteresis: typ ± 1% RH.
	Atmospheric pressure 300 to 1100 mbar
	Accuracy ±2.5 mbar (700 to 1100 mbar) at 23°C±5K
	Calculated quantities see 7.2.1
Atm. pressure compensation	0 to 6500 mbar (programmable)
Refresh rate	2 seconds for all four channels
Connector colors	2 colors, light gray and dark gray, red lever
Standard baud rate	115.2 kbaud
Supply voltage	6 to 13 VDC
Current consumption	5 mA
Sleep mode on the device	Possible (for extensions a 1s delay is necessary)

Figure 66: a) NI board; b) thermostatic bath; c) Almemo D6 FHAD46 connectors, d) characteristics of Almemo D6 FHAD46c connectors

Usually, an accuracy class is specified for every thermocouple sensor. The accuracy applies within the above specified range of validity. The operative range is specified for every sensor – depending on its construction. Various types of thermocouples are available; these can be distinguished in terms of their temperature range, sensitivity, and in particular, their compatibility with the test substance. The most popular thermocouples are the NiCr-Ni (type K). We used a K- type thermocouple T 190 – 2 from Almemo (Figure 65).

Before using them, all used thermocouples were calibrated. To this end, we employed a thermostatic bath LAUDA ECO RE 1225 (Figure 66 a) to create an environment with a stable and known temperature. We immersed all the thermocouples in the thermostatic bath and we

measured the voltages of each thermocouple for different temperatures. The free end was connected to a NI board (Figure 66 b), which make connection between the thermocouple and PC. We were then able to plot the calibration curve for each sensor.



Figure 67: Almemo data loggers used in this study: a) Almemo 710; b) Almemo 2690-8; c) Almemo 2890-9

Calibrated thermocouples were connected to Almemo D6 FHAD46c connectors (Figure 54 c). Almemo D6 FHAD46c connectors are in fact temperature transducers based on the fully adjusted sensor element FH0D46-Cx; this comprises a capacitive temperature, a barometric atmospheric pressure sensor, and an EEPROM. This means that the sensor element can be replaced or adjusted quickly and easily without any loss in accuracy.

The barometric atmospheric pressure sensor is used to determine atmospheric pressure directly at the measuring location. On this basis atmospheric pressure compensation can then be performed automatically in the connector. Information stored in the integrated EEPROM ensures that the sensor element can be adjusted quickly and easily. Calibration curves can be stored also via the Almemo software.

These connectors allow the connection with Almemo data loggers. In our laboratory are available various Almemo data loggers, during the experimental campaigns being used 4 of them: two Almemo 710 with 10 plug-in ports; one Almemo 2690-8 with five plug-in ports; and two Almemo 2890-9 with 8 plug-in ports.

➤ Thermistors

A thermistor is a solid-state transducer made from thermally sensitive semiconductor-based metal oxides with metallized or sintered connecting leads onto a ceramic disc or bead. This technology is allowing to modify its resistive value in proportion to small changes in

temperature.

Negative temperature coefficient of resistance thermistors, or NTC thermistors reduce or decrease their resistive value as the operating temperature around them increases. NTC thermistors are the most commonly used type of temperature sensors. NTC thermistors have a negative electrical resistance versus the temperature (R/T) relationship. The relatively large negative response of an NTC thermistor means that even small changes in temperature can produce significant changes in its electrical resistance response.

Table 5: Technical data of all temperature sensors used

Name	ALHBORN FHAD46-E1	TSI 986	IAQ Calc 7545	Comfort Sense 54T35	AXIOMET AX-DT200
Type	thermocouple	thermistor	thermistor	thermistor	thermistor
Range	-20 ÷ 60 °C	-10 ÷ 60°C	0 ÷ 60°C	-20°C ÷ 80°C	-20°C ÷ 80°C
Precision	10 ÷ 40°C: ±0.4°C -10 ÷ 80°C: ±1.3°C	±0.5°C	±0.6°C	±0.5°C	±0.3°C
Resolution	-	0.1°C	0.1°C	0.1°C	0.1°C



Figure 68: Temperature and relative humidity sensors AXIOMET AX-DT200

Along with the 45 thermocouples used for instrumenting the real vehicles in different set-ups that will be described in the following parts of this chapter, we used also several thermistors such as: 24 AXIOMET AX-DT sensors (measuring also the temperature and the humidity), the TSI 986 probe which is a thermo-anemometer, the temperature probe embedded in the TSI IAQ Calc 7545 data logger, the temperature probe from the 54T35 from the Comfort Sense instrument.

In Table 5 are presented the technical characteristics of all temperature sensors used in this study.

c) *Relative humidity*

➤ **Capacitive humidity sensors**

For applications where cost, space, or fragility are relevant, electronic sensors are used, at the price of a medium accuracy. Capacitive hygrometers are the widest used. For this type of sensors, the effect of humidity on the dielectric constant of a polymer or metal oxide material is measured. With calibration, these sensors usually have an accuracy around 2% in the range that is comprised between 5–95% RH. Without calibration, the accuracy is two to three times worse. These capacitive sensors are robust against all effects such as the water vapour condensation and high temperatures during short lapses of time. In general, the capacitive sensors are subjected to pollution, drift and aging effects, but are suitable for many applications. The measurement principle relies on the hygroscopic properties of a polymer that is contained between two electrodes. The thin polymer sheet absorbs or releases water vapor, depending on the relative humidity of the room. The dielectric properties of the thin sheet of polymer depend on the amount of water vapor that is stored in it. Therefore, depending on how the relative humidity changes, the dielectric properties of the sheet change and thus the capacity of the sensor changes.

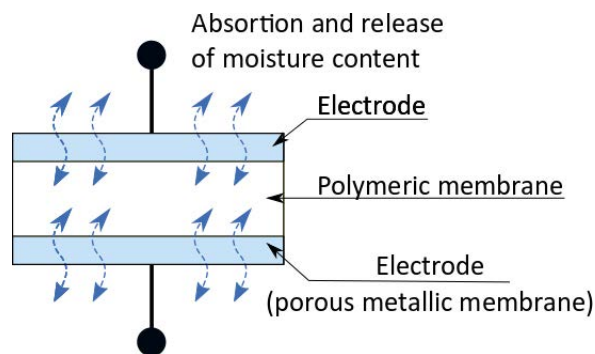


Figure 69: Measurement principle of the polymeric capacitive humidity sensor

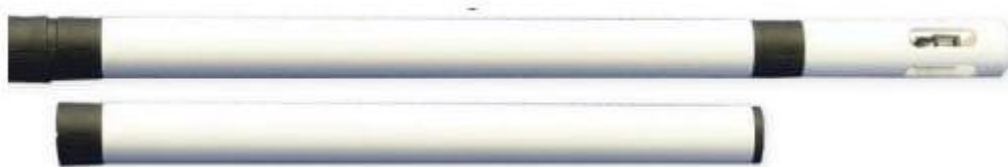


Figure 70: Relative humidity probe FHA646-E1 from Ahlborn

Three types of capacitive humidity sensors were employed in this study: the relative humidity probe FHA646-E1 from Ahlborn, the relative humidity probe from the Comfort Sense system, and AXIOMET AX-DT sensors. In Table 6 are presented the technical characteristics of all temperature sensors used in this study.

Table 6: Technical data of the relative humidity sensors used

Name	ALHBORN FHA646-E1	Comfort Sense 54T37	AXIOMET AX-DT200
Type	capacitive	capacitive	capacitive
Range	5 ÷ 98% RH	0 ÷ 100% RH	0 ÷ 100% RH
Precision	± 2% RH	±2% RH	0÷10°C:+2%; 10÷30°C:+1.5%; 30÷45°C:+2% RH
Resolution	-	0.1% RH	-

d) *Comfort measurements*

➤ Comfort Sense

In this thesis classical comfort evaluation using a measurement device was made with a Comfort Sense system developed by Dantec Dynamics, that determines the comfort in accordance with the following standards EN 13182, ISO 7726, ISO 7730, ASHRAE 55 and 113. The system can provide measurements of air speed, temperature, operating temperature, determining the PMV, PPD and DR indices. In general, the system consists in a main unit that can have up to 16 inputs for measuring probes and different types of probes that measures the parameters mentioned above. The main unit processes and transmits the information to a personal computer (PC) to read and save the data. Thus, it has built-in A/D (analogical/digital) converter with a USB 2.0 interface, microprocessors and other microelectronic components that are required to perform the operations. Also, for cases where there is no possibility to connect the unit to an electricity network the manufacturer offers the possibility of a power battery. The main unit with the input modules and the battery can be seen in Figure 71.

The probes used measure parameters like air temperature, speed or humidity. This are needed to calculate the draught sensation, the PMV and PPD indices or the operative temperature. For draught measurements an omnidirectional sensor is required that has a frequency response of at least 2Hz. The omnidirectional probes used in this system measures both air velocity and temperature. The probe used for measuring the draught is made of a thin film, for measuring the velocity and a small thermistor with fast response, which measures the temperature.

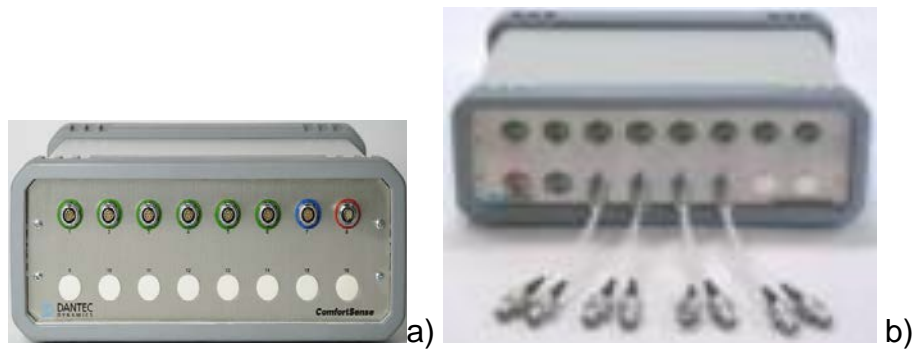


Figure 71: Comfort Sense system: a) Central unit; b) Input module and assembly [223]

The velocity sensor consists of two quartz spheres of 3 mm diameter, wrapped with a thin nickel sheet that is covered with a layer of quartz. The measurement principle was presented earlier in the first paragraph of this chapter. One of the spheres is maintained at a higher temperature than the other while the electrical energy required maintaining it at that higher temperature is measured. A special algorithm makes the conversion between the measured temperature, heat loss, convection coefficients, and air velocity. These two spheres are protected by a cage to prevent mechanical damage. Due to the simple and thin construction, obstruction of the air flow is minimal. The probes can be mounted on tripods or crossing beams systems, which can be static or dynamic during measurements. Comfort Sense has also compact flexible probes, designed to be placed on manikins, for determining the draught sensation (Figure 72). The speed and temperature probe, can measure respectively velocities between 0.1÷30 m/s either temperatures in the ranges -20÷80°C.

The operative temperature probe has an ellipsoidal shape, with a diameter of 56 mm and a length of 160 mm. The sensor element is a nickel wire coil which measures the average temperature on the ellipsoidal surface. The shape and size of the sensor facilitates the direct measurement of the operative temperature, its shape being chosen because different surfaces, that are cooler or warmer, may have similar effects on the sensor as it would have on the human body. The sensor can simulate a person standing when he is positioned vertically, a person seated when it is bent at a 30° angle to the vertical, and a person lying down when positioned horizontally. The measuring element has the surface color and structure as close as possible to an average-dressed person with normal clothing.

The relative humidity probe has a capacitive sensor which principle and characteristics are given in the previous paragraph.



Figure 72: Comfort Sense probes

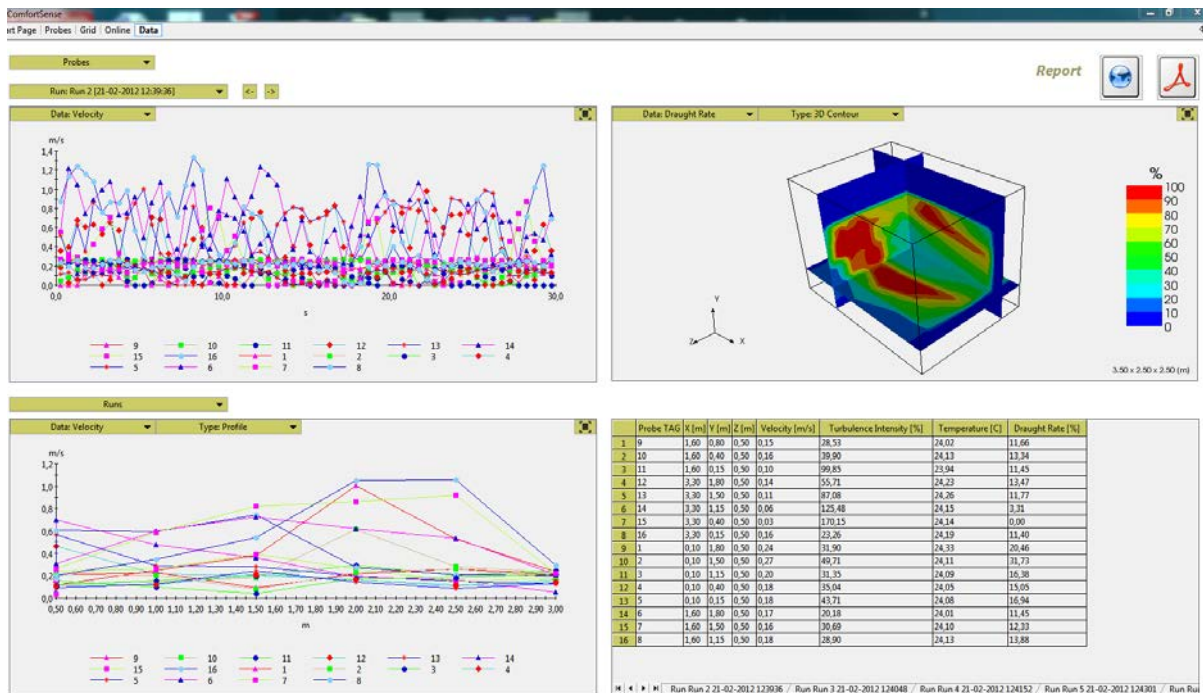


Figure 73: Interface of the Comfort Sense software

Dedicated application software is provided by the manufacturer in order to read and make a graphical presentation with the data received by the probes. The results can be presented in a 2D and 3D graphic. The software includes a library with probes to be easily identified and used. After selecting the probes, the software allows their placement in space and a route if they do not have a fixed position. The temperature and humidity range are defined by the user and the program notifies the user when these values are exceeded. The software performs parameter linearization, statistical calculations and spreadsheet or graphical presentations. It can export the results as text or for programs like Office Excel (Figure 73).

➤ **Thermal manikin measurements**

The thermal manikin that was used in this study represents the object of the entire Chapter 2. In the case of our manikin, the equivalent temperature represents an indication of thermal comfort obtained by evaluating the power consumption of a region of the manikin. Due to the PWM control signal which commutes on and off between maximum and minimum voltage, the power consumed by the thermostatic system was calculated by creating a calibration slope between PWM duty-cycle and the power calculated as a point by point mean of a single pulse period. The voltage drop on the patch was calculated differentially by measuring with the Hantek DSO5102P oscilloscope the voltage difference at the leads of the whole circuit from which it was subtracted the voltage difference on the transistors. The current consumed by the patch was measured with a TH5A current transducer and converted in equivalent temperature.

$$\theta_{ech} = \theta_{reg} - \frac{P}{S \cdot h_{calc}} \quad (26)$$

where:

θ_{ech} = equivalent temperature;

θ_{reg} = mean temperature of surface region calculated using a sliding average over a preset period of time;

S = surface area of manikin's region;

P = mean power consumption calculated using a sliding average over a preset period of time;

h_{calc} = convection coefficient calculated with the previous relation at constant environment temperature (θ_{ech}) of 24 °C and manikin's surface temperature controlled at 34 °C or with an anatomic distribution [67, 145].

Experiments revealed that by modifying the environmental temperature from 20 to 40°C the changes in power consumption were indistinguishable Figure 30. In Figure 74 are shown values of equivalent temperature obtained with the thermal manikin at different flow rates. This test was made in the controlled environment of the climatic chamber.

Compared to classical measurement systems offering the possibility of estimating the global PMV, the thermal manikin gives the advantage of assessing at a local scale and predicts local sensation, through the equivalent temperature or through a derived local PMV. The thermal manikin represents a powerful assessment tool for the thermal comfort analysis in laboratory settings but also and in real field case studies it is a method of investigating local discomfort through the local distributions of the equivalent temperature of the segments of the manikin. This kind of representation allows for instance, the assessment of the environmental parameter's uniformity. In Figure 74, is presented an example of equivalent temperature distributions for

several air flows defined by Nilsson [67, 69, 224] or in the standard EN ISO 14505/2 [14] for a studied air grille used in operating rooms.

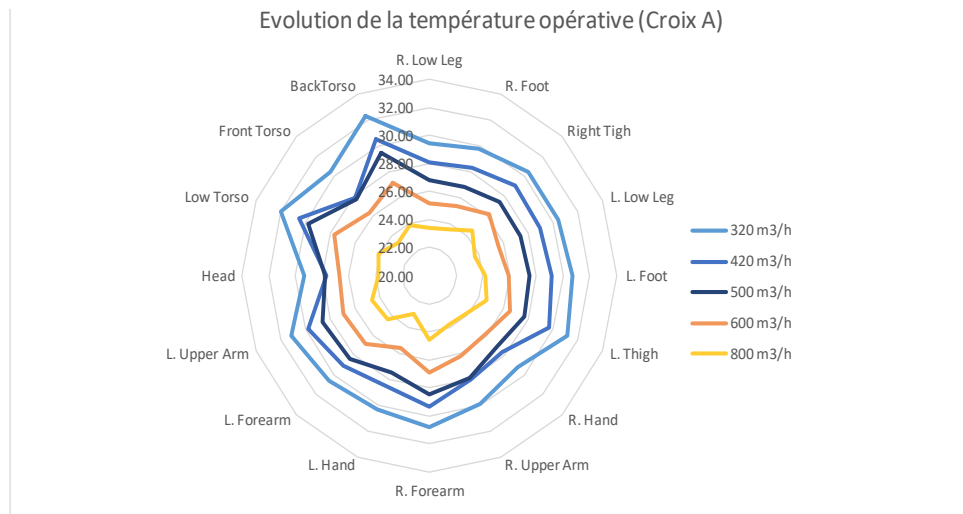


Figure 74: Example of θ_{ech} distributions obtained from the thermal manikin data for different air flow rates in the climatic chamber [225]

Table 7: Ranges of equivalent temperatures for different thermal sensations - winter season [69, 146]

Thermal state	Too cold	Cold but comfortable	Neutral	Warm but comfortable	Too hot
Body part	Equivalent temperature [°C]				
whole body	<18.2	18.2 ÷ 21	21 ÷ 24	24 ÷ 26.7	26.7<
scalp	<12	12 ÷ 17	17 ÷ 22.2	22.2 ÷ 27.5	27.5<
face	<11.9	11.9 ÷ 17	17 ÷ 22.2	22.2 ÷ 27.5	27.5<
chest	<11.8	11.8 ÷ 17.5	17.5 ÷ 23.5	23.5 ÷ 30.1	30.1<
upper back	<11.5	11.5 ÷ 17.5	17.5 ÷ 23.5	23.5 ÷ 30.1	30.1<
left upper arm	<11	11 ÷ 16.8	16.8 ÷ 22.2	22.2 ÷ 27.8	27.8<
right upper arm	<11	11 ÷ 16.8	16.8 ÷ 22.2	22.2 ÷ 27.8	27.8<
left lower arm	<11	11 ÷ 16.8	16.8 ÷ 22.2	22.2 ÷ 27.8	27.8<
right lower arm	<11	11 ÷ 16.8	17.2 ÷ 23.5	23.5 ÷ 30	30<
left hand	<11	11 ÷ 18.5	18.5 ÷ 25.5	25.5 ÷ 32.8	32.8<
right hand	<15	15 ÷ 20	20 ÷ 26	26 ÷ 32	32<
left thigh	<17.9	17.9 ÷ 22.2	22.2 ÷ 26.5	26.5 ÷ 31	31<
right thigh	<17.9	17.9 ÷ 22.2	22.2 ÷ 26.5	26.5 ÷ 31	31<
left calf	<17.9	17.9 ÷ 22.2	22.2 ÷ 26.5	26.5 ÷ 31	31<
right calf	<17.9	17.9 ÷ 22.2	22.2 ÷ 26.5	26.5 ÷ 31	31<
left foot	<17.9	17.9 ÷ 22.2	22.2 ÷ 26.5	26.5 ÷ 31	31<
right foot	<17.9	17.9 ÷ 22.2	22.2 ÷ 26.5	26.5 ÷ 31	31<

Interpretation of the equivalent temperature in terms of perception of thermal sensation and

thermal comfort can be made using following tables proposed by Nilsson [67, 145]. Depending on t_{eq} obtained with the manikin, thermal sensations at different levels can be classified. The asymmetric thermal conditions such as in the vehicle compartment make the determination and evaluation of local t_{eq} particularly useful.

These values were obtained by the author during several measurement sessions using human subjects feedback during a period of 1 h exposure to a variety of asymmetric thermal conditions under typical winter (heating system) and summer conditions (cooling system). The environmental parameters were kept constant during the hour. During the measurements there were used two different thermal manikins to assess the thermal sensation [67, 145].

Table 8: Ranges of equivalent temperatures for different thermal sensations - summer season [69, 146]

Thermal state	Too cold	Cold but comfortable	Neutral	Warm but comfortable	Too hot
Body part	Equivalent temperature intervals [°C]				
whole body	<20	20 ÷ 23.7	23.7 ÷ 26.7	26.7 ÷ 30	30<
scalp	<11	11 ÷ 18.8	18.8 ÷ 26.7	26.7 ÷ 34.1	34.1<
face	<11	11 ÷ 18.8	18.8 ÷ 26.7	26.7 ÷ 34.1	34.1<
chest	<16.9	16.9 ÷ 22.2	22.2 ÷ 28	28 ÷ 33.6	33.6<
upper back	<17.2	17.2 ÷ 22.8	22.8 ÷ 28.5	28.5 ÷ 34.1	34.1<
left upper arm	<16	16 ÷ 21.6	21.6 ÷ 27	27 ÷ 32.6	32.6<
right upper arm	<16	16 ÷ 21.6	21.6 ÷ 27	27 ÷ 32.6	32.6<
left lower arm	<16	16 ÷ 21.6	21.6 ÷ 27	27 ÷ 32.6	32.6<
right lower arm	<16	16 ÷ 21.6	21.6 ÷ 27	27 ÷ 32.6	32.6<
left hand	<14.2	14.2 ÷ 20.9	20.9 ÷ 27.7	27.7 ÷ 34.5	34.5<
right hand	<14.2	14.2 ÷ 20.9	20.9 ÷ 27.7	27.7 ÷ 34.5	34.5<
left thigh	<17	17 ÷ 21.1	21.1 ÷ 25.2	25.2 ÷ 29.9	29.9<
right thigh	<17	17 ÷ 21.1	21.1 ÷ 25.2	25.2 ÷ 29.9	29.9<
left calf	<17	17 ÷ 21.1	21.1 ÷ 25.2	25.2 ÷ 29.9	29.9<
right calf	<17	17 ÷ 21.1	21.1 ÷ 25.2	25.2 ÷ 29.9	29.9<
left foot	<17	17 ÷ 21.1	21.1 ÷ 25.2	25.2 ÷ 29.9	29.9<
right foot	<17	17 ÷ 21.1	21.1 ÷ 25.2	25.2 ÷ 29.9	29.9<

B. Experimental set-ups and measurement protocols

The three main experimental set-ups used during the study were conceived in order to respond to the logical steps that we employed during the conception of our numerical models that will be presented in Chapter 4. In a first time a simple car-cabin numerical model was designed and in our quest of methods of calibration of the correct boundary conditions, we used temperature and air flow measurements in a real car-cabin. In a second time, more complex tests, including the presence of the thermal manikin and of two types of air diffusers were performed both numerically and experimentally. An intermediary experimental campaign considered the

characterization of the three-dimensional isothermal air jets discharged from the diffusers from the dash board of the cabin. Considering the sake of coherence in the development of the present chapter, we will first present the real vehicle that represented the basis of all the experimental set-ups, then we will present the two configurations that were used to inject the numerical models with real boundary conditions and to perform experimental thermal comfort evaluations, and we will end the chapter with the description of the particular experimental set-up used for the elementary air jet flows.

a) Description of the real vehicle

In this study we used a Renault Megane hatchback car (Figure 75) from 2003. It is equipped with a 1.4 liter engine, has 5 seats and 5 doors.



Figure 75: Picture of the real vehicle that was employed during the study

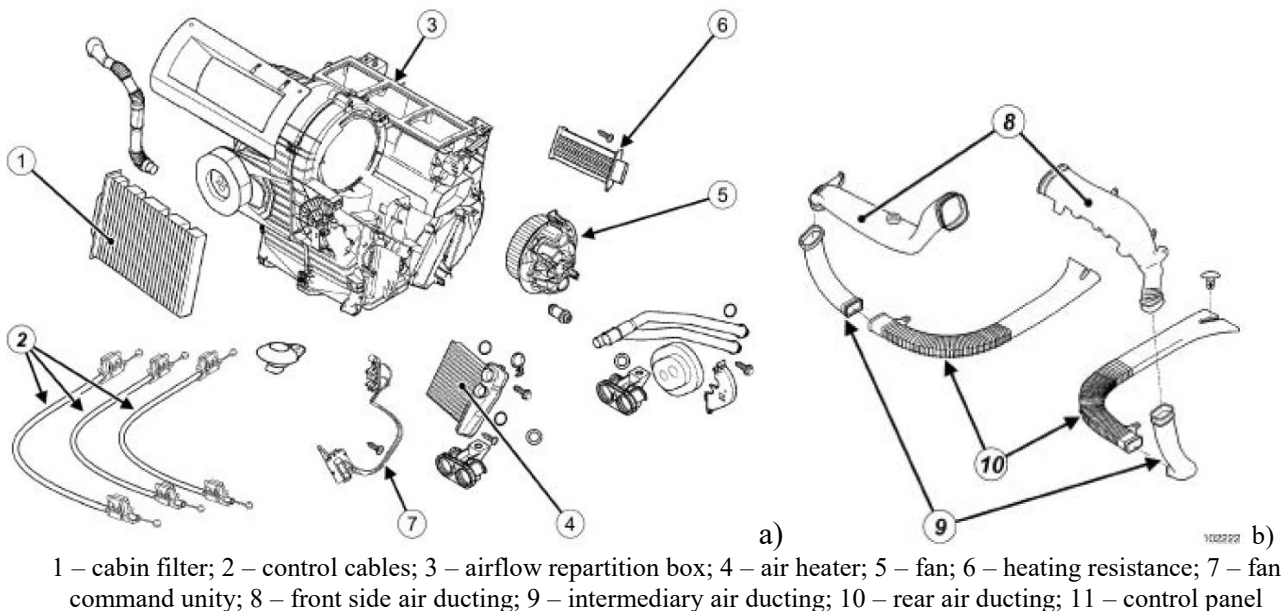
The in-cabin environment is heated or cooled with a manual ventilation/conditioning system. The ventilation and air conditioning system is composed of: the air treatment system (Figure 76a, b c and d). The air that was previously heated or cooled is introduced in the cabin via the ducting system and the discharge air diffusers. The interior environment is considered in this case as one zone thereby, we consider three types of air diffusers, each serving a different purpose.

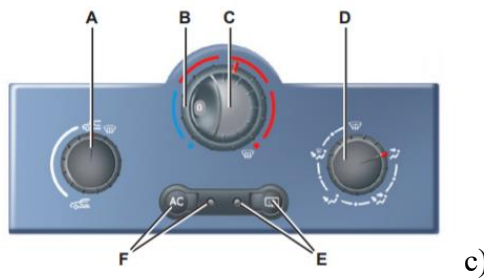
A first category of air diffusers is located at the dashboard level directed to the windshield serving to defrost/dehumidifying the glass. Another category of diffusers is mounted in the dashboard and directed to the passengers of the front part of the vehicle used usually to

cool or to heat the front or the rear part of the cabin. The third type of diffusers are located at the bottom of the front and rear part of the cabin and directed to the legs of all passengers and used mainly to heat the cabin environment during the winter.

The ventilation and air conditioning system is entirely manual for this car model and does not allow imposing a set-point for the in-cabin temperature, but to modify the inlet temperature via the position of marker on a visually intuitive scale on the control panel presented in Figure 76 c – *B scale*. The same control panel allows modifying the air flow rate entering the cabin on a step by step commutator allowing 5 positions - Figure 76 c – *C scale*. The first one is 0 – corresponding to “no ventilation” mode. The other 4 positions that we named hereafter respectively I, II, III and IV. The *A scale* in - Figure 76 c allows switching between the recirculating mode and full fresh air mode with intermediary steps. The *D scale* in - Figure 76 c allows to choose the air distribution strategies, for instance: the air might be fully discharged on the wind shield, the air might be fully discharged through the dashboard diffusers, the air might be fully discharged through the bottom (level at the legs) diffusers, the air might be discharged in the same time through the bottom (level at the legs) diffusers and through the dashboard diffusers, and finally, the air might be in the same time discharged through the bottom (level at the legs) diffusers and through the dashboard diffusers.

During all the experimental campaigns in this study we only considered the case where the air is fully discharged through the dashboard diffusers.





A – air recirculation command; B – air temperature regulator; C – flow rate regulator; D – air distribution regulator; E – heating the rear window command; F – air conditioning system command.

Figure 76: Ventilation/conditioning system of the employed vehicle: a) air treatment system, b) ducting system, c) control panel of the ventilation/conditioning system



Figure 77: Disposal of the air diffusers on the dashboard

b) Preliminary characterization of the air distribution system of the vehicle

All the experiments were made with the car kept inside a hall as shown in in Figure 78. The main reason for this choice was related to our desire to maintain extended steady state conditions and to decouple the in-cabin conditions from solar radiation and to protect measurement equipment from the outdoor meteorological conditions. As a result, indoor thermal conditions varied much slower than outside.



Figure 78: The vehicle placed in the experimental hall during the measurements

Prior to the campaigns of thermal comfort evaluation, inlets flow rate was carefully measured for three running speeds of the fan - V1, V2 and V3 corresponding to positions (stages) I, II and II of the air flow controller. Data regarding the air flow rates were available in the technical manual of the vehicle, but we wanted the real distribution of the flow rates to the discharge diffusers, since that the ducting system is not symmetric. For the fourth step of the fan we did not perform this type of measurements given the very high values of the in-cabin velocities that we did not considered during this study.

In order to evaluate the values of the volumetric flow rate, for each considered diffuser and each velocity step of the fan, we performed integration of the radial air speed profiles measured with the omnidirectional probe from the Comfort Sense system that was described earlier. Our choice to employ the omnidirectional probe rather a directional hot film anemometer was related to the fact that this method is more accurate at very low velocities and for use when the flow direction has strong three dimensional characteristics.

Two TSI AIRFLOW air cone hoods were employed as displayed in Figure 79 and carefully glued in front of the diffuser. Air speed values were recorded in 65 points as shown on the measurement grid presented in Figure 80. The free ends of the air cones have both the diameter of 10 cm. The total sampling time of the air speed in each considered point was 10

seconds. Air flows resulted from the integration of these values on the surface of the free end of the air cones (see Figure 79).



Figure 79: images during air velocity measurement

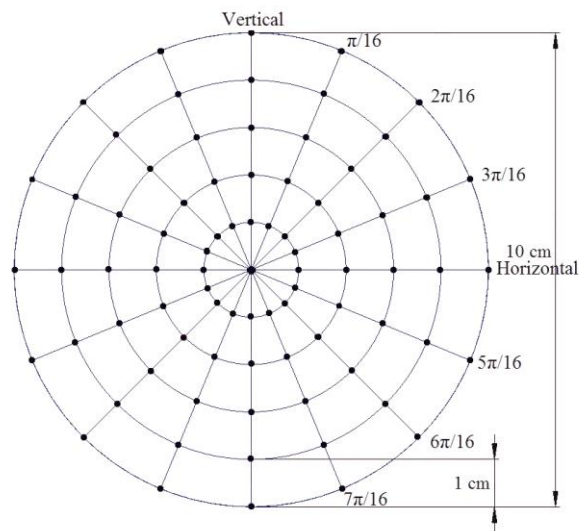


Figure 80: Measurement grid for the evaluation of the volumetric flow rate for each considered diffuser

In Figures 81-83 are represented the air speed profiles obtained for each of the three dash-board diffusers at various fan running speeds. In Table 9 are given the volumetric flow rates and mean air speed values corresponding to each velocity step. From this table it can be observed an important difference between the values obtained for the two lateral air diffusers. This difference is also visible in all three previous figures representing the measured air speed profiles for the lateral diffusers at all three considered air speeds. This is due to the different ducting geometry constrained by the positioning inside the dashboard. The left side ducting is shorter due to the driving wheel and to other embedded devices (such as the displaying panels of the dashboard). This is the first time at our knowledge that such a detailed characterization of the flow rates discharging from the dashboard of a real car is proposed in the literature.

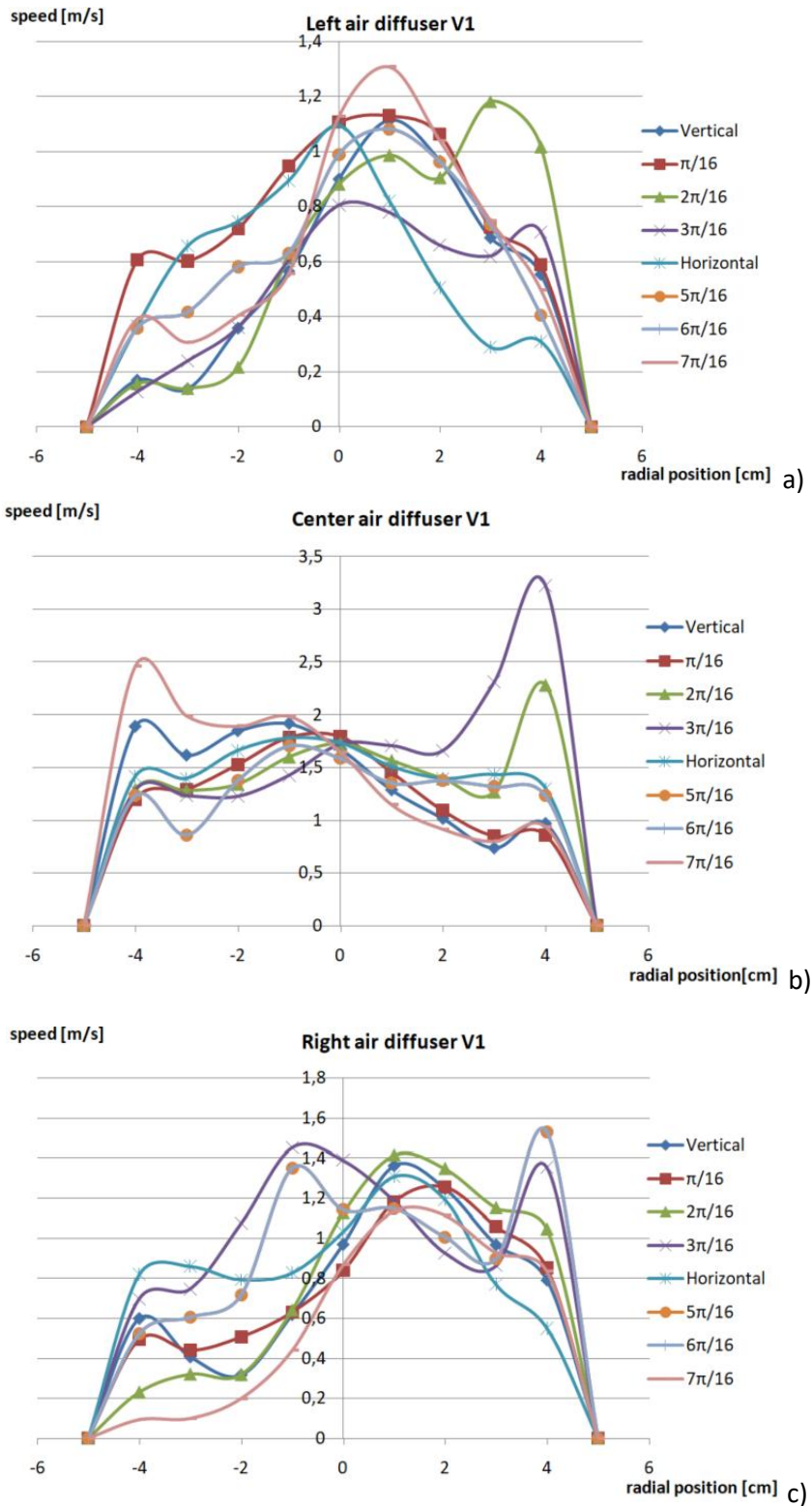


Figure 81: Measured air speed profiles using the air cone for V1 – position I of the fan speed regulator: a) left side diffuser, b) central diffusers, c) right side diffuser

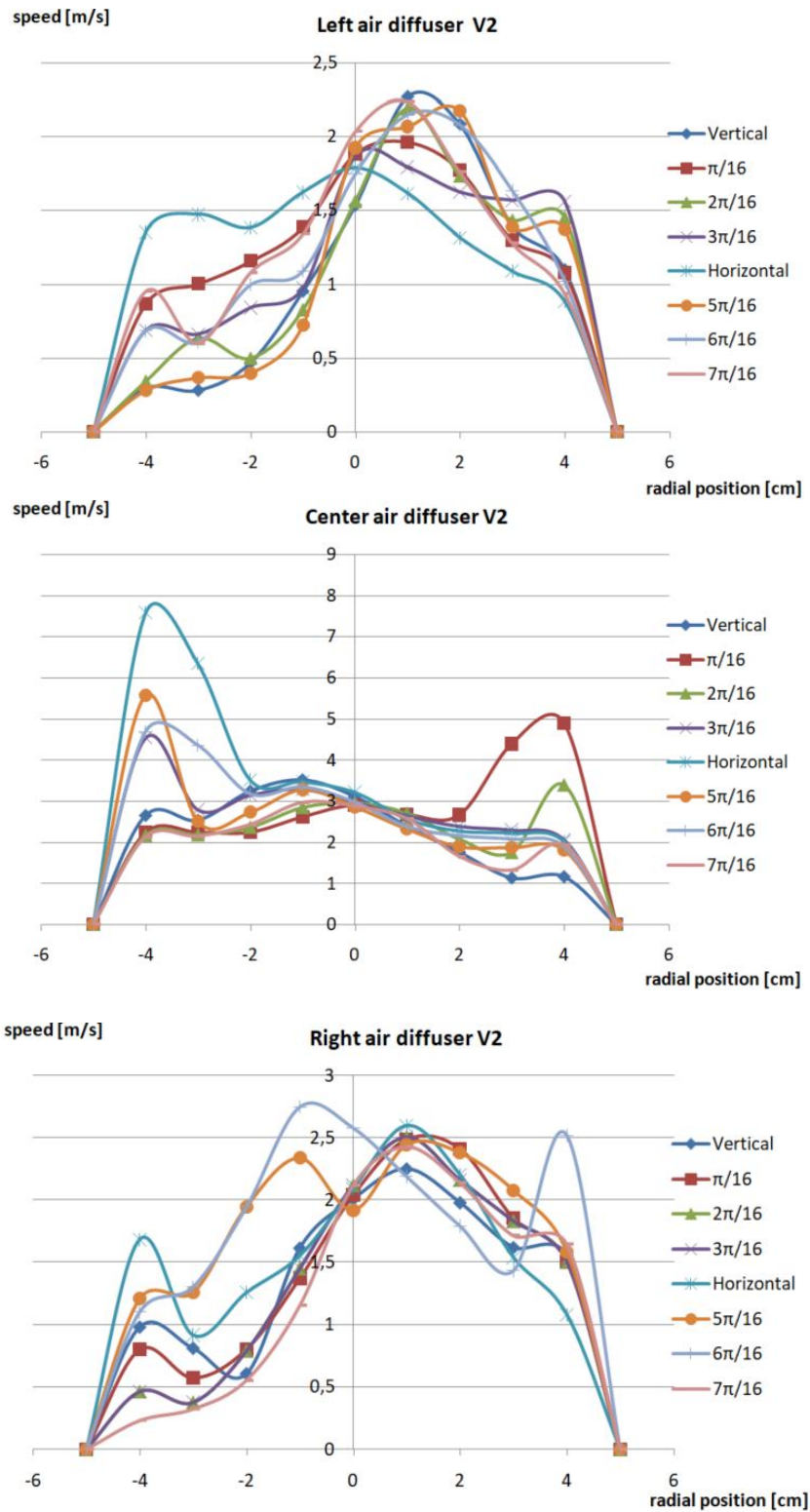


Figure 82: Measured air speed profiles using the air cone for V2 – position II of the fan speed regulator: a) left side diffuser, b) central diffusers, c) right side diffuser

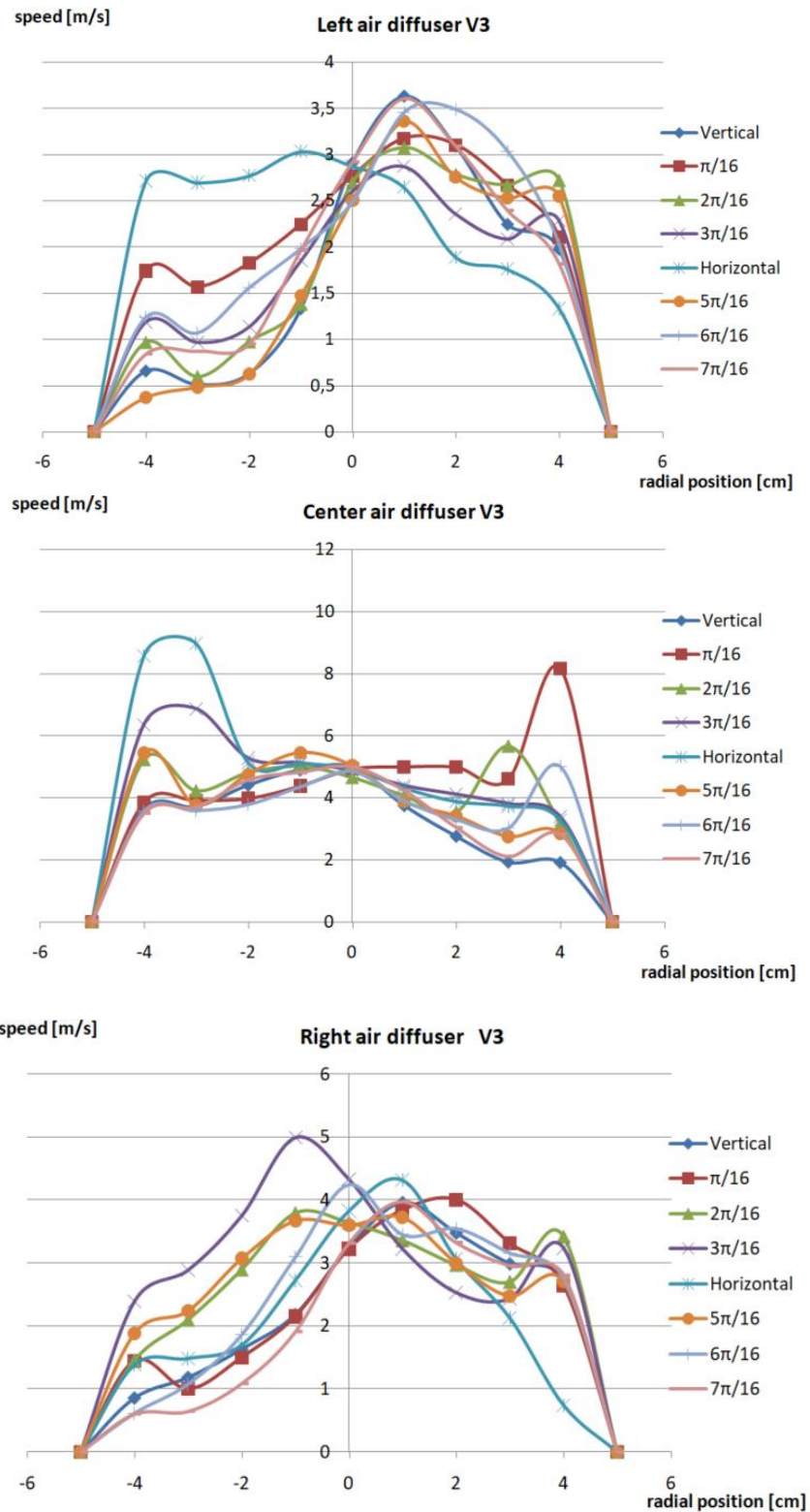


Figure 83: Measured air speed profiles using the air cone for V3 – position III of the fan speed regulator: a) left side diffuser, b) central diffusers, c) right side diffuser

Table 9: Inlets flow rate and mean velocity

	Parameter	V1	V2	V3
Central diffuser	Mean velocity [m/s]	1.66	3.29	4.85
Right side diffuser		0.86	1.58	2.50
Left side diffuser		0.60	1.19	2.02
Central diffuser	Q [m ³ /s]	0.0131	0.0258	0.0380
Right side diffuser		0.0068	0.0124	0.0197
Left side diffuser		0.0047	0.0093	0.0158
Central diffuser	Q [kg/s]	0.0160	0.0316	0.0466
Right side diffuser		0.0083	0.0152	0.0241
Left side diffuser		0.0057	0.0114	0.0194

c) *First in-cabin experimental set-up*

This experimental set-up and the related measurement protocol were designed for calibrating and validating our first numerical modeling approach of the vehicular cabin as it will be shown in the next chapter. In this case, we modeled only the cabin, without passengers, the objective being to obtain a reasonable model of this complex geometry enclosure, and to have experimental data for both imposing boundary conditions and for verifying the numerical results.

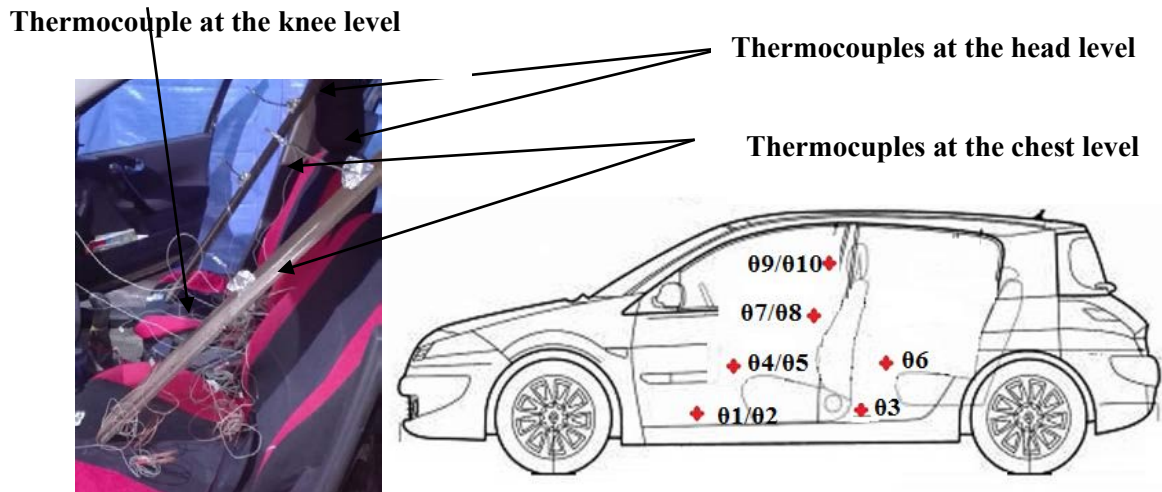


Figure 84: Positions of the thermocouples at the place of passengers' body parts

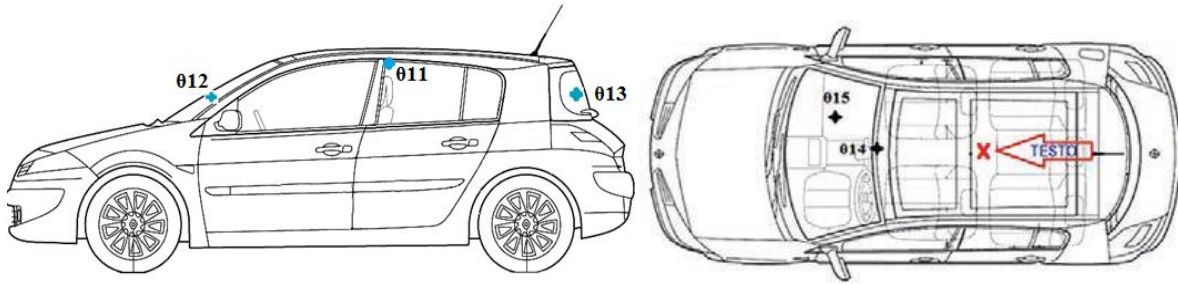


Figure 85: Measuring points for the thermocouples on different cabin surfaces

Table 10: Positioning coding for each thermocouple during the first experimental set-up

No	Place
01	Diver foot
02	Front Passenger foot
03	Back foot
04	Driver knees
05	Front Passenger knee
06	Front Passenger back knees
07	Driver chest
08	Front Passenger chest
09	Driver face
010	Front Passenger face
011	Ceiling
012	Windshield
013	Rear window
014	Vent
015	Dashboard

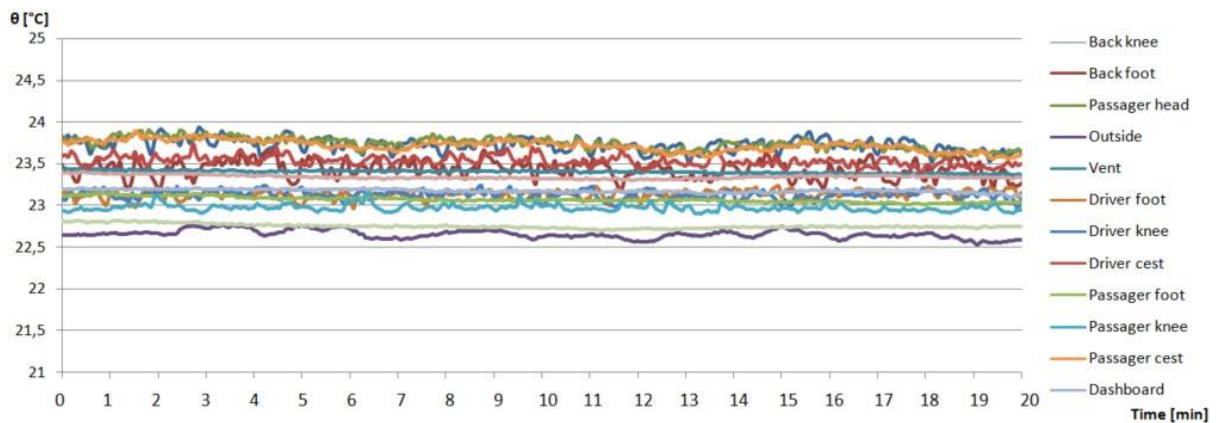


Figure 86: Example of temperatures evolution inside and outside the cabin on a period of 20 minutes considered for V1 – I stage of the fan velocity

A network of 15 K-type thermocouples was used to monitor the evolution of the temperature on different interior surfaces of the vehicle and in different points in the air

where body parts of the driver and of the front passenger could be placed (i.e. head, chest, knee, foot). The positions of the thermocouples are displayed in Figures 74 and 75. Other sensors (omnidirectional velocity probe and its associated thermistor, relative humidity probe and operative temperature probe) were also installed in the vehicle cabin. A total number of 4 measurement sessions was considered, corresponding to intervals of 45 minutes, one for each fan velocity stage.

During this first experimental campaign we considered only the air distribution in the car through the original set of diffusers of Renault Megane, taking care that their ailerons should be oriented in horizontal position.

Measuring sessions were conducted when outdoor temperatures were temperatures relatively similar, so both ambient and cabin temperature had steady-state values between 21-24.5 °C. For the choice of our boundary conditions we considered only cases where the temperature evolutions inside the cabin were constant in time. A typical example of temperatures evolutions inside and outside the cabin is presented in Figure 86. It can be seen that the variation during the considered measurement session is insignificant for all the measurement points.

d) *Second in-cabin experimental set-up*

A second experimental set-up and measurement protocol were designed, in a more complex way for the calibration and the validation of our final numerical models. The objective of the experimental campaign was multiple:

- to record in different conditions, like previously, the evolutions of the temperatures on the surfaces inside the cabin and in different points in the air;
- to test the effect on different flow rates and cold air temperatures on the air distribution inside the cabin;
- to « measure » thermal comfort indices using the Comfort Sense system and the thermal manikin previously developed for different flow rates and two geometries of air diffusers in cooling conditions, and thus to provide data for validation purposes of the numerical models developed in Chapter 4;
- to perform subjective thermal comfort evaluations for the same flow rates and the two geometries of air diffusers in cooling conditions allowing a direct comparison between the subjective response and the data obtained from the dedicated measurement systems;

- to provide data recording air speed values and temperatures in different points inside the car cabin for validation purposes of the numerical models developed in Chapter 4.

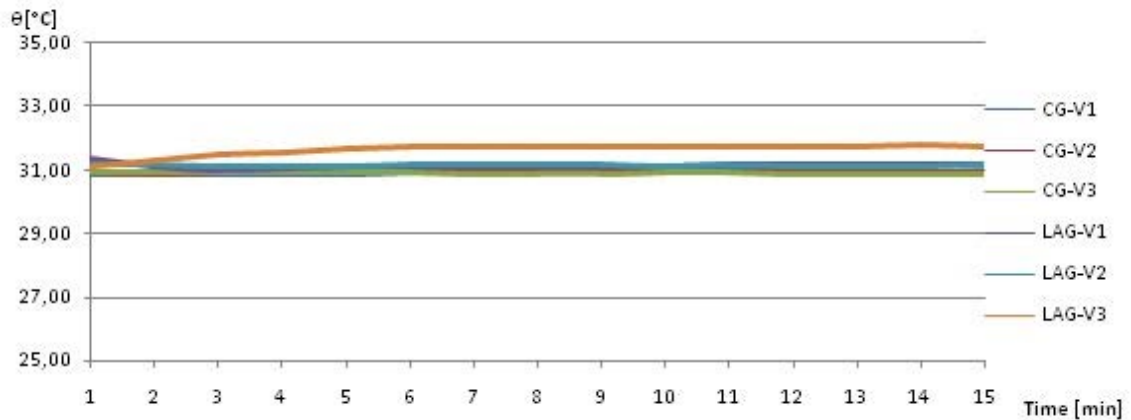


Figure 87: Example of temperature evolution inside and outside the cabin on a period of 20 minutes considered for V1



Figure 88: Photos of the instrumented interior of the car cabin

Measurements were performed made during two days with similar external conditions. Inside the hall where our experimental car was placed, the air temperature variation was between 28 and 31°C. A typical example of a of temperatures evolutions inside and outside the cabin is presented in Figure 87. Before each measurement session, the vehicle was turned on for 30 minutes as required by ISO 14505 standard.

In this case, inside the cabin we installed 41 thermocouples (see Figure 88). Three thermocouples were placed at the dash-board air diffusers level, one in the center, one on the

left side air diffuser and another in the right side air diffuser. Another nine thermocouple were placed on the interior surfaces: e.g. dashboard, windshield, sides windows, ceiling, floor, top cover of the trunk and rear window. Another fifteen thermocouples were placed in the zones corresponding to sensible parts of the passengers as head, chest, abdomen, knee and ankles. The rest of fourteen thermocouples were placed on a horizontal line passing from the middle of the height of the central air diffusers in a median plane between the two front seats and on a vertical line from the floor to the ceiling in the center of the car, also in the median plane. In Figure 89 are presented the thermocouples' positions inside the car cabin.

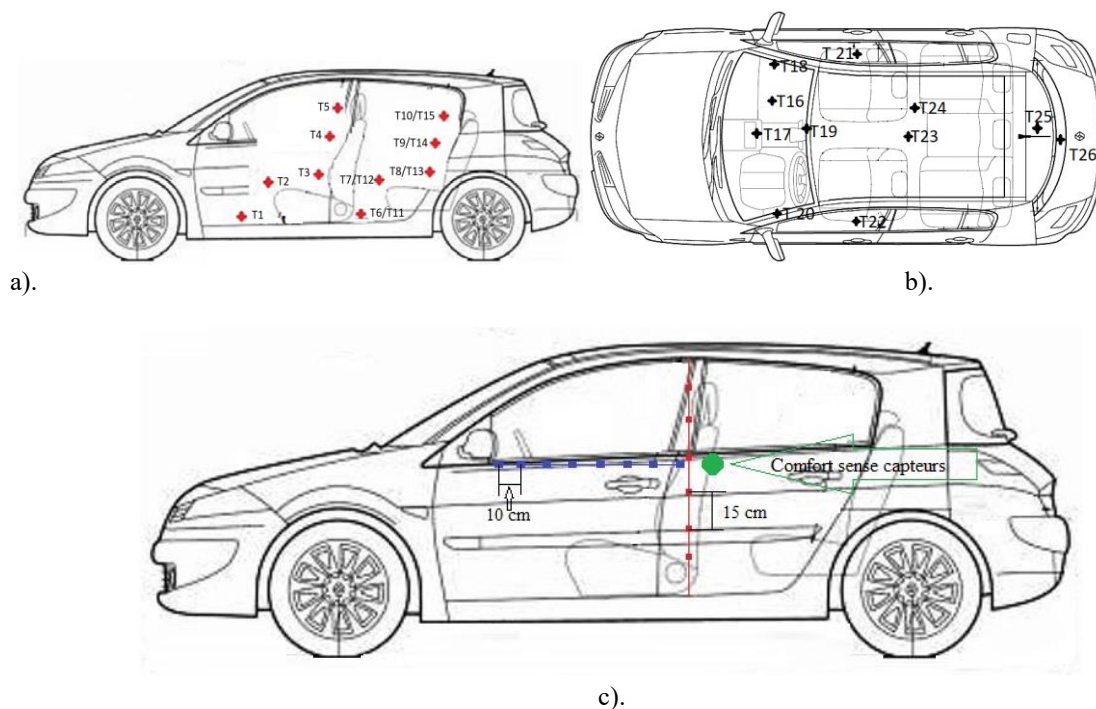


Figure 89: K-type thermocouples distribution in cockpit: a). the place of human body parts; b). on surfaces; c). on vertical and horizontal axes in the center of the car and comfort sense probes

As explained previously, during this this experimental campaign we also performed thermal comfort evaluation using both subjective and measurement methods.

For the determination of thermal comfort indices, we used the Comfort Sense system allowing the direct assessment of PMV, PPD and DR indexes. In the next step we used the thermal comfort manikin that we presented earlier. These measurements sessions were combined with the subjective evaluation sessions as follows.

The ISO 14505-3 gives guidelines and specifies a standard test method for the assessment of thermal comfort of a cabin using human subjects. The questionnaire used in

The sample is not very large but given that this approach is very time consuming, we wanted to respect the minimum prescriptions indicate by the ISO 14505-2 standard in which is specified that the minimum sample of subjects for in cabin environment evaluation is 8.



Figure 91: Ventilation system control panel corresponding to the three considered fan velocity steps

The sample of subjects has ages comprised between 27 and 49 years. 15 persons are males and 6 persons are females. The 21 sessions were respectively divided around two sets of air diffusers: baseline – original air diffusers of the Renault Megane car, and a new innovative set of dashboard air diffusers that will be described later on. Thus, the first 10 sessions were dedicated to the first set of air diffusers and the 11 others to the second set of air diffusers. In this case also we considered that the ailerons of the two sets of air diffusers are oriented in horizontal position.

Each session was completed in 45 minutes, respectively 15 minutes for each step of the fan speed controller corresponding to V1, V2 and V3 as in Figure 91. This way, in the first 15 minutes, the ventilation system was set on the step I, in the following 15 minutes it was set on step II, and in the last 15 minutes being set on step III. The subjects were asked to take the drivers' seat in the running engine car placed in the experimental hall. Each surveyed person had been given a set of 12 questionnaires to fill-out during the entire session of 45 minutes. They were instructed to fill-out the first questionnaire at the very next moment after entering the car. Each of the following questionnaires was filled-out at intervals of 5 minutes. They were instructed to change the velocity step after 15 minute and to fill-out additional questionnaires right after the change of the velocity step.

A total number of 252 questionnaires were filled-in and the time for filling out the questionnaire was considered to be about 30-60 sec. The persons interviewed have been informed briefly about reasons for the questionnaire. The general information requested in the questionnaire was: the date and the time of filling, information about the person who had completed the questionnaire (age, sex and weight). For the assessment of the thermal sensation the subjects had to choose an option on the 7-points rating scale and they also had to choose the thermal preference at the time of filling-in the questionnaires. They had to put a

note on the acceptability of the thermal environment and on the local thermal discomfort.

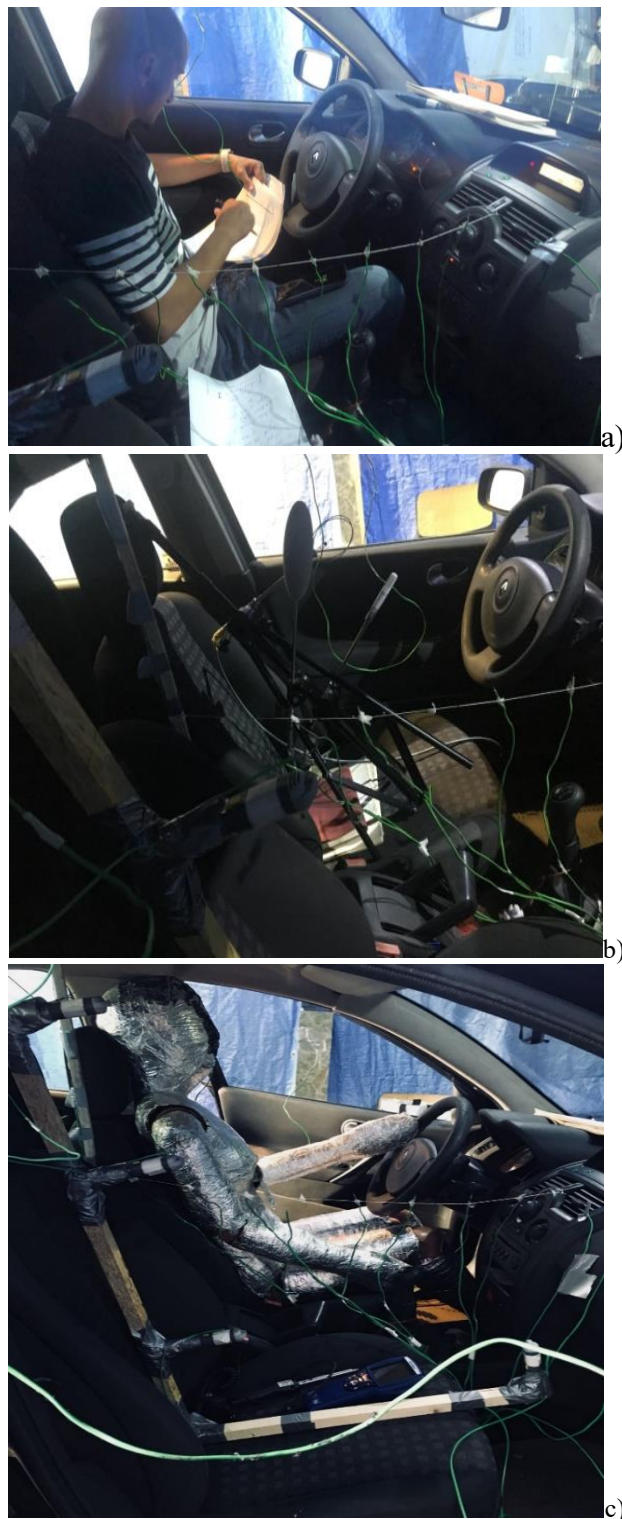


Figure 92: Pictures during the thermal comfort experimental campaign: a) human subject in the car, b) Comfort Sense system on the passenger's place, c) thermal manikin on the passenger's place

With the help of the data that was collected via the questionnaires we could estimate the Thermal Sensation Vote (TSV). Uncomfortable and thermal sensation scales were proposed for 16 parts of human body: head, front torso, back torso, pelvis, hands, forearms, upper arms, front and back thighs, front lower legs, back lower legs and foot. The heart rate of each person was monitored during the entire experimental campaign and the corresponding values were noted on each questionnaire. The subjects were also asked to note down some observations regarding a particular state that could affect their vote (i.e previous physical effort, coffee consumption, etc.)

For each set of considered air diffusers and each value of the flow rate we performed additional sessions using the Comfort Sense system placed on the drivers' place and respectively the thermal manikin as the driver.

e) *Third experimental campaign – elementary air jets characterization*

Competition for space in new vehicles is intense, so the HVAC ducts are often squeezed between different components and the ducts geometry is very complex. In Figure 93 is presented the ventilation duct system for the studied vehicle.

The third experimental campaign was designed in an intermediary phase of our study. Once developing our numerical models, the question of the three-dimensionality of the studied flow arisen. In all studied references from the literature, numerical models consider the distribution of the velocity profile from the inlet vents as being uniform, thus the diffusers are reduced to orifices in the dashboard where complex elements such as ailerons are not taken into consideration. A shortcoming of this work hypothesis is that the a uniform distribution of the velocity on the entire inlet surface is not a solid assumption

A first idea was to reproduce at least the ducting system upstream the air diffusers and to simulate the air flow through them. Using a 3D CAD software, left and right ducts were reproduced as displayed in Figure 94. As shown in the next chapter, in our case the complex surfaces inside the cabin are leading to a large number of elements for the numerical mesh grids. These ducts have many details introducing more complexity in the meshing process. Even more, resolving numerically the flow through the elements of the considered air diffusers was not an option our case, given that the boundary layer on these elements has another scale than the global scale of the car cabin. This way we decided to perform a detailed characterization of the velocity fields at the exit plane of the diffusers and at other

axial distances of the jet flows through Laser Doppler Velocimetry. To this end, a special experimental set-up was conceived.



Figure 93: Renault Megane air front air ducts geometry

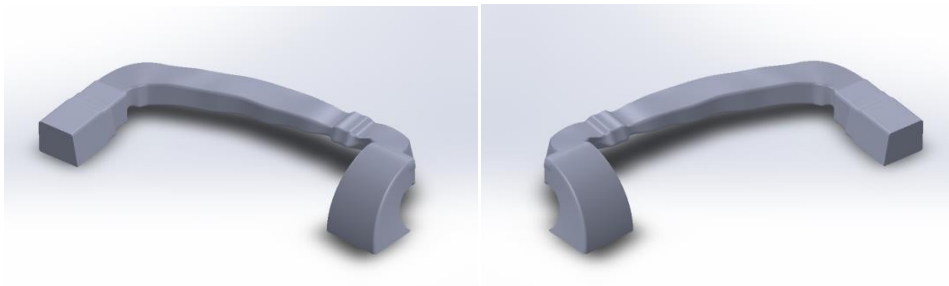


Figure 94: geometry of the air ducts reproduced in SolidWorks

Coming to the idea of the main goal of the doctoral research that was since the beginning the improvement of thermal sensation of vehicle driver and passengers, by implementation of innovative air diffusers we wanted whether the innovative concept for optimized air diffusion using passive control of air jet through lobed grille diffusers [10] could be applied in the case of a car cabin. To this end we oriented our research towards diffusers with the special lobed geometry presented earlier. As shown in the first chapter, in the light of some previous studies [158] the trailing edge of the lobed ailerons is generating strong longitudinal large scale vortices that favor mixing and entrainment.

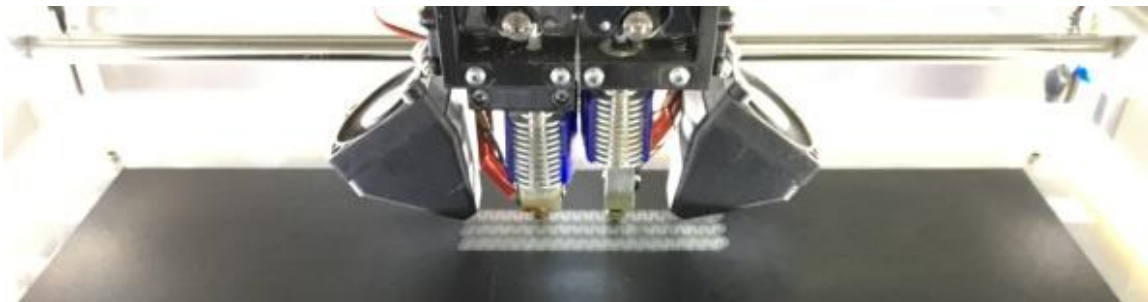
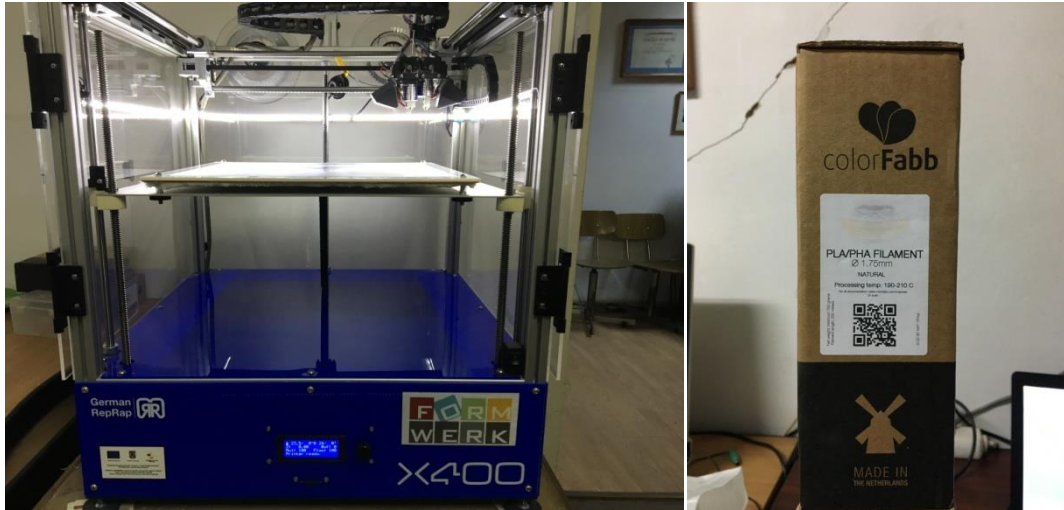


Figure 95: Images during the prototyping process of the new air diffusers

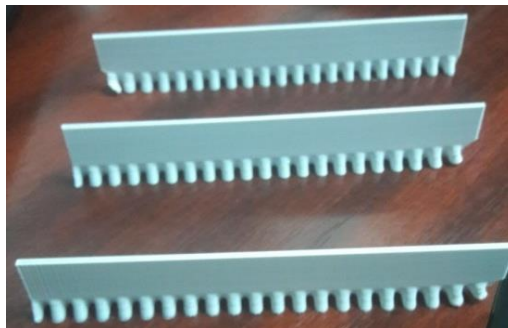


Figure 96: Newly printed ailerons before painting



Figure 97: Air diffusers with lobed ailerons before printing

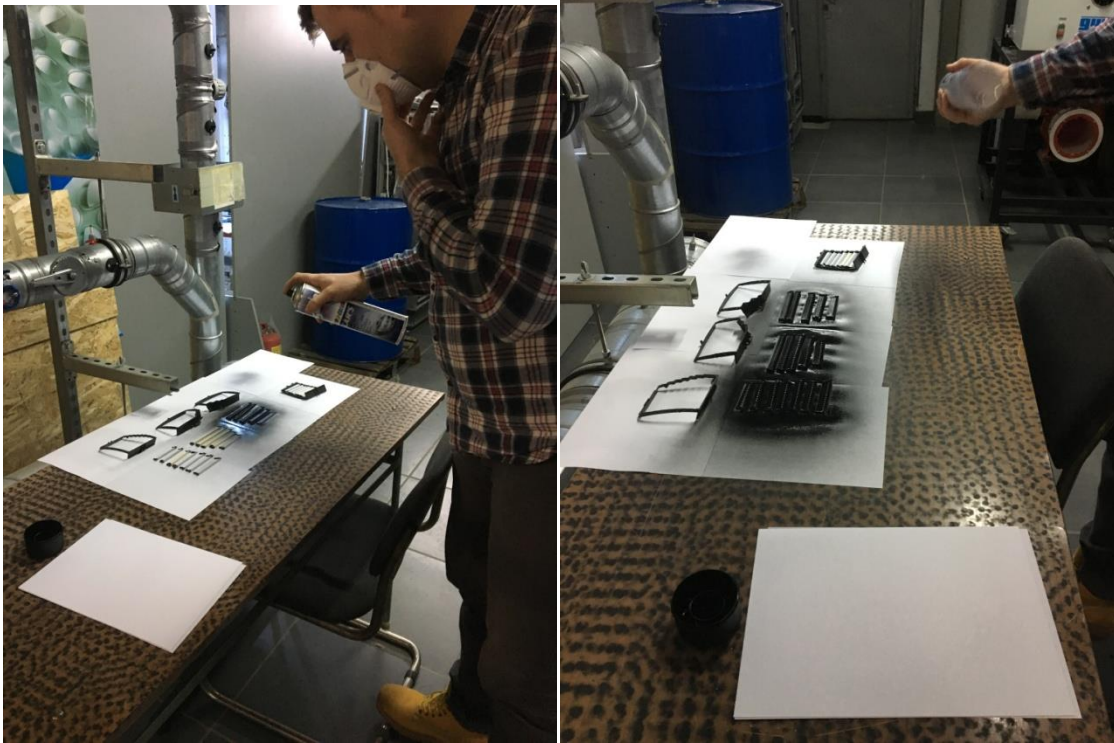


Figure 98: Pictures from the painting process.

The considered set of lobed ailerons air diffusers is presented in Figure 97. The new diffuser geometries were designed and manufactured at UTCB. They were first designed in SolidWorks CAD software. The processing necessary for 3D printing was done in 3D Simplify software. The printing process was ensured with a German RepRap X400 3D printer. The printing material used is a (PLA) Poly-Lactic Acid, it is a thermoplastic polymer which was processed (Figure 95). To avoid reflections after printing the new diffuser geometries were coated with black paint (Figure 98).

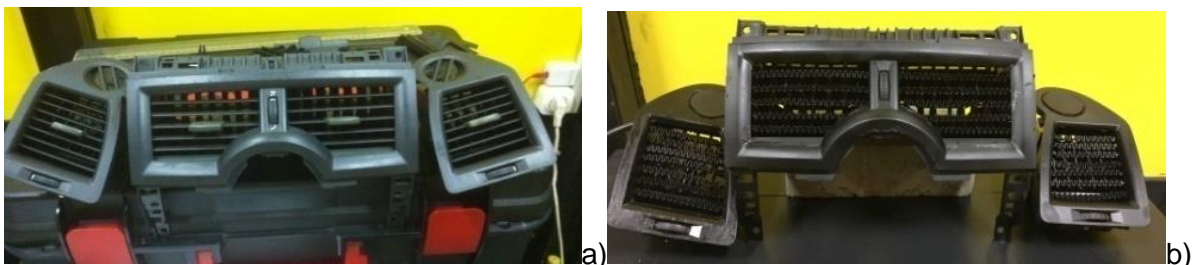


Figure 99: Lobed ailerons diffusers compared to the baseline original Renault Megane air diffusers: a). CG – classical grilles air diffusers; b) LAG – lobed ailerons grilles air diffusers



Figure 100: Dashboard and front air ducts mounted on a specially designed structure

In order to make possible Laser Doppler Velocimetry measurements, we created a distinct experimental facility, composed of an entire ventilation system with its own dashboard, mounted on a specially designed support to ensure mobility (see Figure 100) allowing to modify its inclination angle.

The distributions of the three velocity components were measured in vertical transverse planes aligned as possible with the diffusers, at different distances from the exit planes as shown in Figure 102. The rounded shape of the dashboard did not allow getting closer than $X=14$ mm. The nearest velocity distribution field was used as boundary condition for the numerical model, the others being used to validate our numerical model as presented in the next chapter.

The LDV sampling time during measurements was in the range of 60 to 100s and the mean data rate ranged between 500 Hz to 4.8 KHz depending on the flow velocity at the measurement point. The uncertainty of the measurement was estimated to be in the range of ± 0.1 to $\pm 0.6\%$ for the U, V and W mean components, and in the range of ± 1 to $\pm 5\%$ for the corresponding RMS components. This estimation was based on the evaluation of a global bias error, depending on all the parameters susceptible to bias the measurements [219, 221, 227-229], and of a statistical uncertainty related to the data scattering around the mean values [229-231].

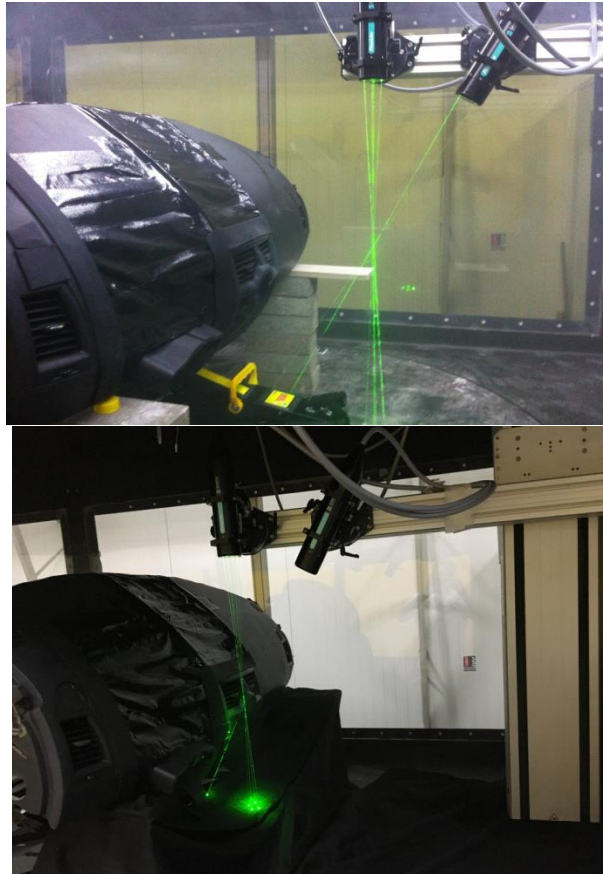


Figure 101: LDV probes in the front of the central air diffusers

The probe was mounted on a three-dimensional traverse system with the ranges on the X, Y, and Z axis, as 1000mm, 1000mm and 1000mm respectively, and with the movement resolution and reproducibility of $6.25\mu\text{m}$. LDV data was acquired on a grid in the (YZ) plane at each X location. The grid spacing was kept the same, of 5mm in the Y and Z directions and varied from 16 mm close to the jet exit for a $100\text{mm}\times 100\text{mm}$ grid to 25mm at $X=100\text{mm}$ for a $250\text{mm}\times 250\text{mm}$ grid in the case of the lateral air diffusers.

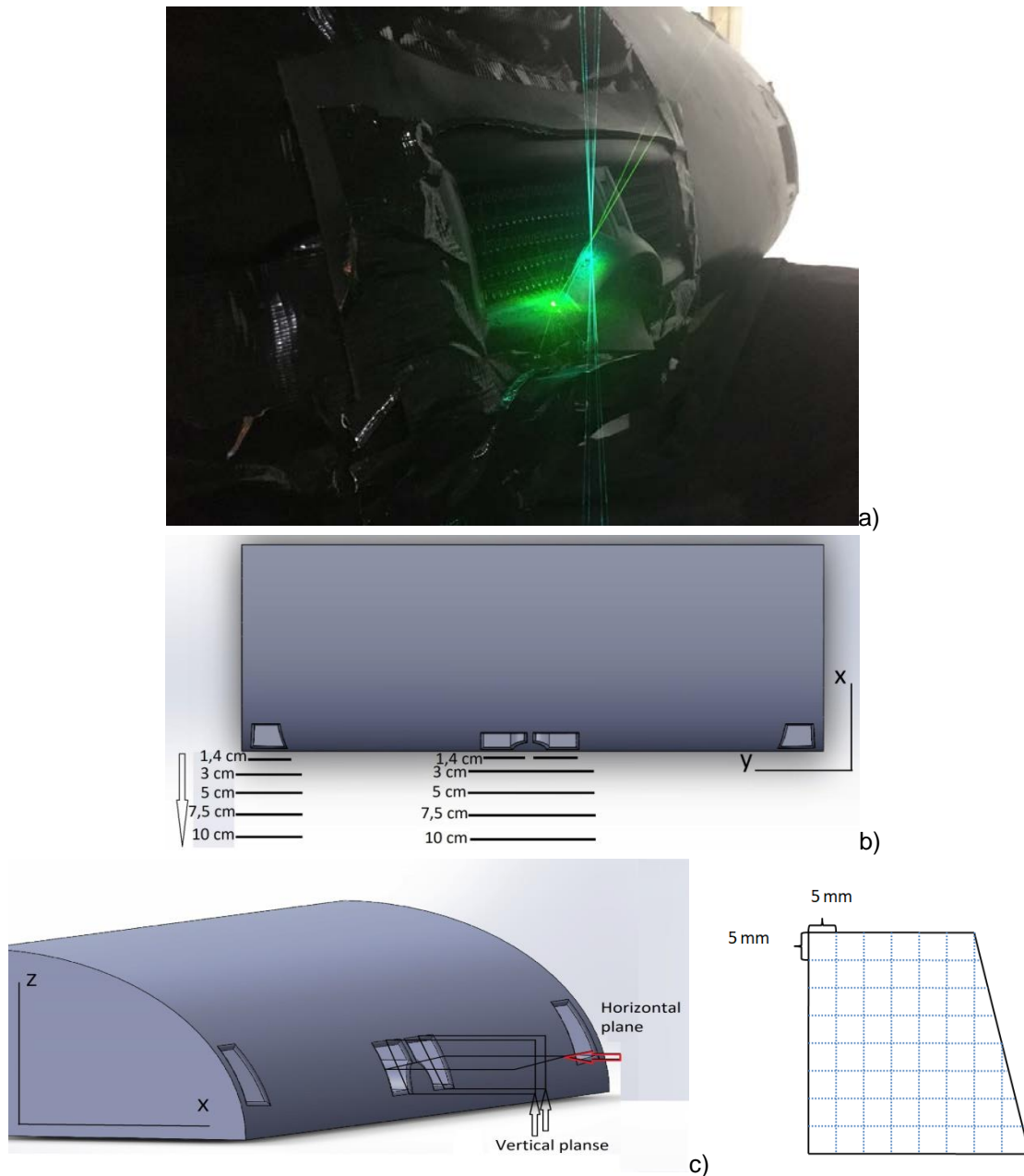


Figure 102: Velocity measurements planes

In Figure 103 are presented the velocity field distributions for the left central air vent position at the exit plane ($X=14\text{mm}$) for the classical air diffuser CG and for the lobed air diffuser LAG. In Figure 104 are shown the same results in the case of the left side air vent position. The velocity fields distributions at other distances will be presented in the next chapter through a comparison with results from the numerical model. As it could be observed in this figure the initial distribution of the velocity fields is different for the CG and LAG cases. The difference is more important at the lateral diffusers especially for the axial component of the velocity U and inherently for the velocity magnitude. This will have an impact on the whole field distribution as we will observe later.

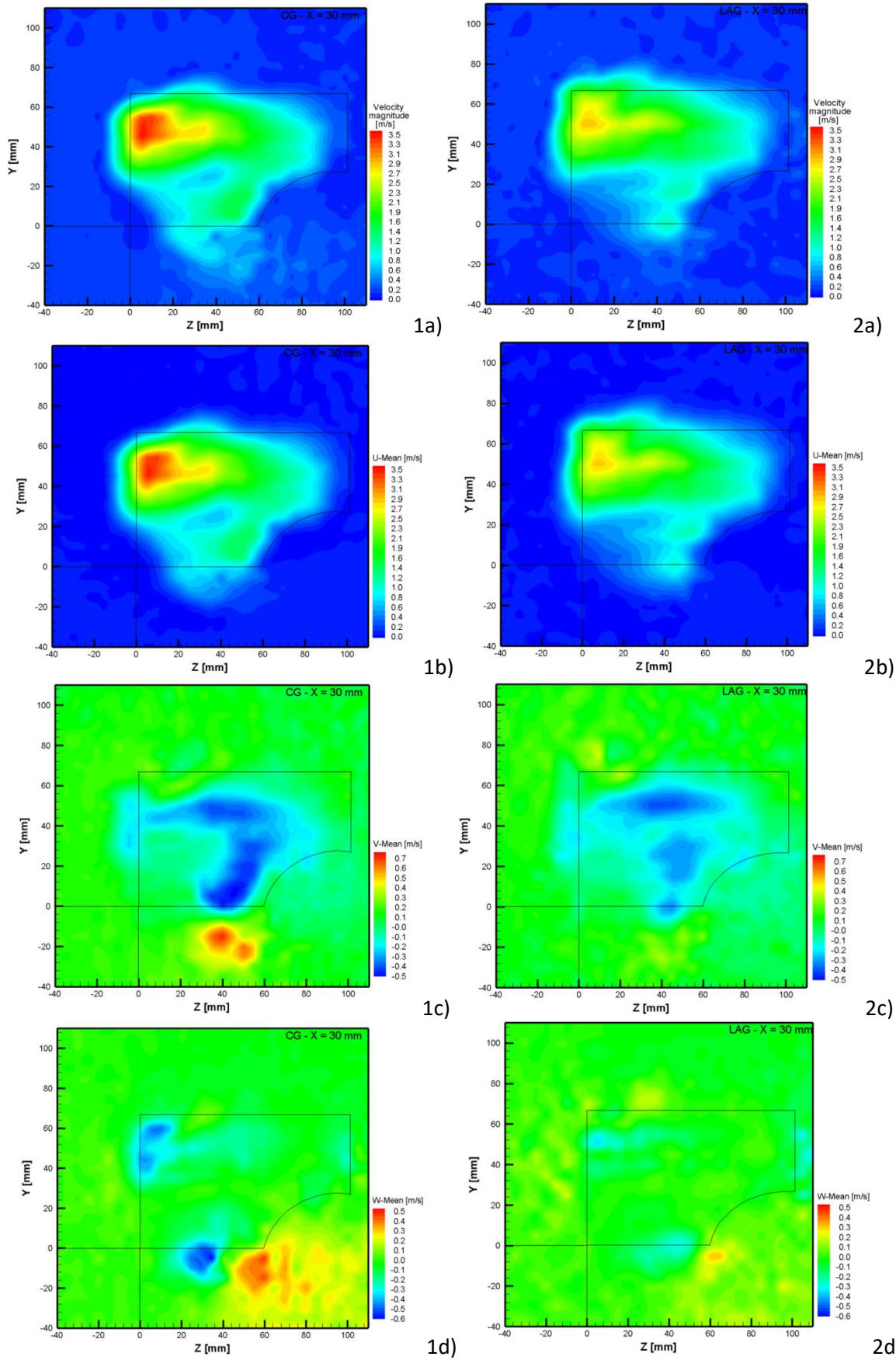


Figure 103: Velocity distributions for the center left air diffuser at the exit plane ($X=14$ mm): 1) classical air diffuser - CG, 2) lobed air diffuser- LAG : a) velocity magnitude, b) U component, c)V component, d) W component

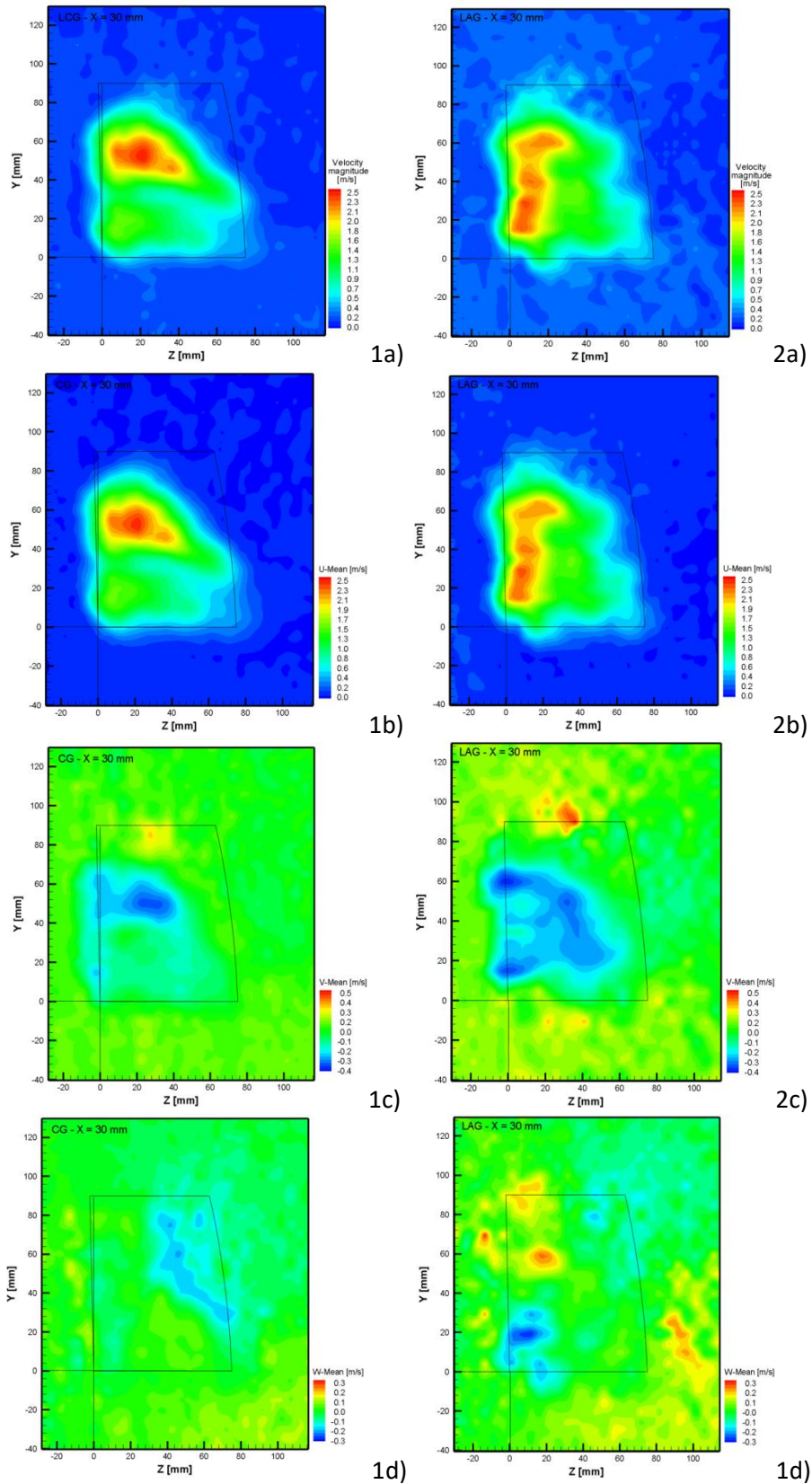


Figure 104: Velocity distributions for the left side air diffuser at the exit plane (X=14 mm): 1) classical air diffuser - CG, 2) lobed air diffuser- LAG : a) velocity magnitude, b) U component, c)V component, d) W component

CHAPTER 4 – NUMERICAL MODEL

In the introduction of this chapter we propose to pass briefly through the currently developments related to Computational Fluid Dynamics applied to air distribution and thermal comfort. In the bibliographical chapter we have put in evidence several numerical studies that we found in literature relevant for our subject. Still, the vast majority of these studies lack details and justifications of modeling choices, this way we decided to rely on the knowledge gained in the much more studied domain of air distribution and thermal comfort in buildings. We will start this chapter with a synthesis of the mathematical models and methods that were available for us for allowing in the following parts to justify our choices

In the following parts of the chapter we will present the steps employed in our numerical approach. In a first time a simple car-cabin numerical model was designed and in our quest of methods of calibration of the correct boundary conditions, we used temperature and air flow measurements in a real car-cabin. In a second step, a complex numerical model has been developed. This model includes a passenger with anatomic shape and takes into consideration to types of air diffusers. The validation of the chosen approach for introducing the effect of the flows generated by the two types of diffusers is also presented in this chapter.

A. Numerical modeling: limitations for thermal comfort domain

For numerical modeling in fluid dynamics problems, the equations of conservation of mass, momentum and energy are used, in the structure of a system of partial differential equations. Numerical models generally use three methods: finite difference method, finite element and finite volume method. Depending on the spatial scale of the investigated area (building, room, enclosure, vehicle cabin) and the phenomena investigated we distinguish nodal models, zonal and CFD type. The latter will be referenced and discussed below because they are our choice in this study. The choice of CFD models was motivated by the possibilities of deepening the analysis of the considered cases. These models are used to replace the experimental methods when the experimental approach would raise special problems or when parametric studies would require a long time. CFD models are based on numerical solving of Navier-Stokes equations for all mesh points of the studied domain. Solving the equations of conservation of mass, momentum and energy allows knowledge at any point of the distribution of a various state variables. The particularity of a fine or very fine mesh (million elements) allows a very detailed simulation of airflow, in our case in

enclosures with complex shapes and different thermal states. This is the main reason why we turned to this type of numerical approach since the intention is to study the influence of parameters correlated with fluid dynamics and fine and very fine resolution of the airflow.

a) Equations and mathematical models

CFD modeling involves using a type of partial differential equations that consists of:

- continuity equation expressing conservation of fluid mass:

$$\frac{\partial \rho}{\partial t} + \frac{\partial(\rho u_i)}{\partial x_i} = 0 \quad (27)$$

- Navier-Stokes equations of motion, expressing the conservation of quantity of motion:

$$\frac{\partial(\rho u_i)}{\partial t} + \frac{\partial(\rho u_i u_j)}{\partial x_j} = \frac{\partial \sigma_{ij}}{\partial x_j} + F_i \quad (28)$$

- Fourier-Kirchhoff energy equation expressing energy conservation:

$$\rho \frac{\partial E}{\partial t} + \frac{\partial}{\partial x_i} (\rho u_i H) = - \frac{\partial q_i}{\partial x_i} + \dot{Q} + \frac{\partial \sigma_{ij} u_i}{\partial x_j} + \rho f_i u_i \quad (29)$$

In our field we introduce the following simplifying assumptions for the flow and heat transfer phenomena: the fluid is considered Newtonian, usually single phase, incompressible, subject to the gravitational field and a constant viscosity.

CFD modeling type can be achieved with different degrees of smoothness and approximation of the temporal and spatial variation of fluid parameters, such models can distinguish between DNS (Direct Numerical Simulation), LES (Large Eddy Simulation) and statistical models such RANS (Reynolds Averaged Navier - Stokes).

b) Turbulence modeling

Turbulence is a dominant feature of the air flows around us. It is a property of the flow, not of the fluid in question. Turbulence doesn't have a specific definition but rather is characterized by its properties [232, 233]. When a flow is turbulent, physical quantities such as velocity and pressure vary rapidly and randomly, and the momentum, energy and concentration are characterized by an increased diffusivity. Statistical approach (RANS), resulting in less time than the previous calculation is often used in industrial computing codes for preliminary designs and seems appropriate for flows inside buildings. The objective of this method is to neglect the instantaneous turbulent small scale shucking in fluid flows motion, too complex, and to seek simple equations to predict the evolution of mean fields.

Thus, the equations of motion are averaged to reduce the fluctuating terms, and the new unknowns are taken into account in models of turbulence closure [234]. The more the models are elaborate, the more the physical representation of the flow is real, but computing time increases considerably. Thus, for each type of flow, we must find the best compromise between accuracy and complexity of the used model.

Turbulent viscosity

By analogy with the law that connects the efforts due to viscosity tensor, Boussinesq propose in 1877 connecting turbulent efforts $-\overline{u_i u_j}$ with velocity gradient of the mean flow by the concept of turbulent viscosity. To close the turbulence model, is necessary to determine this turbulent viscosity. There are many models for solving the equations:

- Turbulent viscosity models based on Boussinesq's hypothesis;
- Transport models for Reynolds efforts;

In function of the correlations order introduced for solving the undetermined system of equations we can have:

- First order models that calculate the Reynolds efforts in function of the mean flow with or without additional equations;
- Second order models that treat anisotropic the Reynolds tensor (additional equations that take into account all the turbulent efforts and turbulent heat fluxes);

Thus, we meet first-order models without transport equation, where we deduce mean fields in simple cases, first-order models with equation/equations of transport for more complex mean fields and characteristic turbulence quantities, second-order models with closure models, where we deduce mean fields and fluctuating mediated fields. In the following paragraphs we will review the characteristics of different types of turbulence models proposed in the commercial code Fluent and used during the numerical study. We will not detail other existing models or those proposed by Fluent that were not used in this study. Among these we include second order RSM model that could not be implemented in the work because of limitations of computing resources. We synthetized a review of turbulence models used in previous relevant studies in Table 11.

Near wall modeling of the flow can be achieved using several methods:

- wall functions method: the region where molecular viscosity is taken into account is not resolved, the turbulence models for large Reynolds numbers are coupled to a global

formulation of boundary layer;

- two layers method: near wall region is resolved with specific models, turbulence models for large Reynolds numbers are coupled with simpler models;
- small Reynolds numbers method (LRN-Low Reynolds Number): resolution is to the wall by introducing damping functions in the transport equations of k and ϵ .

Table 11: Popular turbulence models comparaison

Model	Advantages	Disadvantages
Spalart-Allmaras	Low time consuming -1 equation;	Not suitable for many cases;
k-ϵ standard	Robust, economic, reasonable accuracy;	Weak results for complex flows; errors for special cases like boundary-layer, jets ;
k-ϵ RNG	Indicated for medium to complex flows;	Same disadvantages;
k-ϵ realizable	Same benefits and additional near wall treatment;	Limitations due to turbulent viscosity isotropicity hypothesis;
k-ω standard	Applicable for flows around obstacles and boundary layer flows; For airflows interior buildings- good accuracy and numerical stability [235];	Sensible to correct boundary layer conditions for turbulence [235];
k-ω SST	k- ω std model's accuracy near walls and k- ϵ model's independency for free flows;	It is necessary to have a very fine mesh for the boundary layer ;
laminar	Not applicable for the airflows considered in the studied cases; (Reynolds numbers are in the turbulent regime)	

c) CFD models in thermal comfort domain

Starting with the first CFD studies for indoor airflow research, in 1973, Nielsen [236] presented an attractive alternative to pure experimental investigations. Thus, for our domain of research related to airflows in occupied flows, the development of CFD methods opened the door to tremendous opportunities. Indeed, it is now possible to study the prediction of the indoor environment, with the great advantage of the flexibility offered by the numerical

simulation. Information on thermal comfort, air quality, effectiveness of the ventilation/air conditioning systems can be extracted from the velocity, temperature and mass concentration distributions. In the literature, numerical modeling has been used successfully for several applications. An important area of interest is represented by the interaction between body and ambient microclimate with emphasis on indoor air quality. However, despite the results, the issue of occurring flows has not been fully resolved, with an often problem of the approach uncertainty. Validation of CFD simulations and quality of the applied model remains an intrinsic part of the process, being often overlooked due to limitations of computing power or experimental cost. Indeed, the relatively limited possibilities of obtaining validation data restrict sometimes the certainty of the CFD approach for the study of air flow in occupied spaces.

An important step in comfort studies was the introduction of human body models. Complex shape and thermal potential of the human body affects the air path and evaluation in terms of thermal comfort of an ambience. Research in this field have gone further, extensive studies detaching the correct choice of turbulence model, the appropriate geometry, for different ventilation strategies in buildings [237] etc.

Research directions with virtual thermal manikins (VTM) are well developed. Murakami et al. [238], Bjorn and Nielsen [187], Hayashi et al. [239] simulated pollutants dispersion around the human body and their impact on the inhaled air quality. Sorensen [240] calculated the view-factors for the radiation heat flux between a human body and surrounding surfaces. Other researches [116, 241, 242] focused on the study of velocity field and radiative and convective heat flux released by the body, using CFD simulations.

Developing models for the human body inside the buildings was made step by step, starting from 2D simulations for air flow around simplified geometries without involving temperature field. Transition in three-dimensional allowed the study of more realistic air flows and the introduction of radiation between surfaces. With increasing computing power, realistic forms and complex geometries were introduced, virtual manikins being sometimes equipped with an air flow simulating human breath, or a generation of moisture in the skin or a control model imitating the thermo-physiologic adjustment system.

In 1996, Murakami et al. [116] CFD introduced human model in CFD study, being interested in the dynamic effect of air flow around the body. This model is called "computational thermal manikin" used to predict thermal comfort. Article describes the development of virtual thermal manikin, being analyzed in a first phase the convective heat transfer between body and air flow, using a CFD code. The novelty of this study comes from

the analysis of convective transfer, analysis difficult to realize experimentally to human body skin. The virtual manikin used in this study is detached from other CFD studies by the curved shape that looks like the human body.

CFD calculations using virtual thermal manikins (VTM), with simple geometries involving low computing resources, but an anthropomorphic geometry can lead to more accurate results. VTM differ in size, posture and geometric complexity. In general, we meet VTM's closest in size to adult human body, with heights between 1.65 and 1.90 m and areas between 1.6 m^2 and 1.8 m^2 . Depending on the study, three positions are used: lying, sitting and standing.

The level of geometric details of the body depends on the computational resources that are available and the objective of the numerical approach involving a VTM. In [117] the authors used an elliptical section to reproduce a person and Niwa et al. [118] simulates a human body in seated position by a cubical geometry. To simulate an upright human body, it was used a parallelepiped of the same height for flow field visualizations [119] and thermal comfort indexes determination [120]. Other researchers have used three dimensional rectangular shape to model airflow around a seated [121] or standing person [122-125]. Intricate geometries of the human body can be generated using a specialized CAD software or with a laser scanner usually used for geodetic studies. An example of such use of a laser scanning method is given in [242]. In the study three thermal manikin models were created, each with 125.000, respectively 250.000 and 500.000 elementary triangular surfaces for a coarse mesh, medium and fine. The presence of small areas of skin allows calculation of the form factor between the body and the surrounding surfaces, which leads to the exact flow exchanged by radiation. Topp and Nielsen [237, 243] investigated by numerical simulations difference between the different forms of VTM in the sitting position and placed in an unidirectional flow field. They conclude that only in the region very close to the body geometry has influence. This result must to be considered in the studies which involve breath or air flow to the face.

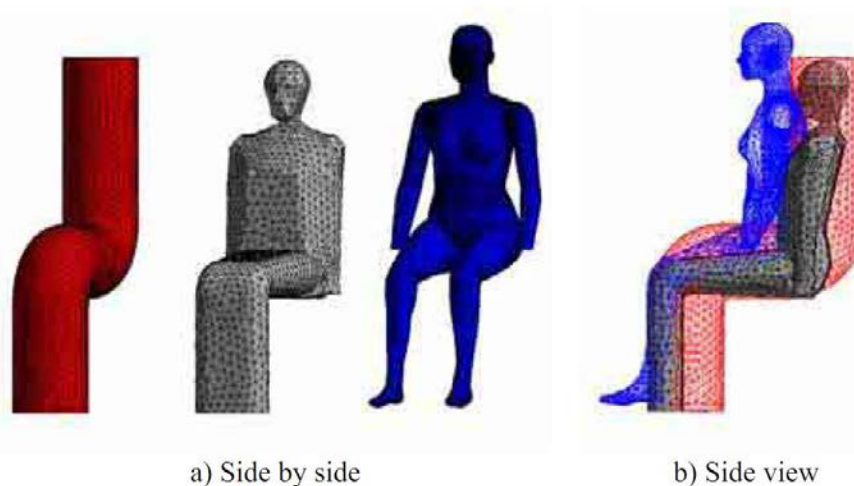


Figure 105: Different shapes of virtual thermal manikin [237, 243]

A more realistic geometry is necessary in numerous studies that aimed the convection currents generated by the body, local thermal comfort and air breath quality because the body plays an important role in determining local discomfort or the transport of pollutants.

All these studies show that the influence of the geometry when numerical research is focused on global air flow a more simplistic model can be used. However, if we want to investigate local air flow around the human body, a detailed geometry is required. This need is encountered in the automotive industry or for other personalized ventilation systems, in which the investigated flow contains a part of the boundary layer around the body [244, 245].

Choosing a turbulence model involves a procedure that takes into account many considerations such as: the pattern of the flow, the accuracy needed, computational resources, accounted physical phenomena etc. The most used turbulence models for the numerical simulation of the air flow around a human body are $k-\epsilon$ type models. Murakami et al. [116] reveals that the only way to calculate the convection heat transfer in sensible area is to use a fine mesh. However, in simulations using $k-\epsilon$ turbulence model for small Reynolds numbers, for a fine mesh of complex geometries, it is difficult to achieve convergence [246].

In the past, several turbulence models were used, either based on the case study or the involved resources. In 1998 Chen and Xu [247] demonstrates the feasibility of zero equation turbulence model, for the air flow prediction for the general purpose spaces, having the advantage of low computational resource needed. Another model which involves a short computing time was tested by Torano et al. [248], and comparing the results from simulations with Spalart-Allmaras model and the usual $k-\epsilon$ experimental data, both models showing satisfactory results. The two $k-\epsilon$ standard equations model of turbulence used is the most used model, with many variants. Studies have shown that the model predicts quite well the mixture

of pollutants in an environment [249] or the air flow and particle distribution for different ventilation strategies [250]. For special conditions different variants of the previous model were used, for example, the $k-\varepsilon$ realizable model is better adapted for turbulence or flow involving separation and $k-\varepsilon$ Low-Reynolds - Number treats better the flows near walls, Bosbach et al. [251] showing that fact through simulations carried out within the cabin of an aircraft, experimental results validated by PIV measurements. Posner et al. [252] evaluates in 2003 several $k-\varepsilon$ models to simulate air flow in a room, the results indicating a better validation for the model $k-\varepsilon$ RNG compared with $k-\varepsilon$ standard. In 1988 Wilcox [253] introduced $k-\omega$ turbulence model, trying to improve $k-\varepsilon$ model. A comparison of several models showed that $k-\omega$ SST model demonstrates additional accuracy in the calculation of velocity and temperature distribution for a an office [254], fact also demonstrated in 2007 by Kuznik et al. [255] by comparing profiles resulted by $k-\varepsilon$ realizable, RNG $k-\varepsilon$, $k-\omega$ standard and $k-\omega$ SST simulations of a mechanically ventilated room with a jet outlet. Improving $k-\omega$ model with low Reynolds number correction (Low Reynolds Number - LRN) has led to a robust model with accuracy in the results, especially in cases with heat transfer, which involves a reasonable calculation time. More complex models, which tend to approach the DNS model involving direct solution of the equations, could be implemented on high performance computing machines, simulation time being no longer an impediment. The LES models compared to other classic models offers the possibility to characterize the dynamic details of the studied fields, especially in closed spaces [256]. DES method is used in most recent studies when RANS models are not sufficiently precise and LES unapproachable. Comparative studies between DES, LES and RANS indicated that DES seems to be a promising model, being accurate in terms of velocity measured field. However, the method should be studied further before being widely applied for simulations of indoor environment.

Regarding the generation of a computational grid, complex geometry of the human body has led to special requirements. Fairness and accuracy of the simulations are highly dependent on the quality of the calculation domain. In general, mesh generation is the most laborious of the whole process of CFD calculation. Accuracy is actually influenced by mesh size, the shape of cells, topology, etc. The difficulty of meshing for complex geometries generation especially requires the use of unstructured cells. Since structured grids lead to better results than unstructured in our domain, the calculation volume is generally divided into two, one in which there is the manikin and the rest of the room [242]. The first area is generally a parallelepiped meshed in unstructured cell, the rest can be meshed by a structured

grid.

Number of calculation cells varies from case to case. Simulations involving humanoid forms require a large number of cells. For example, in 1996, a 3D calculation domain was divided by Murakami et al. [116] in 125.568 cells, then Sorensen and Voigt [242] reached almost one million cells for another organic shape, these days we find studies with over two million cells [257].

Tracking solution of CFD calculations must be carried out according to grid dependency study [258]. It should be taken into consideration the computing grid for which the solution no longer varies. This study also depends on computational resources that should be able to generate the computing grid and then run simulations themselves. Coarse grids are generally used in the far areas and fine mesh near walls where is needed to capture accurately the physical phenomena in the boundary layer. In areas that have high spatial gradients (velocity, temperature, etc..) fine grid are used for capturing accurately the variation of physical quantities and coarse grids are used in areas where these variations of the physical quantities are very small - and they are usually located in areas outside the boundary layer, undisturbed areas of jets, chemical reactions, etc.

In CFD simulations, the boundary conditions required for thermal mannequin varied from case to case. The first approach that integrated a humanoid form only, considered the convective transfer between the body and the environment. Thus, in 1996 Murakami performed the first CFD simulations, integrating into the domain rounded shape geometry. The boundary layer conditions of the manikin for the case without jet were imposed with a constant flux of 20 W/m^2 , and for case with a uniform flow ($v_{\text{inlet}} = 0.25 \text{ m/s}$) skin temperature was imposed to $33.7 \text{ }^\circ\text{C}$. Computational domain was meshed into 125 000 cells at the skin surface boundary layer is created. For the case with no jet flow a mean velocity of 0.26 m/s in the plume generated by the body was obtained, a value which is in good agreement with experimental data [259]. Distribution of body temperatures, the convection coefficient values on the skin surface are also in agreement with experimental data found in various studies, but they don't make any statement relating to thermal comfort. Where there is an air flow around the body, different values for local convective flow are found to be not similar with the experiments (ex. 500 W/m^2 at head's level). These values are explained by the absence of radiation model and other models of specific heat transfer of the human body. Despite the simple geometry boundary conditions of the model, the study paves the way for research involving virtual thermal mannequins.

One of the challenges, still unresolved in the literature, remains the modeling of the

transitory response of the human body and especially its prediction of the state of comfort in an indoor environment in the presence of air flows generated by HVAC systems. CFD models' development offers new opportunities for solving these challenges. Usual comfort prediction models such as PMV and DR described in Chapter 1 can be supplied with data from numerical studies being applied in many situations. However, as shown in the same chapter, thermal comfort indexes have shortcomings, being contested in many studies [260-263]. The main problem is that the thermal control mechanism of the human body is a complex and difficult to model depending on the factors influencing the heat exchange between human body and environment.

In 2000, the previous authors Murakami et al. [241] introduced the model of radiation coupled with convection and the transport of moisture for a simple geometry model of the human body, coupled with two nodes thermo-physiological model [22] imposing the heat transfer between the body and the environment, which, through an iterative process is controlled the temperature at surface skin. The results found indicate convection current velocity of 0.23 m/s, and a metabolic flux distribution flows of 100.4 W/m² the convective, radiative, evaporative and breathing flux being: 29.1 W/m², 38.3 W/m², 24.3 W/m², respectively 8.7 W/m². These results are in good agreement with experimental results found by that time, the radiation heat transfers coefficients being not calculated. The only reference to the thermal comfort is related to skin temperature resulting from the calculation with a value of 33.3° C and inside of the body with a value of 36.9° C, the state of thermal neutrality being at 33.7° C, respectively 36.8° C. There were no references to local discomfort factors.

In 2003, Al-Mogbel [264] resumes Murakami's study, implementing the same two nodes model, air temperature being imposed as a criterion for convergence rather than skin temperature, questionable approach because the room temperature is insensitive to the temperature distribution of the skin. The paper does not specify how the model was implemented in CFD code.

Another approach is mentioned in a study by Tanabe [78] where a radiation model and 65 nodes thermo-regulatory model are integrated in a CFD code. The model has 16 segments, each with 4 layers. These are: the bone layer, the muscle layer, the fat layer and the skin layer and a central component, the circulatory system. Because heat transferred by radiation and convection was calculated empirically heat transfer coefficients, the CFD code was used only for simulation the air flow patterns around a of a virtual thermal manikin. Another study from 2004 [265] coupled the CFD code with Fanger's model, the results being validated with experimental data obtained using a thermal mannequin. In other studies it was imposed either

the body surface heat flux [266], or various temperatures [242]. With the appearance of the thermo-physiological models, the coupling between this type of models and CFD simulations has gain interest. This type of coupling requires an initial temperature which is iteratively adapted according to the environmental conditions [74, 244], or requires an imposed heat flux depending on local temperature and velocity [257, 267].

B. First simplified model of the car cabin

The concrete objective of the numerical approach was to develop a realistic CFD model of a vehicular environment including a virtual manikin as driver. From the previous literature review it appears to us that the anatomic shape of the driver is very important. In this paragraph we present the first step in this numerical approach which consisted in the set-up of the model for the cabin car itself. We first wanted to check if we can reproduce the environment without passengers, confronting the numerical environment with the real experimental set-up that we presented in Chapter 3 B c).

The development of the numerical model was divided in a few steps: the first step - generation of the cabin geometry, the second step - generation of the numerical grid and grid independence study, the third step - validation of the numerical results.

a) Generation of the Renault Megane geometry

This first model comprises the interior of the car geometry with all the relevant details for our study but does not include the human geometry. The model for the vehicle geometry was designed in Catia software and then imported in Ansys Design Modeler in order to be prepared for the numerical simulation.

b) Generation of the numerical grid and grid independence study

The numerical mesh grid was developed in Ansys Workbench. In Figure 106 can be observed the developed geometry and an example of the boundary mesh in the interest domain.

In order to obtain a fairly accurate solution for the studied case at the expense of the least computational resources a mesh independence study was carried out. A *fairly accurate* solution from the mesh point of view is the solution in which the accuracy of results is enough to capture the flow characteristics and it does not significantly vary with an increase of t grid resolution. For example, a poor-quality grid will cause inaccurate solutions and/or slow convergence or even no convergence. On the other hand, more cells can give higher accuracy, the downside being the increased memory and Central Processing Unit (CPU) time

needed for the solution calculation.

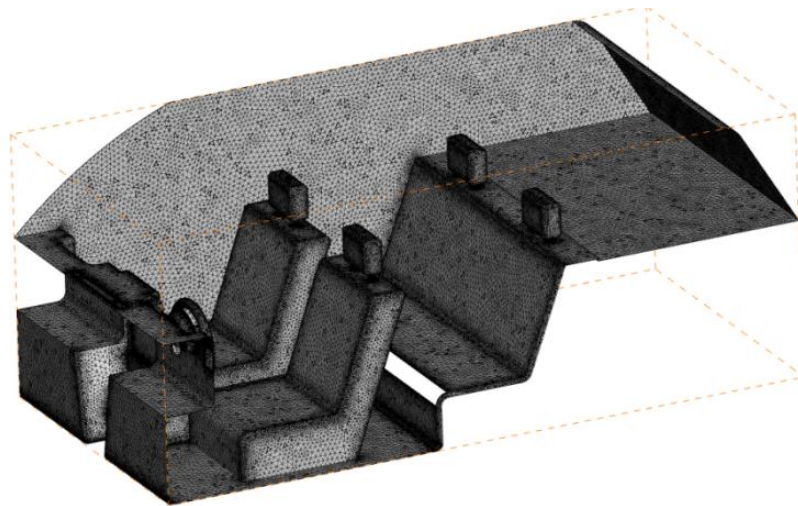


Figure 106: Investigated geometry and numerical model mesh detail

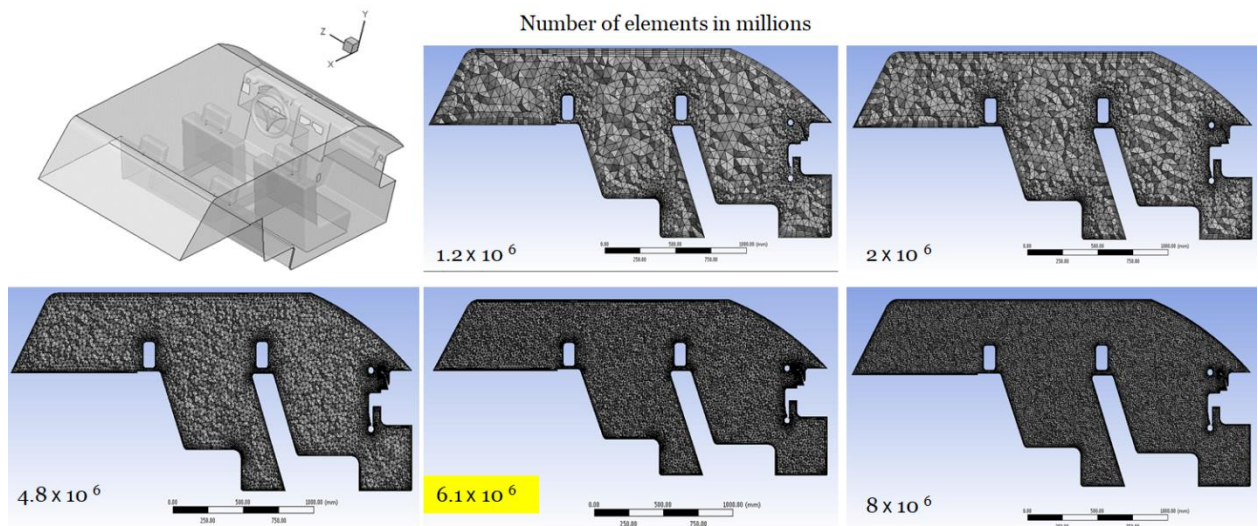


Figure 107 Numerical grids used for the mesh independence study for the numerical case without thermal manikin

In Figure 107 are shown 5 of the numerical grids used for the mesh independence study. The elements used for the numerical grid are prisms in the boundary layer and tetrahedral in the rest of the domain due to the high complexity of the studied geometry. The boundary layer consists of 5 layers. The size of the five different grids used for the grid independence test was: 1.2, 2, 4.8, 6.1 and 8 million elements. The numerical results obtained with the 6.1 and 8 million elements showed small differences, so we choose the 6.1 million elements numerical grid for the next studies from computational reasons.

The pressure-velocity coupling was achieved with the COULPED algorithm. The pressure-based coupled algorithm displays a more robust and efficient implementation for the

steady-state flows [268]. A second order upwind scheme was used to compute the convective terms in the equations, integrated with the finite volume method. For the near-wall modeling we used a standard wall function.

The studies from the recent literature show that $k-\omega$ SST turbulence model is proving to be the most reliable of the two equation models when the desiring the reproduction of relatively complex flow, characterized by relatively low values of Reynolds number as thermal plumes currents generated by the body or a jet of air used for ventilation [235]. The overall performance of this model is one of the best for the indoor environment modeling when studying globally jet flows [269]. Also, Zhang [270] have identified RNG $k-\varepsilon$ $k-\omega$ SST turbulence model as appropriate to be used for numerical simulation for the indoor environment. We chose then this model for our numerical approach, and further study intended to mesh the computing space was made for this model of turbulence.

c) Validation of the numerical results

Aside mesh independence study, a very important part in the process of a numerical simulation is the validation of the numerical results. Validation is the process of determining the degree to which the results obtained from a numerical model are an accurate representation of the real world from the perspective of the intended use of the studied model. Validation deals with the assessment of the comparison between sufficiently accurate computational results and the experimental data. The necessary data for this the second step was obtained from an experimental measurement session. Most of the experimental studies having the purpose to validate numerical models of the passenger compartment that are available in the literature, have been conducted in spaces in which, was attempted to maintain constant the values of thermal parameters [98, 204]. In this case the boundary conditions imposed to the model, can be imposed also to the experimental facility. In our case, the boundary conditions imposed to the numerical model were the experimental data obtained through measurements from the first experimental session for the studied vehicle.

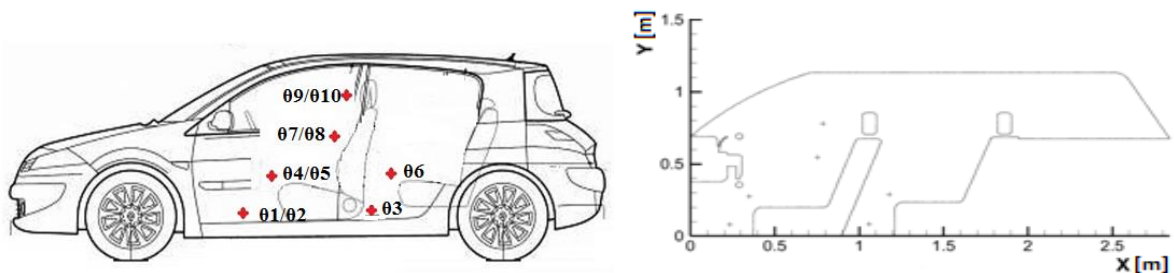


Figure108: a). thermocouples at different passenger’s position points; b). monitored

points in the CFD model

The variation of internal cabin parameters was monitored in the experimental measurement sessions described in the previous chapter.

One of studied parameters inside the vehicle was the air velocity in different location points. The location of the monitored points was chosen with regard to different body parts as described in Table. 3. We checked which are the “maximum allowable mean air speeds” - according to the guidelines given by ISO 7730 [19] - as a function of the local air temperature (see Table 12) and the turbulence intensity (we considered the maximum value which is 40 % according to ISO 7730). We found that, for the third and fourth flow rate positions of the ventilation system (the forth being the last), the measured velocity in cabin at the body levels was higher than the maximum allowable velocity and an unpleasant draft sensation was created. In conclusion we decided to take into account only the values of the parameters measured for the second air flow rate position of vehicle ventilation system.

For the inlet boundary conditions, we imposed a mass flow rate of 0.042 kg/s for the central diffusers and a mass flow rate of 0.039 kg/s for the sides’ diffusers which corresponds to a volumetric flow rate of 123 m³/h and 114 m³/h respectively. The imposed flow rates correspond for the second air flow rate position of vehicle ventilation system. The air temperature for the inlet diffusers was imposed at 23 °C for all the diffusers. The temperature of the walls was imposed the same as in the studied experimental case (between 22.2-23.2°C).

The turbulence intensity, I , is defined as the ratio of the root-mean-square of the velocity fluctuations, u' , to the mean flow velocity, u_{av} .

A turbulence intensity of 1% or less is generally considered low and turbulence intensities greater than 10% are considered high. Ideally, a good estimate of the turbulence intensity at the inlet boundary is obtained from external, measured data. For example, for a wind-tunnel experiment, the turbulence intensity in the free stream is usually available from the tunnel characteristics. In modern low-turbulence wind tunnels, the free-stream turbulence intensity may be as low as 0.05%. For internal flows, the turbulence intensity at the inlets is totally dependent on the upstream history of the flow. If the flow upstream is under-developed and undisturbed low turbulence intensity could be used. If the flow is fully developed, the turbulence intensity may be as high as a few percent.

The value inlet turbulence intensity at the diffusers was imposed as 5% being calculated using an empirical method proposed in [271]:

$$I = 0.16Re^{-1/8}. \quad (30)$$

The Reynolds number at the exit of the central diffusers based on streamwise mean velocity and equivalent diameter ($D_{e1} = 0.093$ m) was $Re = 17763$, and for the sides diffusers $Re = 13924$ ($D_{e2} = 0.073$ m).

$$(31)$$

Table 12: Air speed measured at different body parts locations

Inlet grills	Dashboard				Foot				Dashboard and foot			
Fan controller position	V1	V2	V3	V4	V1	V2	V3	V4	V1	V2	V3	V4
Air speed	v_a [m/s]											
Passenger head	0.08	0.12	0.15	0.19	0.03	0.05	0.13	0.21	0.06	0.07	0.2	0.17
Driver chest	0.12	0.13	0.12	0.12	0.05	0.05	0.17	0.21	0.06	0.11	0.24	0.23
Driver knee	0.06	0.08	0.12	0.12	0.06	0.07	0.09	0.09	0.04	0.07	0.15	0.12
Driver foot	0.08	0.17	0.16	0.15	0.15	0.16	0.23	0.24	0.08	0.15	0.17	0.19
Passenger head	0.1	0.1	0.13	0.14	0.05	0.07	0.13	0.13	0.07	0.06	0.09	0.15
Passenger chest	0.08	0.11	0.15	0.15	0.05	0.06	0.16	0.17	0.06	0.08	0.12	0.13
Passenger knee	0.06	0.07	0.1	0.09	0.03	0.07	0.25	0.22	0.03	0.05	0.11	0.11
Passenger foot	0.1	0.1	0.23	0.24	0.27	0.26	0.62	0.51	0.2	0.31	0.32	0.41
Back knee	0.1	0.1	0.12	0.12	0.09	0.15	0.22	0.24	0.14	0.21	0.21	0.16
Back foot	0.14	0.2	0.3	0.25	0.32	0.39	0.85	0.98	0.2	0.34	0.42	0.44

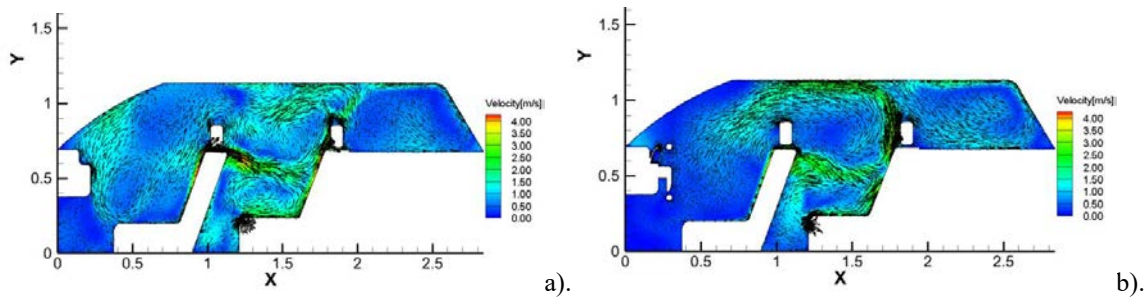


Figure 109: Velocity vectors distribution in a). the left part of the car; b). the right part of the car

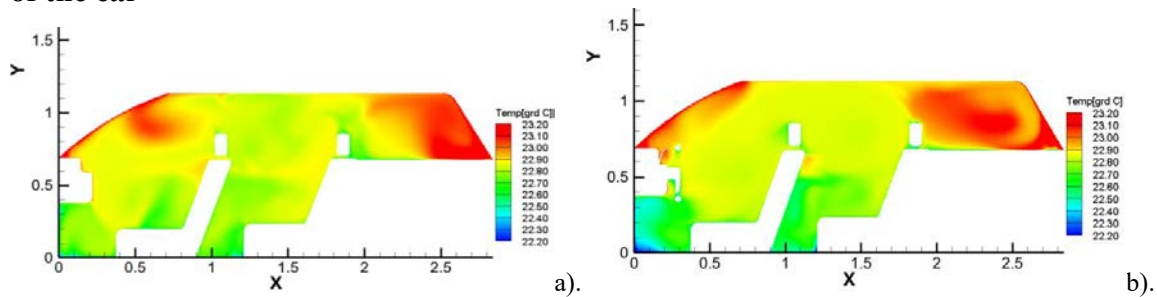


Figure 110: Temperatures contours in a). the left side of the car; b). the right part of the car

Figure 109 displays the results obtained for the velocity vectors distribution in the median plane passing through the driver's seat and through the right passenger seat with the flow on both the left and the right part of the vehicle. A local recirculation flows in the front

compartment and the recirculation in the rear part of the cabin could be observed.

The temperature fields distributions in the vehicle cabin display values between 22.2 °C and 23.2 °C, the resulted temperature fields from numerical simulation can be seen in Figure 110. The lowest temperature can be found at the bottom of the vehicle cabin because of the lowest value for the temperature imposed on the surface the floor.

In the Figure 111 the iso-contours of three velocities are represented with different colors: with red 3.8 m/s; with green 2.8 m/s; with blue 2 m/s.

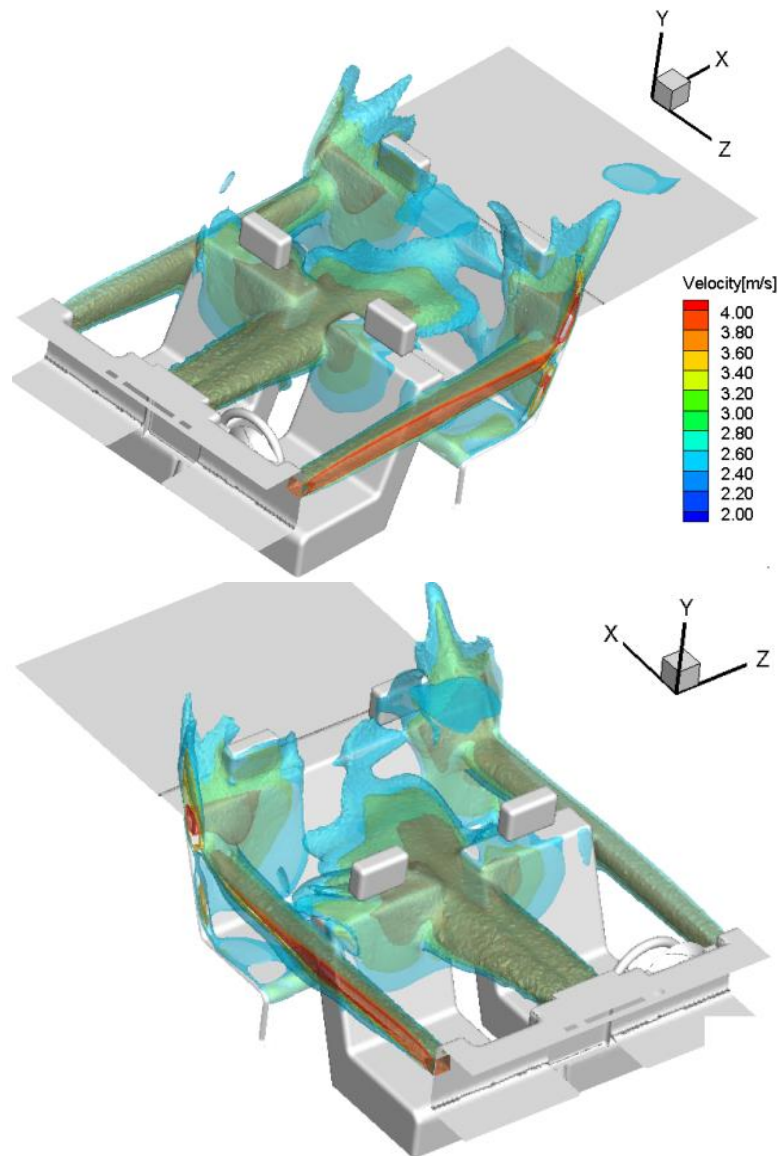


Figure 111: Iso-contours of velocity (red - 3.8 m/s, green 2.8 m/s, blue 2 m/s)

Table 13: Comparison between numerical and experimental results of the values of air speed, temperature and thermal indexes

Point/parameter of measurement	v_a [m/s]		Θ [°C]		PMV		PPD	
	Exp	CFD	Exp	CFD	Exp	CFD	Exp	CFD
Passenger Head	0.1	0.38	23.62	22.91	-0.38	-1.13	8.11	32.18
Driver Chest	0.13	0.35	23.3	22.83	-0.54	-1.11	11.24	31.09
Passenger Chest	0.11	0.18	23.61	22.77	-0.42	-0.58	8.73	9.31
Driver Knee	0.08	0.17	22.41	22.64	-0.58	-0.79	12.03	18.28
Passenger Knee	0.07	0.14	22.94	22.79	-0.47	-0.71	9.71	10.86
Back Knee	0.1	0.2	23.53	22.8	-0.40	-0.84	8.37	19.85
Driver Foot	0.17	0.12	22.2	22.63	-0.88	-0.63	21.51	13.52
Passenger Foot	0.1	0.17	22.57	22.8	-0.57	-0.71	11.79	15.55
Back Foot	0.2	0.25	23.44	22.68	-0.70	-0.97	15.29	25.11



Figure 112: Renault Megane dashboard and the considered left air diffuser for the parametric variation of the angle of the guiding vanes

In Table 13 can be seen the comparison between numerical and experimental results of the values of velocity, temperature and thermal sensation indexes. Comparing the values for the PMV and PPD indices, small differences can be observed. Some values are indicating a state of discomfort in the case of the numerical model because of the higher air speeds resulting from, the differences between the temperature values being very small. Considering the temperature values, we found a good correlation between the temperature in the measuring points. Larger differences between measured and numerical results can be observed in the case of comparative speeds. In some cases, the difference is small (foot area) but in others the difference is quite large (head and chest region). Since the comparison was made in terms of speed for a given point, even a slight difference between the digital velocity

field and the actual velocity field could lead to this result. An important parameter conducting to these differences between the numerical and experimental results is that in the numerical case, a uniform velocity has been imposed for the entry of the domain.

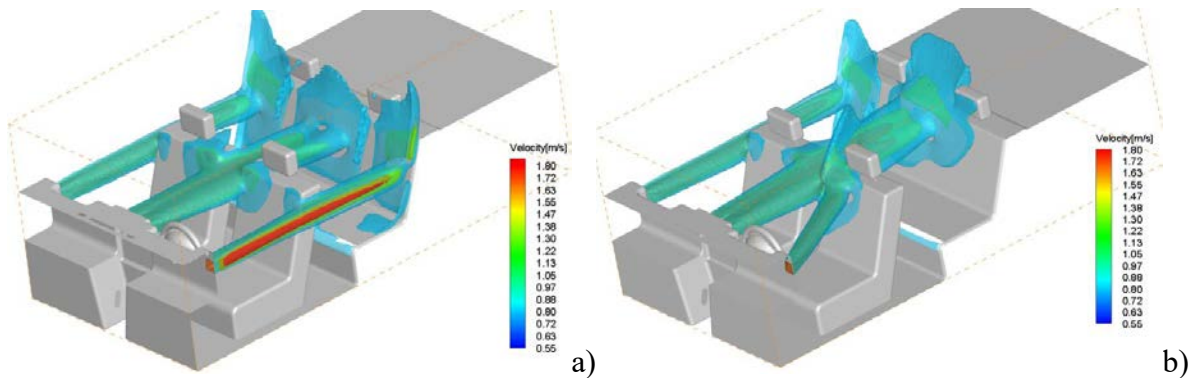


Figure 113: Iso-contours values of the velocity magnitude a) 0°; b) 30°

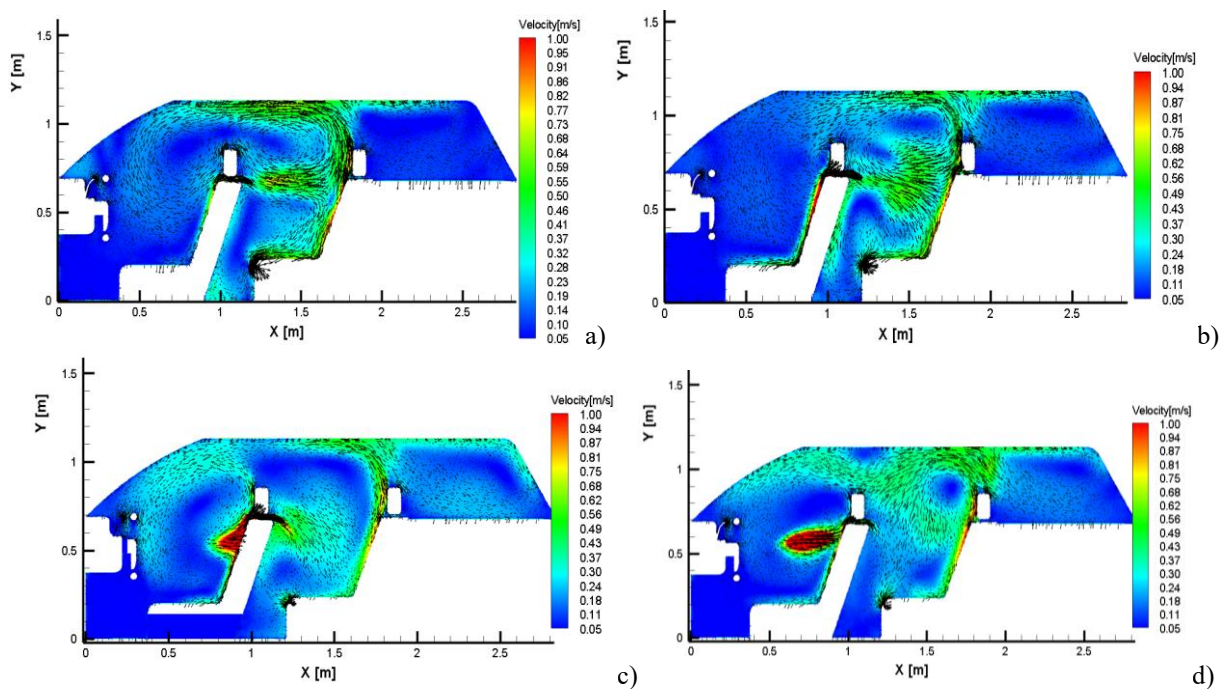


Figure 114: velocity magnitude distribution in plane vectors for the median place of the driver seat: a). 0°; b). 10°; c) 20°; d) 30°

Given the fact that only for the comparison of the velocity values in some areas we have larger differences we considered the validation acceptable.

After the previous global validation of the numerical model, a first case study was to investigate the effect of different angles of the diffuser airflow (left side only) over thermal sensation (Figure 111). We considered this step in our study in order to have a first quantitative response of the importance of the flow dynamics inside the car cabin on the

presumptive thermal sensation response as predicted by the PMV/PPD indices.

For the left side air diffuser, we modified the angle of the vertical guiding vanes in the horizontal plane from 0° to 30° , with a 5° step angle. The Figure 113 is showing the iso-contours of the velocity magnitudes corresponding to those two extreme angles. We considered isothermal conditions, maintaining the same flow rate as previously for all studied cases. Figure 114 is presenting the distributions of the velocity magnitude and of the in-plane vectors for the median plane of the driver and Figure 115 is presenting the same distributions of parameters for the median plane of the front passenger. The global pattern of the flow inside the cabin is changing very much with the variation for only one air vent. This changing of the position was performed only in the horizontal plane. Beginning with an angle of 20° , the velocity magnitude values in the drivers' chest region are higher than 1m/s . In the region of the face and chest for the rear left passenger the velocity magnitude displays values over 0.5m/s . The same observations could be done for the median plane of the front passenger. In this case, in the rear right passenger region, the velocity magnitude displays even higher values with the increase of the guide vanes angle of the left side air diffuser.

In Figure 116 are presented the distributions of the velocity magnitude and of the in-plane vectors, in a horizontal plane, at the chest level for the two extreme angles 0° and 30° . It is interesting to note that the central flow displays a larger spread in the horizontal plane, and the central core is much shorter in the first case. This behavior could be understood in correlation with Figure 4 where one could observe that the left side air jet enters in interaction with the central flow, resulting in an acceleration of the latter one. For 30° the side jet enters the central region between the front seats and impinges on the rear right seat.

With the air speed values from the numerical model and considering the metabolic rate value of 1 met and clothing insulation of 0.7 clo, the Predicted Mean Vote (PMV) and the Predicted Percentage of Dissatisfied (PPD) indexes were calculated. Tables I and II present values for the PMV and PPD indexes obtained at the right of each passenger place in the cabin for respectively the head, the chest, the knees and the feet. It appears from these tables that the most favorable position of the guiding vanes of the studied air vent is for an angle of 0° , knowing that most of PMV and PPD values fall in the acceptable range close to thermal neutrality. As the angle of the guiding vanes of the left air vent increases, values of PMV decreases showing an increased sensation of cooling.

This is rendered by higher vales of the percentages of dissatisfied. Driver's head location seems to be not much unaffected by this variation, excepted for the 20° angle where the velocity magnitude is increasing. For the front passenger head location, we could not

distinguish a clear trend for the variation of PMV-PPD values, most of them indicating much higher values for the velocity magnitude of air. As for the head region located at the position of the two rear passengers, all the values of PMV fall in the range between slightly cool and cool.

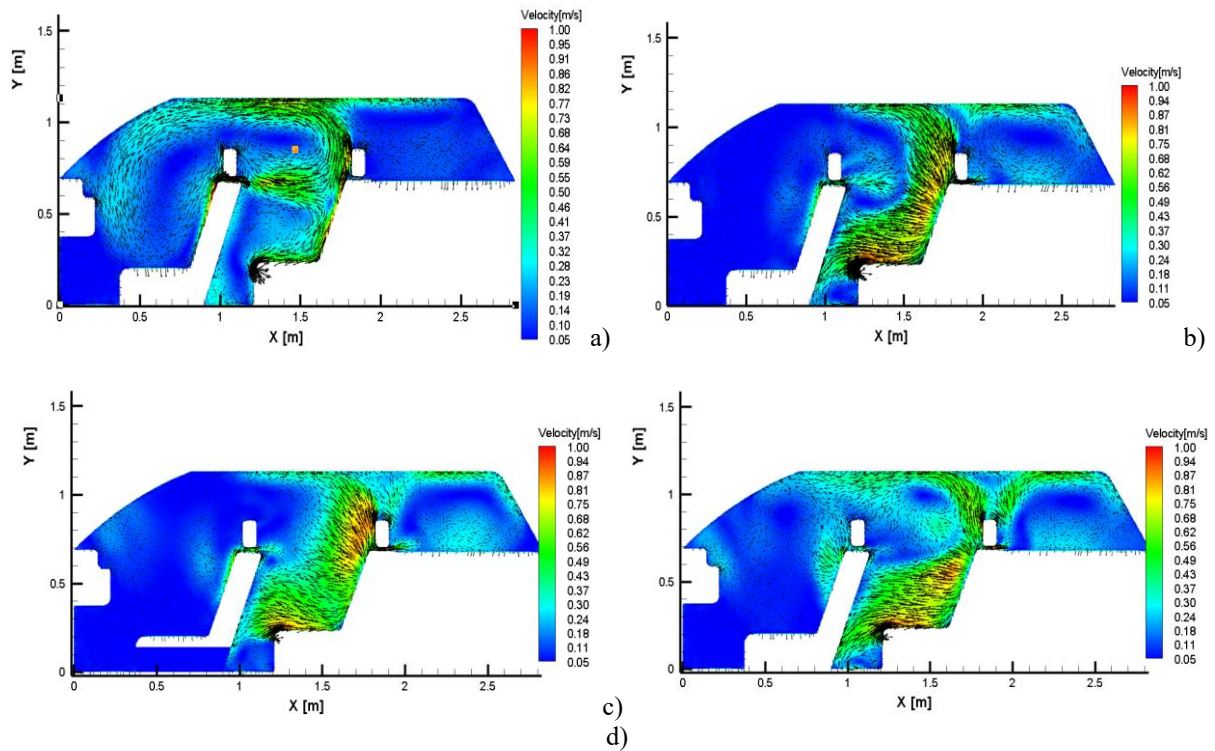


Figure 115: Distribution of the velocity magnitude and of the vectors in median plane of the driver: a). 0°; b). 10°; c) 20°; d) 30°

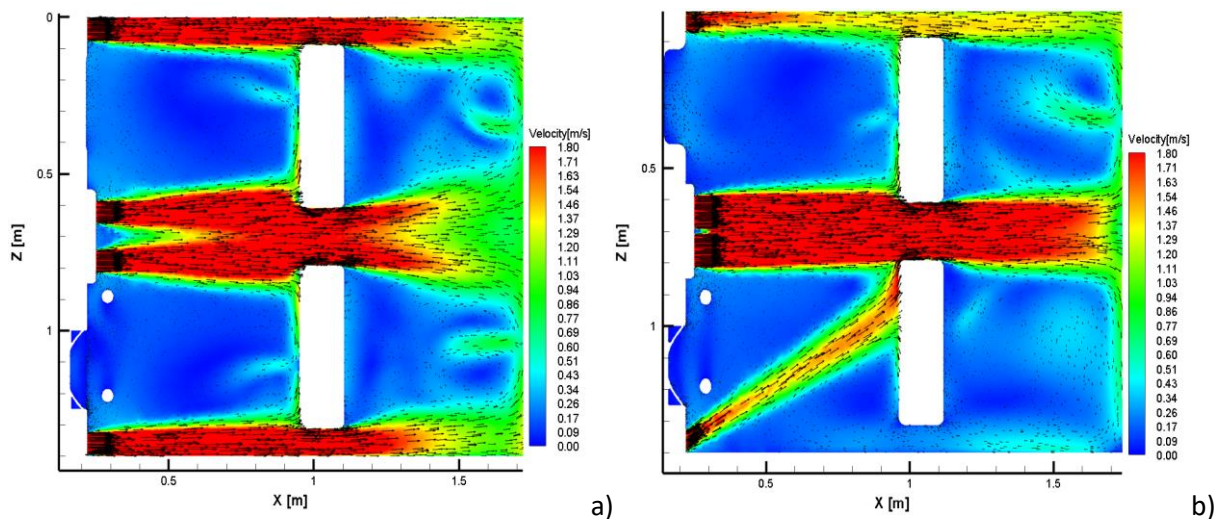


Figure 116: Distribution of the velocity magnitude and of the vectors in at the chest level in horizontal: a) 0°; b) 30°

All the points situated at the knees and feet locations for the front passengers seem to

be unaffected by this variation, while for the rear passengers the same observation as for the head region could be done: all values of PMV fall between slightly cool and cool range.

Table 14: PMV index values for different angle values

Point/ parameter	PMV						
	0°	5°	10°	15°	20°	25°	30°
D. Head	-0.54	-0.56	-0.69	-0.73	-0.98	-0.76	-0.54
P. Head	-0.54	-0.78	-0.60	-0.76	-0.54	-0.54	-1.00
R.R. Head	-1.44	-1.40	-1.12	-0.96	-0.94	-1.05	-1.08
R.L. Head	-1.50	-1.19	-1.53	-1.53	-1.59	-1.42	-1.23
D. Chest	-0.54	-0.66	-0.66	-0.71	-1.66	-2.10	-1.87
P. Chest	-0.59	-0.66	-0.75	-1.04	-0.86	-0.70	-1.04
R.R. Chest	-1.53	-0.77	-1.19	-1.08	-0.94	-0.61	-1.07
R.L. Chest	-1.49	-1.57	-1.56	-1.55	-1.47	-1.62	-1.61
D. Knee	-0.54	-0.54	-0.55	-0.54	-0.54	-0.54	-0.54
P. Knee	-0.54	-0.77	-0.54	-0.54	-1.08	-0.54	-0.54
R.R. Knee	-0.98	-0.65	-0.77	-0.94	-1.02	-1.08	-0.83
R.L. Knee	-1.44	-0.54	-1.46	-1.41	-1.45	-1.48	-1.48
D. Foot	-0.54	-0.54	-0.54	-0.54	-0.54	-0.54	-0.54
P. Foot	-0.54	-0.62	-0.54	-0.54	-0.54	-0.54	-0.54
R.R. Foot	-0.58	-0.90	-0.72	-0.77	-0.72	-0.92	-0.54
R.L. Foot	-0.80	-0.85	-0.80	-0.85	-0.54	-0.98	-0.83

Legend: D. – driver; P. - front passenger; R.R – rear right passenger; R.L. – rear left passenger

Table 15: PPD index values for different angle values

Point/ parameter	PPD						
	0°	5°	10°	15°	20°	25°	30°
D. Head	11.22	11.70	15.18	16.39	25.36	17.31	11.22
P. Head	11.23	17.77	12.66	17.14	11.22	11.23	26.23
R.R. Head	48.05	45.64	31.45	24.57	23.75	28.47	29.94
R.L. Head	51.16	34.82	52.81	52.81	55.98	46.62	36.77
D. Chest	11.22	14.09	14.28	15.65	59.84	81.30	70.61
P. Chest	12.28	14.19	16.85	28.17	20.87	15.37	28.09
R.R. Chest	52.81	17.68	34.82	29.94	23.75	12.95	29.21
R.L. Chest	50.73	54.76	54.38	53.61	49.42	57.76	57.06
D. Knee	11.23	11.24	11.31	11.23	11.23	11.23	11.23
P. Knee	11.23	17.50	11.24	11.24	29.75	11.24	11.24
R.R. Knee	25.37	13.91	17.68	23.75	26.94	29.94	19.48
R.L. Knee	48.05	11.23	48.97	46.14	48.51	49.86	49.86
D. Foot	11.25	11.25	11.24	11.23	11.24	11.24	11.25
P. Foot	11.24	13.23	11.23	11.23	11.23	11.23	11.24
R.R. Foot	11.99	22.08	15.84	17.68	15.84	22.92	11.23
R.L. Foot	18.59	20.36	18.59	20.36	11.23	25.37	19.48

Legend: D. – driver; P. - front passenger; R.R – rear right passenger; R.L. – rear left passenger

As a general observation, we note that this parametric study was performed for air flow rates corresponding to the second position of the manual control of the fan speed, which is a popular selection for this vehicle model in usual circumstances of driving. Maximum

values of the velocity magnitude are rather high compared to the limits of the PMV-PPD models from the standards. Moreover, the locations of these maximum values are changing with the angle of the guiding vanes. However, given the high values recorded for the air velocities, it is obvious for us that the PMV/PPD approach is not adapted, giving as a qualitative method of comparison in this case. These values are rather high at some points when compared to the limits of the PMV-PPD model given in EN ISO 7730 [19]. In the same time, the same study should be performed taking into account the thermal components, like the radiative transfer since the creation of recirculation regions with high velocities, that are a consequence of the impinging of the lateral flows on the windows could be interesting through the perspective of an enhanced heat transfer.

All these observations based on our preliminary tests allowed us to conclude with the following ideas:

- Having measured values for all temperatures on the boundaries of our computational domain and in the air, in a quasi-steady state environment, gives us an interesting possibility to calibrate and validate a numerical model;
- Reasonable flow patterns are obtained for the unoccupied cabin when we compare air temperature and air speed values from the numerical model with the ones measured in the real car cabin;
- The presence of the human body inside this complex and confined cabin geometry is needed in order to model the serious impact upon flow fields;
- A slight change in the initial orientation of one of the air jets is generating a dramatic change in the whole cabin flow pattern. This is raising the question of the validity of the hypothesis of a uniform distribution of the velocity fields at the exit planes of the air diffusers as is the case in most of the available literature.

c. Car cabin with enhanced boundary conditions and human body: final model

Since the beginning, even for the case where only the cabin was considered, several issues were encountered, one of them being the small space from the cabin with a lot of details. We tried to overcome this shortcoming, by simplifying the geometry as much as possible without interfering with the elements that are affecting the flow. When we decided to introduce the virtual human body inside the cabin, another issue was to find a relevant position. We wanted to have the virtual manikin in the driving position with a hand on the steering wheel and as much as possible introduced in to the seat to avoid narrow spaces

formation which will lead to mesh of poor quality in those areas.

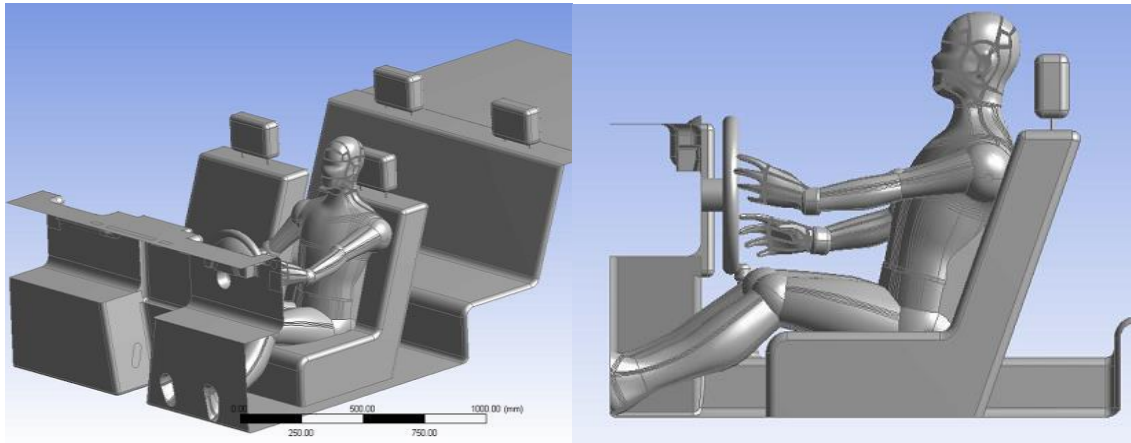


Figure 117: Isometric and side view of the studied geometrical model

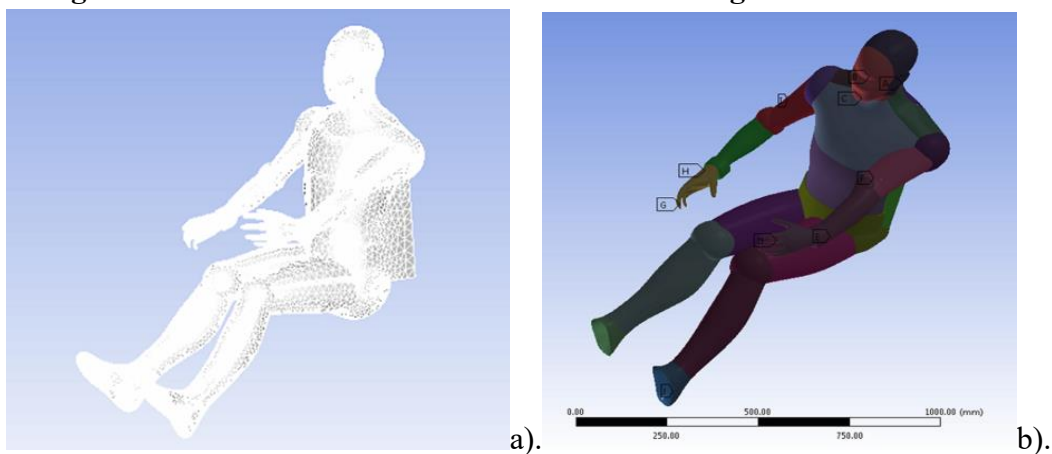


Figure 118: Virtual manikin zones

After several trials a virtual manikin was installed in the automobile on the driver's seat. Since we did not have the time and skills to draw a virtual manikin, we studied tens of virtual manikins' geometries available on the web. We tried the majority of the virtual manikins in Ansys Design Modeler, Solid Works and Catia. Most of the virtual manikins could not be opened as a solid and we could not obtain a solid part from the manikins' surfaces. Some geometries had other problems like adjacent surfaces that overlap or did not close. Also, some geometries could not be meshed properly because of the high density of details. We could use only one geometry for the virtual manikin which was posed in a driver position but we had to reconstruct some parts from his body. This final reconstructed virtual manikin in driving position is presented in Figure 117. The reconstruction and the scaling of the virtual manikin was made considering our real thermal manikin developed at UTCB. The virtual manikin was split in 16 larger zones as the measuring parts of the equivalent temperature of the previously developed experimental thermal manikin. These zones are

composed of smaller parts (Figure 118 b) related with the anatomic parts of a real human. This manikin was scaled in order to have a standard height of 1.70m and its surface area is 1.81m^2 being suitable for a standing posture. It has a total surface in contact with the cabin air (1.20 m^2) for a sitting posture. The rest of the total surface was in contact with the solid surfaces of the automobile cabin (seat).

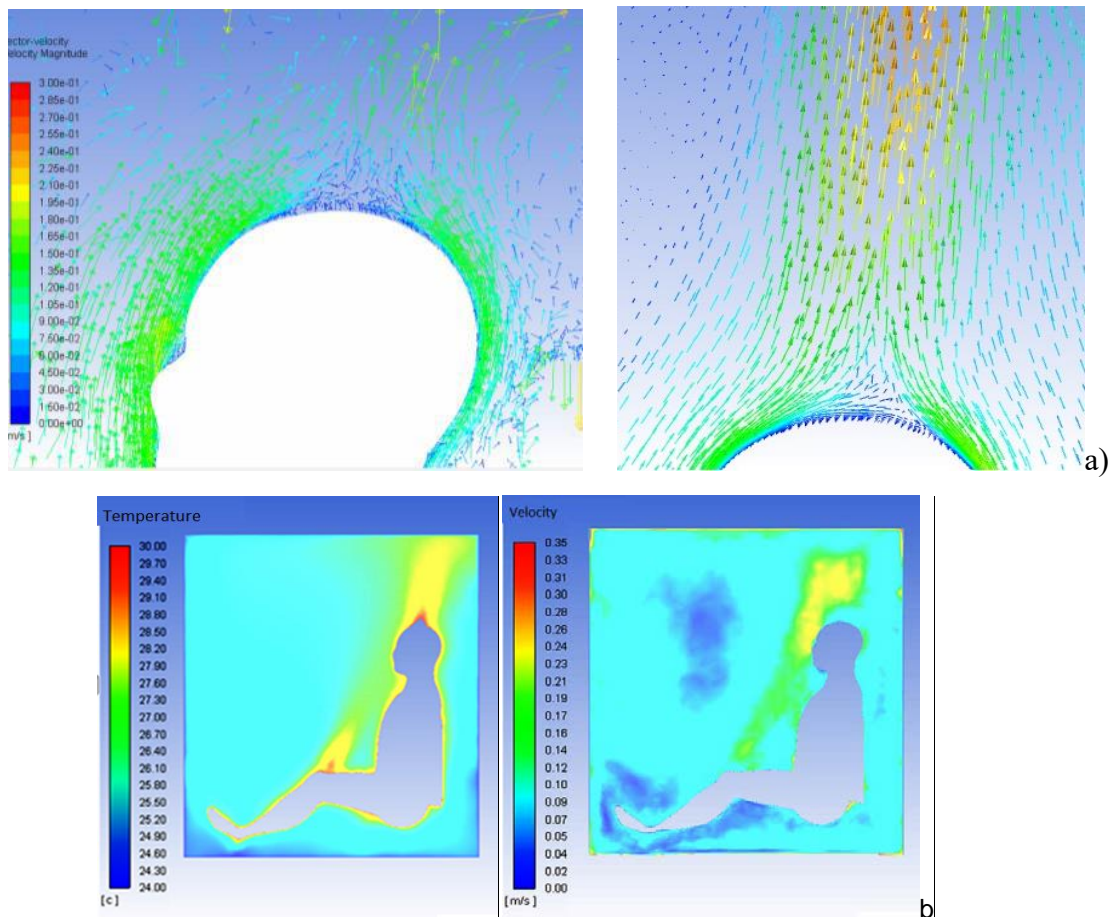


Figure 119: Manikin thermal plume evolution placed in the testing box: a) Velocity vectors field detail; b) temperature distribution in the sagittal plane; c) velocity magnitude distributions in the sagittal plane

Once chosen the final virtual manikin geometry, prior the mesh dependency tests in the vehicle cabin geometry, the manikin was first meshed and tested in a virtual box, to simulate the evolution of the thermal plume Figure 119. The imposed temperature on the manikin surface was 34°C and the ambient temperature 24°C with no air velocity, our desire being to create a natural convection flow around the virtual thermal manikin.

Maybe the most difficult to validate flow in this case would be the human thermal plume and we decide to compare our results from the testing box with an experimental study performed at UTCB [276] and with other data from the literature. As expected we noted the existence of a recirculation region above the head, corresponding to a small low-pressure

zone just above the head. This stagnant area is well evidenced in both numeric and experimental cases. In addition, we can see in both situations the existence of a smaller convective flow in the direction of the forehead, which meets the main convective flow. This secondary flow seems to meet with another flow coming from behind the manikin. General shape of the three fields is similar and we emphasize once again the previous finding, namely that $k-\omega$ SST model satisfactorily reproduces the dynamics of convection plume. In addition, we note that the values obtained for the case without the jet, both by numerical and experimental way are similar to those obtained by Sorensen and [242]. If we observe the distribution of temperature fields obtained by numerical and experimental method outlined above, we remark that the values scale obtained in the two cases is similar.

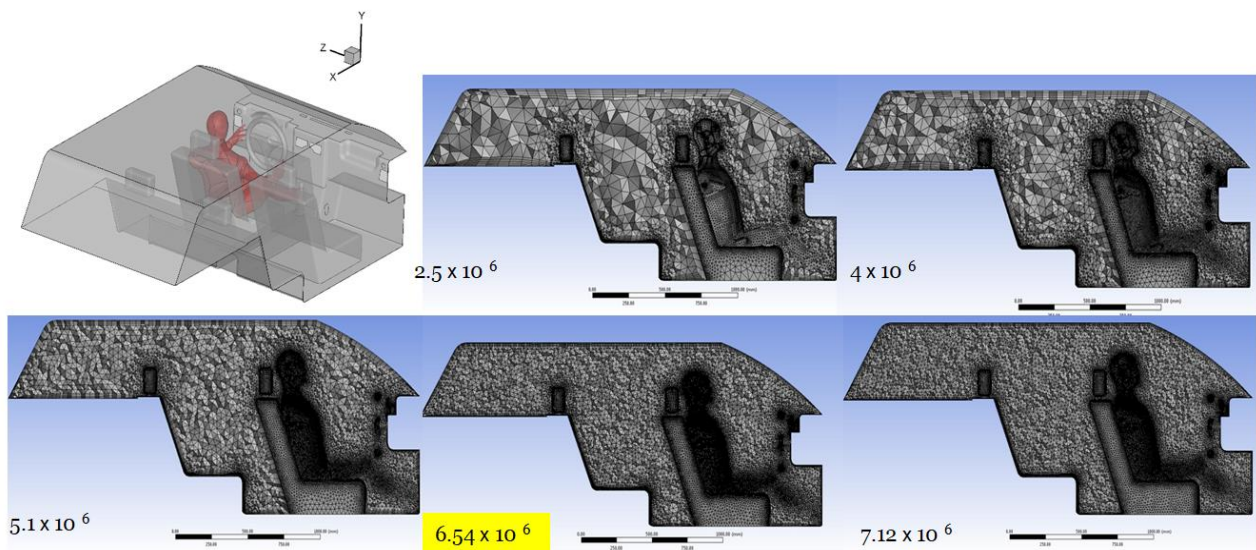


Figure 120: Numerical grids used for the mesh independence study of the numerical model with virtual thermal manikin introduced (driver position)

Given the satisfactory tests from the testing box we proceeded to the meshing of the final domain of the cabin car with virtual driver. The mesh grid was as previously realized in Ansys Workbench. The elements used for the mesh grid are prisms in the boundary layer and tetrahedral in the rest of the domain due to the high complexity of the studied geometry. Several meshes were tested to check the independence of the solution (Figure 120). A fine mesh consisting of 6.5 million elements was chosen based on the experience from the previous studies where we performed the grid dependence test [272]. The boundary layer consists in five layers, with the first cell height of 0.75mm and a growth factor of 1.2. As a first case study, for a first evaluation of the new numerical model we decided to go back to the previous case where we investigated the change of the inclination angle of the flow in the horizontal plane and to investigate the influence of the driver presence without taking for the

moment the thermal plume into consideration. Further we will call “Case I” –the numerical simulations without virtual manikin; and “Case II” – numerical simulations with virtual manikin in the cabin. In each of these cases the left air diffuser angle of the guiding vanes was modified on horizontal plane with one step of 5° towards the interior cabin from 0° to 30°. In conclusion 14 numerical simulations were made for each case, each having a different angle.

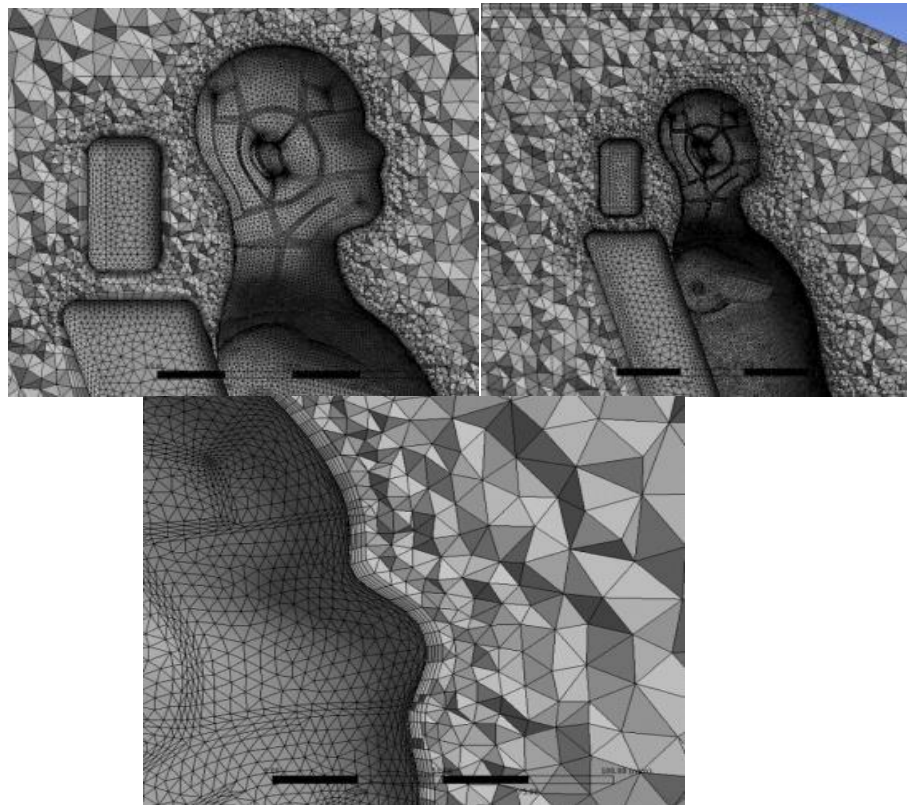
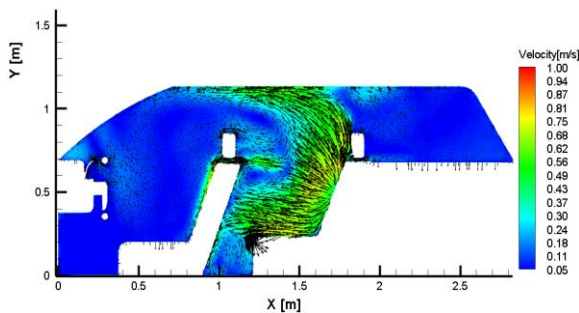
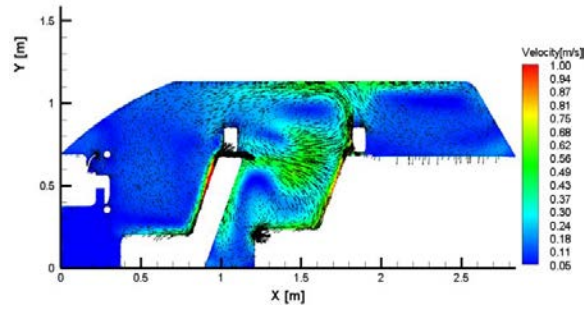


Figure 121: Numerical grid used for numerical simulation (different close-ups)

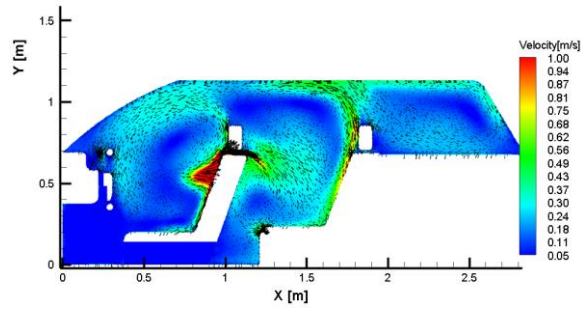
As previously a value of 23°C was imposed for the inlet air temperature, internal and external ambient temperature and on the cabin and manikin surfaces temperature. For the air diffuser that is placed on the left side of the car, the angle that is orienting the vertical guiding vanes inside in the horizontal plane was modified from 0° to 30°, with a 5° elementary angle.



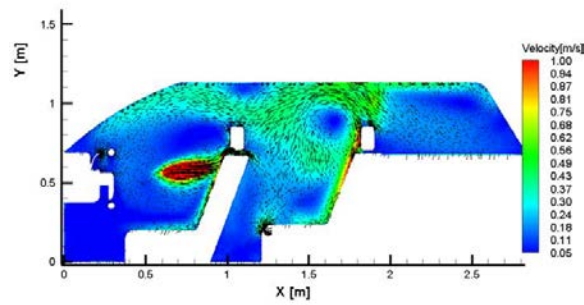
a).



b).

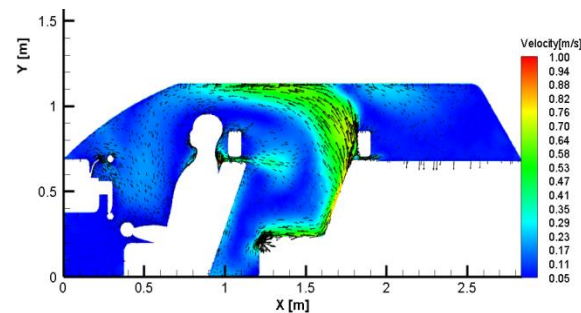


c).



d).

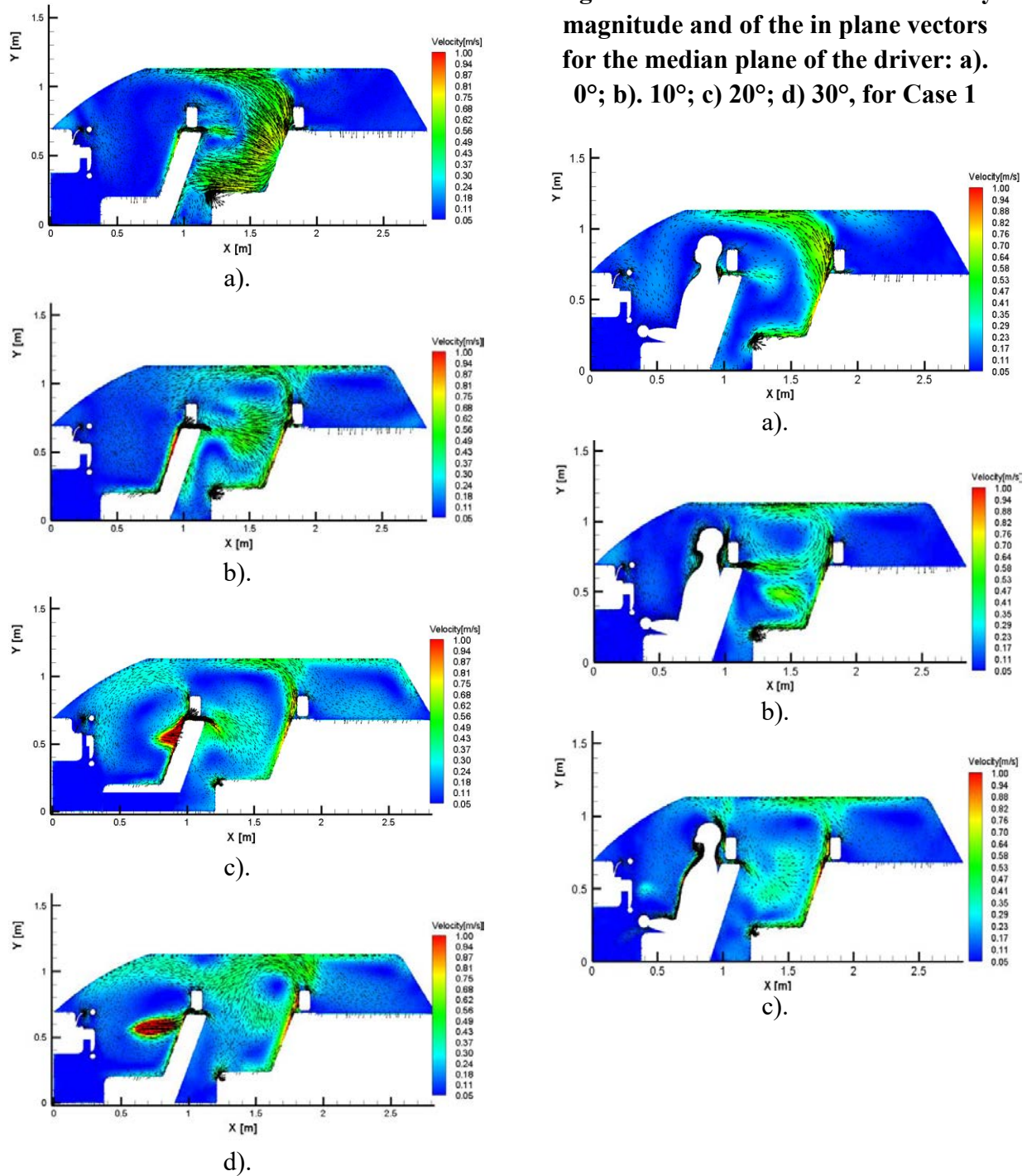
Figure 122: Distribution of the velocity magnitude and of the in plane vectors for the median plane of the driver: a). 0°; b). 10°; c) 20°; d) 30°, for Case 1

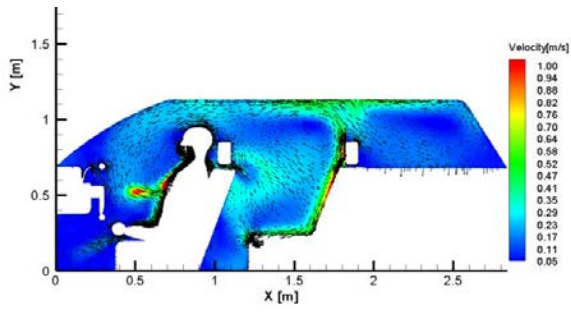


and Figure 123 are presenting the velocity magnitude map and of the in-plane vectors for the median plane passing through the center of the driver seat for both studied cases. As the effect produced by the presence of a human body, the air passing on the rear part of the cabin is obstructed, also his presence produces vortices in the neck and head zone of the virtual driver. For an angle value of 20°, the velocity magnitude values in the driver's chest region are higher than 1m/s. At the location of the face and the chest for the rear left passenger the

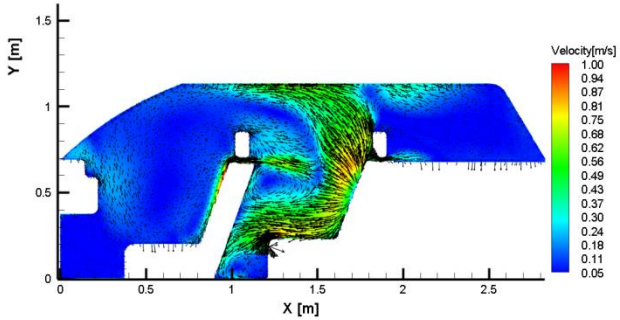
velocity magnitude displays values over 0.5m/s. The same observations could be done for the median plane at the place of the right passengers. The pattern of the flow is modified substantially with the angle changing, while the presence of the manikin body diminishes air velocity in the rear part of the cabin. Comparing the velocities found in rear part of the vehicle, high velocities was found in the rear right part of the car comparing with the rear left part. The causes are the inlet angle modification and the presence of the driver.

Figure 122: Distribution of the velocity magnitude and of the in plane vectors for the median plane of the driver: a) 0°; b) 10°; c) 20°; d) 30°, for Case 1



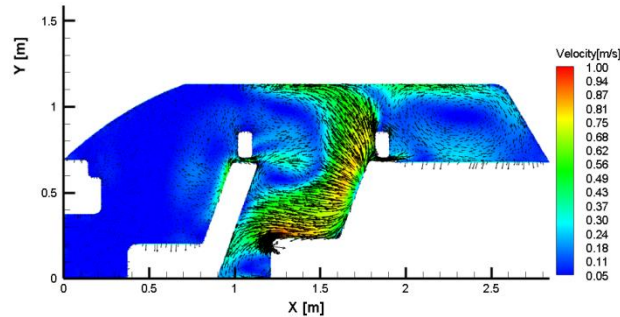


d).
Figure 123: Distribution of the velocity magnitude and of the in plane vectors for the median plane of the driver: a). 0°; b). 10°; c) 20°; d) 30°, for Case 2

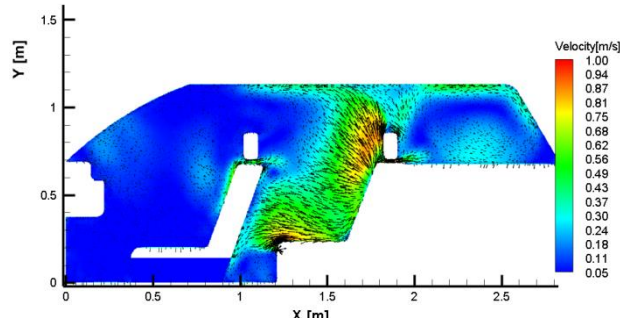


d).
Figure 124: Distribution of the velocity magnitude and of the in plane vectors for the median plane of the passenger: a). 0°; b). 10°; c) 20°; d) 30°, for Case 1

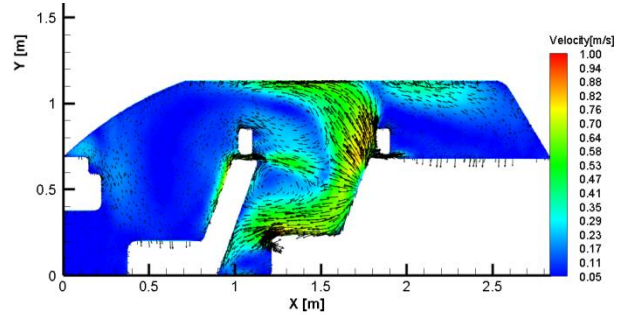
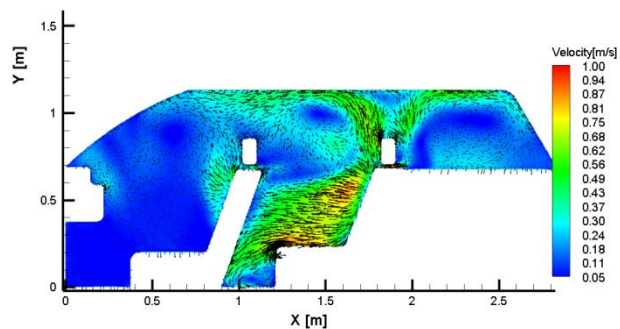
a).



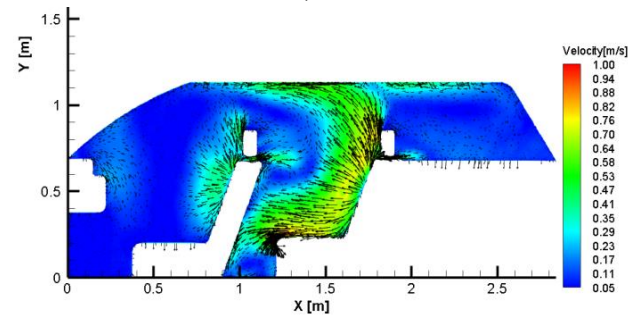
b).



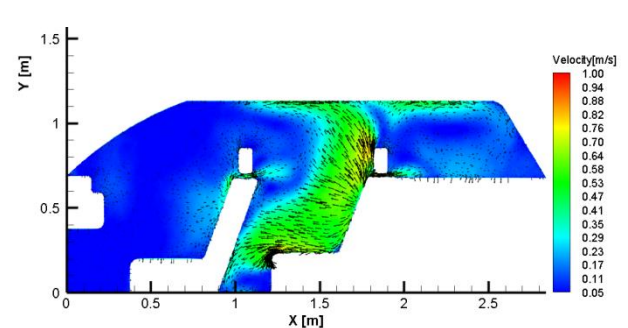
c).



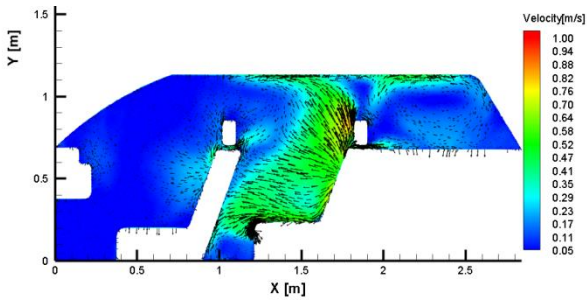
a).



b).



c).



d).
Figure 125: Distribution of the velocity magnitude and of the in plane vectors for the median plane of the passenger: a). 0°; b). 10°; c) 20°; d) 30°, for Case 2

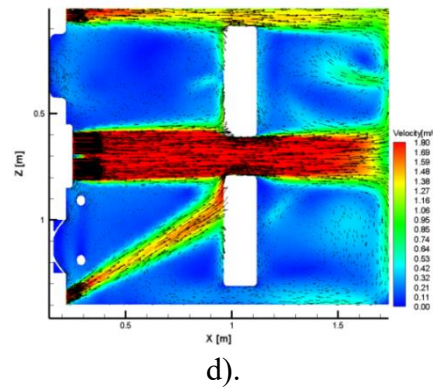
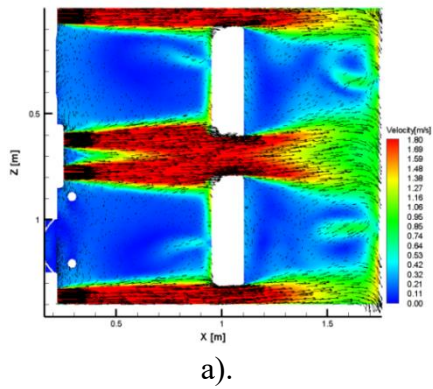
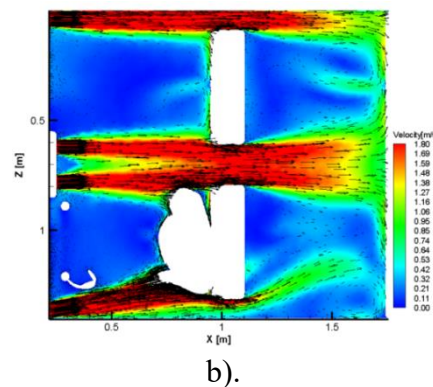
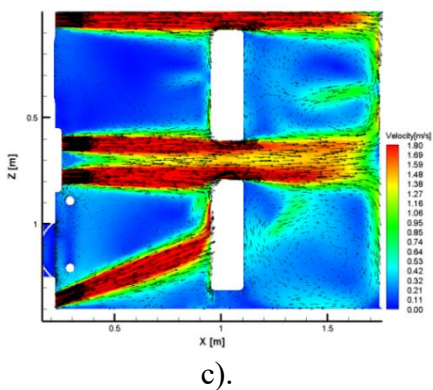
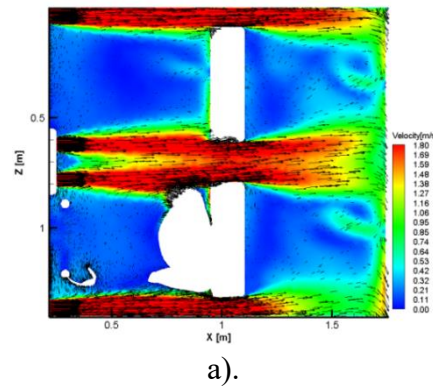
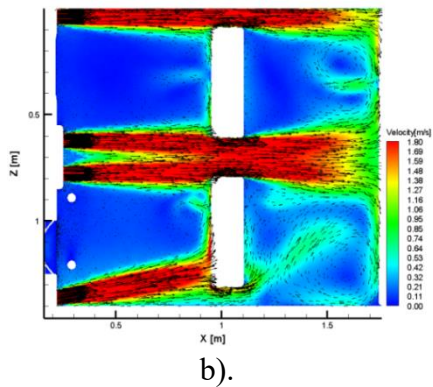
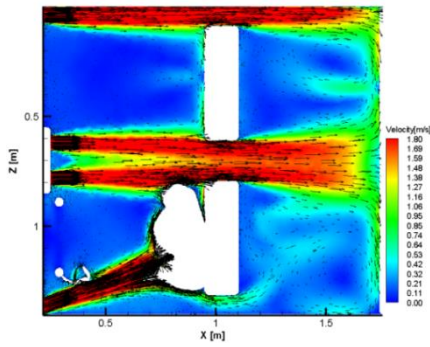
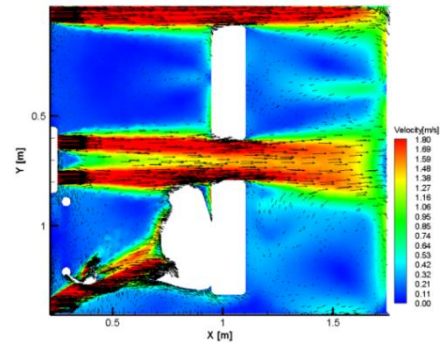


Figure 126: Distribution of the velocity magnitude and of the in plane vectors for the median plane of the passenger: a). 0°; b). 10°; c) 20°; d) 30°, for Case 1





c).



d).

Figure 127 :Distribution of the velocity magnitude and of the in plane vectors for the median plane of the passenger: a). 0°; b). 10°; c) 20°; d) 30°, for Case 2

Table 16: PMV index comparison for Cases I and II

Point/ parameter	0°		10°		20°		30°	
	Case I	Case II	Case I	Case II	Case I	Case II	Case I	Case II
D. Head	-0.54	-0.54	-0.54	-1.00	-0.54	-0.54	-0.54	-0.58
P. Head	-0.54	-0.54	-0.54	-0.58	-0.65	-0.54	-0.71	-0.54
R.R. Head	-1.44	-1.45	-1.12	-1.15	-0.94	-0.93	-1.08	-0.85
R.L. Head	-1.50	-1.56	-1.53	-1.54	-1.59	-1.50	-1.23	-1.50
D. Chest	-0.54	-0.54	-0.58	-1.02	-0.80	-1.95	-2.08	-1.92
P. Chest	-0.54	-0.54	-0.74	-0.72	-0.72	-0.71	-0.60	-0.74
R.R. Chest	-1.53	-0.90	-1.19	-0.92	-0.94	-0.99	-1.07	-0.92
R.L. Chest	-1.49	-1.39	-1.56	-1.51	-1.47	-1.45	-1.61	-1.34
D. Knee	-0.54	-0.54	-0.54	-0.54	-0.54	-0.54	-0.54	-0.55
P. Knee	-0.63	-0.54	-0.54	-0.54	-0.54	-0.54	-0.54	-0.54
R.R. Knee	-0.98	-0.68	-0.77	-0.95	-1.02	-0.87	-0.83	-1.00
R.L. Knee	-1.44	-1.41	-1.46	-1.46	-1.45	-1.39	-1.48	-1.26
D. Foot	-0.54	-0.54	-0.54	-0.54	-0.54	-0.54	-0.54	-0.54
P. Foot	-0.54	-0.54	-0.54	-0.54	-0.54	-0.54	-0.54	-0.54
R.R. Foot	-0.58	-0.82	-0.72	-0.68	-0.72	-0.80	-0.54	-0.77
R.L. Foot	-0.80	-0.76	-0.80	-0.72	-0.54	-0.74	-0.54	-0.54

Table 17: PPD [%] index comparison

Point/ parameter	0°		10°		20°		30°	
	Case I	Case II	Case I	Case II	Case I	Case II	Case I	Case II
D. Head	11.23	11.23	11.24	26.16	11.23	11.23	11.23	11.99
P. Head	11.23	11.23	11.23	11.99	13.81	11.23	15.55	11.23
R.R. Head	48.05	48.51	31.45	32.83	23.75	23.25	29.94	20.36
R.L. Head	51.16	54.27	52.81	53.01	55.98	51.03	36.77	50.99
D. Chest	11.23	11.23	12.18	26.94	18.59	74.45	80.41	73.40
P. Chest	11.23	11.23	16.49	15.84	15.93	15.65	12.57	16.68
R.R. Chest	52.81	22.08	34.82	22.92	23.75	25.69	29.21	22.92
R.L. Chest	50.73	45.04	54.38	51.37	49.42	48.60	57.06	42.73
D. Knee	11.23	11.23	11.23	11.23	11.23	11.23	11.23	11.32
P. Knee	13.33	11.23	11.23	11.23	11.23	11.23	11.23	11.23
R.R. Knee	25.37	14.90	17.68	24.16	26.94	20.93	19.48	26.16
R.L. Knee	48.05	46.19	48.97	48.97	48.51	45.39	49.86	38.22
D. Foot	11.23	11.23	11.23	11.23	11.23	11.23	11.23	11.23
P. Foot	11.23	11.23	11.23	11.23	11.23	11.23	11.23	11.23
R.R. Foot	11.99	19.39	15.84	14.90	15.84	18.59	11.23	17.68
R.L. Foot	18.59	17.32	18.59	15.84	11.23	16.77	11.23	11.23

With the air speed values from the numerical simulation and with a metabolic rate value of 1 met and clothing insulation of 0.7clo, the Predicted Mean Vote (PMV) and the Predicted Percentage of Dissatisfied (PPD) indexes were calculated. Tables 16 and 17 give values for the PMV and PPD indexes obtained at the right of each passenger place in the cabin for respectively the head, the chest, the knees and the feet. Although, as visible in Figures 123-128, the global pattern of the flow in the cabin is affected by the presence of the human body, if we take a look to the PMV and PPD values from the Tables 16 and 17 we can observe that the differences are very slight, questioning ourselves once again about the sensitivity of these indexes.

The final step in our numerical model was to find a way to reproduce a more realistic boundary condition than the uniform velocity at the air vents. To this end we imposed at the inlets representing the air diffusers on the dashboard, the measured velocity fields that we measured with the help of our third experimental set-up that was presented in Chapter 3, B, e).

In these final cases we also considered the isothermal situation, therefore the value of 23°C was imposed for the inlet air temperature, internal and external ambient temperature and on the cabin and manikin surfaces temperature. A comparison between the Case 2 with uniform inlet velocity (as boundary conditions for the ventilation flow a mass flow rate of 0,0057 on the central air vents and a mass flow rate of 0,0043 kg/s on the side air vents) and Cases 3 and 4 corresponding respectively to the measured velocity fields at the exit of the classical air diffuser grilles (CG) and at the lobed ailerons air diffusers grilles (LAG).

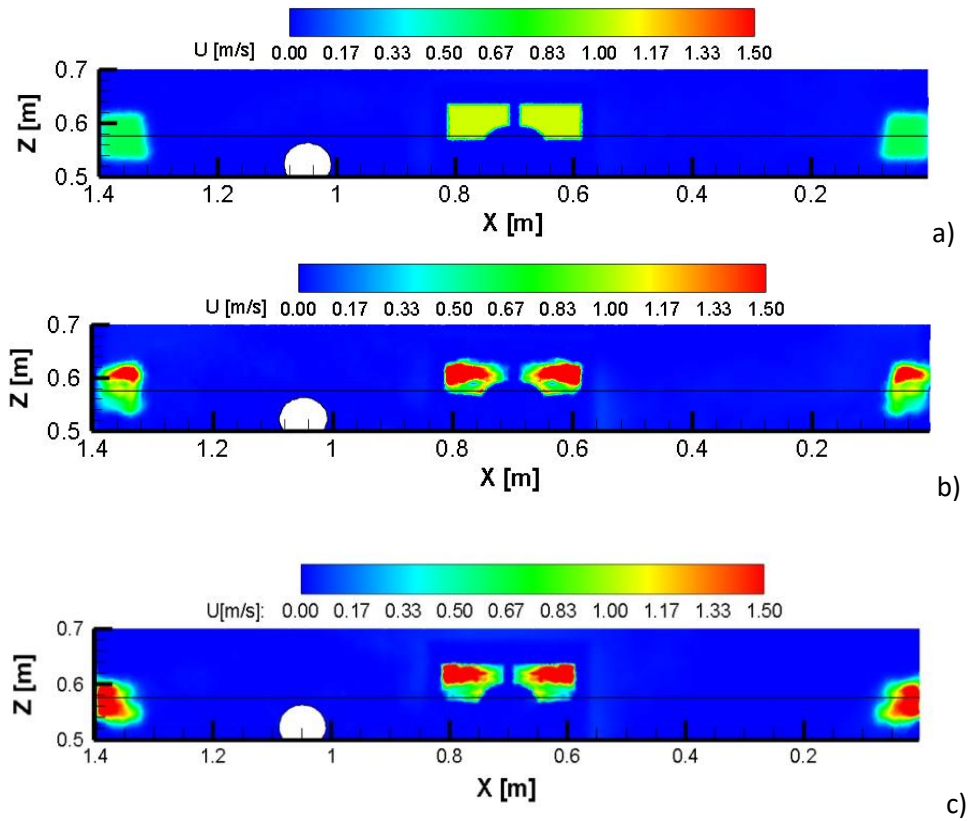


Figure 128: Axial velocity component distribution at the outlets: a) Case 2; b) Case 3 - CG, c) Case 4 - LAG

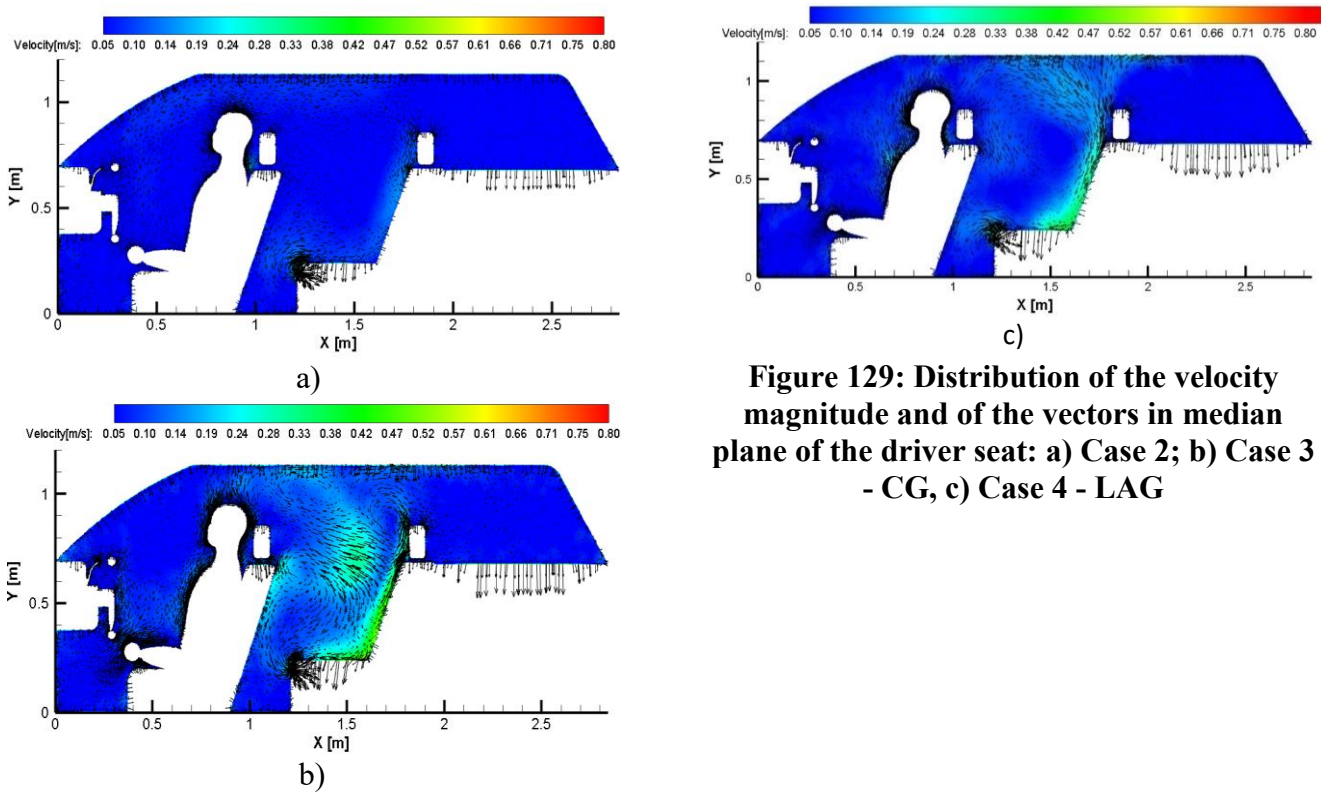


Figure 129: Distribution of the velocity magnitude and of the vectors in median plane of the driver seat: a) Case 2; b) Case 3 - CG, c) Case 4 - LAG

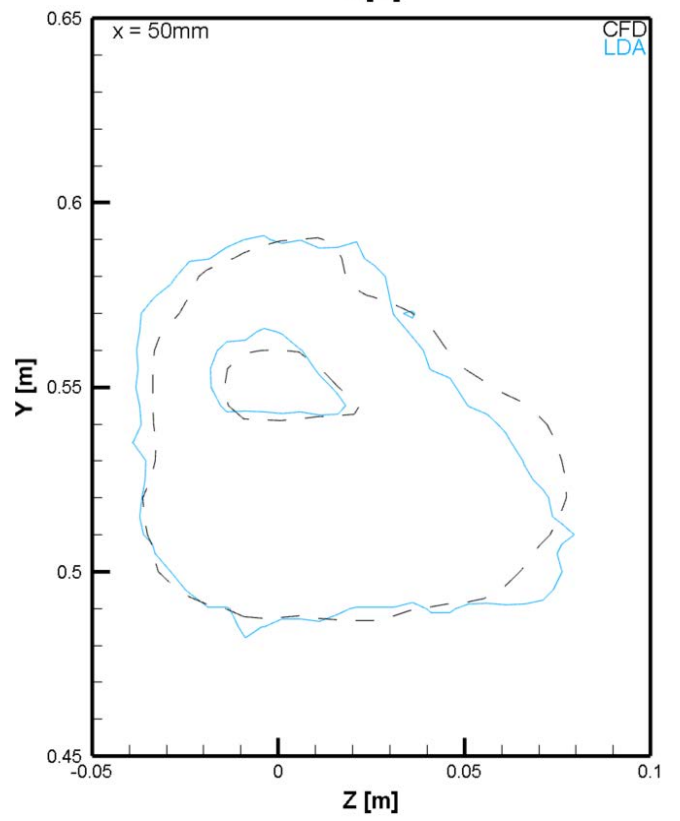
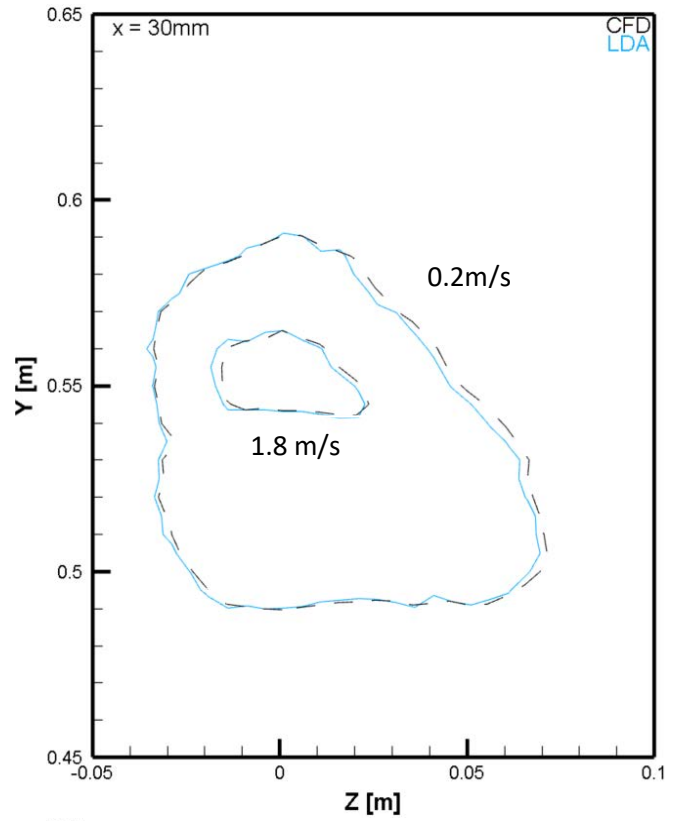
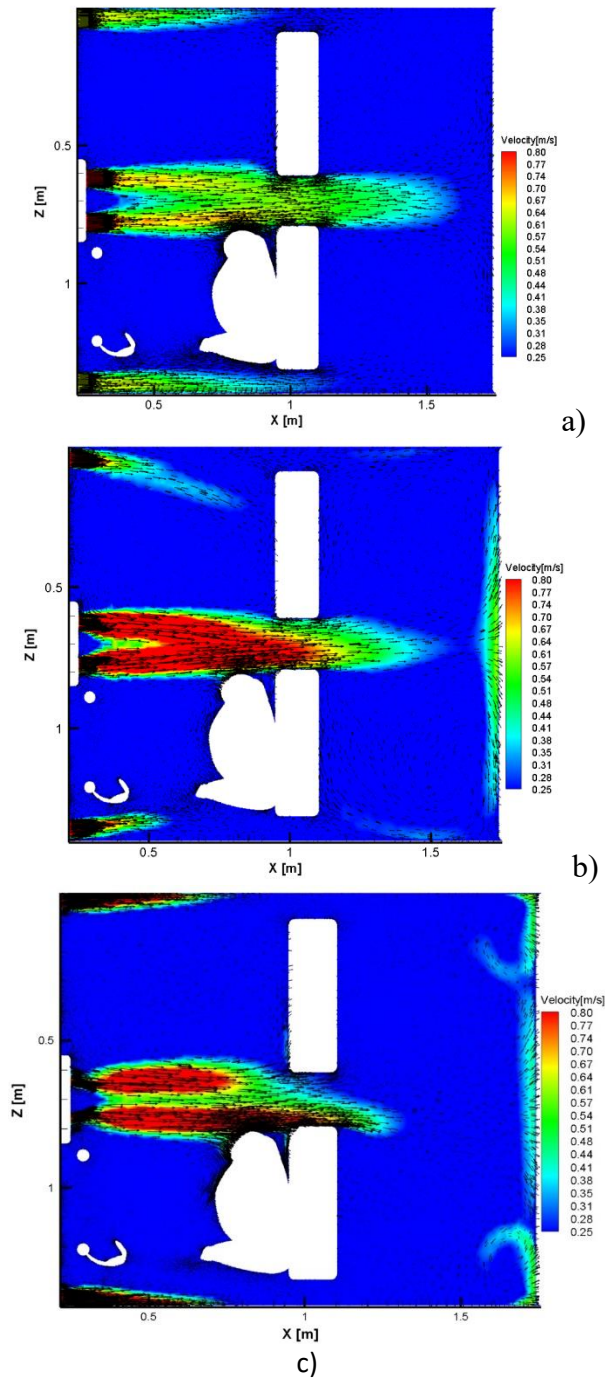


Figure 130: Distribution of the velocity magnitude and of the vectors in at the chest level in horizontal for: a) Case 2; b) Case 3 - CG, c) Case 4 - LAG

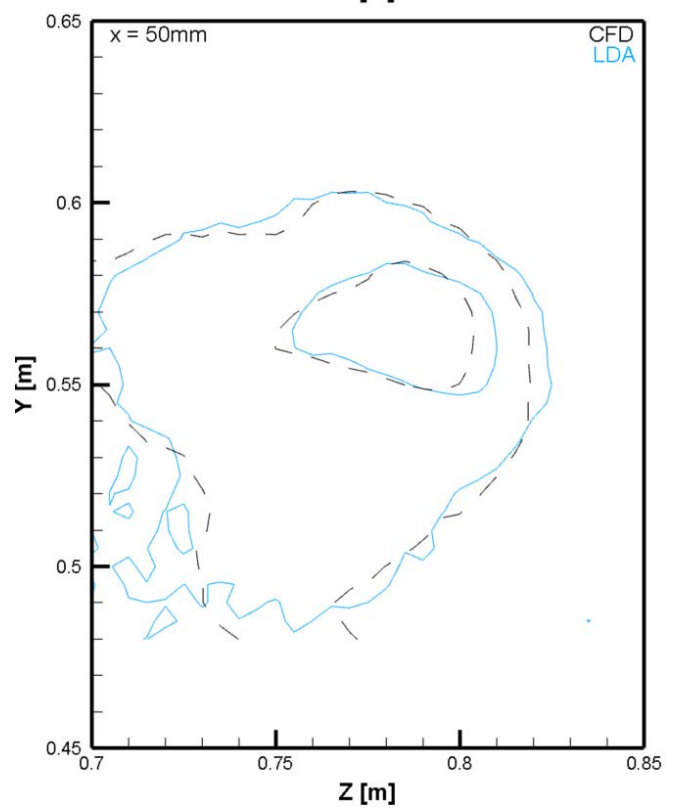
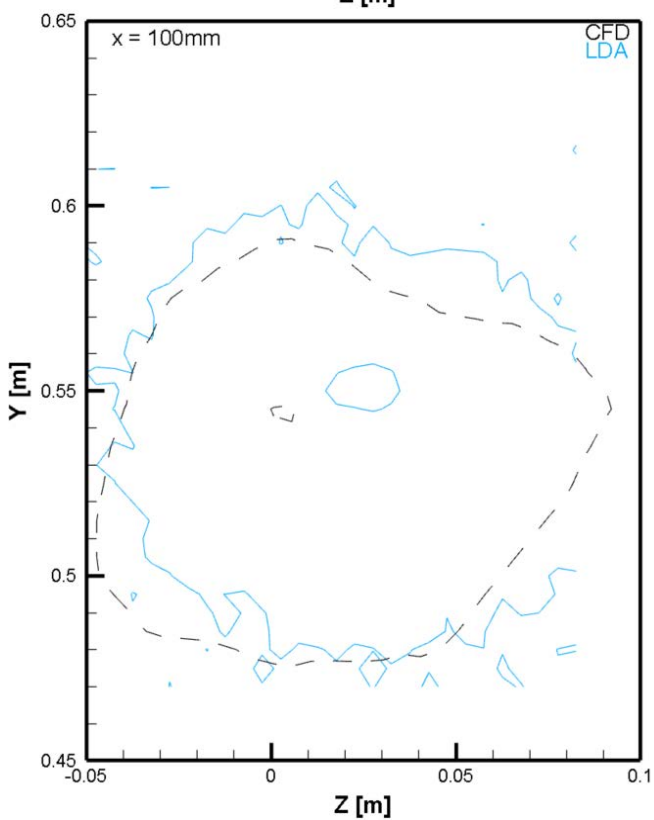
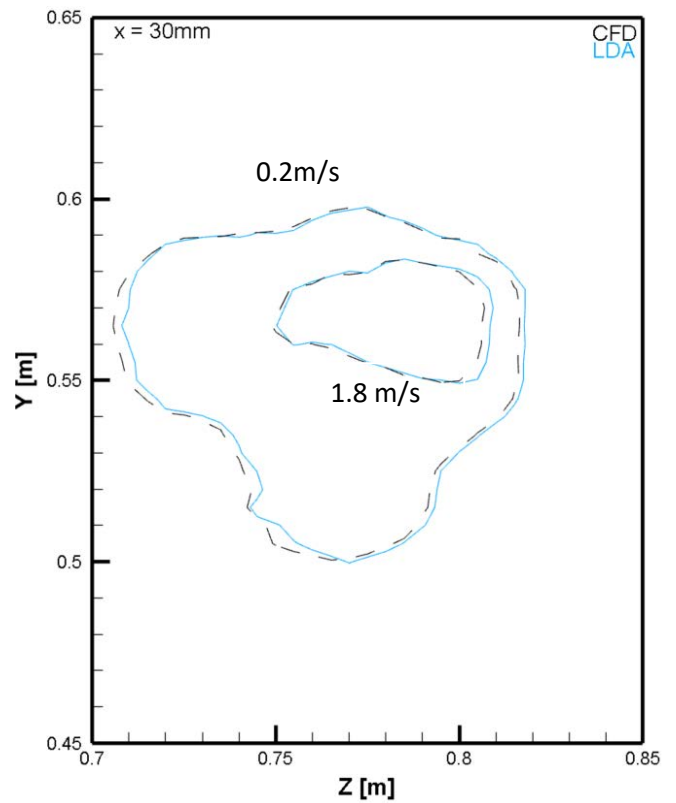
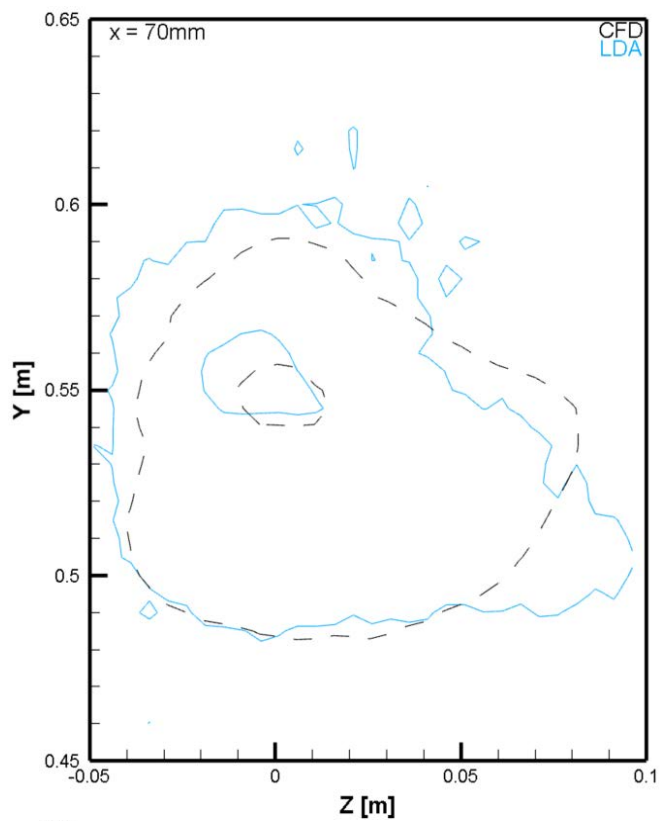


Figure 131: Side Classical grills - Side grille CG (The inner contours are corresponding to 1.8m/s and the outer contours are corresponding to 0.2 m/s)

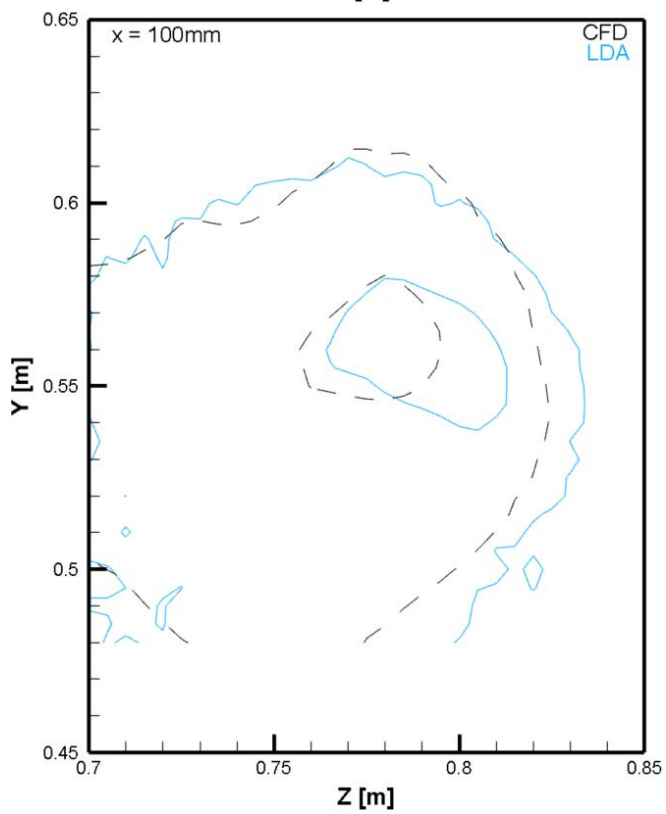
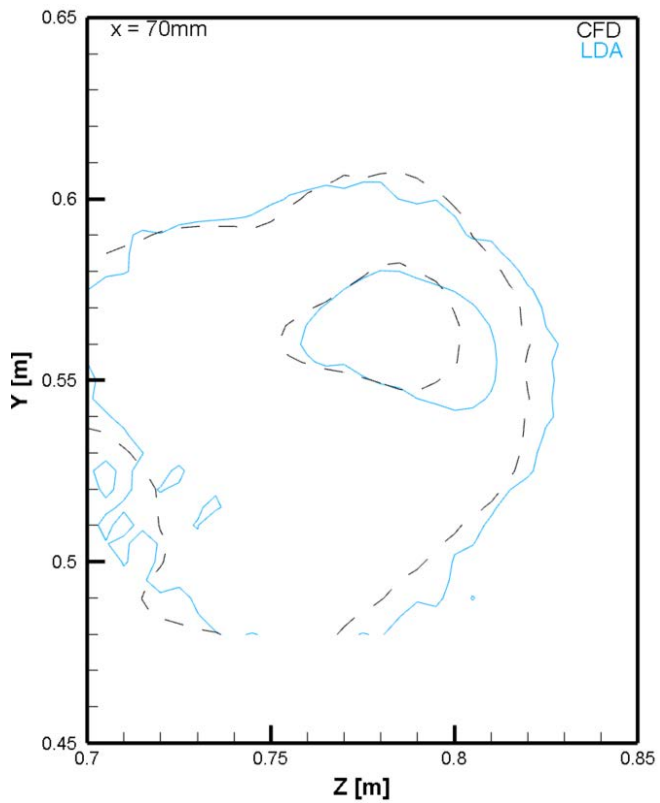


Figure 132: Center Classical grills - Side grille CG (The inner contours are corresponding to 1.8m/s and the outer contours are corresponding to 0.2 m/s)

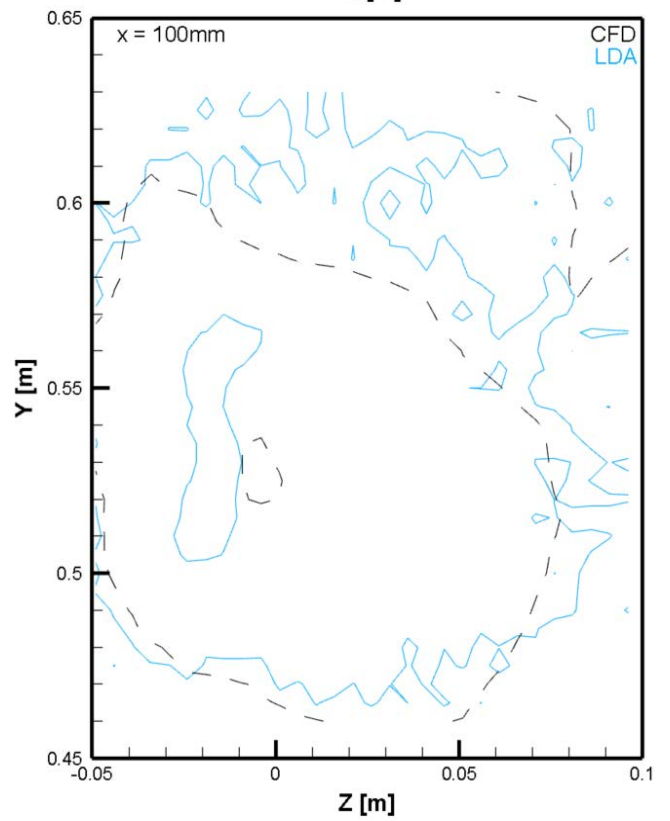
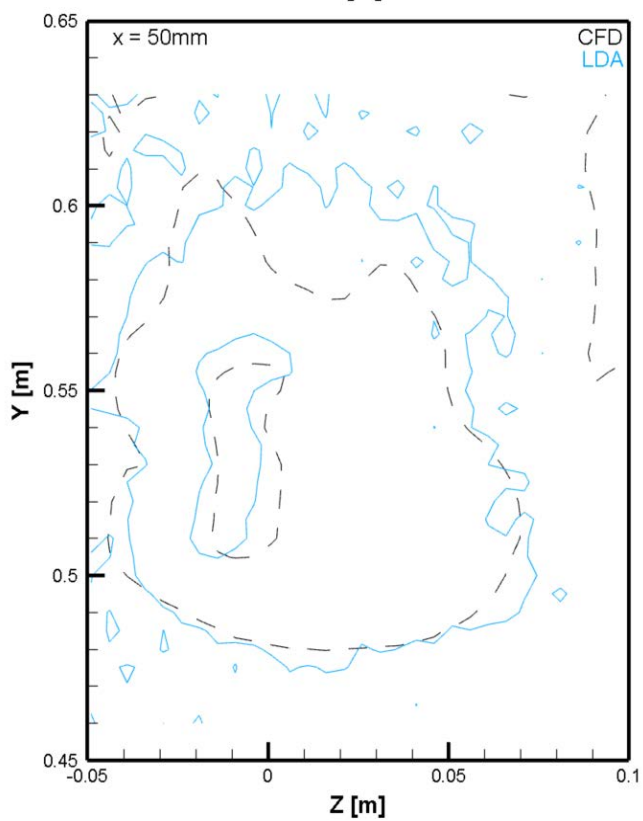
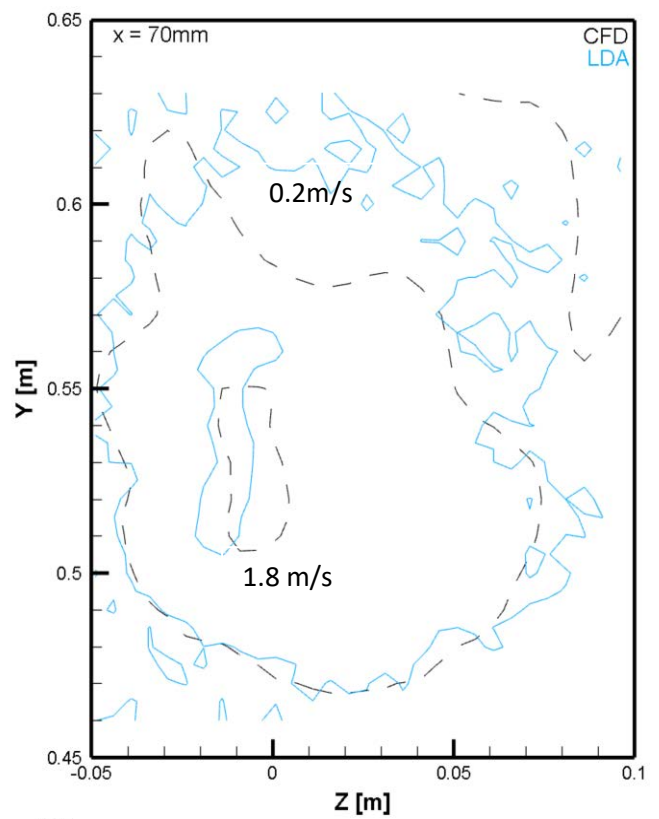
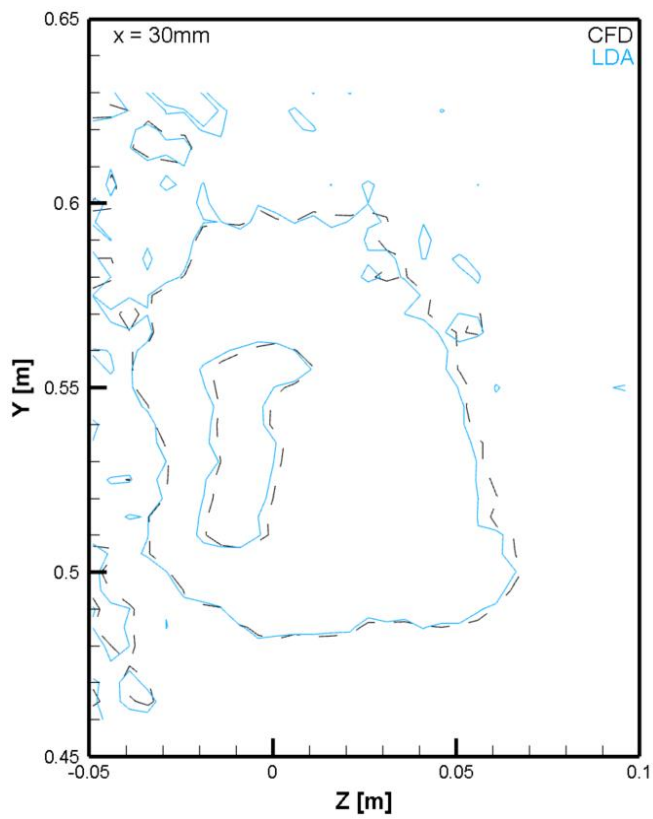


Figure 133: Side Lobed aileron grills grille LAG (The inner contours are corresponding to 1.8m/s and the outer contours are corresponding to 0.2 m/s)

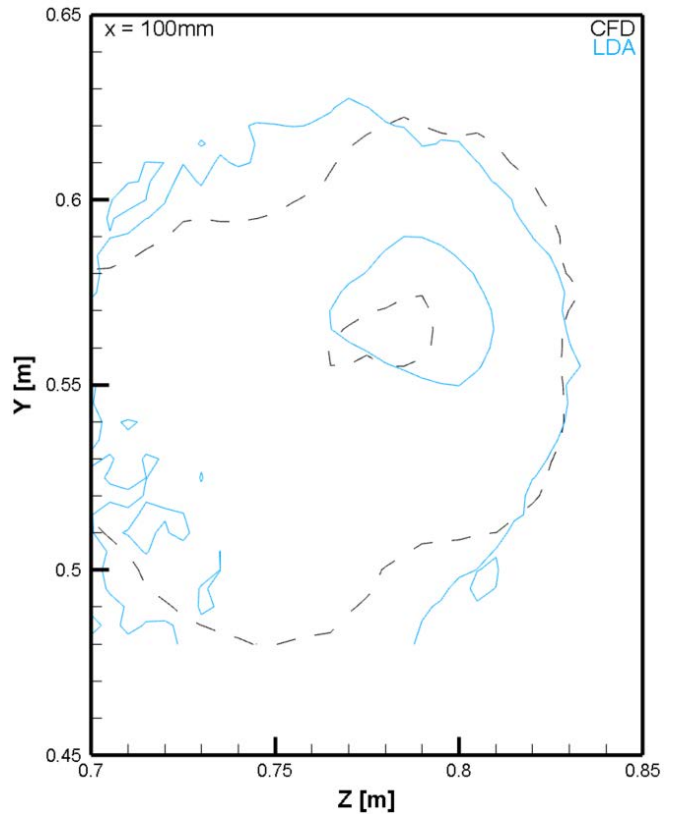
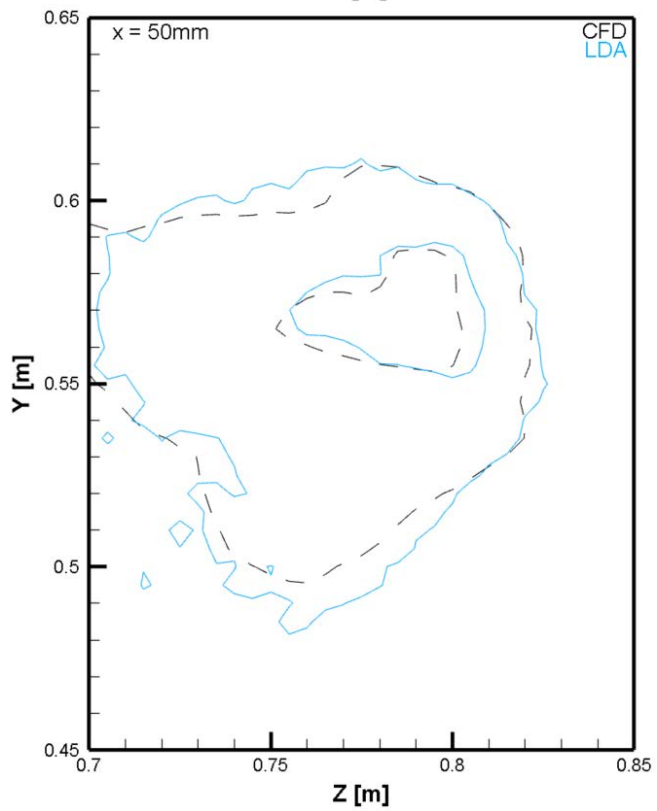
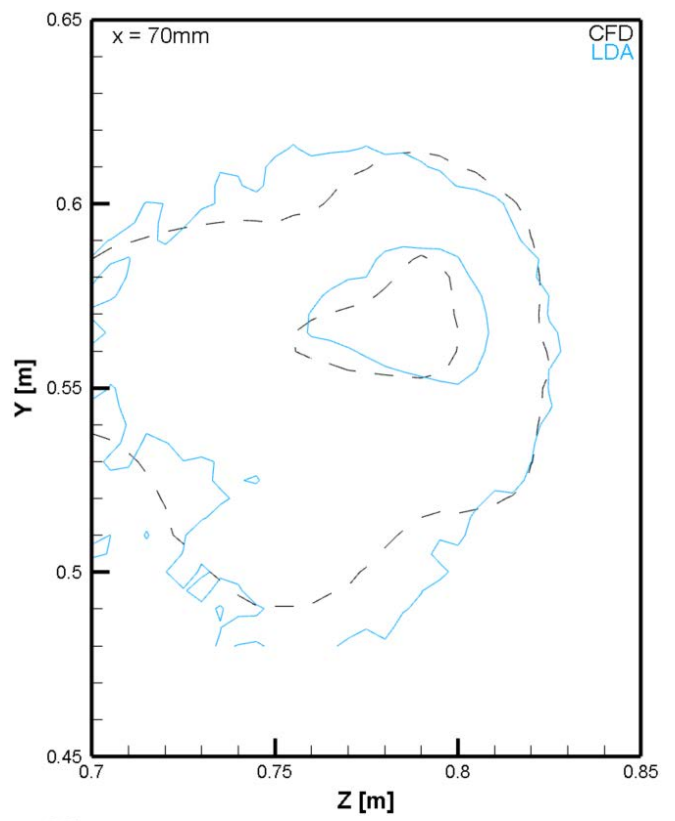
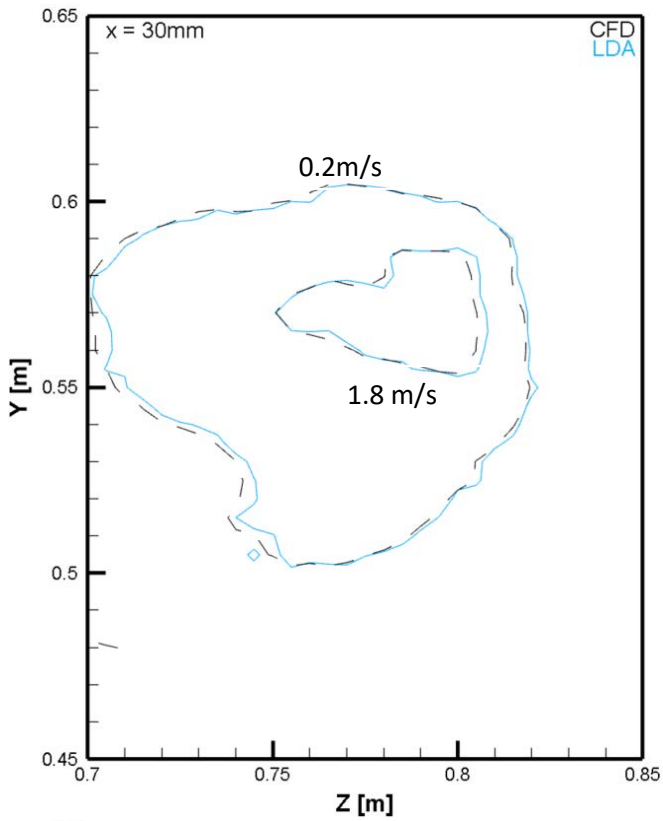


Figure 134: Center Lobed aileron grills grille LAG (The inner contours are corresponding to 1.8m/s and the outer contours are corresponding to 0.2 m/s)

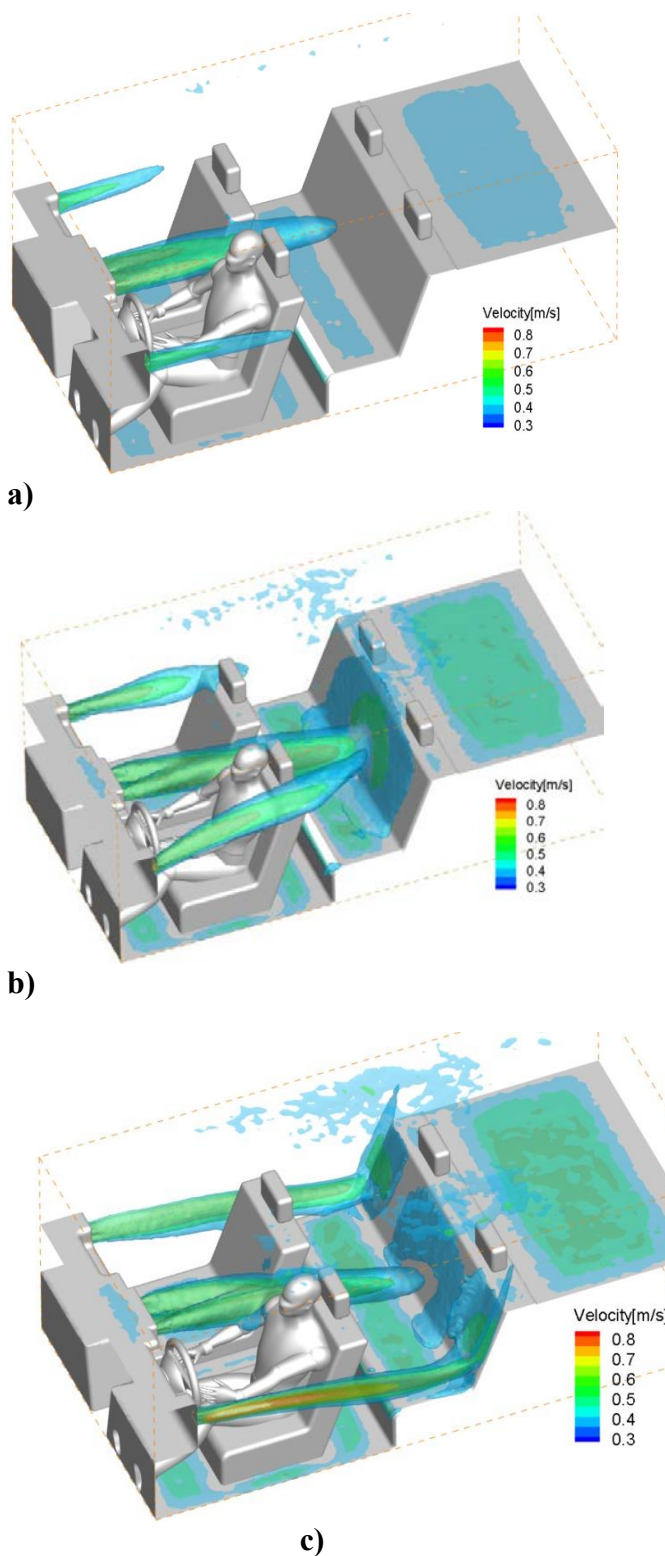


Figure 135: Velocity isocontours : a) Case 2; b) Case 3 - CG, c) Case 4 - LAG
Legend: blue – 0.3 m/s green – 0.55 m/s; red – 0.75 m/s

Figure 129 and Figure 130 are showing the distributions of the velocity magnitude and

of the in-plane vectors for the median plane of the driver for both cases. One could observe that the global pattern of the flow inside the cabin is changing with the change of the boundary conditions. The distribution of the flow is dramatically changing. Even if the mean velocity at the air grilles is the same, the local velocity profiles on the surface of the grilles have a different aspect as shown in Figure 128. The black line is corresponding to the horizontal planes from Figure 130.

At this point we wanted to check which is the accuracy of the predicted jet flows using the measured velocity fields imposed as boundary conditions. To this end we decided to compare the transverse numerical velocity distributions with their counterparts measured further downstream at the locations presented in Chapter 3. In Figures 132-135 are given the iso velocity contours for the transverse velocity distributions at one lateral air diffuser at one central air diffuser. Only two levels are represented in these figures. The inner contours are corresponding to 1.8m/s and the outer contours are corresponding to 0.2 m/s. We superimposed the experimental contours (blue continuous lines) with the numerical contours (dashed black lines). The comparisons in these figures are showing that for the axial distances, of each jet flow, at which we could measure the velocity fields, the correspondences are quite satisfactory. Other comparisons with experimental data were performed in the non-isothermal cases were the final goal of the

study.

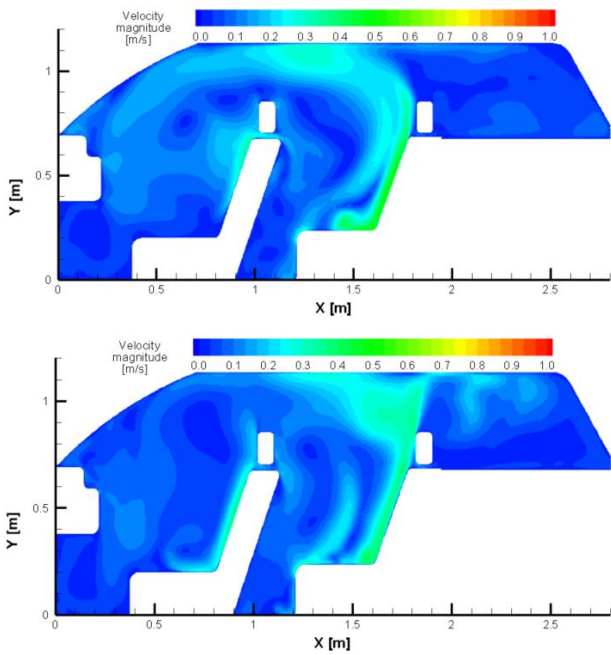


Figure 136: Velocity distribution in the middle of the passenger plane for the isothermal case: a) CG ; b) LAG

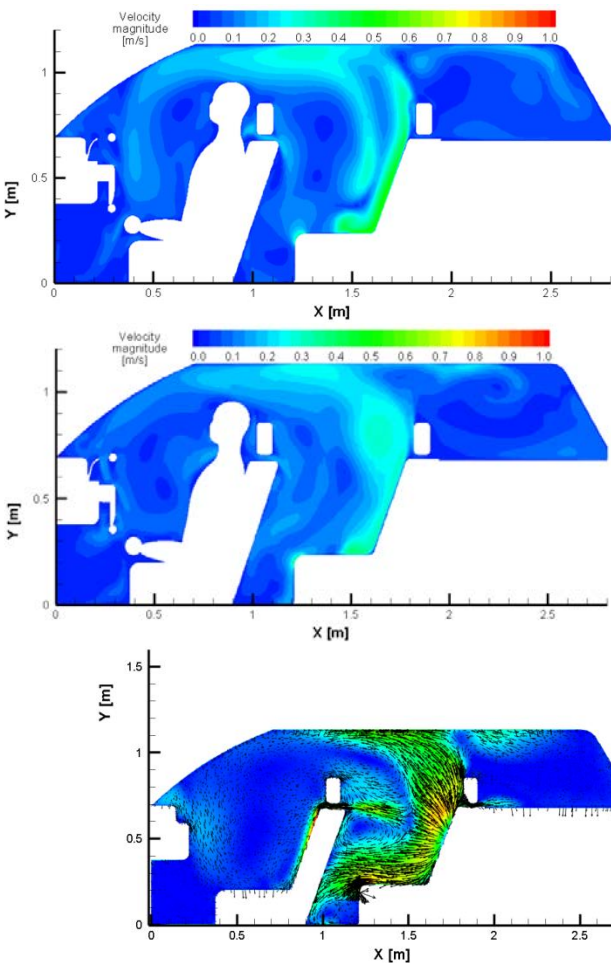


Figure 137: Velocity distribution in the median plane of the driver for the isothermal case: a) CG ; b) LAG

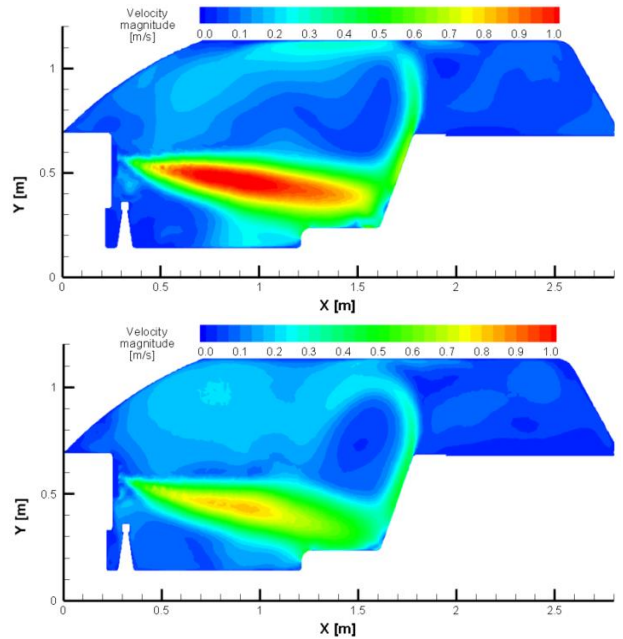
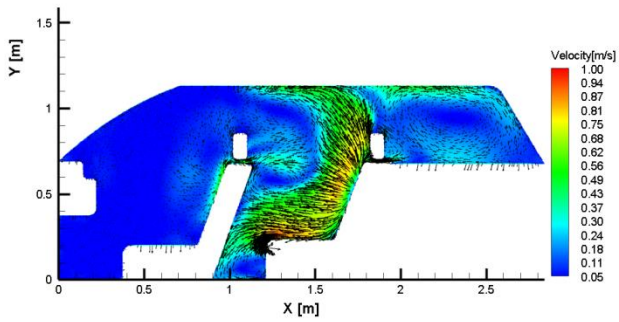


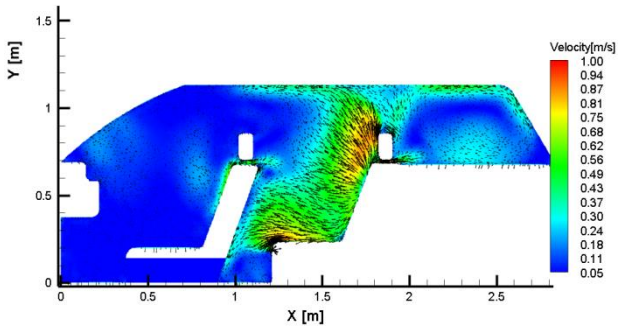
Figure 138 : Velocity distribution in the median plane of the right passenger place for the isothermal case: a) CG ; b) LAG

Once again for finishing this chapter we calculated values of the PPD/PMV indexes, knowing the air speed extracted the numerical model and imposing the metabolic rate value of 1 met and clothing insulation of 0.7 clo (summer time).

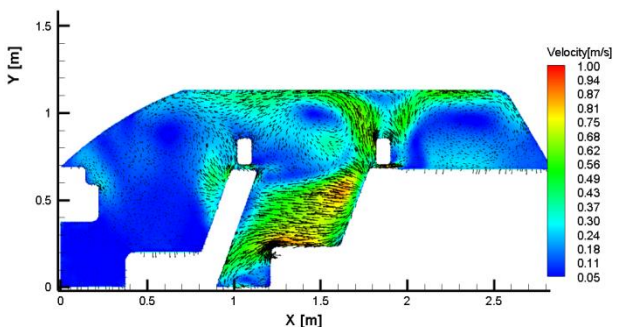
a).



b).

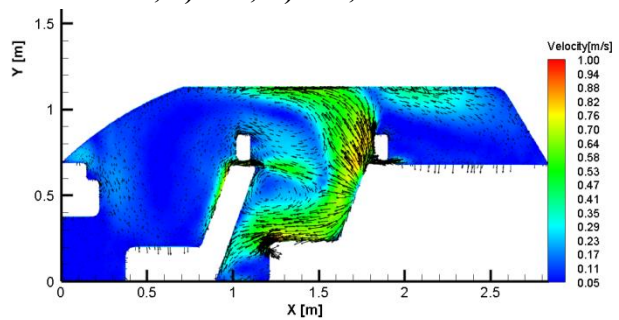


c).

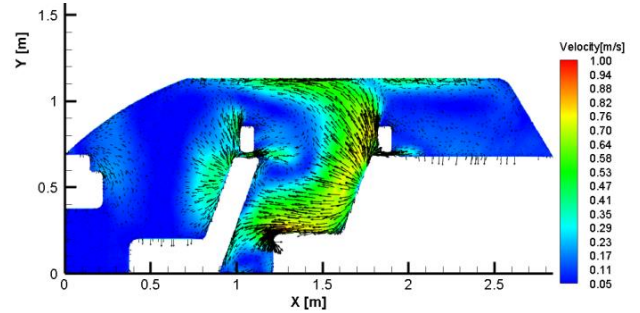


d).

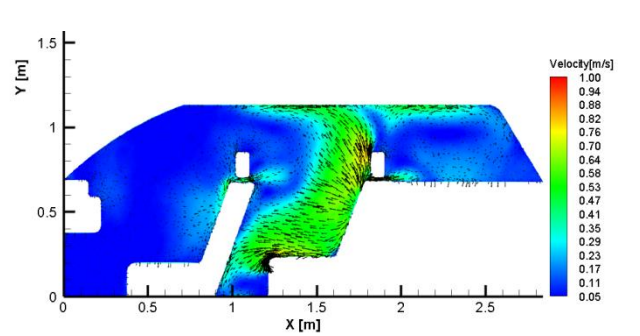
Figure 124: Distribution of the velocity magnitude and of the in plane vectors for the median plane of the passenger: a). 0°; b). 10°; c) 20°; d) 30°, for Case 1



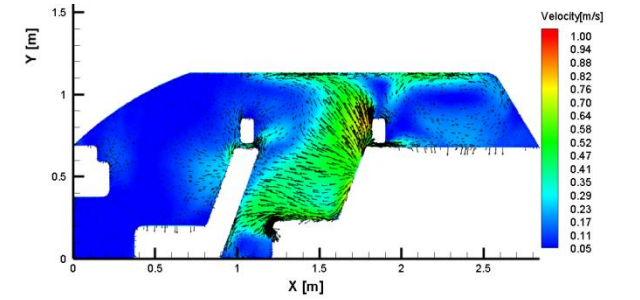
a).



b).

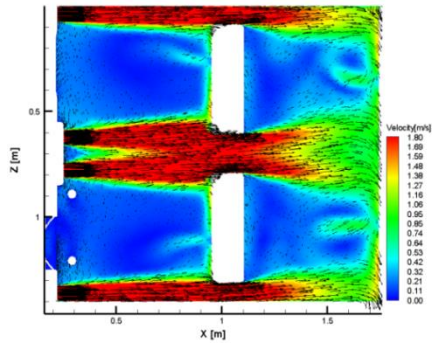


c).

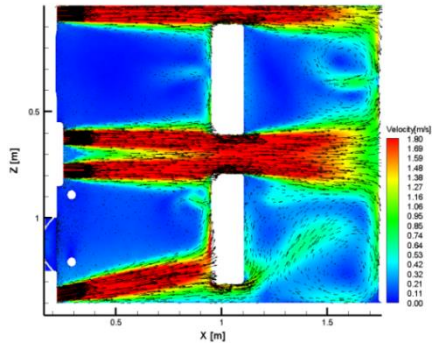


d).

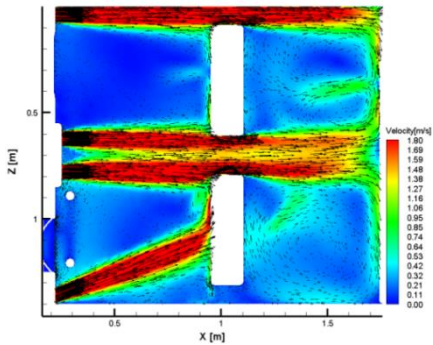
Figure 125: Distribution of the velocity magnitude and of the in plane vectors for the median plane of the passenger: a). 0°; b). 10°; c) 20°; d) 30°, for Case 2



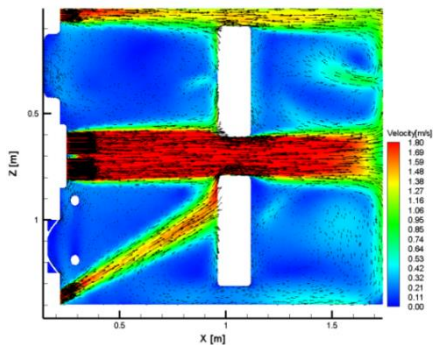
a).



b).

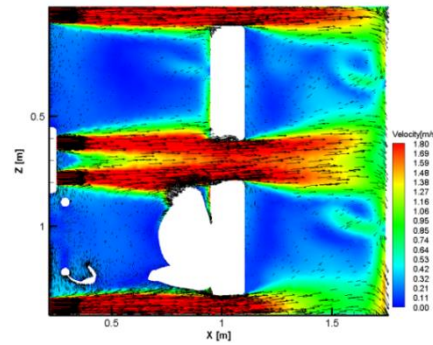


c).

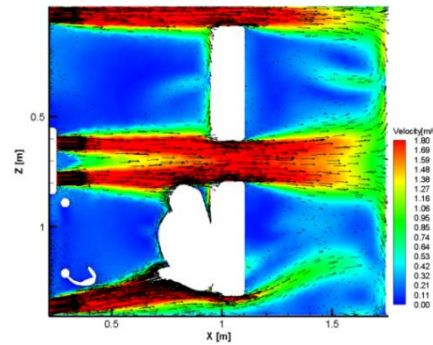


d).

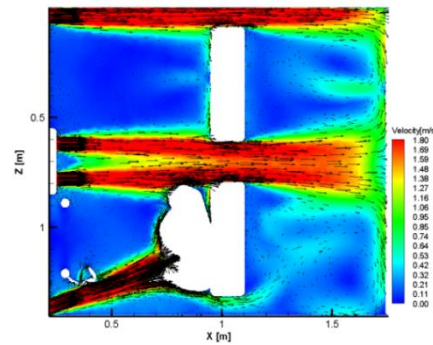
Figure 126: Distribution of the velocity magnitude and of the in plane vectors for the median plane of the passenger: a). 0°; b). 10°; c) 20°; d) 30°, for Case 1



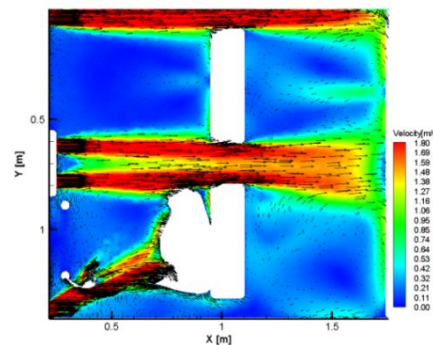
a).



b).



c).



d).

Figure 127 :Distribution of the velocity magnitude and of the in plane vectors for the median plane of the passenger: a). 0°; b). 10°; c) 20°; d) 30°, for Case 2

Table 16 presents values for the PMV and PPD indexes obtained at the right of each passenger place in the cabin for the head, the chest, the knees and the feet. We observe that even the mean velocity in the inlet is the same, the case when measurement data imposed as boundary conditions leads to a different airflow distribution inside the cabin. The jets have different jet throws, influencing the overall comfort, the percentage of dissatisfied increasing in the second case.

Table 18: Comparison of cabin comfort parameters

Point/parameter	CV	CG	LAG	θ [°C]	clothing insulation [clo]	metabolic rate [met]	RH [%]	θ_{mr} [°C]	CV	CG	LAG	CV	CG	LAG
	v_a								PMV			PPD		
	[m/s]								-			[%]		
Driver Head	0.05	0.08	0.07	23	0.7	1.0	57	23	-0.5	-0.5	-0.5	11.2	11.2	11.2
Passenger Head	0.04	0.04	0.04						-0.5	-0.5	-0.5	11.2	11.2	11.2
Rear right pass head	0.07	0.12	0.09						-0.5	-0.6	-0.5	11.2	13.7	11.2
Rear left pass head	0.07	0.21	0.12						-0.5	-0.9	-0.6	11.2	21.9	13.9
Driver Chest	0.02	0.12	0.08						-0.5	-0.7	-0.5	11.2	14.1	11.2
Passenger Chest	0.02	0.06	0.03						-0.5	-0.5	-0.5	11.2	11.2	11.2
Rear right pass chest	0.05	0.13	0.08						-0.5	-0.7	-0.5	11.2	14.6	11.2
Rear left pass chest	0.06	0.08	0.09						-0.5	-0.5	-0.5	11.2	11.2	11.2
Driver Knee	0.01	0.13	0.05						-0.5	-0.7	-0.5	11.2	14.9	11.2
Passenger Knee	0.03	0.07	0.04						-0.5	-0.5	-0.5	11.2	11.2	11.2
Rear right pass knee	0.10	0.10	0.10						-0.6	-0.6	-0.6	11.9	12.5	12.0
Rear left pass knee	0.11	0.15	0.12						-0.6	-0.8	-0.6	12.5	17.1	13.9
Driver Foot	0.03	0.05	0.03						-0.5	-0.5	-0.5	11.2	11.2	11.2
Passenger Foot	0.02	0.03	0.03						-0.5	-0.5	-0.5	11.2	11.2	11.2
Rear right pass foot	0.05	0.05	0.05						-0.5	-0.5	-0.5	11.2	11.2	11.2
Rear left pass foot	0.05	0.06	0.05						-0.5	-0.5	-0.5	11.2	11.2	11.2

The final numerical models that we retained, with virtual manikin as a driver, in non isothermal conditions, allowed us to simulate six cases that we will present in the next chapter. Three of them are dedicated to the classical air diffusers – CG, and three of them are dedicated with the new air diffusers – LAG.

In Tables 19, 20 and 21 we present the synthesis of the boundary conditions that we applied to these models apart the measured velocity fields that we discussed earlier. The imposed temperatures on the surfaces and at the inlets are temporal mean values from the experimental set-up presented in Chapter 3, B, d). Note that, the imposed flow rates in these cases are also different between the diffusers in this case. In order to obtain the corresponding values we used a weighting coefficient that we applied to the velocity fields.

Table 19: Mean air temperatures from measurements for the three fan controller positions such as imposed as boundary conditions in the final model

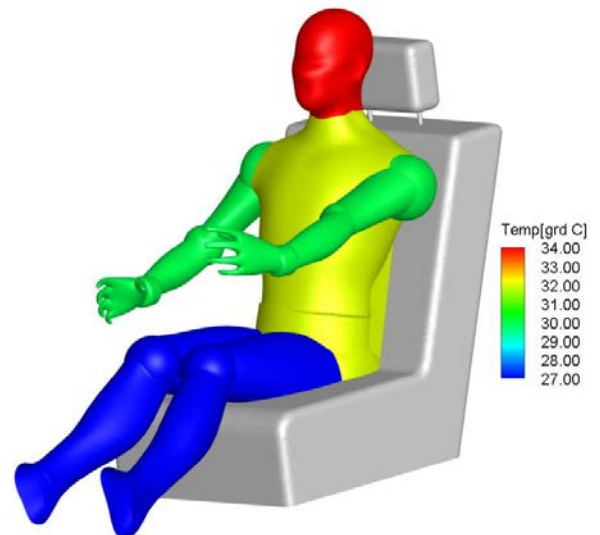
Diffuser position	V1	V2	V3	V1	V2	V3
	Temperature [°C]			Q [m3/s]		
Left diffuser	9.85	9.83	12.07	0.0131	0.0258	0.0380
Right diffuser	6.99	8.02	12.57	0.0068	0.0124	0.0197
Central diffusers	2.96	5.79	11.14	0.0047	0.0093	0.0158

Table 20: Mean surface temperatures from measurements for the three fan controller positions such as imposed as boundary conditions in the final model

Vehicle interior surface	V1	V2	V3
	Temperature [°C]		
Windshield	28.83	28.62	27.63
Ceiling	26.63	26.23	22.37
Right side	25.16	25.72	24.70
Left side	25.16	25.72	24.70
Rear window	28.41	28.13	27.29
Floor	21.08	21.05	22.65
Driver seat	29.00	28.00	27.00
Passenger seat	29.00	28.00	27.00
Back seat	29.00	28.00	27.00
Trunk	27.44	26.86	25.92
Dashboard	25.23	24.93	23.77

Table 21: Surface temperatures of the virtual manikin

Region	Temperature [°C]
1. Right foot	27
2. Right leg	27
3. Right thigh	27
4. Left foot	27
5. Left leg	27
6. Left thigh	27
7. Right hand	30
8. Right arm	30
9. Right upper arm	30
10. Left hand	30
11. Left arm	30
12. Left upper arm	30
13. Head	34
14. Pelvic region	32
15. Chest	32
16. Back	32



The in depth analysis the experimental work performed and the elaborated numerical simulations, allows us to formulate relevant conclusions in *finding what is the influence of the inlet conditions upon the flow field and evolution of the thermal comfort by the two types of air diffusers*. This way, we wanted to check first what is happening with the global distribution of the flow inside the cabin in non-isothermal conditions. Next, we wanted to gain a deeper perspective in the thermal comfort aspects. To this end we compared thermal indexes from the numerical data with the measured values of the parameters characterizing the thermal environment from the car such as described in the experimental set-up from Chapter 3.

We finish this last chapter dedicated to our study with a comparison between the numerical study and the experimental results obtained in the real car cabin from measurements and from the subjective studies.

A. Numerical results obtained using the complex model with realistic boundary conditions and virtual manikins

As it has been shown by Fanger [273], the velocities and the turbulent characteristics of the flows may generate a thermal discomfort translated by the sensation of “draught” was defined as “an undesired cooling of the human body caused by air movement” [273, 274]. This way, we wanted to check first, the influence the different boundary conditions and of the variation flow rate on the global temperature and velocity fields inside the car cabin. Therefore, we represented the temperature and velocity fields in various planes defined inside the car cabin – for instance through the sagittal plane of the driver or the median plane that passes through the right passenger’s place, or the vertical median planes for each diffuser.

In Figures 140-143, we represent for the isothermal case, for both diffusers (CG and LAG) the velocity magnitude distribution respectively in the median plane of the driver, in the median horizontal plane of the right passenger’s place, and in the median horizontal planes of the central diffusers and of the side diffusers. This case was considered only for V2.

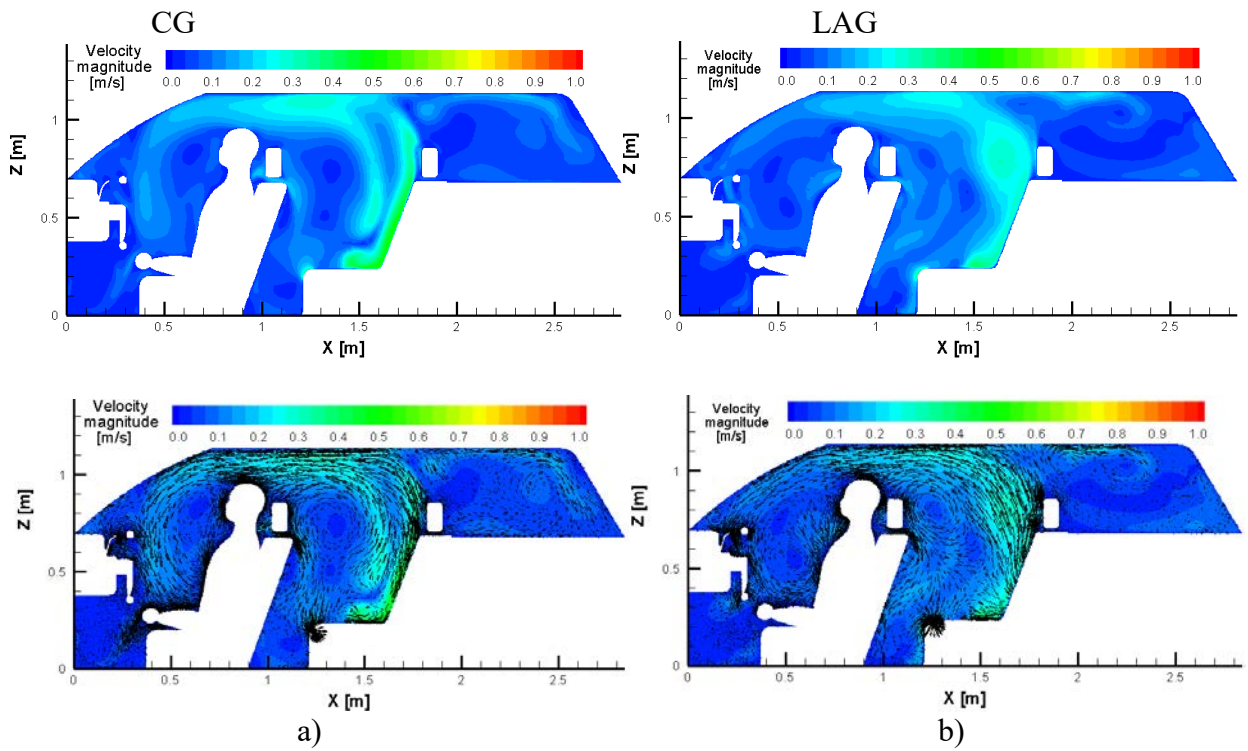


Figure 139: Velocity magnitude and in plane components distribution in the median plane of the driver for the isothermal case, V2: a) CG ; b) LAG

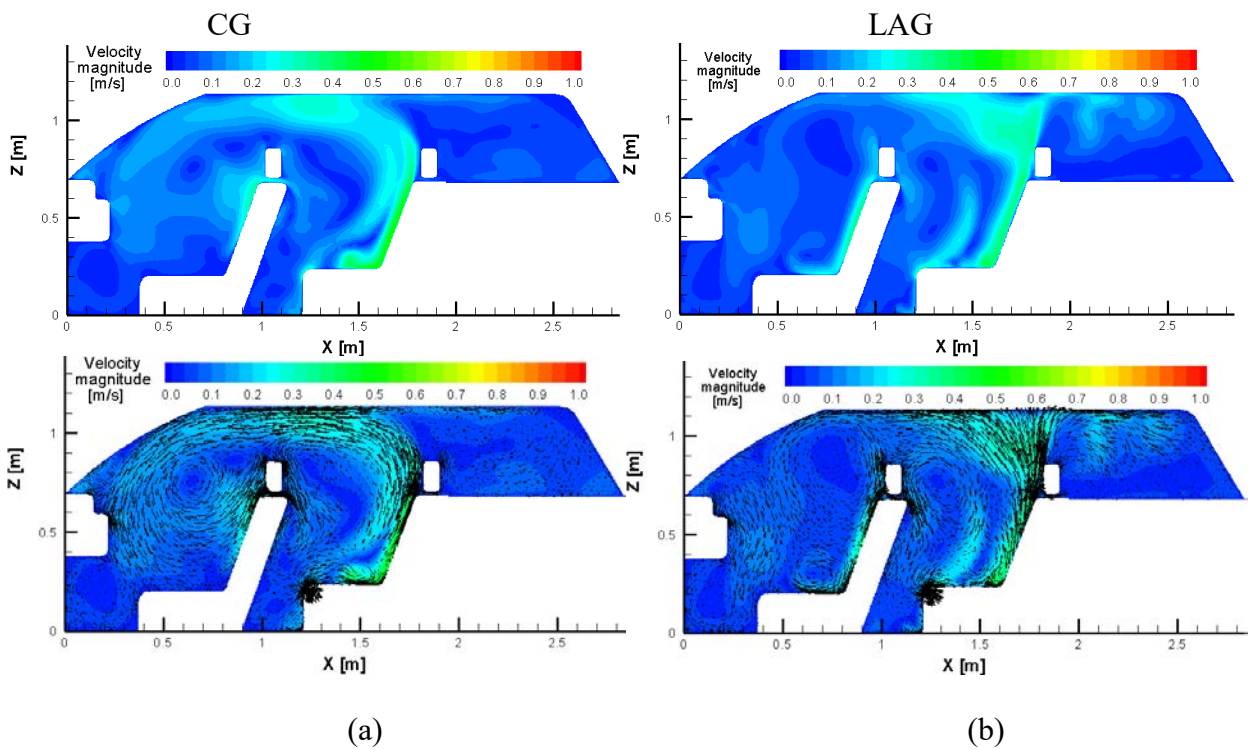


Figure 140: Velocity magnitude and in plane components distribution in the median plane of the right passenger place for the isothermal case, V2: a) CG ; b) LAG

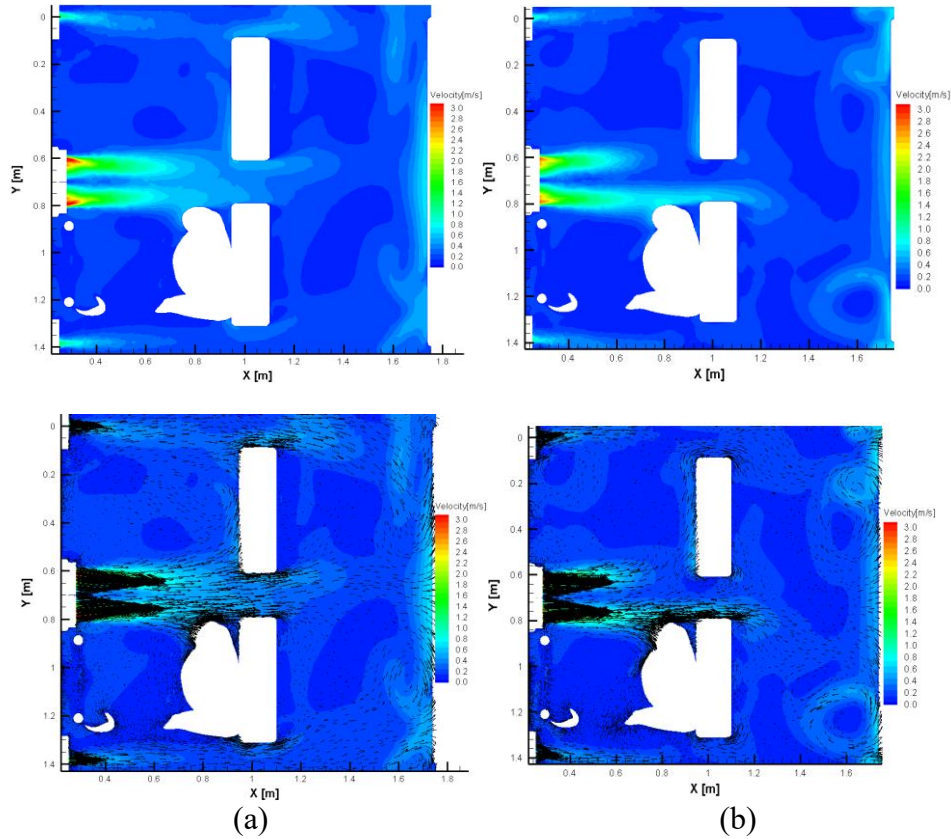
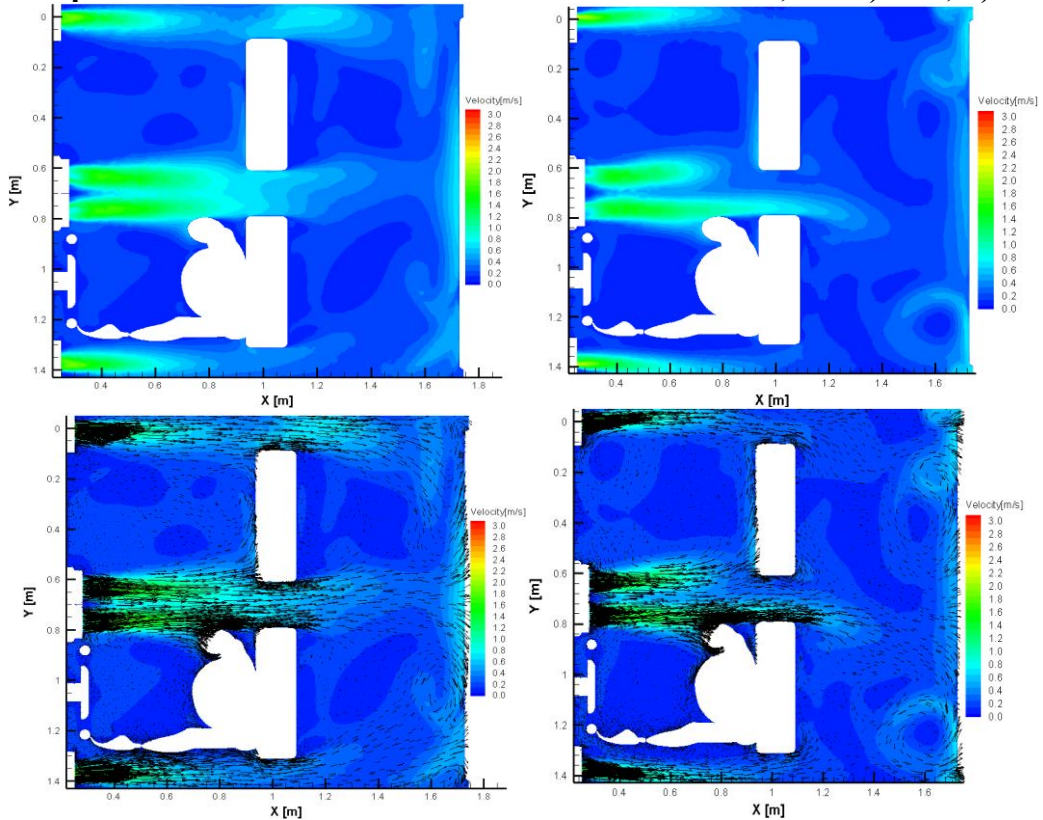


Figure 141: Velocity magnitude and in plane components distributions in the median horizontal plane of the central diffusers for the isothermal case, V2: a) CG ; b) LAG



(a) (b)
Figure 142: Velocity magnitude and in plane components distributions in the median horizontal plane of the side diffusers for the isothermal case, V2: a) CG ; b) LAG

In Figures 141 and 143 one could observe an asymmetry of the global pattern of the flow, obviously caused by the presence of the individual. The flow from the left side central diffuser is passing in the proximity of the human body, attaching itself to its surface through the Coanda phenomenon, thus its throw becomes longer. The observed phenomenon is however more pronounced for the LAG case. Moreover, the air jets emerging from the LAG seem not to coalesce in the considered horizontal plane for this case of flow rate.

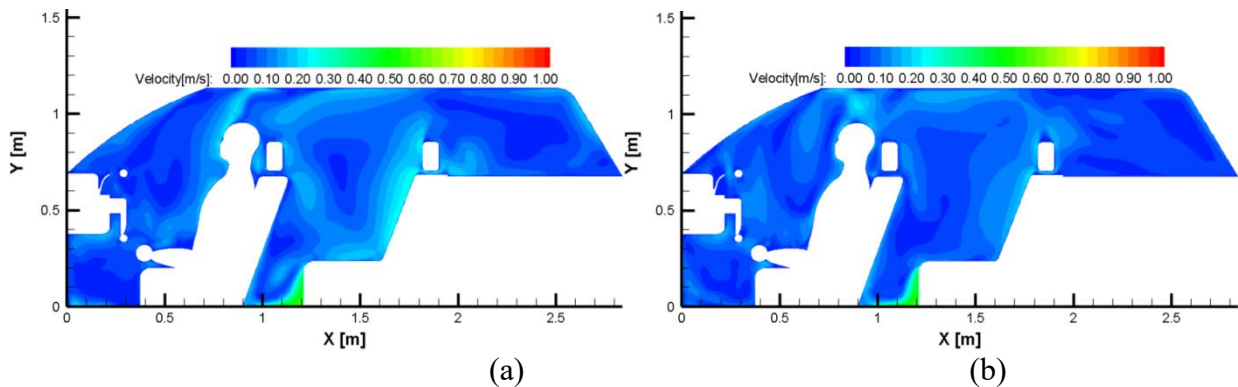


Figure 143: Velocity magnitude distribution in the median plane of the driver for the non-isothermal case, V1: a) CG ; b) LAG

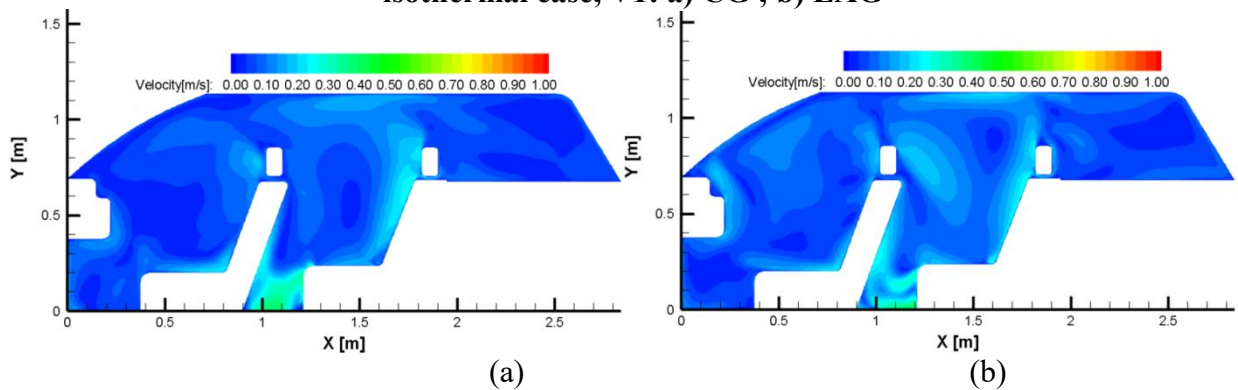


Figure 144: Velocity magnitude distribution in the median plane of the right passenger place for the non-isothermal case, V1: a) CG ; b) LAG

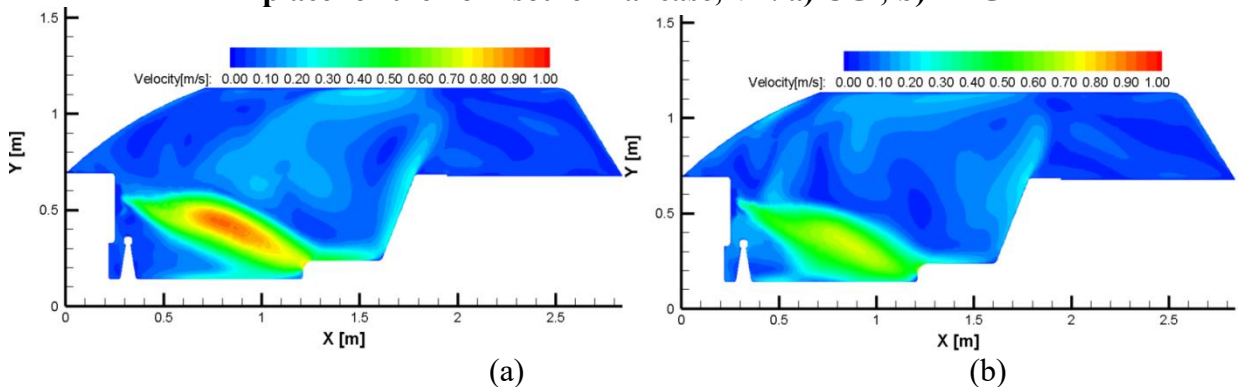
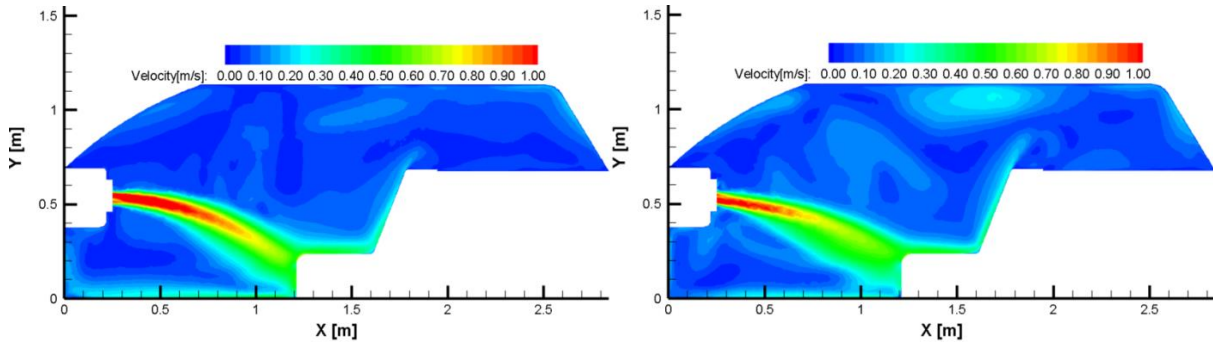


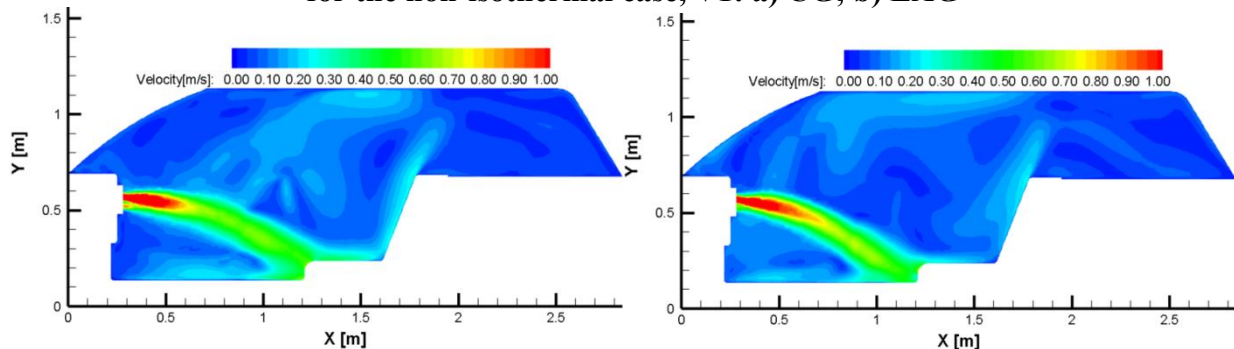
Figure 145: Velocity magnitude distribution in the median plane of the car for the non-isothermal case, V1: a) CG ; b) LAG



(a)

(b)

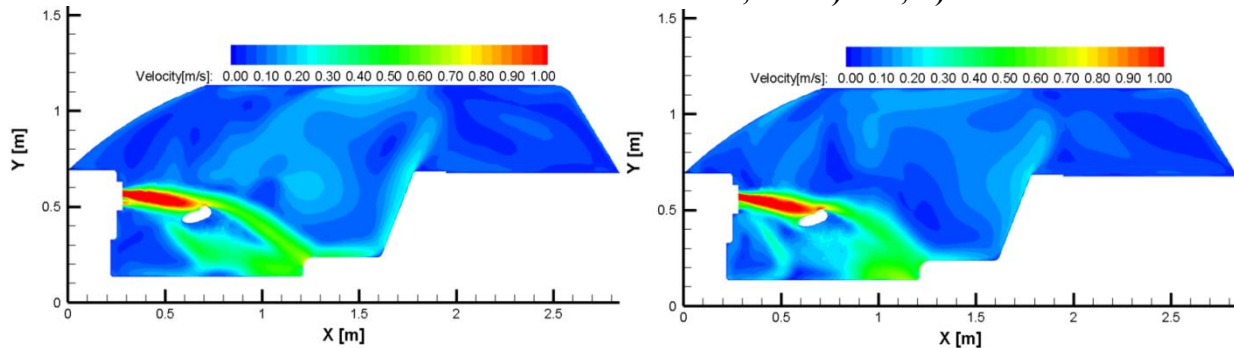
Figure 146: Velocity magnitude distribution in the median plane of the right side diffusers for the non-isothermal case, V1: a) CG; b) LAG



(a)

(b)

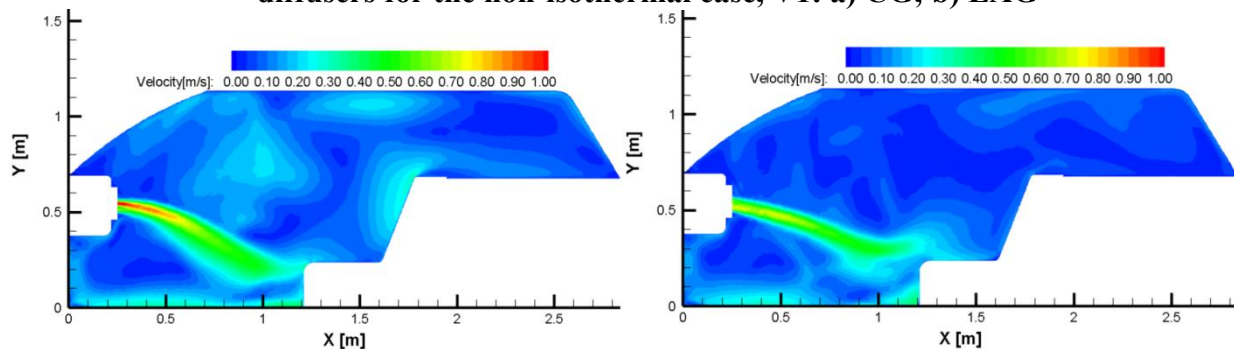
Figure 147: Velocity magnitude distribution in the median plane of the right central diffusers for the non-isothermal case, V1: a) CG; b) LAG



(a)

(b)

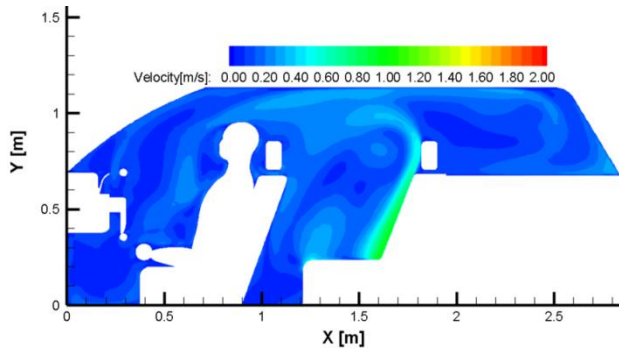
Figure 148: Velocity magnitude distribution in the median plane of the left central diffusers for the non-isothermal case, V1: a) CG; b) LAG



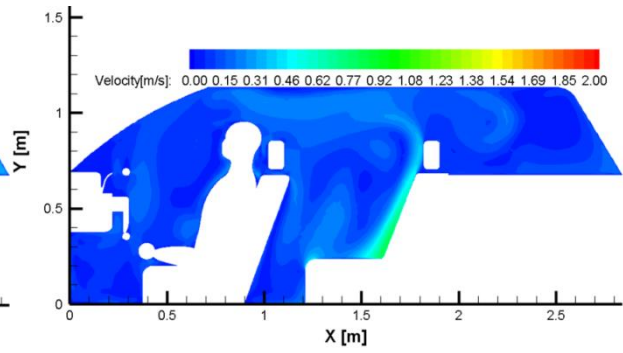
(a)

(b)

Figure 149: Velocity magnitude distribution in the median plane of the left side diffusers for the non-isothermal case, V1: a) CG; b) LAG

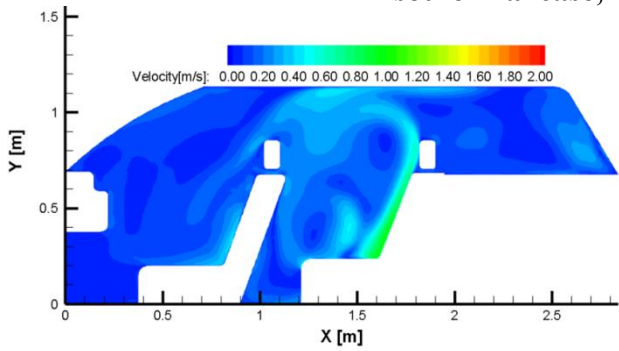


(a)

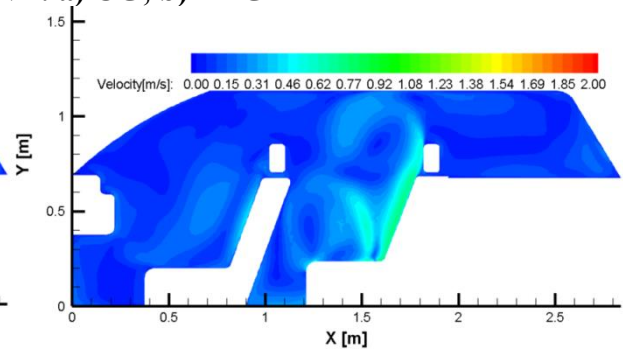


(b)

Figure 150: Velocity magnitude distribution in the median plane of the driver for the non-isothermal case, V2: a) CG; b) LAG

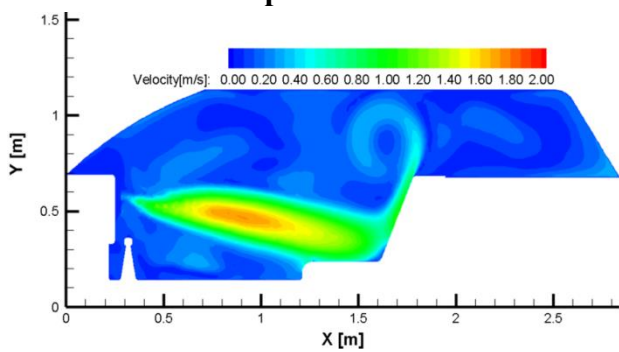


(a)

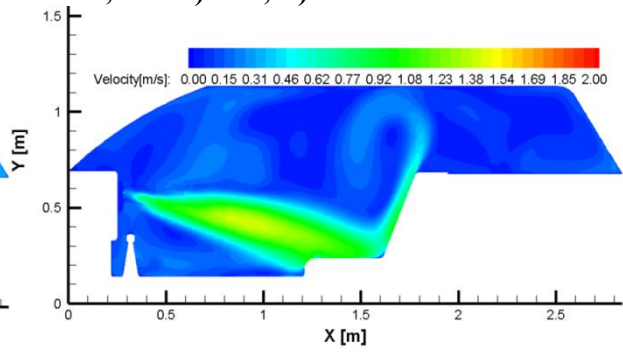


(b)

Figure 151: Velocity magnitude distribution in the median plane of the right passenger place for the non-isothermal case, V2: a) CG; b) LAG



(a)



(b)

Figure 152: Velocity magnitude distribution in the median plane of the car for the non-isothermal case, V2: a) CG; b) LAG

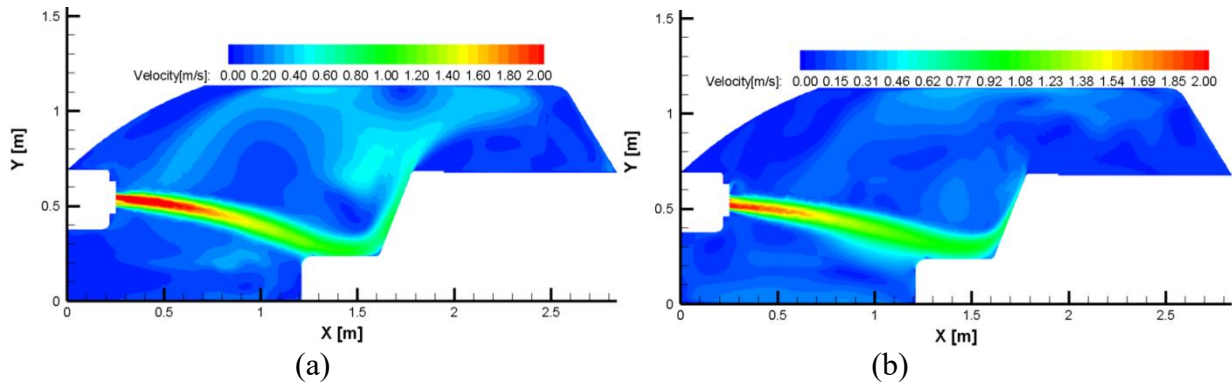


Figure 153: Velocity magnitude distribution in the median plane of the right side diffusers for the non-isothermal case, V2: a) CG; b) LAG

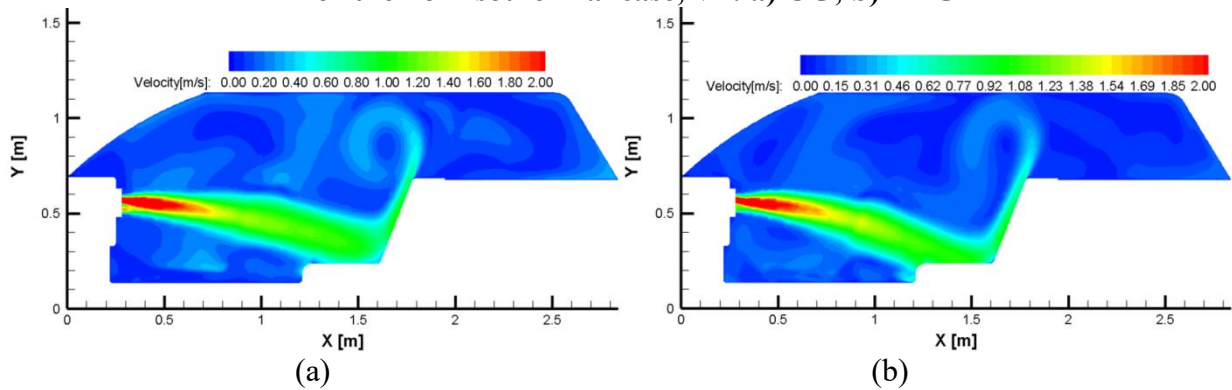


Figure 154: Velocity magnitude distribution in the median plane of the right central diffusers for the non-isothermal case, V2: a) CG; b) LAG

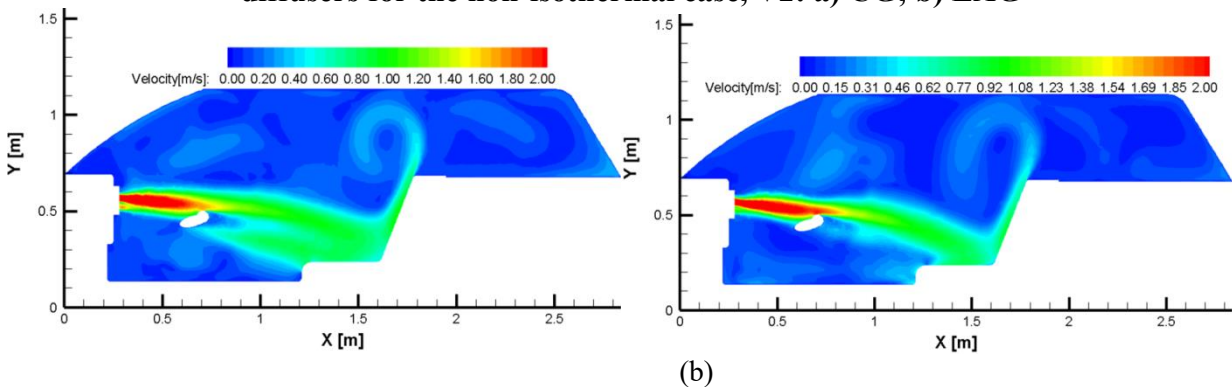


Figure 155: Velocity magnitude distribution in the median plane of the left central diffusers for the non-isothermal case, V2: a) CG; b) LAG

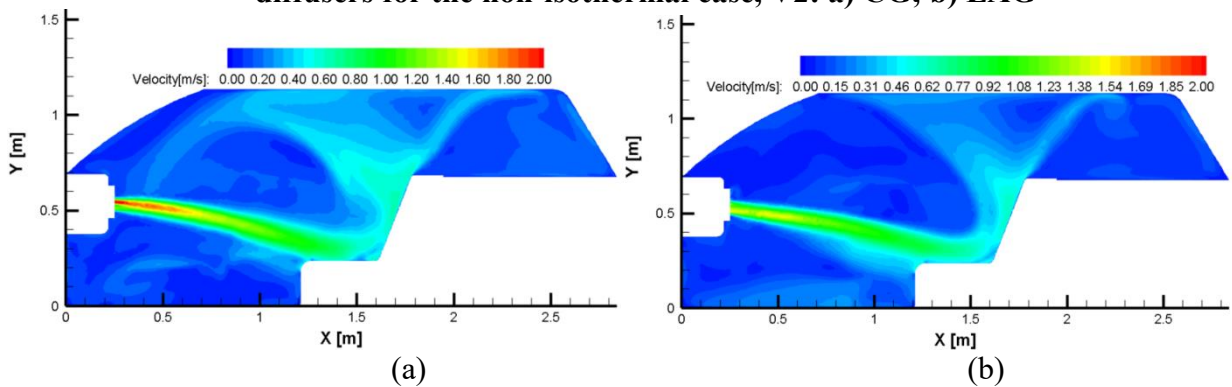
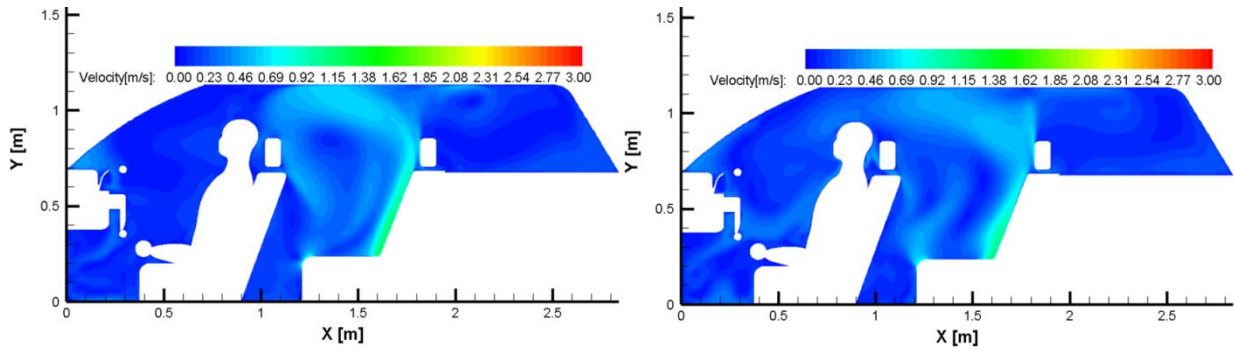


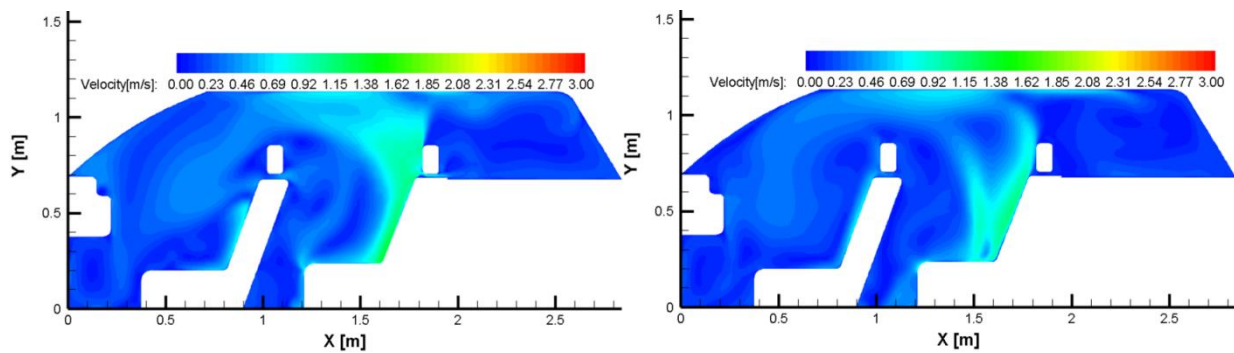
Figure 156: Velocity magnitude distribution in the median plane of the left side diffusers for the non-isothermal case, V2: a) CG; b) LAG



(a)

(b)

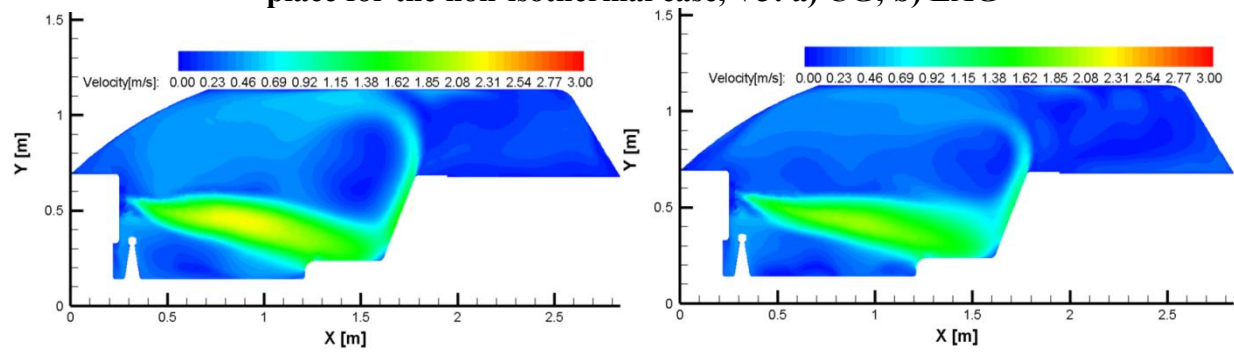
Figure 157: Velocity magnitude distribution in the median plane of the driver for the non-isothermal case, V3: a) CG; b) LAG



(a)

(b)

Figure 158: Velocity magnitude distribution in the median plane of the right passenger place for the non-isothermal case, V3: a) CG; b) LAG



(a)

(b)

Figure 159: Velocity magnitude distribution in the median plane of the car for the non-isothermal case, V3: a) CG; b) LAG

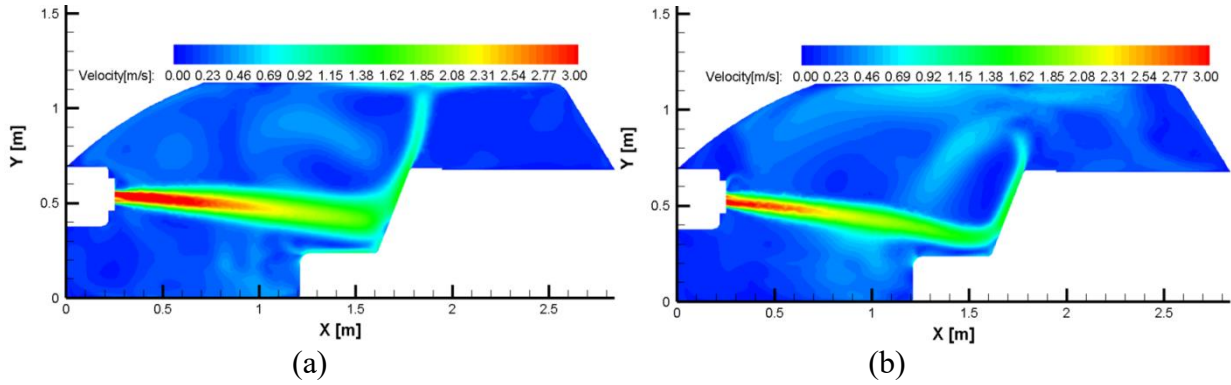


Figure 160: Velocity magnitude distribution in the median plane of the right side diffusers for the non-isothermal case, V2: a) CG; b) LAG

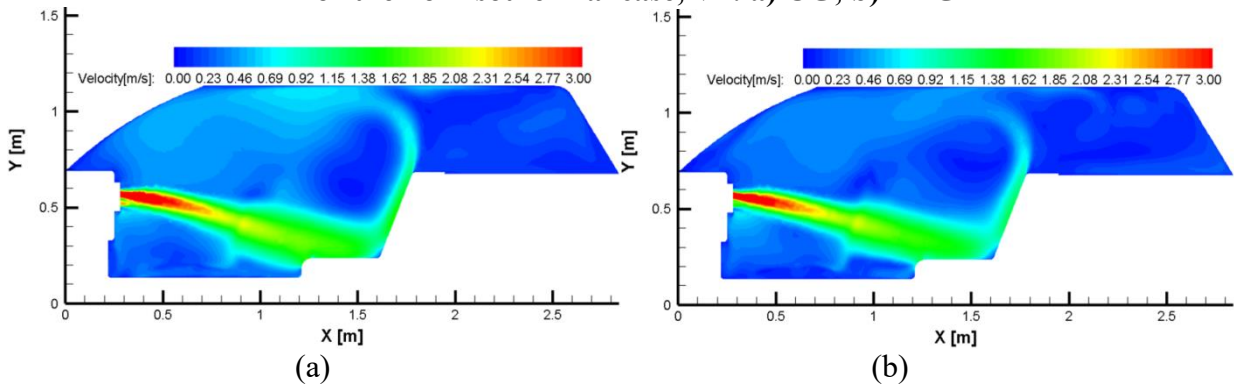


Figure 161: Velocity magnitude distribution in the median plane of the right central diffusers for the non-isothermal case, V2: a) CG; b) LAG

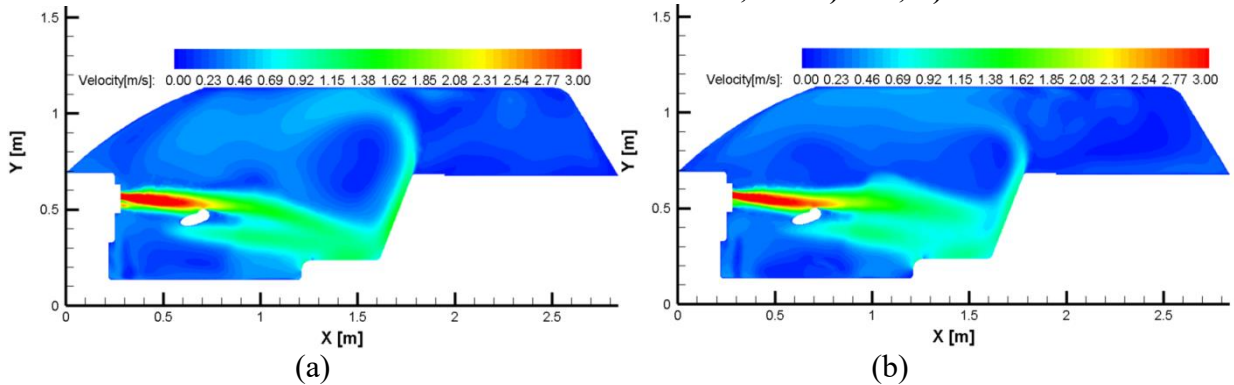


Figure 162: Velocity magnitude distribution in the median plane of the left central diffusers for the non-isothermal case, V2: a) CG; b) LAG

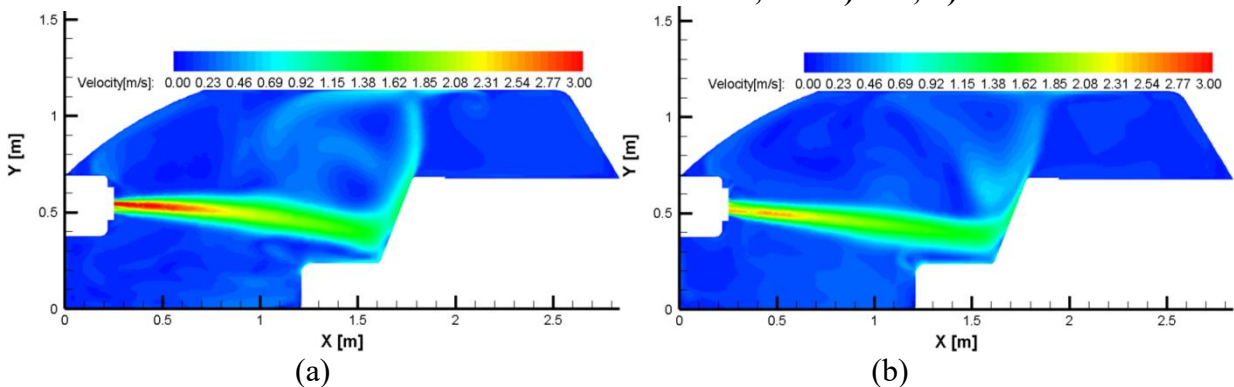


Figure 163: Velocity magnitude distribution in the median plane of the left side diffusers for the non-isothermal case, V2: a) CG; b) LAG

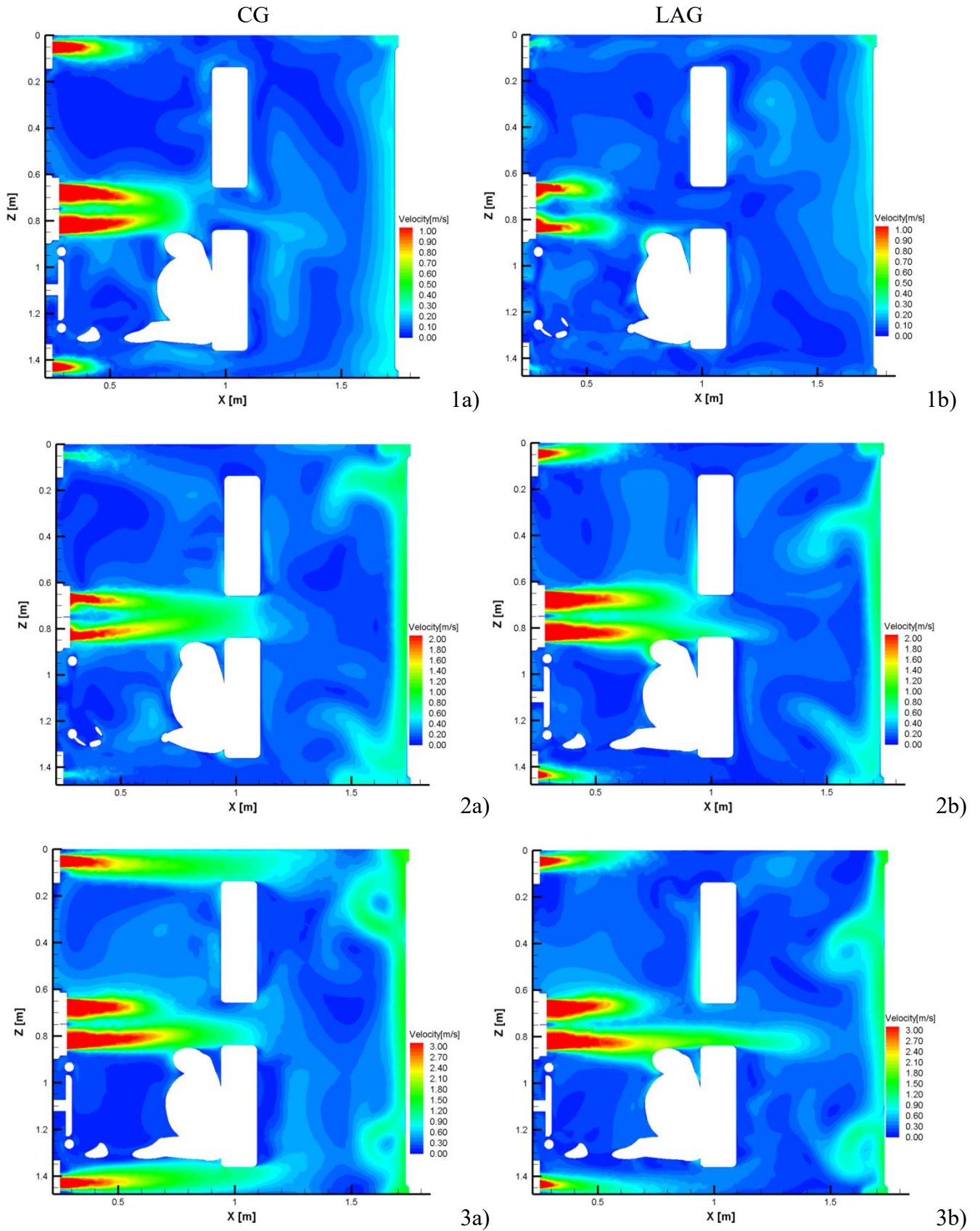


Figure 164: Velocity magnitude distribution in the median horizontal plane of the central diffusers for the isothermal case: a) CG ; b) LAG; 1) V1, 2) V2, 3) V3

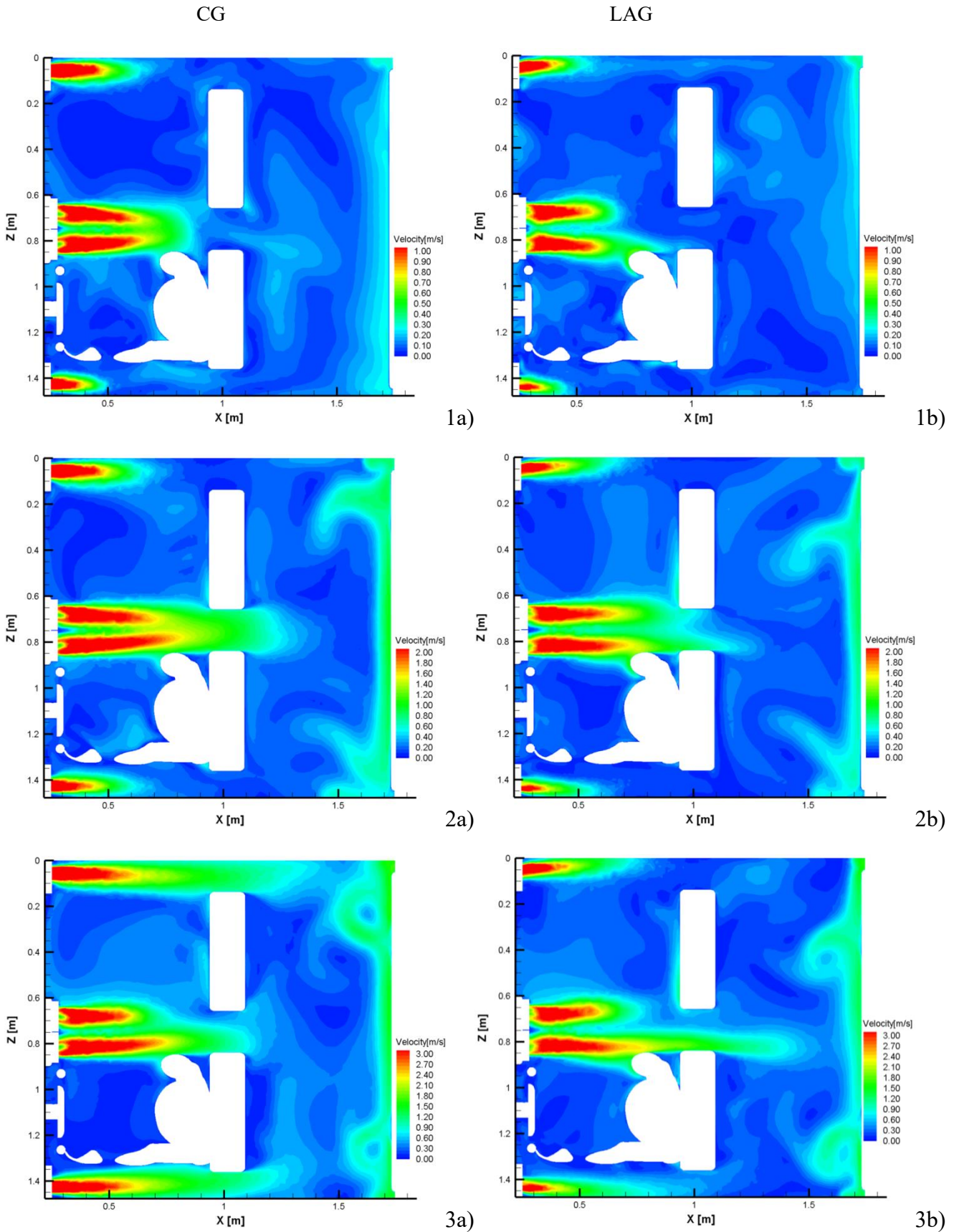


Figure 165: Velocity magnitude distribution in the median horizontal plane of the side diffusers for the isothermal case: a) CG ; b) LAG; 1) V1, 2) V2, 3) V3

In Figures 144-164 we represented this time, for the non-isothermal case, for both diffusers (CG and LAG) the velocity magnitude distributions respectively in the median plane of the driver, in the median horizontal plane of the right passenger's place, and in the vertical median plane of each diffuser. All the volumetric flow rates corresponding to each step of the flow controller for which we had experimental data was considered.

In Figures 165-166 we represented for both diffusers (CG and LAG) the velocity magnitude distributions in the median horizontal planes of the central diffusers and of the side diffusers, also for all three positions of the fan controller.

The previous global asymmetry of the flow seems to be amplified by the differences of temperature between the jet flows and the ambient. There is no noticeable difference between the velocity magnitude distributions in the vertical median planes that are passing through the centre of the diffusers, but once again in the horizontal plane the evolution of the flows is globally very different for the LAG and CG cases and for the three considered air flows.

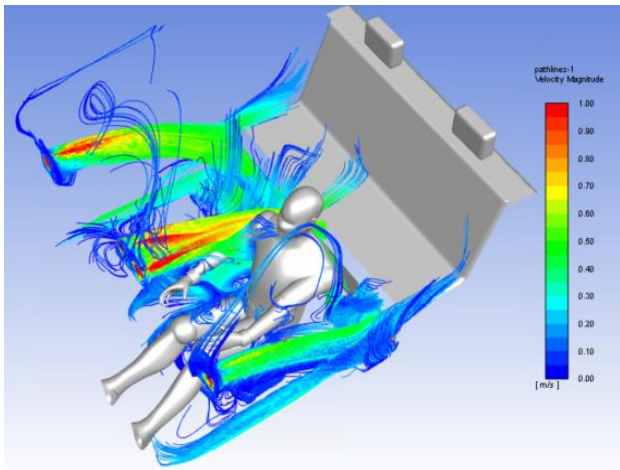
Globally, for all LAG cases the air jet flows seem to have a larger throw, fact that is confirmed in Figure 167 where we represented the path lines for the flows emerging from the diffusers.

As this phenomenon is quite similar to what it was previously found for the lobed aileron grilles in the study of Nastase et al. [161] we decided to take a look to the entrainment rates of the studied diffusers in isothermal conditions for the three fan controller positions. These flow rates were obtained from the integration of the stream wise velocity profiles from the transverse planes across the entire cabin.

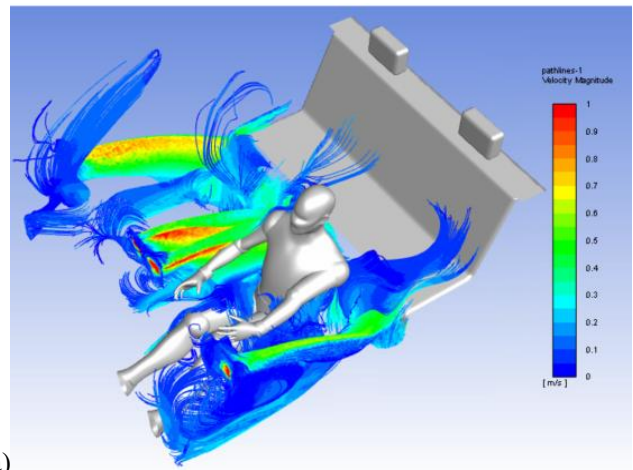
An interesting result is observed for V2 position of the fan air controller. As in the case of the throw of other lobed air diffuser flow [157] the LAG jet throw is not reduced despite its higher induction. The results presented in Figure 168 provide us with valuable information, giving an indication on the entrainment and the throw improvement by the lobed grille. Our wish is to confirm the entrainment results given in Figure 4a, through the integration of the entire cross fields of the two flows.

For the other flow rates, no distinctive advantage of the LAG diffusers compared to the CG could be observed.

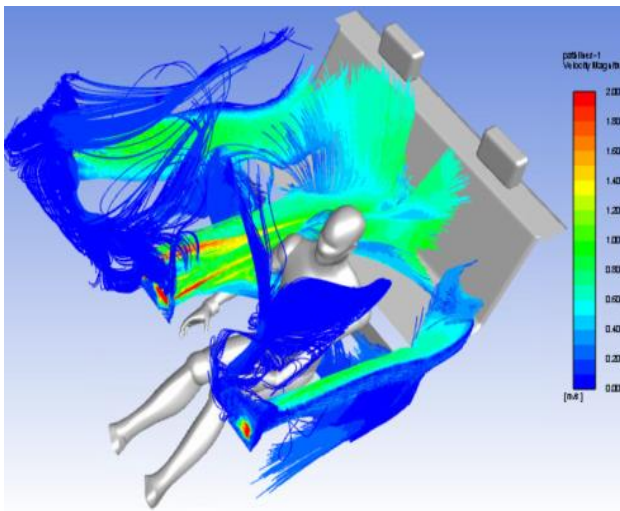
A three-dimensional representation of the flows is given in Figures 169-171 where we compare the velocity magnitude iso-contours for the two types of diffusers and for the three volumetric flow rates. In Figures 172-173 we represented the temperature distributions in the median plane of the driver for both diffusers and for all the three volumetric flow rates.



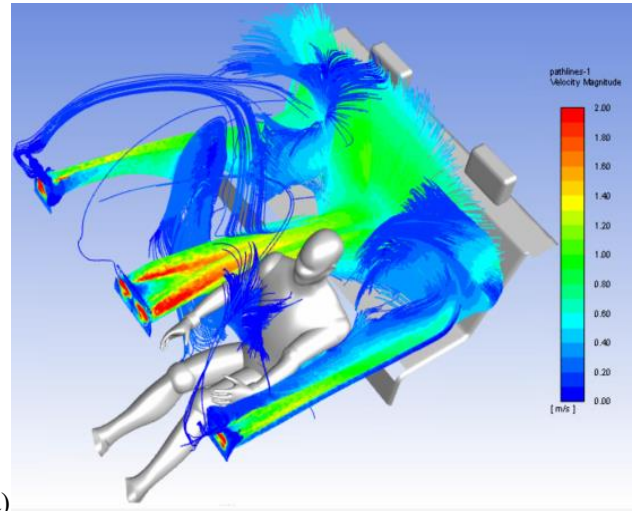
1a)



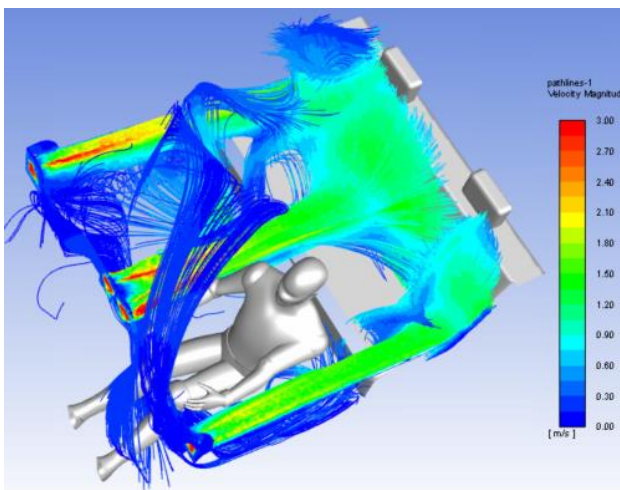
1b)



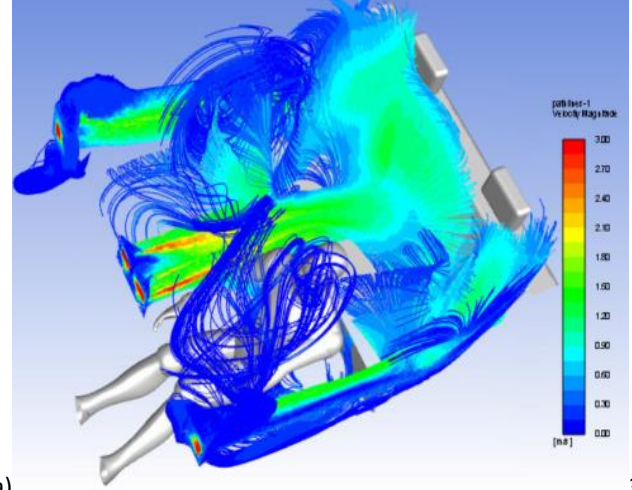
2a)



2b)



3a)



3b)

Figure 166: Path lines for the flows emerging from the diffusers a) CG ; b) LAG; 1) V1, 2) V2, 3) V3

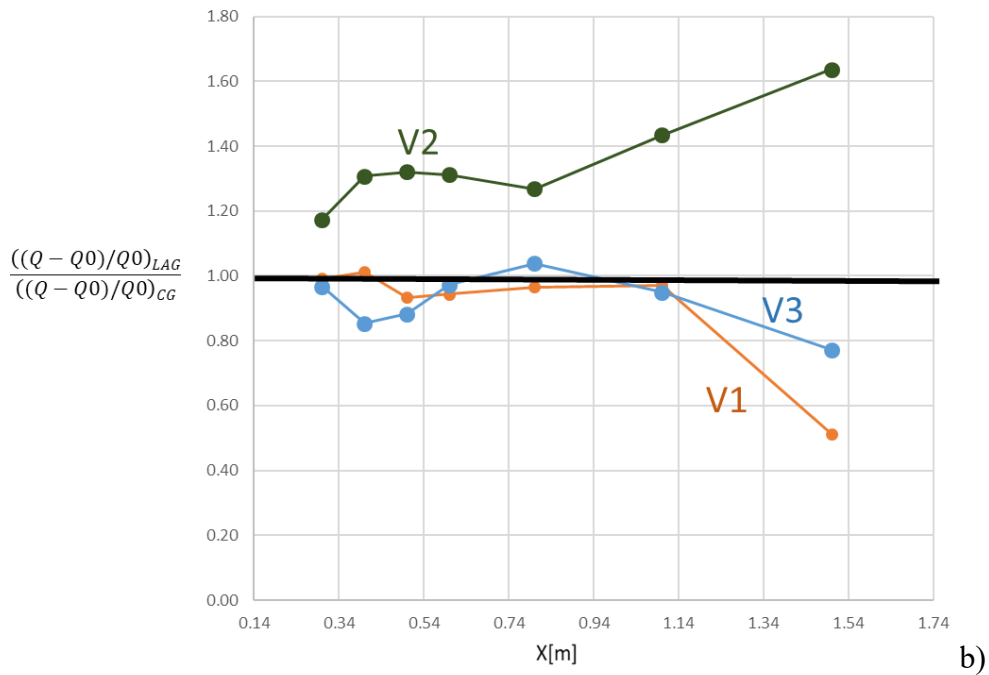
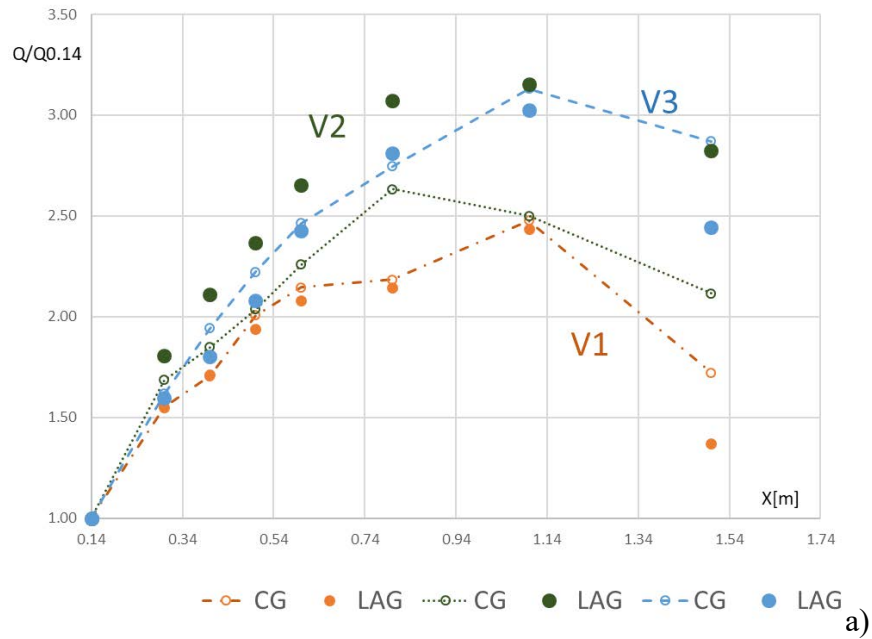
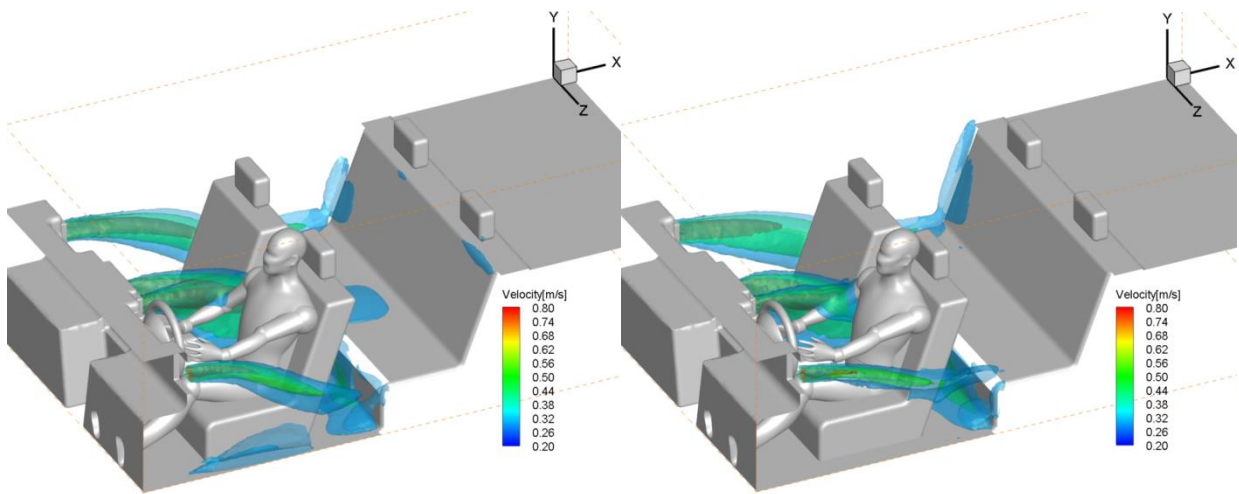
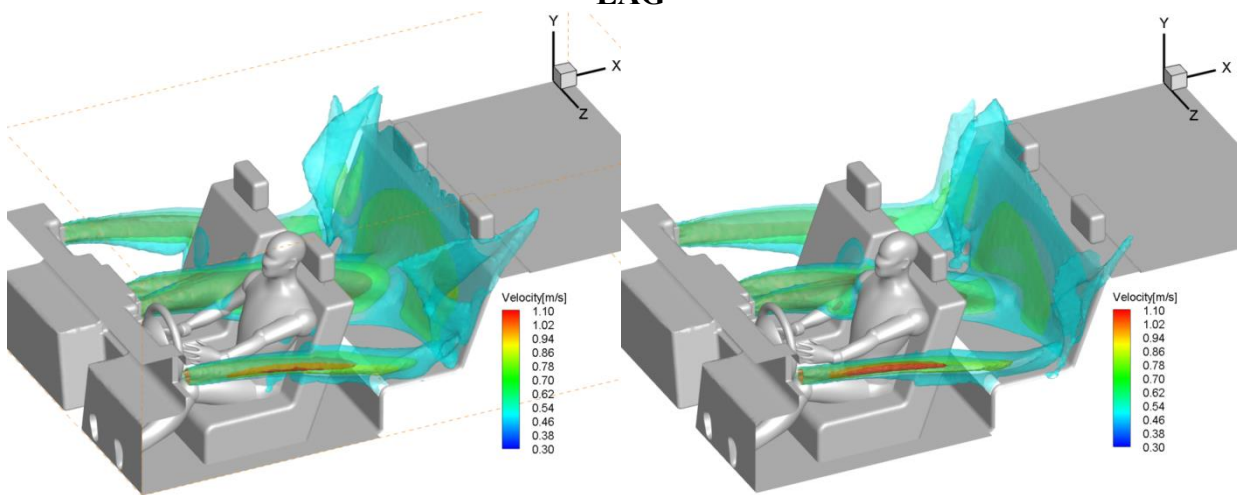


Figure 167: a) Global normalized volumetric flow rates for the three fan controller positions and for the two types of diffusers, b) normalized entrainment rates (LAG compared to CG)



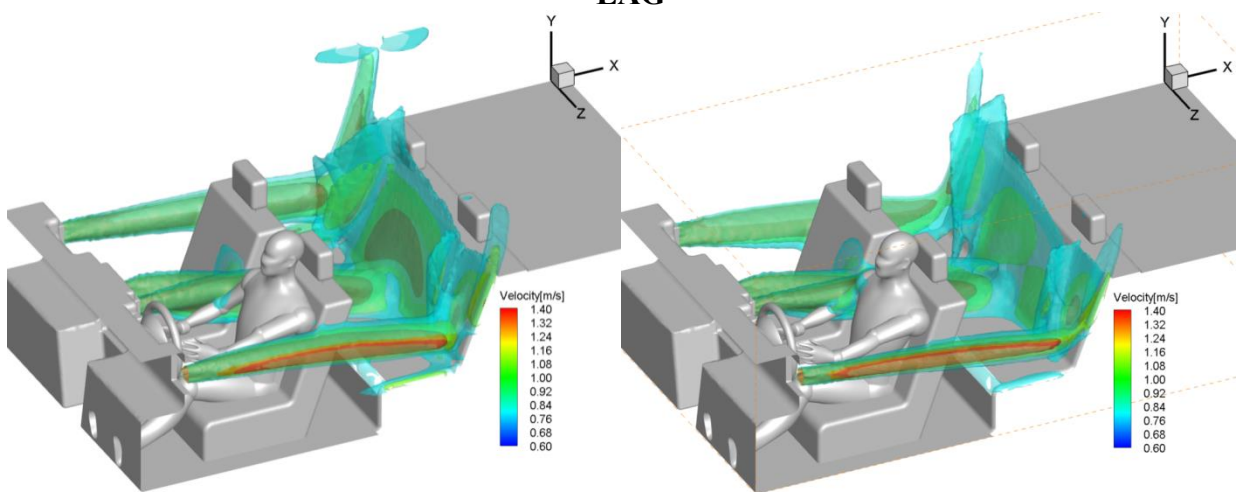
Legend: red - 0.3 m/s; green - 0.5 m/s; blue - 0.8 m/s

Figure 168: Velocity magnitude isocontours for the non-isothermal case, V1: a) CG; b) LAG



Legend: red - 0.3 m/s; green - 0.5 m/s; blue - 0.8 m/s

Figure 169: Velocity magnitude isocontours for the non-isothermal case, V2: a) CG; b) LAG



Legend: red - 0.8 m/s; green - 1.1 m/s; blue - 1.4 m/s

Figure 170: Velocity magnitude isocontours for the non-isothermal case, V3: a) CG; b) LAG

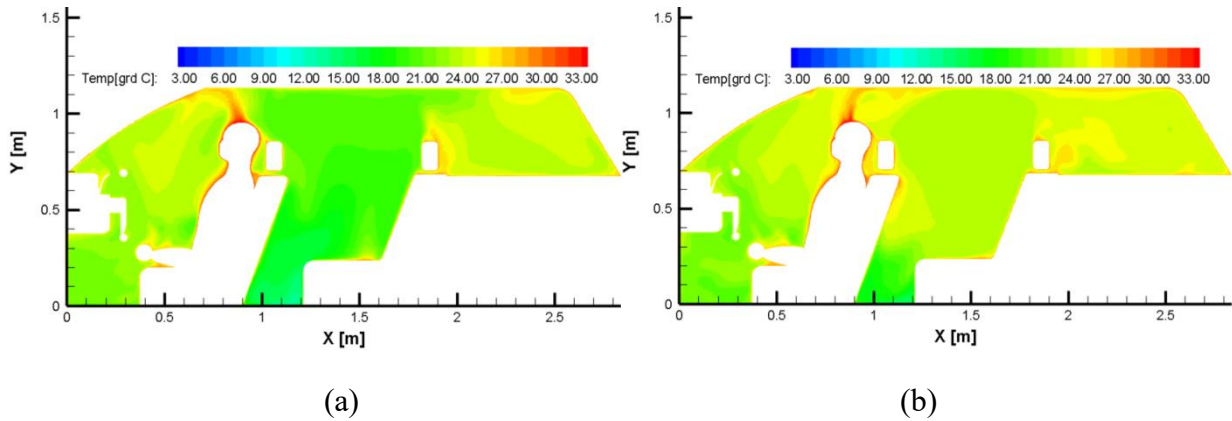


Figure 171: Temperature distribution in the median plane of the driver for the non-isothermal case, V1: a) CG; b) LAG

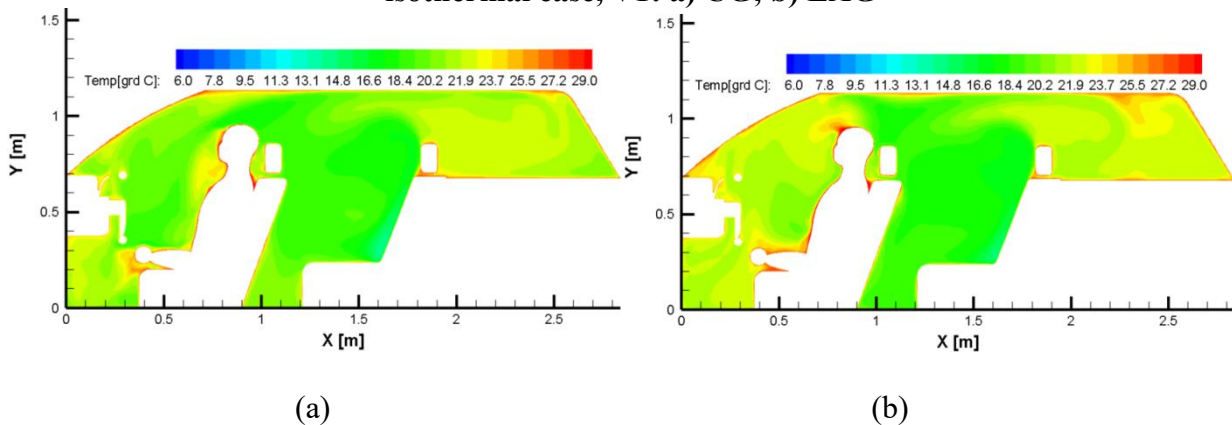


Figure 172: Temperature distribution in the median plane of the driver for the non-isothermal case, V2: a) CG; b) LAG

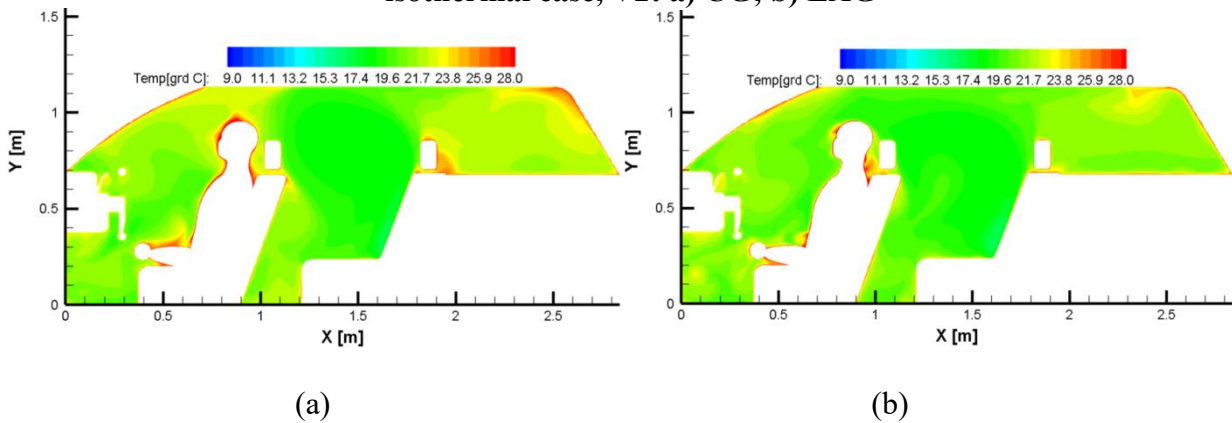


Figure 173: Temperature distribution in the median plane of the driver for the non-isothermal case, V2: a) CG; b) LAG

Observing the results presented in these figures it appears that the thermal plume generated by the virtual manikin is very sensitive to the inlet velocity condition. Indeed, initially, for the low velocity values (Figure 170) the plume has a slender, symmetric shape. We observe however that for the two types of diffusers the orientation is different – for the CG this is towards the windshield while for the LAG the orientation is towards the backseats of the car.

Another representation of the thermal plume, but in its integrality, is proposed in Figure

182, where are given for the six cases, the streamlines starting from the virtual body and coloured by the velocity magnitude. The same observation as in the case of the air temperature distributions could be done – for the CG it is oriented towards the windshield, for the LAG it is oriented towards the backseats of the car.

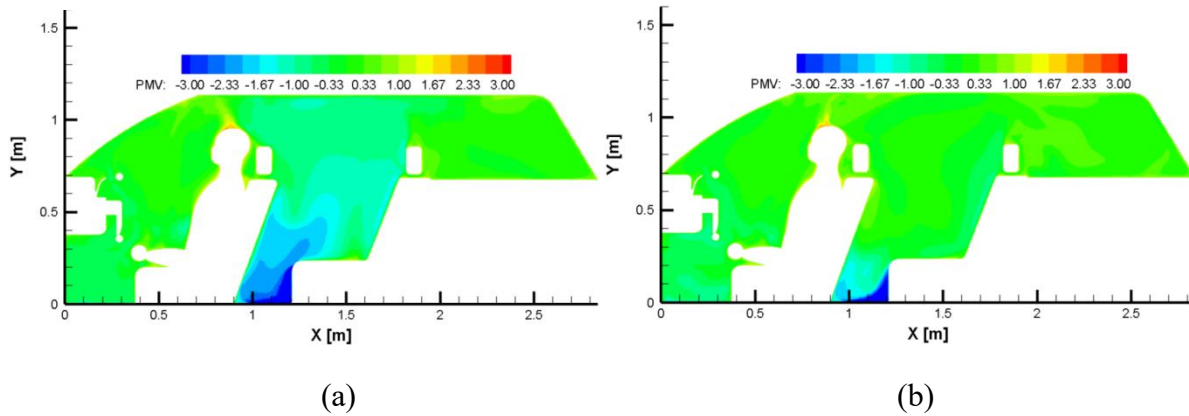


Figure 174: Local PMV distribution in the median plane of the driver for the non-isothermal case, V1: a) CG; b) LAG

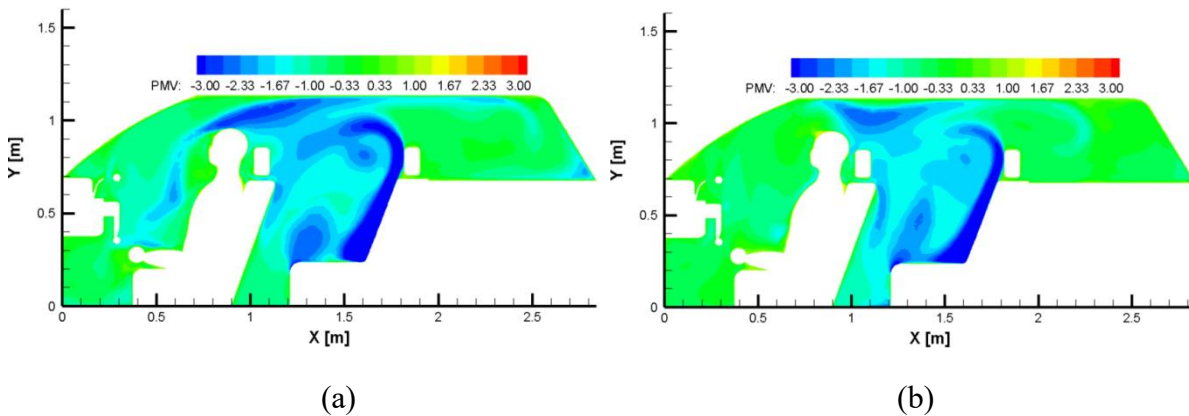


Figure 175: Local PMV distribution in the median plane of the driver for the non-isothermal case, V2: a) CG; b) LAG

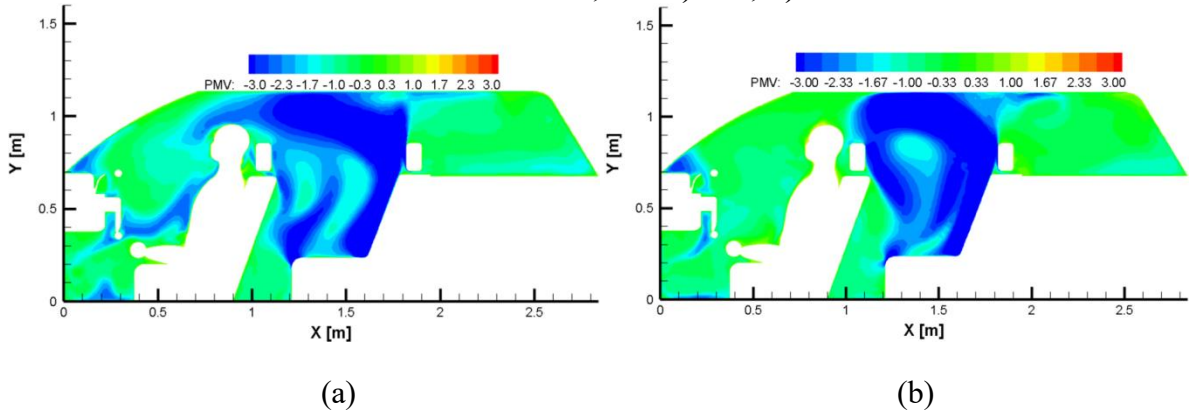


Figure 176: Local PMV distribution in the median plane of the driver for the non-isothermal case, V3: a) CG; b) LAG

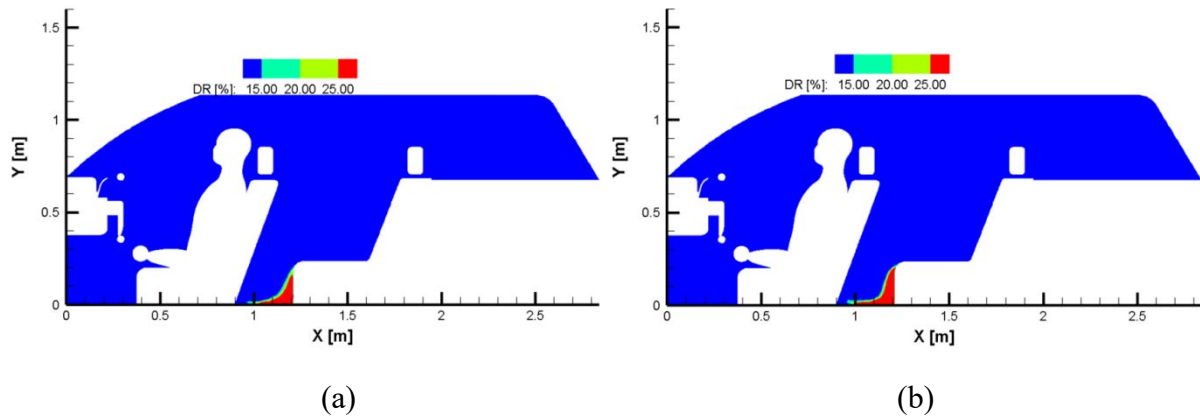


Figure 177: DR distribution in the median plane of the driver for the non-isothermal case, V1: a) CG; b) LAG

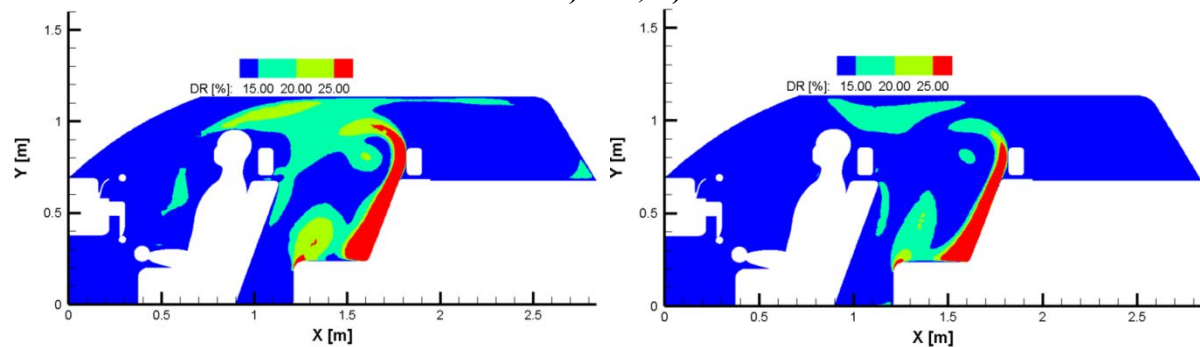


Figure 178: DR distribution in the median plane of the driver for the non-isothermal case, V2: a) CG; b) LAG

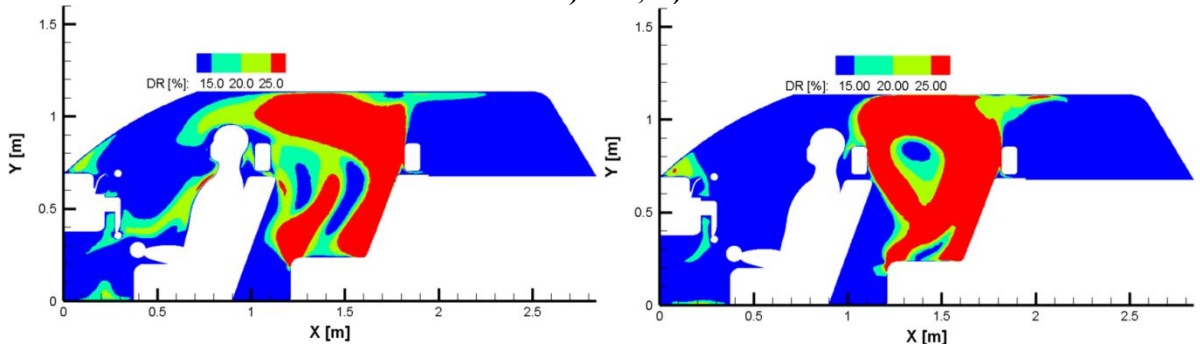


Figure 179: DR distribution in the median plane of the driver for the non-isothermal case, V3: a) CG; b) LAG

As the thermal environment in this study is nonuniform we also decided to estimate the local Predicted Mean Vote (*PMV*) distributions in the test cell [275]. The local *PMV* distributions maps from Figures 175-177 are revealing the presence of zone with the local values of this index related to a sensation of cold. This zone is very constrained for V1, for both CG and LAG cases. For V2 and V3 cases the discomfort zone is extended in the back part of the car cabin. If we compare CG with LAG we could observe that the discomfort zone tends to extend also in the front region of the car cabin in front of the virtual driver in the first case.

The CFD simulation results allow us to easily evaluate the Draft Risk (DR) index as defined by Fanger:

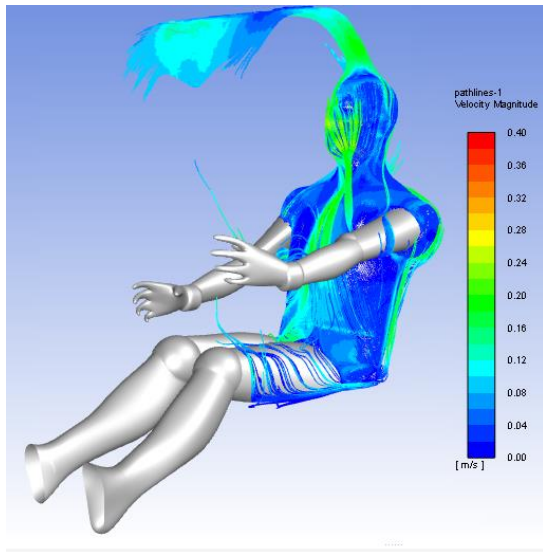
$$DR = (34 - T_a)(U - 0.05)0.622(0.37U \cdot T_u + 3.14) \quad (32)$$

where T_a is the local air temperature, and U and T_u are the local air speed values and turbulence intensity. The spatial distributions of the DR are divided in four main regions. These four regions correspond to a classification of the indoor ambiance regarding its comfort level. This way, the blue color ($DR \leq 15\%$), is associated to the zones with a high comfort level and the red color ($DR > 25\%$) corresponds to region with unacceptable conditions where the sensation of draught might create a serious discomfort.

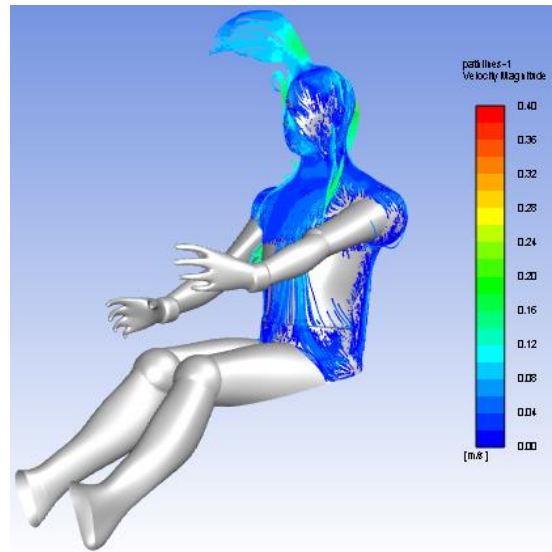
As it could be observed in Figures 170-180, the innovative diffusers offer a larger zone with high comfort level and a more reduced region at the driver's side corresponding to unacceptable conditions. On the other hand, in both cases the zone corresponding to the backseats seems to be more uncomfortable.

As it is obvious that the virtual body suffers a non-uniformly distributed convective heat transfer, with high differences between the various studied cases, there is a need to quantify the status of these cases. The equivalent temperature t_{eq} , which takes into account the combined effect of the local air temperature, local thermal radiation, local air velocity based on the local heat transfer rate at the skin surface [69] represents a good candidate for this quantification.

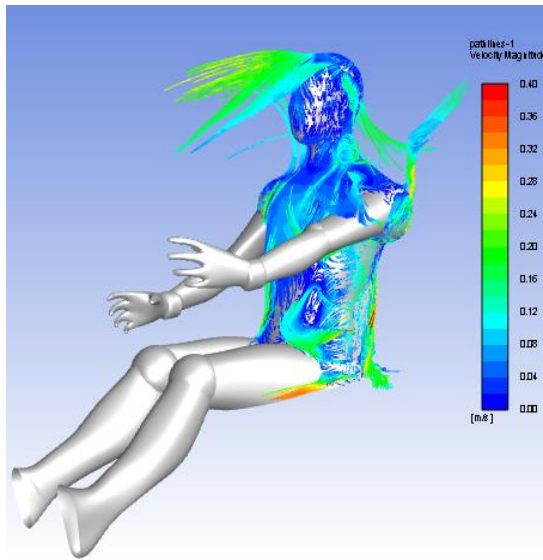
In Figure 182 we represented the equivalent temperature distributions for each part of the body for the five cases with jet flow. It could be noticed in this figure that relatively large variations of the equivalent temperature for each considered body parts occur, indicating variations of the local convective fluxes on the surface of the manikin [69]. This remark brought us to represent in Figure 183 the distributions of the convective fluxes on the surface of the manikin for the five main studied cases. Figure 183 allows observing the convective flux dynamics on the surface of the virtual body being probably explained by subtle changes in the air flow at the solid/fluid interface between the manikin and its ambient. [276]. It allows also to qualitatively observing that thermal transfer occurs differently for each part of the body and each considered case. If we look to the right hand of the manikin which is exposed to the flow of the central air diffusers, it could be observed that in the case of the LAG the heat transfer between the body and the air flow is less intense. In the same time the results are consistent with the previous distributions of the PMV and DR values that were displaying that in the case of the LAG, in the front part of the cabin the thermal discomfort related to draught would be reduced.



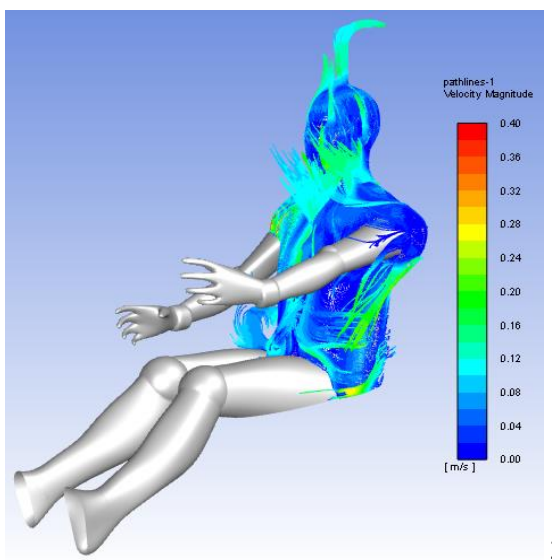
1a)



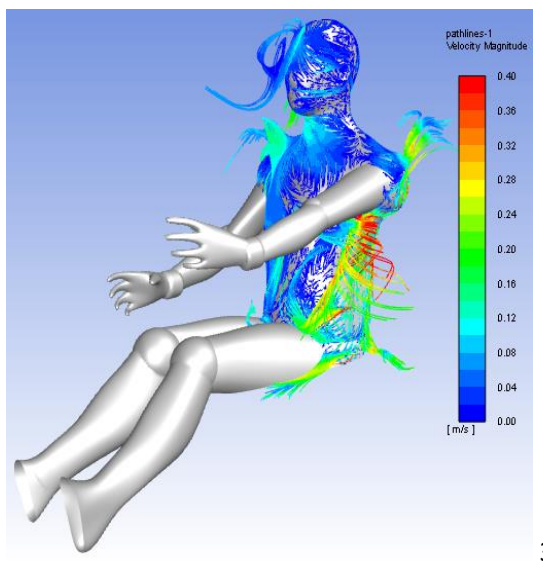
1b)



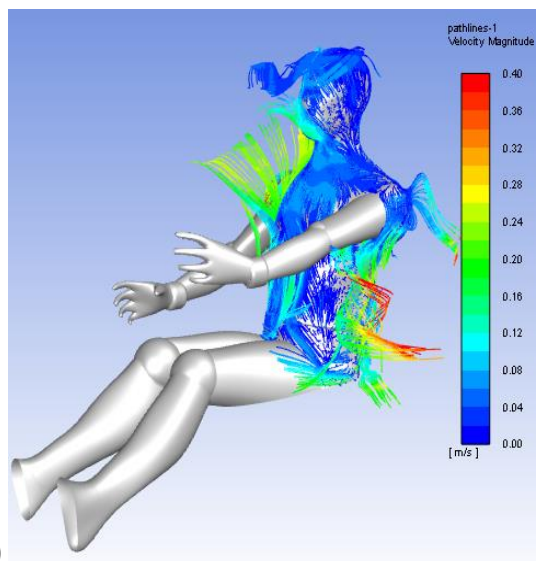
2a)



2b)



3a)



3b)

**Figure 180: Path lines showing the thermal plumes from the virtual thermal driver's body:
a) CG ; b) LAG; 1) V1, 2) V2, 3) V3**

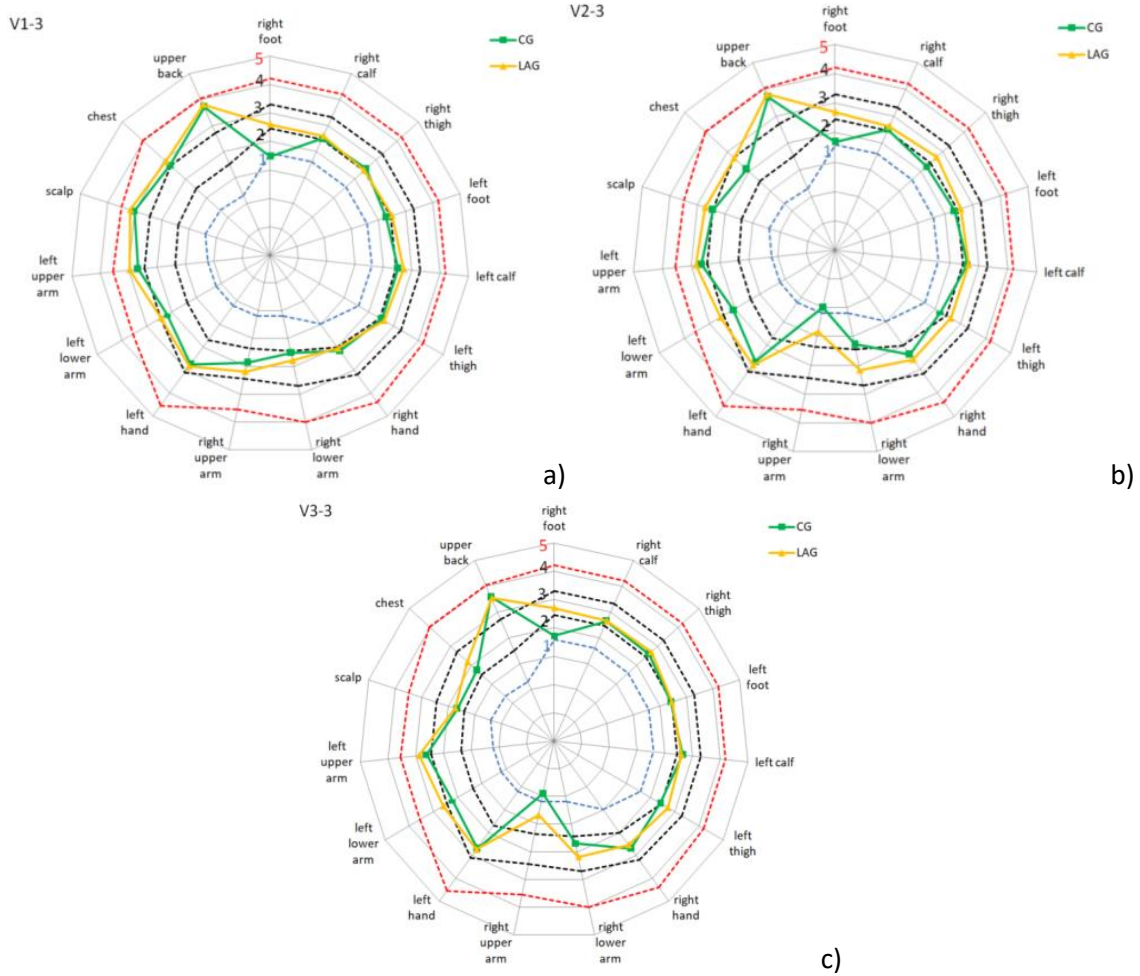
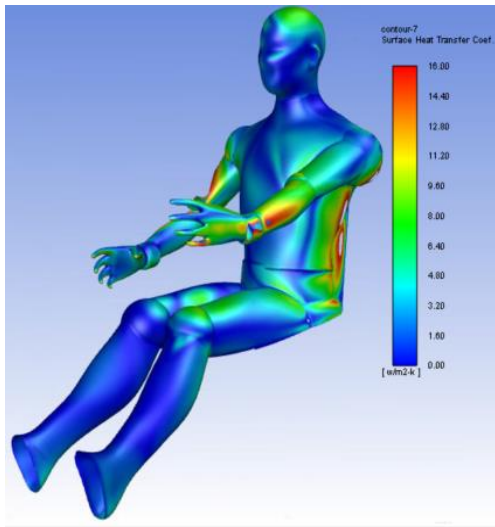
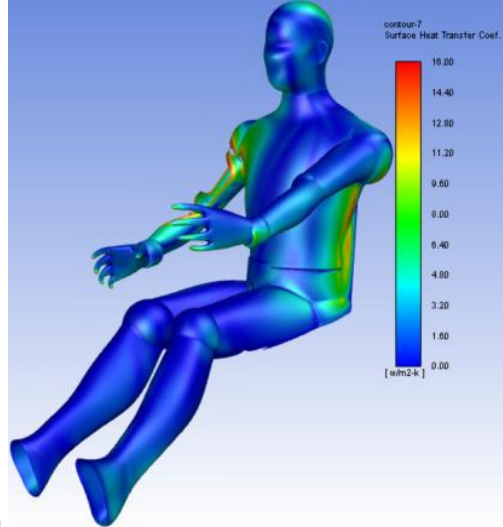


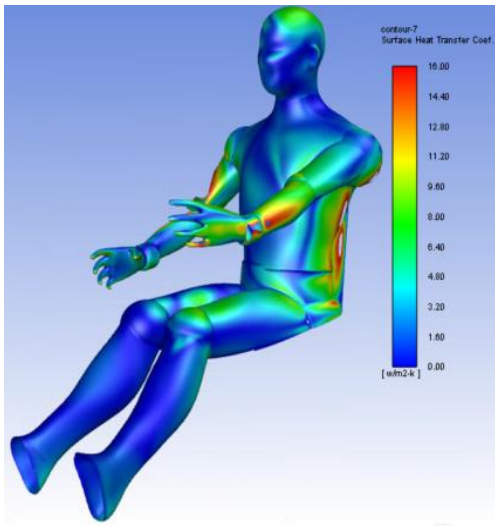
Figure 181: Equivalent temperatures on the surface of the virtual thermal manikin: a) V1, b) V2, c) V3



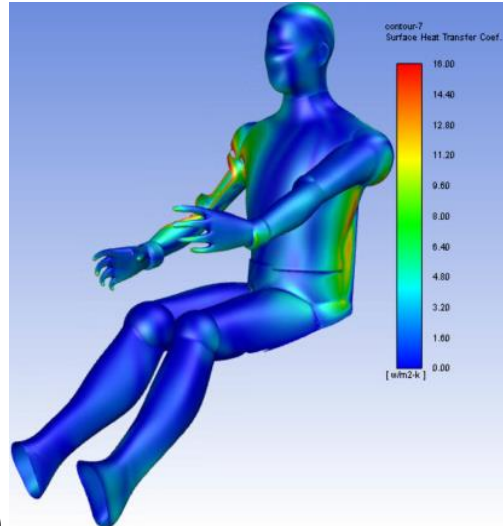
1a)



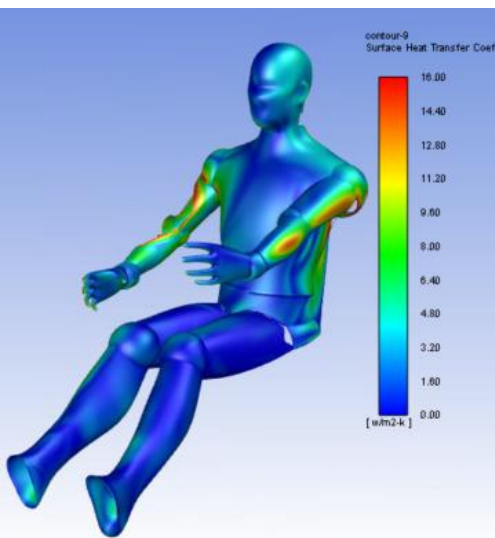
1b)



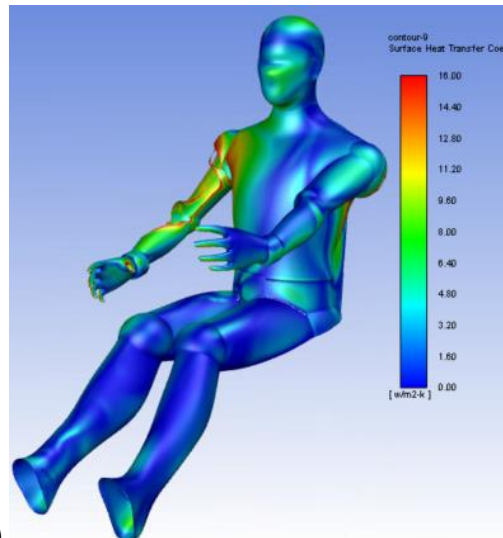
2a)



2b)



3a)



3b)

Figure 182: Convective heat flux on manikin surface a) CG ; b) LAG; 1) V1, 2) V2, 3) V3

B. Experimental results obtained from the third experimental campaign

The second experimental set-up presented in Chapter 3, and was designed partially for the calibration and the validation of our final numerical models, partially in order to gain insight on the phenomena from the car cabin reported to the subjective human component of the thermal sensation. The objectives of the experimental campaign were multiple:

- to record in different conditions, the evolutions of the temperatures on the surfaces inside the cabin and in different points in the air in order to inject these data in the numerical model therefore the effect on different flow rates and cold air temperatures on the air distribution inside the cabin could be quantified;
- to provide data for validation purposes of the numerical models developed in Chapter 4, data that were also displayed in this previous chapter, by recording air speed values and temperatures in different points inside the car cabin;
- to « measure » thermal comfort indices using the Comfort Sense system and the thermal manikin previously developed for different flow rates and two geometries of air diffusers in cooling conditions, and thus to provide data for validation purposes of the numerical models developed in Chapter 4;
- to perform subjective thermal comfort evaluations for the same flow rates and the two geometries of air diffusers in cooling conditions allowing a direct comparison between the subjective response and the dedicated measurement systems.

As explained in Chapter 3 measurements were performed inside an experimental hall during two days with quasi identical external conditions. Inside the hall where our experimental car was placed, the air temperature remained around 30°C. A typical example of a of temperature evolutions inside and outside the cabin is presented in Figure 87. Another example is given in the Figure 182, where we represented the recorded temperature outdoor (15 min same interval) for each considered flow rate (V1, V2, V3), for the tests using the Comfort Sense system, in the case of both diffusers. In this figure it could be observed that the outside temperature is constant during the considered test. Before each measurement session, the vehicle was turned on for 30 minutes as required by ISO 14505 standard.

For all the experimental sessions, the temperature was monitored on the interior surfaces, outdoor and inside the vehicle at different heights. Probe sensors were placed inside the cabin, on different surfaces and at different heights according to sensitive body parts. Inside the cabin we installed 41 thermocouples as explained in Figure 88. Three thermocouples were placed at the

inlets level, one in the center, one on the left side air diffuser and another in the right-side air diffuser. Another nine thermocouple were placed on the interior surfaces: dashboard, windshield, sides windows, ceiling, floor, top cover of the trunk and rear window. Another fifteen thermocouples were placed in the zones corresponding to sensible parts of the passengers as head, chest, abdomen, knee and ankles.

As explained previously, during this experimental campaign we also performed thermal comfort evaluation using both subjective and measurement methods. For the evaluation of thermal comfort indices, we used the Comfort Sense system allowing the direct assessment of PMV, PPD and DR indexes. In another step we used the thermal comfort manikin that we presented in Chapter 2. These measurements sessions were combined with the subjective evaluation sessions as follows.

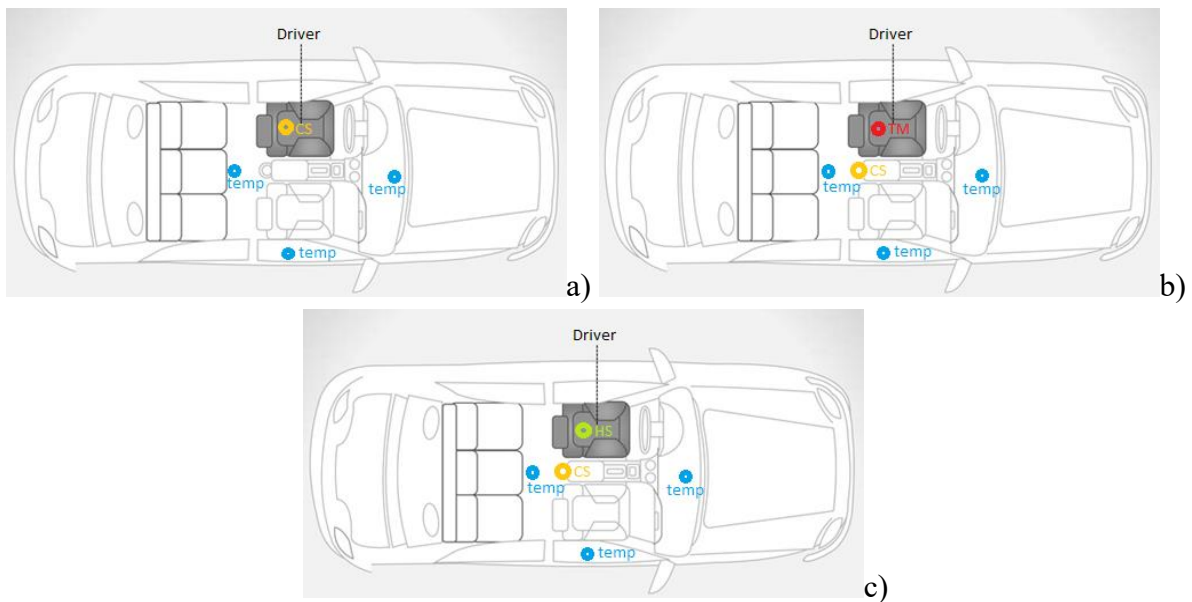


Figure 183: Experimental setup sketch with the synthesis of the performed tests: a) Comfort Sense system at the place of the driver, b) thermal manikin as the driver and Comfort Sense system in the center of the cabin, c) human subjects on the drivers place and Comfort Sense system in the center of the cabin

The following part of this subchapter is organized around the three types of experimental approaches:

- Comfort Sense system on the driver's place ;
- Thermal manikin as driver and Comfort Sense system placed in the center of the cabin ;
- Human subjects as driver and Comfort Sense system placed in the center of the cabin.

In the Figure 181 is presented a synthesis of the experimental setup sketches with the locations of the evoked measurement equipment and subjects.

As explained in Chapter 3, the temperature distributions were evaluated for three different airflow levels (V1, V2, V3) for both grilles types: Classical Grille (CG) and Lobed Aileron Grille (LAG). The measurement of temperature distributions was accomplished for all experimental sessions. Only similar cases as outdoor and inlet temperature were analyzed. For each airflow level, we have plotted the temperature evolution during periods of 15 minutes. The results can be considered relevant for all other measurement set-ups (with ComfortSense, thermal manikin, human subjects). The experimental sessions can be divided into three categories, studying the CG and LAG impact on thermal comfort and these three cases will be detailed further. All other temperature sensors excepted the thermocouples were positioned in the same way for all the cases.

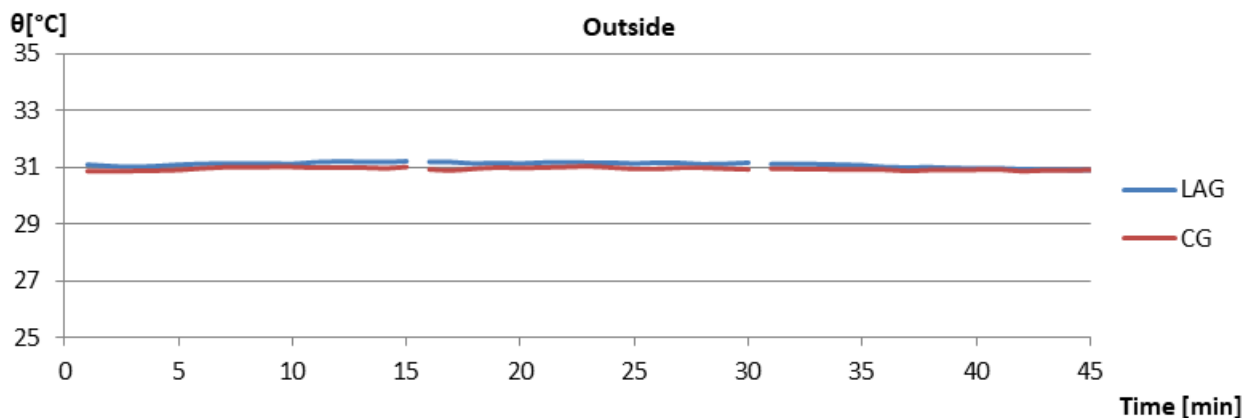


Figure 184: Outside temperature evolution in 15 minutes intervals for each airflow range for the tests using the Comfort Sense system. Comparison between CG and LAG case

In the following figures we present the temperature variations on the interior surfaces of the cabin, for the three different airflow levels (V1, V2, V3). The results do not indicate a significant improvement in the LAG case.

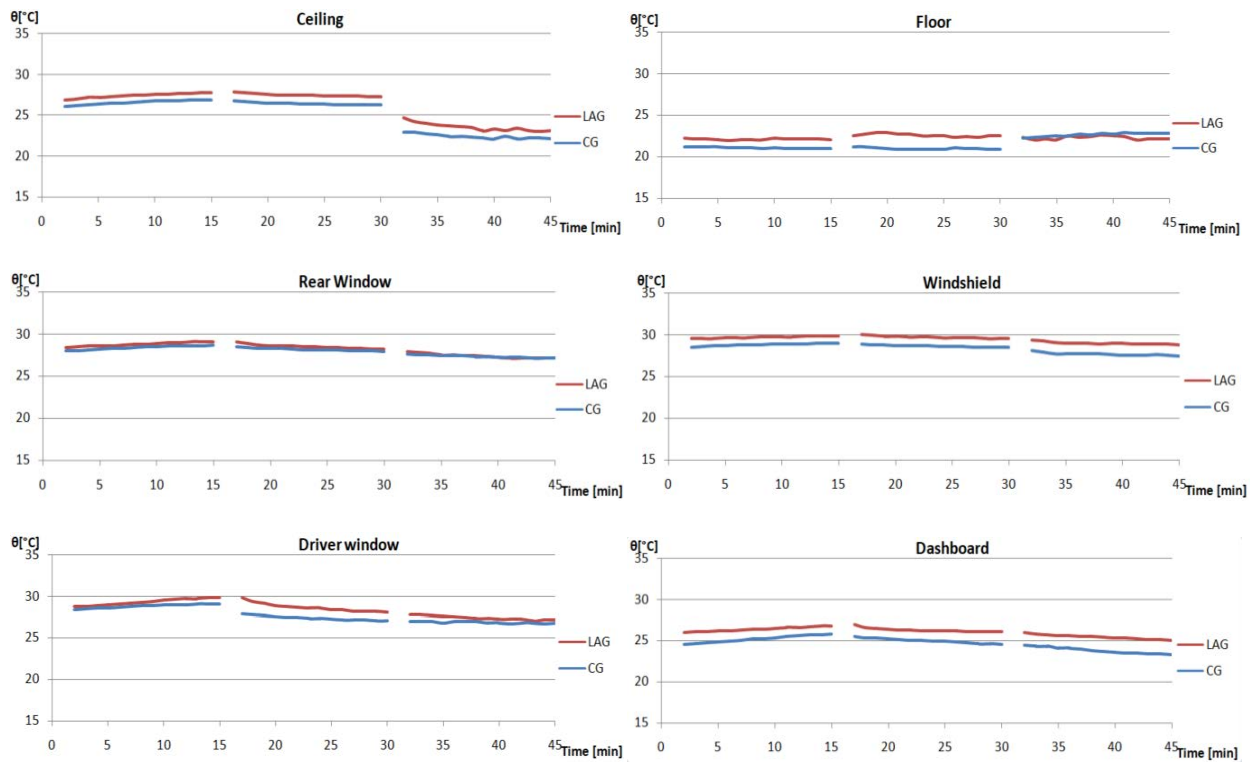


Figure 185: Temperature evolution in 15 minutes intervals for each airflow range, on different surfaces. Comparison between CG and LAG case

We have measured the temperature of inlet airflow for the three intervals. We can observe that the temperatures can be different for certain airflow ranges for the two grilles cases. However, no significant differences can be identified.

Regarding the vertical temperature gradients, temperature sensors were placed at the heights of, the head, the chest, the abdomen, and the knees and the feet. The results are presented in Figure 187. For the lower airflow rates, there is not a significant difference in terms of temperatures for the two air diffusers under investigation. In the case of the highest airflow rate, all the sensors installed at the level of the head show a faster decrease of temperature, indicating that for the case of the lobed grilles the thermal sensation might be different.

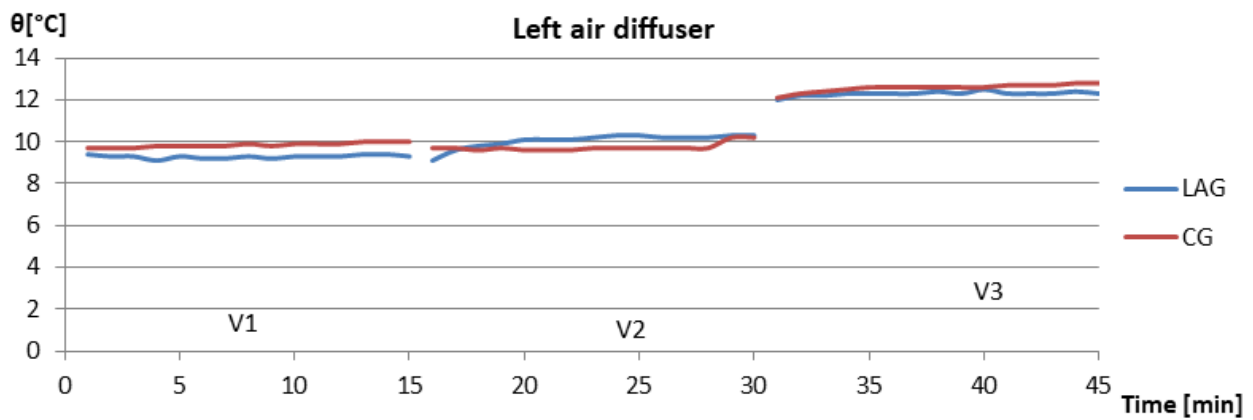
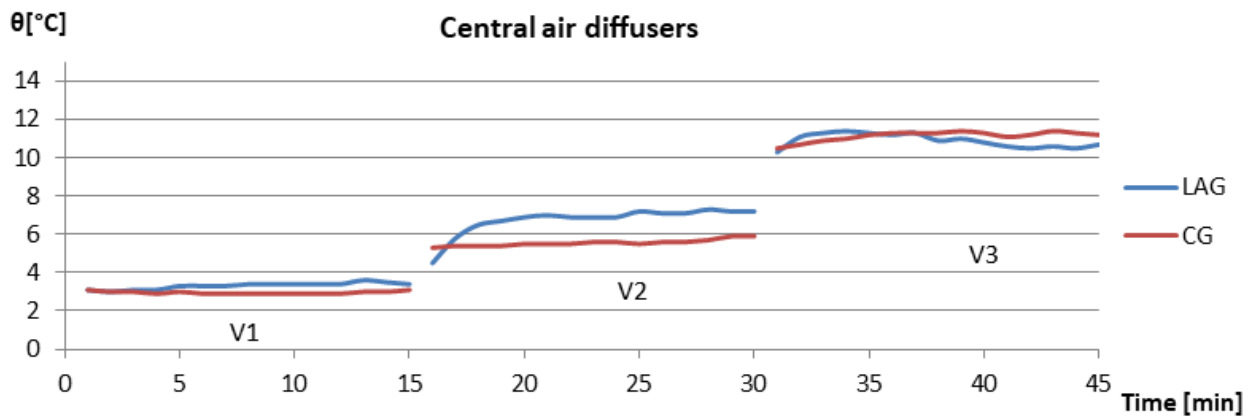
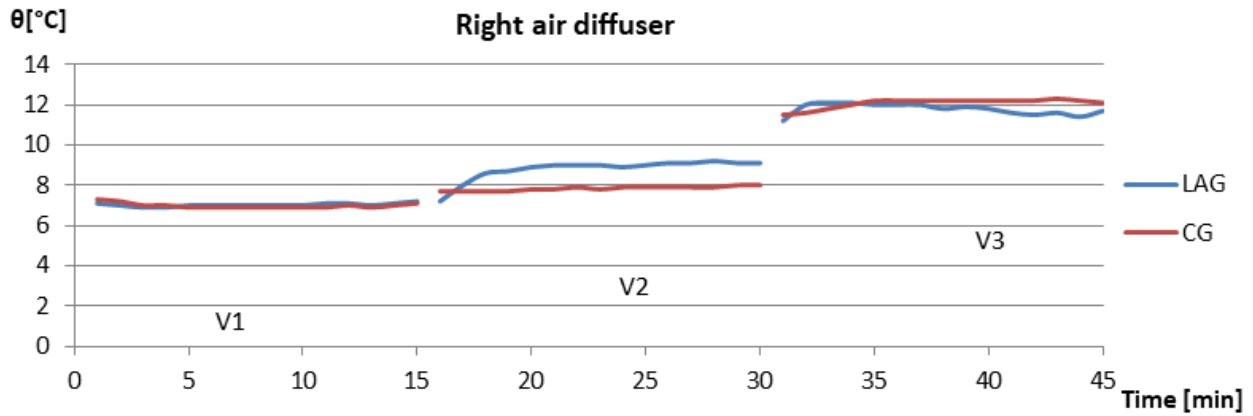


Figure 186: Temperature evolution in 15 minutes intervals for each airflow range, at measured at diffuser grille level. Comparison between CG and LAG case

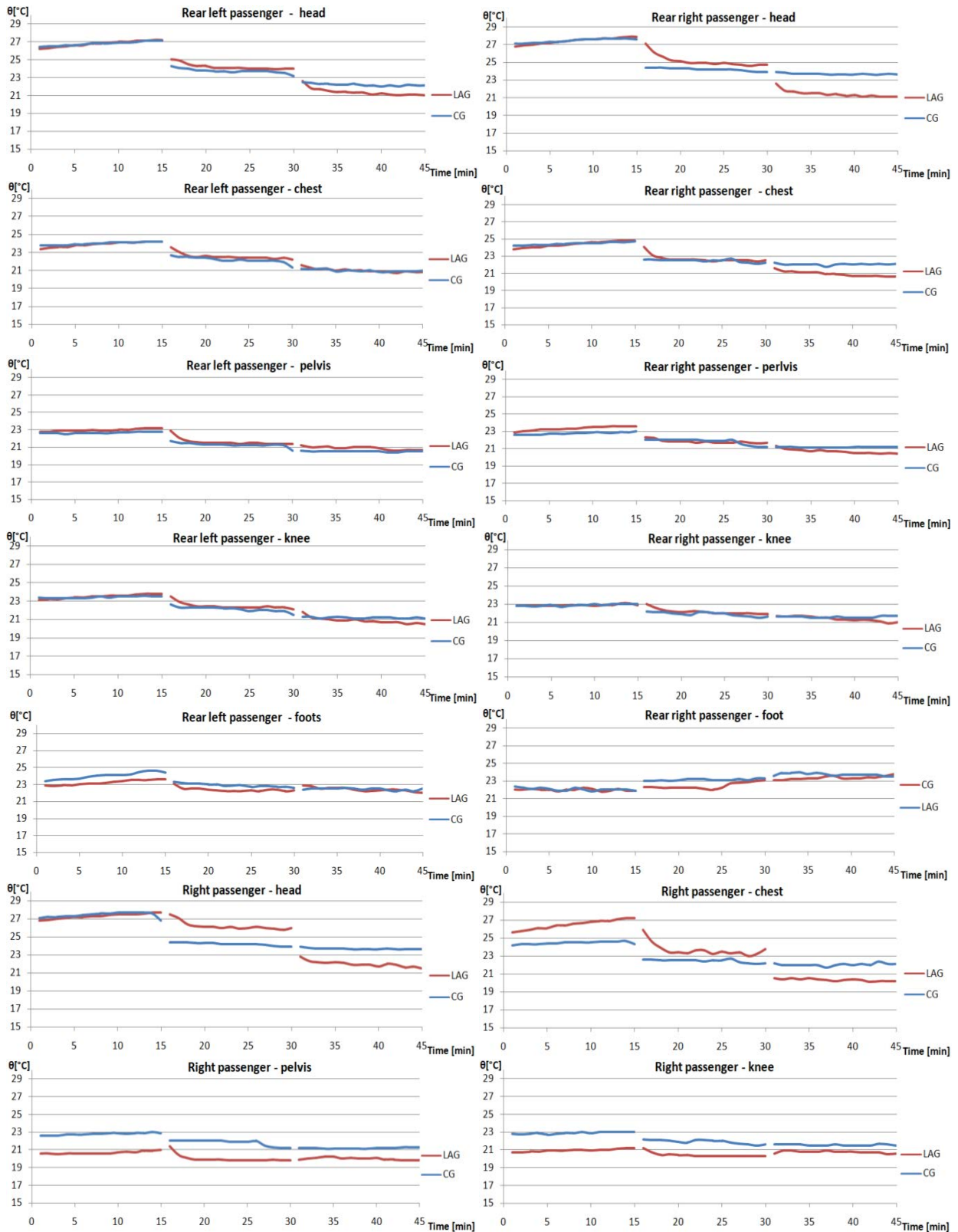


Figure 187: Temperature evolution in 15 minutes intervals for each airflow range, at for different heights. Comparison between CG and LAG case

a) Configuration 1: Comfort Sense placed on driver seat

The Comfort Sense system was installed on the driver place in order to assess thermal comfort and compare the results with Suzy manikin results and with the survey answers from the questionnaires. The big disadvantage of PMV index obtained with Comfort Sense is that the related global assessment of thermal comfort in a single point in such non-uniform and transient environment cannot be relevant to the real situation.

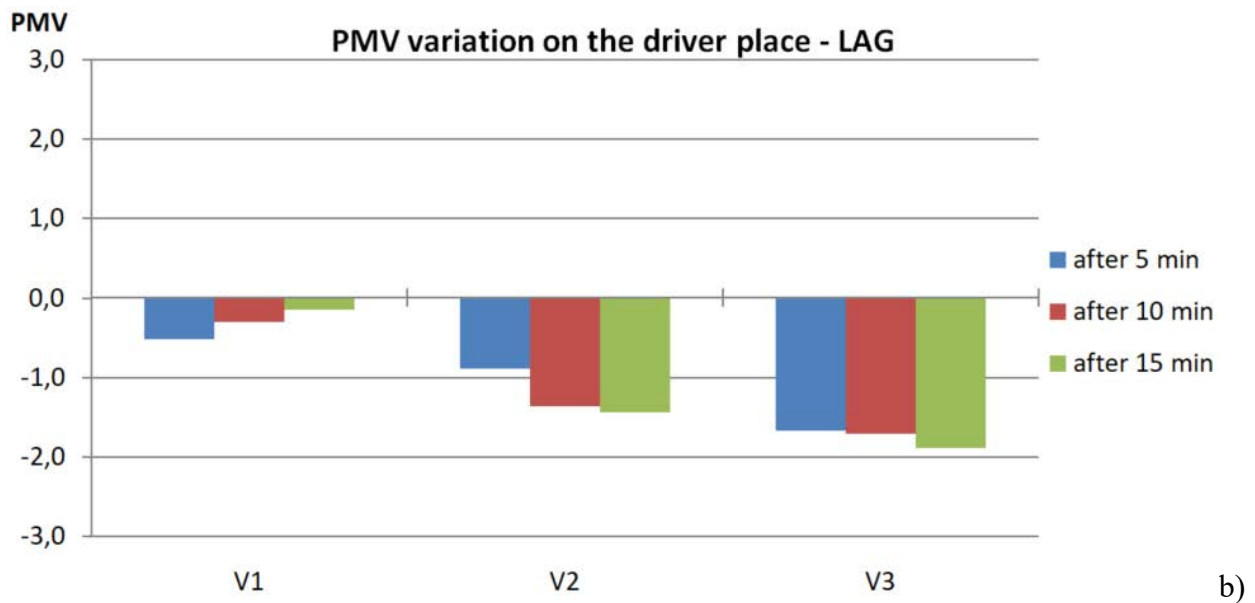
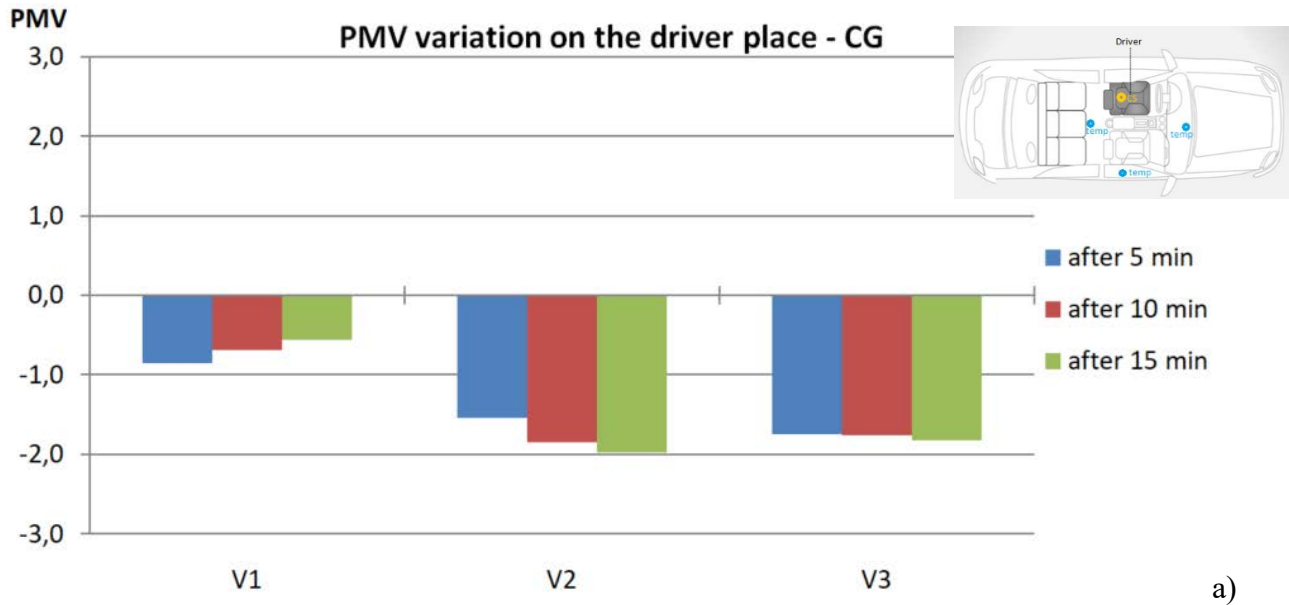


Figure 188: PMV as given by the Comfort Sense system, each 5 minutes during the experiments : a) CG; b) LAG

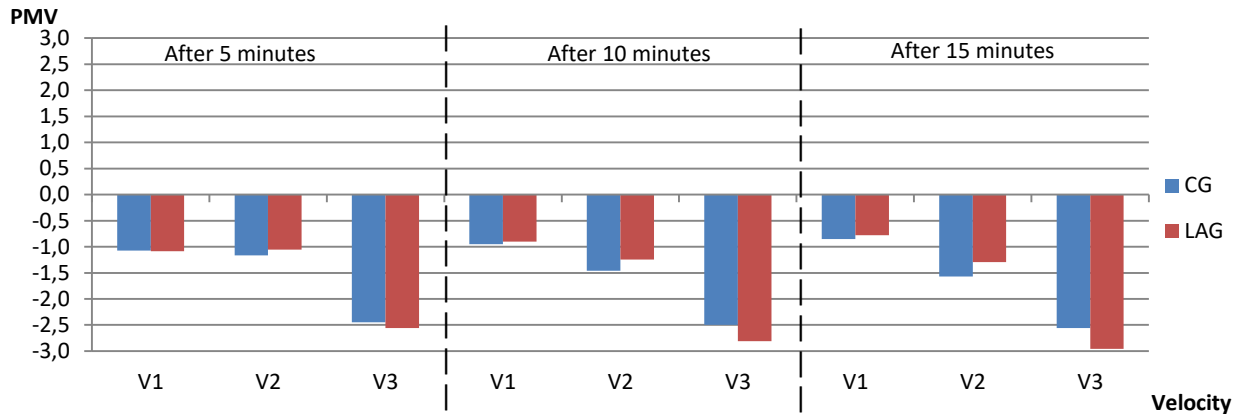


Figure 189: PMV as given by the Comfort Sense system, each 5 minutes during the experiments - Comparison between CG and LAG case

In Figure 187 the PMV values for the two types of investigated air diffusers are compared : classical grille CG and lobed ailerons grille LAG. By imposing a Metabolic rate of 1.1 met and a clothing insulation of 0,7 clo, the PMV index was calculated in a fixed point correlated to the driver seat. The Comfort Sense system was placed in exactly the same place during all the experimental campaigns with the two types of grilles.

We observe that for lower values of the airflow (V1 and V2), the LAG performs slightly better, indicating a better PMV value. However, for the highest airflow, the situation is reversed.

b) Configuration 2: Thermal manikin placed on driver seat and Comfort Sense placed in the center of the cabin

In the next configuration, the thermal manikin was placed on the driver seat and the Comfort Sense system was installed in the center of the cabin vehicle. Figure 188 represents the equivalent temperature distribution for each airflow range (V1, V2, V3) during 3 intervals (after 5, 10 and 15 minutes). The equivalent temperature should be placed between lines 2 and 3, in order to consider achieved thermal comfort. We can observe that, for the LAG case, the equivalent temperature indicates an increased thermal comfort state in comparison with CG case, especially for the right foot, right arm, left thigh etc.

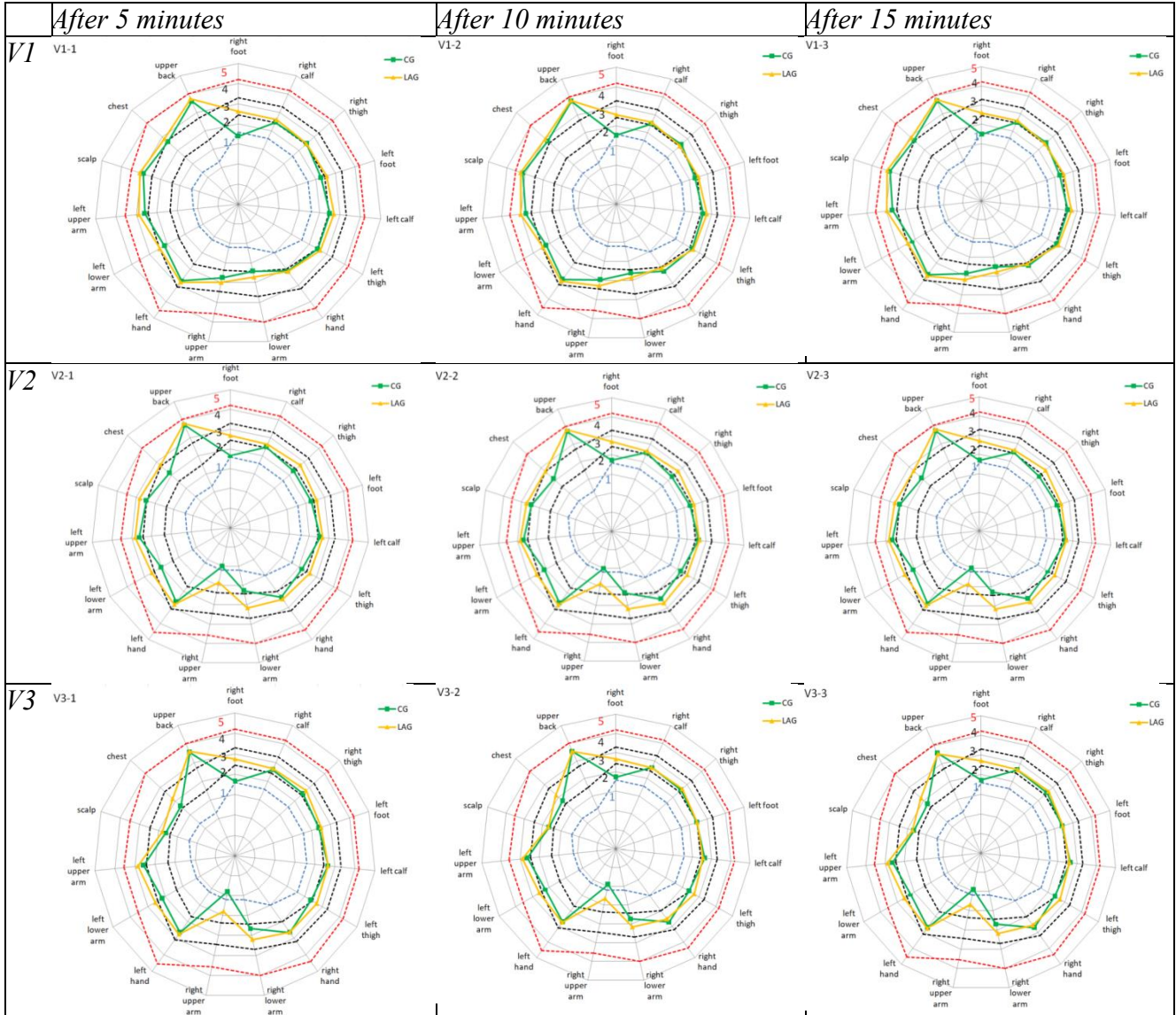
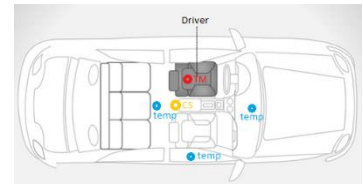


Figure 190: Equivalent temperature for different parts of the body, for CG and LAG case measured for all three ranges of airflows during 5, 10 and 15 minutes

Table 22: Experimental values obtained for t_{eq} using the thermal manikin

Experimental t_{eq} values						
Body part/Velocity step/Diffuser type	V1		V2		V3	
	CG	LAG	CG	LAG	CG	LAG
Whole Body	27.8	27.0	27.7	27.2	27.7	27.2
Right Foot	22.4	23.4	21.2	23.2	21.3	22.6
Right Leg	17.3	23.0	18.4	23.5	18.5	23.5
Right Thigh	22.4	23.0	22.5	23.0	23.1	23.2
Left Foot	22.7	22.3	21.3	23.6	22.8	23.5
Left Leg	21.4	22.6	21.6	22.8	22.1	22.3
Left Thigh	22.6	23.6	22.9	23.3	23.3	23.0
Left Hand	22.6	23.1	21.0	23.1	22.0	23.5
Right Forearm	20.9	20.4	22.0	22.9	23.4	22.8
Right Arm	17.6	18.9	16.4	20.9	18.5	20.9
Hand	19.3	20.8	10.0	14.2	9.4	13.5
Left Forearm	23.7	24.2	23.4	24.1	23.4	23.7
Left Arm	20.9	22.1	20.3	22.9	21.0	22.9
Head	23.3	24.8	23.2	24.2	23.0	24.3
Pelvic region	25.0	25.8	22.2	23.7	18.2	18.7
Chest	23.6	24.6	20.6	23.6	18.5	20.9
Upper back	28.4	28.9	28.5	29.0	27.8	27.8

c) *Configuration 3: Human Subjects placed on driver seat and Comfort Sense placed in the center of the cabin*

After the thermal manikin measurements, several live campaigns were performed with random chosen individuals, to obtain the Thermal Sensation Vote. Multiple sessions were performed to avoid subjective responses. In parallel, the Comfort Sense monitored the PMV index in the center of the cabin’s vehicle.

The majority of votes resulting from the questionnaires are indicating a neutral thermal state. However, this environment cannot be considered neutrally thermal, because this majority does not attain 80%. The resulting TSV index range is between +2 (warm) and -3 (cold).

In the first part of the tests, when the airflow range was set on the first position, most of the TSV was neutral (69% for CG; 56% for LAG) while some of human subjects rated the vehicle environment like warm (11% for CG; 4% for LAG), slightly warm (20% for CG; 25% for LAG) and slightly cool 15% only for the LAG grilles measurements. From these results we can conclude the Lobed Aileron Grilles have the tendency to faster cool down cockpit environment due to the 15% of "Slightly cool" votes more than CG case. In the first period after the entrance in the vehicle from a exterior warm environment, passengers are experiencing "alliesthesia" of the cool indoor environment, a state of thermal pleasure, even if the initial TSV

is warm.

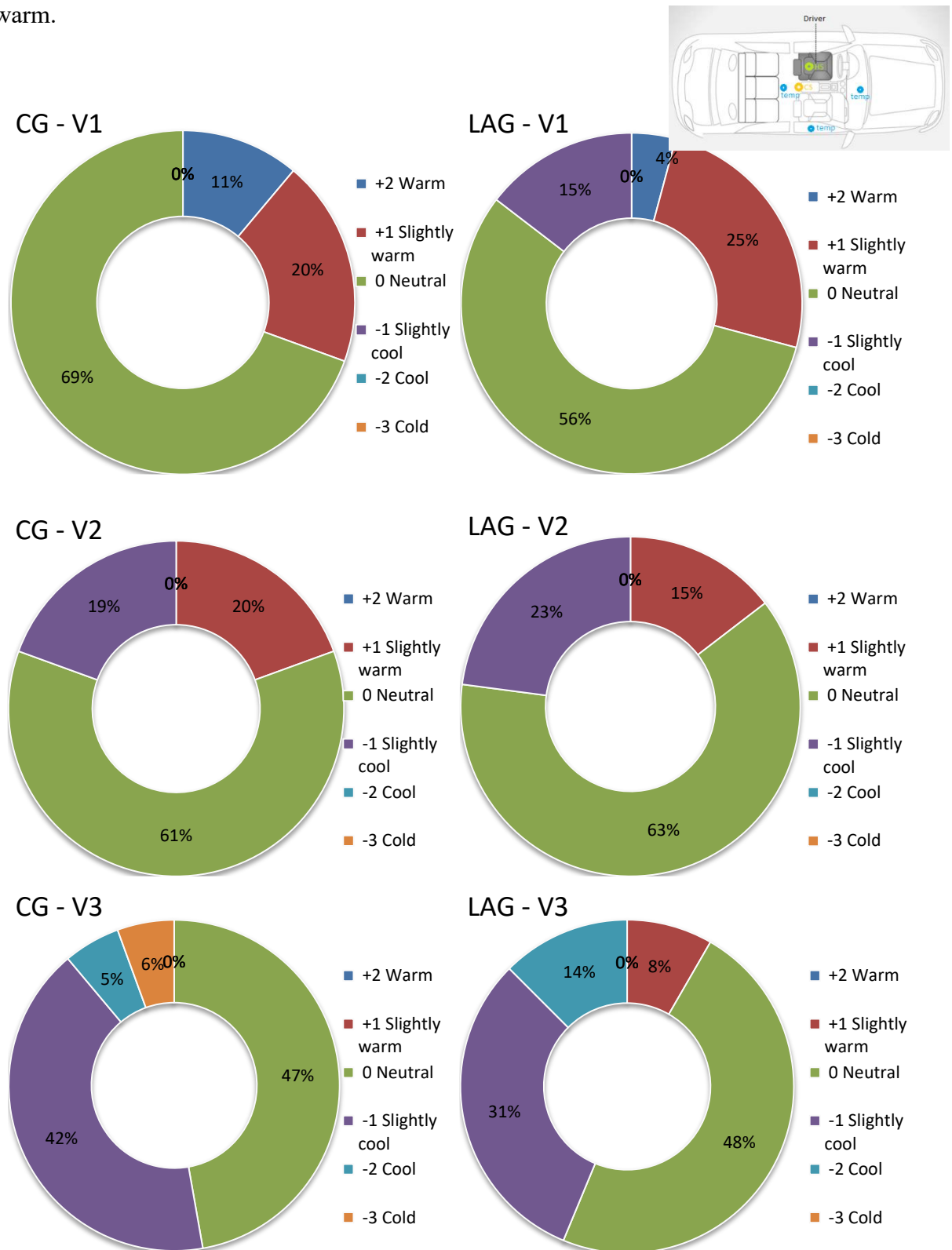


Figure 191: Thermal state percentages field at the level of whole body, from TSV, for both cases CG and LAG in all three airflow ranges

Table 23: TSV values for different parts of the body for CG

Table: TSV index obtained for CG												
Time	0			5			10			15		
Velocity step	V1	V2	V3	V1	V2	V3	V1	V2	V3	V1	V2	V3
Body parts	1	2	3	4	5	6	7	8	9	10	11	12
Whole Body	0.56	0.22	-0.56	0.44	0.11	-0.56	0.33	0.00	-0.78	0.33	-0.39	-0.89
Right Foot	0.67	0.44	-0.11	0.33	0.44	-0.22	0.56	0.44	-0.22	0.22	0.56	-0.22
Right Leg	0.44	0.33	-0.22	0.22	0.33	-0.22	0.44	-0.11	-0.56	0.11	0.22	-0.56
Right Thigh	0.67	-0.22	-0.33	0.11	-0.11	-0.33	0.11	-0.33	-0.56	0.11	0.00	-0.78
Left Foot	0.67	0.67	0.22	0.78	0.56	0.00	0.67	0.78	0.11	0.67	0.44	-0.22
Left Leg	0.78	0.56	0.00	0.78	0.44	-0.11	0.56	0.44	-0.33	0.78	0.22	-0.33
Left Thigh	0.78	0.33	-0.11	0.67	0.22	-0.22	0.44	0.33	-0.22	0.78	-0.11	-0.22
Left Hand	-0.11	-0.22	-0.67	-0.33	-0.44	-1.00	0.00	-0.44	-1.00	-0.11	-0.56	-0.89
Right Forearm	-0.22	-0.67	-1.00	-0.44	-0.89	-1.33	-0.33	-0.89	-1.33	-0.67	-1.00	-1.22
Right Arm	0.00	-0.67	-1.22	-0.22	-0.89	-1.33	-0.33	-0.89	-1.44	-0.44	-0.89	-1.33
Hand	0.44	0.33	-0.11	0.33	0.33	-0.56	0.33	0.22	-0.56	0.44	0.11	-0.89
Left Forearm	0.56	0.33	-0.44	0.33	0.22	-0.78	0.44	0.11	-0.56	0.44	-0.22	-0.56
Left Arm	0.56	0.33	-0.56	0.44	0.22	-0.78	0.44	0.11	-0.67	0.44	-0.22	-0.78
Head	0.78	-0.11	-0.78	0.44	-0.11	-0.89	0.56	0.11	-0.89	0.56	0.11	-0.89
Abdomen	0.78	0.00	-0.22	0.56	0.22	-0.22	0.44	0.33	-0.22	0.44	0.00	-0.33
Chest	0.56	-0.11	-0.56	0.33	-0.22	-0.56	0.44	-0.22	-0.78	0.44	-0.33	-0.78
Upper back	0.67	0.56	0.22	0.33	0.56	0.22	0.67	0.56	0.22	0.89	0.33	0.22

Table 24: TSV values obtained from questionnaires for different parts of the body for the LAG case

Table: TSV index obtained for LAG												
Time	0			5			10			15		
Velocity step	V1	V2	V3	V1	V2	V3	V1	V2	V3	V1	V2	V3
Body parts	1	2	3	4	5	6	7	8	9	10	11	12
Whole Body	0.08	0.00	-0.38	0.08	0.00	-0.50	0.17	-0.08	-0.46	0.42	-0.17	-0.46
Right Foot	0.25	0.00	0.00	0.33	0.00	-0.33	0.08	-0.25	-0.25	0.00	-0.33	-0.42
Right Leg	0.33	0.08	-0.25	-0.08	-0.42	-0.42	0.08	-0.42	-0.42	0.00	-0.58	-0.33
Right Thigh	0.17	-0.08	-0.42	-0.08	-0.42	-0.58	0.00	-0.42	-0.75	-0.25	-0.42	-0.67
Left Foot	0.42	0.25	-0.08	0.33	0.00	0.08	0.25	0.08	-0.08	0.33	0.00	-0.08
Left Leg	0.50	0.25	-0.17	0.08	0.08	-0.08	0.33	0.00	0.00	0.25	-0.17	-0.08
Left Thigh	0.25	0.00	-0.33	0.17	-0.17	-0.33	0.25	-0.25	-0.25	0.08	-0.25	-0.33
Left Hand	-0.25	-0.33	-0.75	-0.33	-0.71	-0.82	-0.33	-0.50	-0.92	-0.42	-0.67	-0.92
Right Forearm	-0.50	-0.58	-0.75	-0.50	-0.96	-0.83	-0.42	-0.50	-0.83	-0.33	-0.63	-0.83
Right Arm	-0.50	-0.67	-0.92	-0.50	-0.63	-0.92	-0.42	-0.67	-0.67	-0.25	-0.79	-0.92
Hand	0.00	-0.08	-0.17	-0.08	0.00	-0.50	-0.08	-0.25	-0.36	-0.17	-0.17	-0.42
Left Forearm	-0.17	-0.08	-0.25	-0.08	-0.08	-0.33	-0.08	0.00	-0.25	0.08	0.00	-0.25
Left Arm	-0.33	-0.08	-0.42	-0.17	-0.17	-0.50	-0.08	-0.25	-0.42	0.08	-0.25	-0.42
Head	0.58	-0.50	-0.92	0.33	-0.54	-0.75	0.00	-0.58	-0.75	0.25	-0.71	-0.92
Abdomen	0.25	0.17	0.08	0.25	0.00	0.00	0.17	0.17	0.00	0.42	-0.08	-0.08
Chest	0.25	-0.67	-0.83	-0.08	-0.54	-0.58	-0.42	-0.50	-0.58	0.08	-0.54	-0.58
Upper back	0.33	0.00	-0.25	0.25	0.17	-0.08	0.17	0.33	0.00	0.33	0.25	0.00

“Alliesthesia” is one of the recent concepts of researchers who are studying physiology and psychology in dynamic state conditions, which proposes that any thermal stimuli sensed by the skin that diminishes or balances the effect of contrary thermal stimuli will be perceived as

pleasant [12]. “Alliesthesia” can be positive or negative. It is depending on people’s current thermo-physiological state and on the effect of the stimuli forms their cause environment on their thermoregulation. As an example, when the body core temperature is raised above its normal value, a cold stimulus will be perceived as pleasant. The same cold stimulus will be unpleasant if the core temperature is below the normal value. From this perspective, a thermal sensation cannot be correlated to specific situations, it is connected to a dynamic equilibrium between human thermoregulation and the thermal impulse of the thermal environment [111] at which in our opinion is added the psychological component. After this period, the subjects are experiencing all other thermal states previously described. The TSV for all the cases, at different time periods are written in the Tables 23 and 24.

Questionnaire survey reveals that the lobed air diffusers are improving thermal comfort state. The most sensible human body parts are feet, ankles, head and the neck. To these sensitive parts we can add arms, forearms and hands which are on the direction of the jet flow from the diffusers. In the following graphics we have compared Thermal Sensation Vote from questionnaires at the level of these body parts for the CG and LAG case.

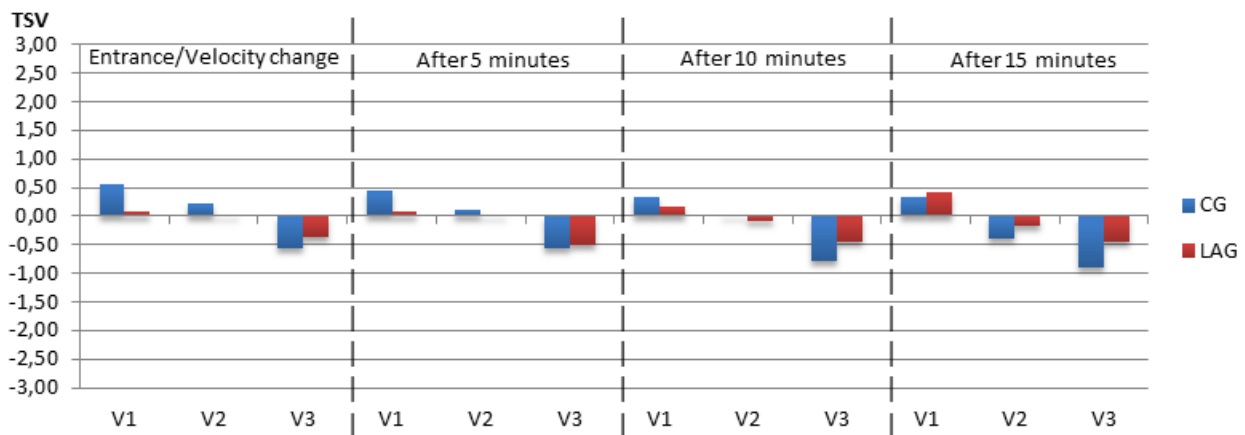


Figure 192 : Whole body TSV for CG and LAG cases

We can observe the CG TSV evolution to “cold” for the largest airflow V3, while for LAG case, the TSV remains the same, while for V2 airflow the TSV is close to neutral. Close to the head of the driver, the LAG case indicates a more comfortable environment.

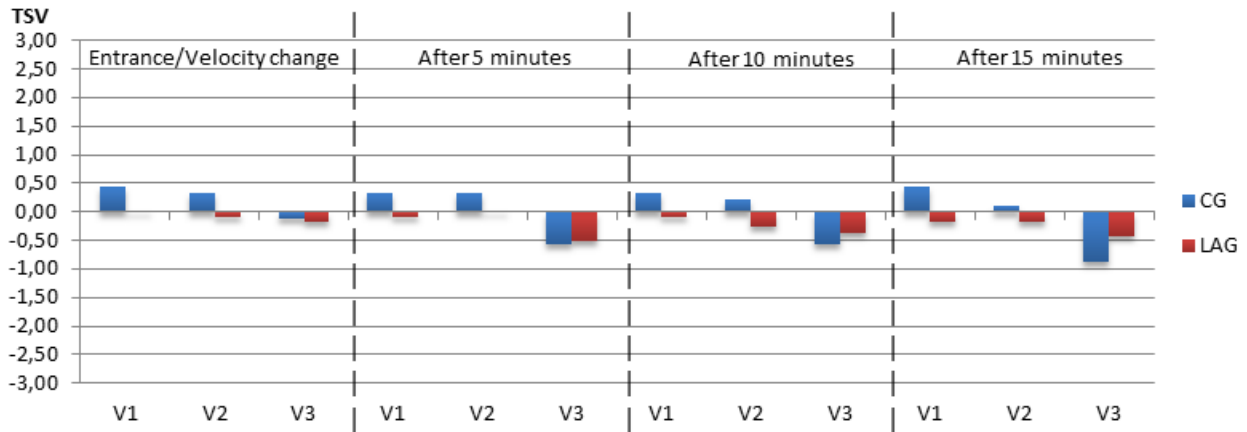


Figure 193: Head TSV for CG and LAG cases

The thermal sensation vote for the right arm, the body part where the most complaints were encountered, can be seen in Figure 194 and Figure 195. We can observe that the CG case leads to more acute cold sensations than the LAG case.

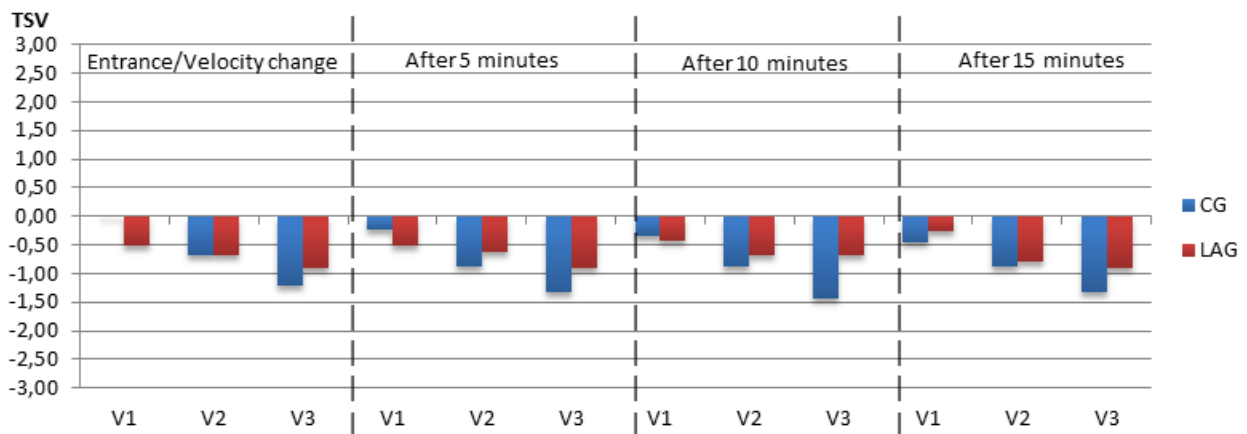


Figure 194: Right Arm TSV for CG and LAG cases

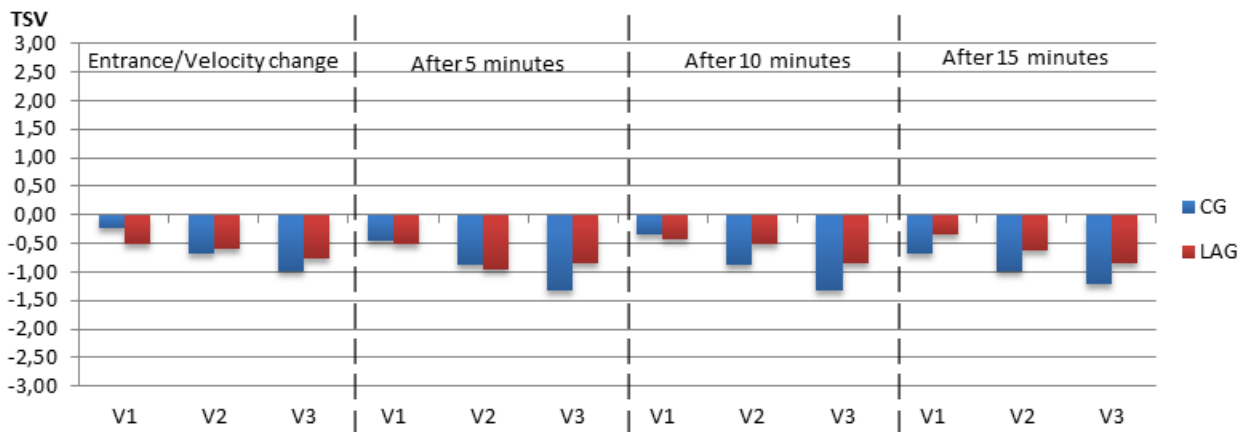


Figure 195: Right Forearm TSV for CG and LAG cases

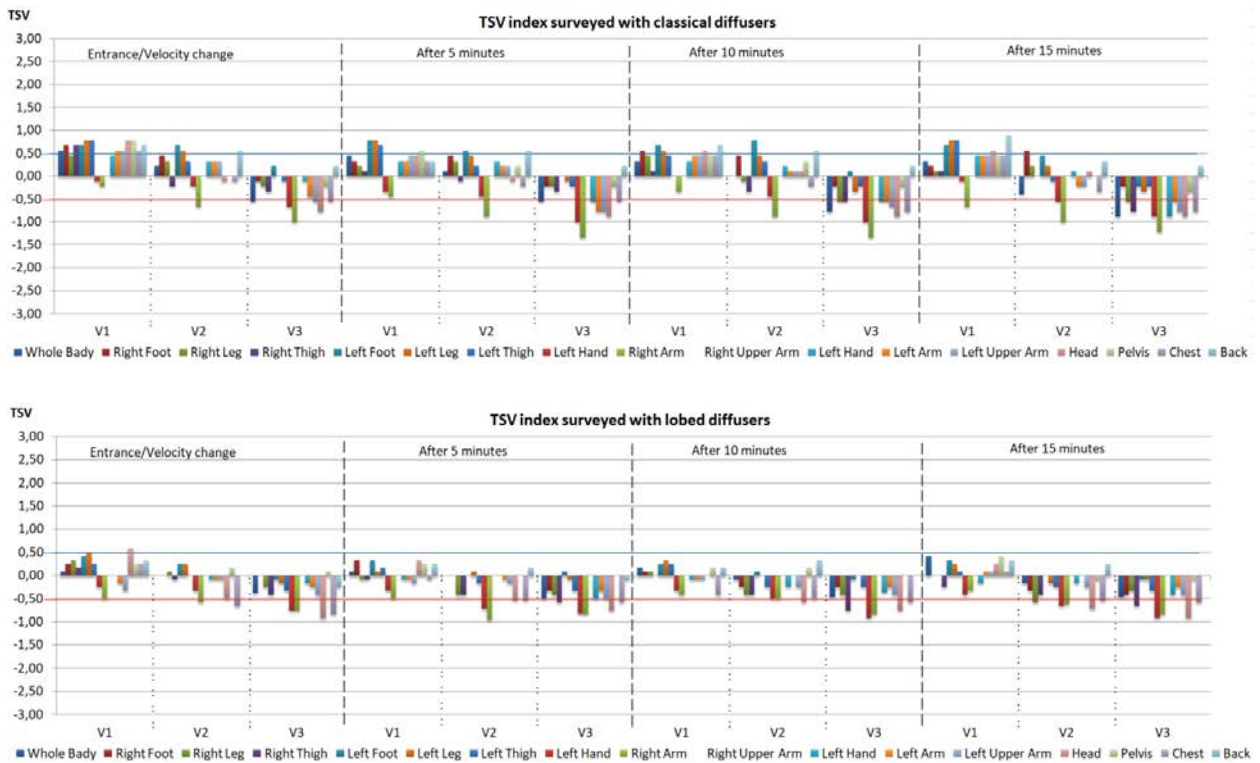


Figure 196: All local TSV values for CG and LAG cases

c. Discussion of the results

In Tables 25 and 26 we are presenting a synthesis of the data recorded by the Comfort Sense system for the CG case and for the LAG case. In Tables 27 and 28 we gathered all data regarding all recorded thermal indexes for CG and LAG cases. A direct interpretation of the values seems to be difficult. The TSV index captures besides the subjective nature of the persons that are filling in the questionnaires, the inherent dynamics of the environmental parameters, such as the protocol was designed after the prescriptions of the standard.

Tables 25: Synthesis of the data recorded by the Comfort Sense system for the CG case

Mean values when the CS was placed on the driver seat

Velocity step	θ_{op}	θ_{MRT}	PMV	PPD	Velocity	θ_{air}	DR
[-]	[°C]	[°C]	[-]	[%]	[m/s]	[°C]	[%]
V1	24	24	-0.70	16	0.02	25	0
V2	26	23	-1.79	66	0.18	22	21
V3	22	22	-1.78	66	0.15	22	20

Mean values when the CS was placed in the center of vehicle and human subject was in the driver seat

Velocity step	θ_{op}	θ_{MRT}	PMV	PPD	Velocity	θ_{air}	DR
[-]	[°C]	[°C]	[-]	[%]	[m/s]	[°C]	[%]
V1	26	25	-0.11	15	0.01	27	0
V2	24	24	-0.61	13	0.04	26	0
V3	21	22	-2.37	90	0.23	21	39

Mean values when the CS was placed in the center of vehicle and thermal manikin was in the driver seat

Velocity step	θ_{op}	θ_{MRT}	PMV	PPD	Velocity	θ_{air}	DR
[-]	[°C]	[°C]	[-]	[%]	[m/s]	[°C]	[%]
V1	23	22	-0.96	25	0.02	25	0
V2	22	22	-1.40	46	0.06	24	3
V3	21	20	-2.50	93	0.19	21	29

Tables 26: Synthesis of the data recorded by the Comfort Sense system for the LAG case

Mean values when the CS was placed on the driver seat

Velocity step	θ_{op}	θ_{MRT}	PMV	PPD	Velocity	θ_{air}	DR
[-]	[°C]	[°C]	[-]	[%]	[m/s]	[°C]	[%]
V1	24	23	-0.92	23	0.01	49	25
V2	23	22	-1.20	35	0.03	60	24
V3	21	23	-2.78	97	0.37	60	20

Mean values when the CS was placed in the center of vehicle and human subject was in the driver seat

Velocity step	θ_{op}	θ_{MRT}	PMV	PPD	Velocity	θ_{air}	DR
[-]	[°C]	[°C]	[-]	[%]	[m/s]	[°C]	[%]
V1	25	25	-0.32	10	0.01	68	11
V2	24	24	-0.92	31	0.13	50	21
V3	23	25	-1.93	72	0.31	37	35

Mean values when the CS was placed in the center of vehicle and thermal manikin was in the driver seat

Velocity step	θ_{op}	θ_{MRT}	PMV	PPD	Velocity	θ_{air}	DR
[-]	[°C]	[°C]	[-]	[%]	[m/s]	[°C]	[%]
V1	24	23	-0.92	23	0.01	25	0
V2	23	22	-1.20	35	0.03	24	0
V3	21	23	-2.78	97	0.37	20	76

The majority of studies using human subjects in dynamic states, for buildings mainly, have been conducted in climatic chambers, and only a few of them have been validated in real in situ conditions. However, an accurate prediction of people’s thermal perception in dynamic state does not yet exist PPD and PMV models do not accurately reflect people’s thermal perception in such a unsteady state such as passengers who are experiencing “alliesthesia” of the cool indoor environment.

Some important discrepancies can be noticed between the results derived from the Comfort Sense and the Thermal Manikin measurements and the subjective ones from questionnaires. Generally, sensations of coldness are amplified in the response of the Comfort Sense system, in comparison with the TSV and the thermal manikin. Moreover, it can be observed that the correlation is not significant.

Tables 27: All recorded thermal indexes for CG case

Classical Diffusers					
Time	Velocity	PMV	TSV	PMV center	PMV manikin
after 5 min	V1	-0.85	0.44	-0.11	0.26
after 10 min		-0.69	0.33		0.27
after 15 min		-0.56	0.33		0.28
after 5 min	V2	-1.54	0.11	-0.61	0.39
after 10 min		-1.85	0.00		-0.09
after 15 min		-1.97	-0.39		-0.22
after 5 min	V3	-1.75	-0.56	-2.37	-0.23
after 10 min		-1.76	-0.78		-0.21
after 15 min		-1.82	-0.89		-0.22

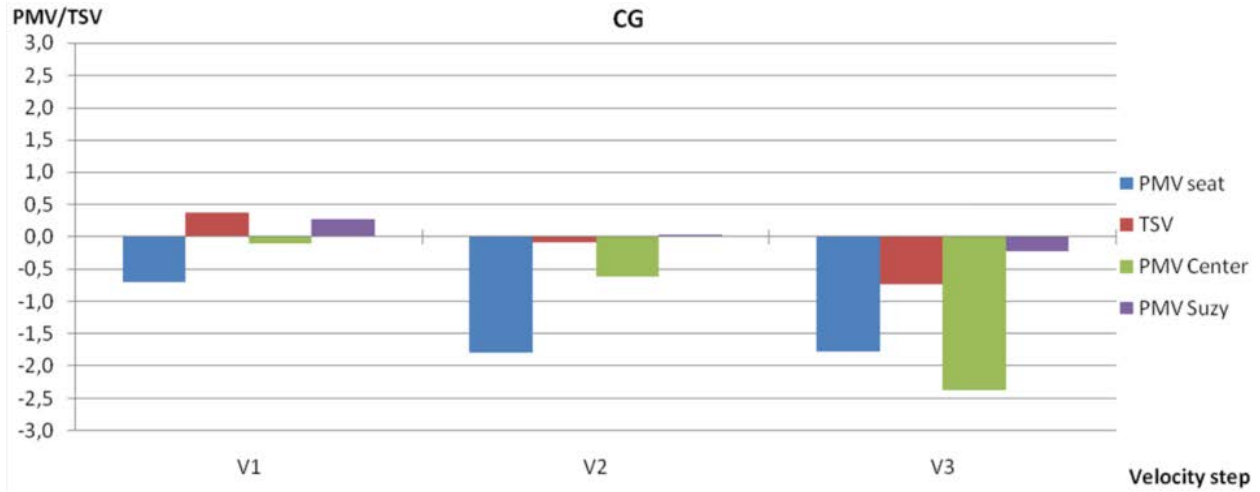


Figure 197: All recorded thermal indexes for CG case

Table 28: All recorded thermal indexes for LAG case

Lobed Diffusers					
Time	Velocity	PMV seat	TSV	PMV Center	PMV manikin
after 5 min	V1	-0.51	0.08	-0.32	0.20
after 10 min		-0.30	0.17		0.39
after 15 min		-0.15	0.42		0.41
after 5 min	V2	-0.89	0.00	-0.92	0.41
after 10 min		-1.37	-0.08		0.39
after 15 min		-1.44	-0.17		0.28
after 5 min	V3	-1.67	-0.50	-1.93	0.15
after 10 min		-1.71	-0.46		0.04
after 15 min		-1.89	-0.46		0.04

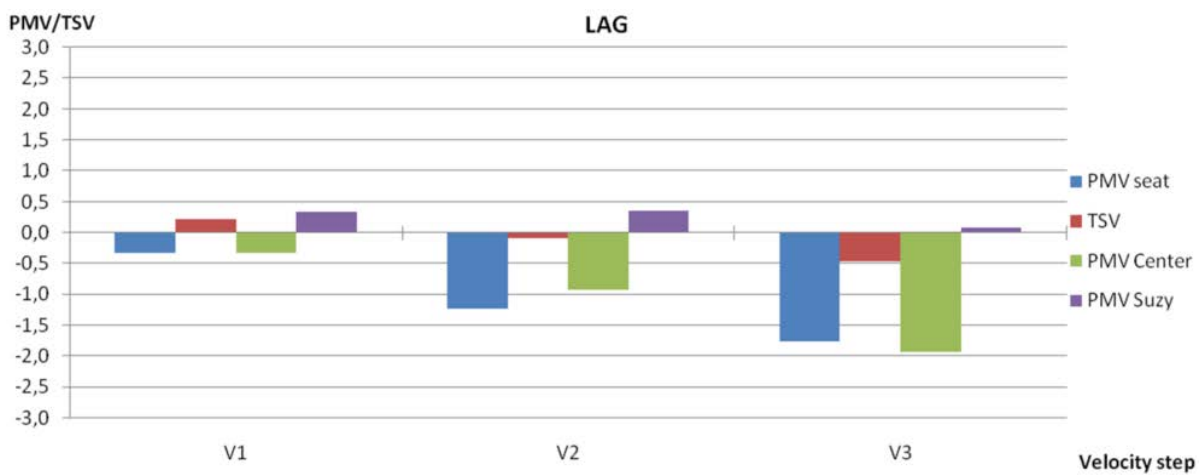


Figure 198: All recorded thermal indexes for CG case

Tables 29: Synthesis of the data recorded by the Comfort Sense system for the CG case

Time	Velocity	PMV CS driver seat		TSV		PMV Suzy		PMV center CS	
		CG	LAG	CG	LAG	CG	LAG	CG	LAG
after 5 min	V1	-0.85	-0.51	0.44	0.08	0.26	0.20	-0.11	-0.32
after 10 min		-0.69	-0.30	0.33	0.17	0.27	0.39		
after 15 min		-0.56	-0.15	0.33	0.42	0.28	0.41		
after 5 min	V2	-1.54	-0.89	0.11	0.00	0.39	0.41	-0.61	-0.92
after 10 min		-1.85	-1.37	0.00	-0.08	-0.09	0.39		
after 15 min		-1.97	-1.44	-0.39	-0.17	-0.22	0.28		
after 5 min	V3	-1.75	-1.67	-0.56	-0.50	-0.23	0.15	-2.37	-1.93
after 10 min		-1.76	-1.71	-0.78	-0.46	-0.21	0.04		
after 15 min		-1.82	-1.89	-0.89	-0.46	-0.22	0.04		

This result is a confirmation of previous analysis carried out in another typology of environment [277]. In the same time the figures 198 and 199 we are representing values of the TSV from the questionnaire survey and the PMV estimated from measured data from the Manikin and the Comfort Sense system versus the operative temperature for the entire experimental campaign show once again a great dispersion of the data collected from the questionnaire survey compared to the measured and predicted comfort indexes. However, the subjective data and the thermal manikin are giving globally very close responses. This finding correlated with the evidence of the same discomfort zones put in evidence by the subjects, the manikin and the numerical results, shows that the thermal manikin represents a worthy tool for the thermal comfort analysis in laboratory configurations and in real field case studies.

CHAPTER 6 – PERSONAL CONTRIBUTIONS

Before going to the general conclusions chapter, a synthesis of the original contributions developed in the research study is presented.

The doctoral thesis addresses a complex, interdisciplinary subject, which required the study of a large number of relevant literature to get an idea of the state of the art. In the first part, the thesis is organized around the study of current research, mainly aiming two directions: methods, models and indicators for prediction of vehicular thermal comfort and numerical simulation techniques for turbulent flows. Thus Chapter 1, offers an overview of the main concepts and results of numerous studies from literature for numerical and experimental research in the field of thermal comfort. This chapter is the summary of our initial search of landmarks in the literature that allowed us to get directions to a study and to choose a specific numerical and experimental validation, based on existing results and the available means. This chapter is a bibliographical one, proposing an extensive and exhaustive introduction in the thermal comfort research field with focus on cabin thermal environment, a synthesis of theoretical aspects concerning thermal comfort, vehicle environments and related environmental factors, that have a major effect on the vehicular space mainly aiming two directions: methods, models and indicators for the prediction of indoor thermal comfort and numerical simulation techniques for the turbulent flows used for the study of air flow in the cabin environment. It represents the summary of our initial extensive search of milestones in the existing literature. It allowed us to set the main directions for our research and to define specific numerical and experimental validation based on the existing data and on the available methods.

Thus, a first personal contribution consists of the literature review in Chapter 1, given the absence of such an analysis at present for the vehicular spaces, in the literature, taking into account all the aspects mentioned above.

In this study, the numerical approach was focused on CFD (Computational Fluid Dynamics) and experimental studies. The CFD type approach has the advantage of providing the opportunity to analyze a large number of cases, thus filling costs related to the need for a relatively large number of experiments whenever a parametric study is required. In this context, CFDs have gained great popularity in our field over the last decade. A problem presented in the literature is related to the fact that insufficient importance is still given to convective flows generated by heat sources such as the human body, which can themselves affect the distribution of room air [280]. Generally speaking, when it comes to studies that perform simulations of the

thermal and flow behavior of ventilated spaces, the investigators' attention is captured by the airflows generated by the air intake devices, although the location of the maximum air speed values in a room is influenced by the intensity of heat sources and their distribution in the room. Consequently, the interaction between the different flow types (convection currents, uniform flows and / or air jets) should be taken into account when a study focuses on estimating comfort from these simulations. *One of the main contributions of this study is related to the fine modeling of convective flow generated by the human body and the study of its interaction with the environment in terms of flow dynamics in the vehicular spaces.*

At the same time, the results obtained from any type of numerical approach should be validated experimentally in conditions as close as possible to real ones, to allow their exploitation. Knowing that experimental studies using human subjects are costly, long lasting and subjective, being hard to validate, a good compromise is the use of thermal manikins. *This is the motivation of developing thermal manikins in our research group and thus one of the most important objectives of the thesis was consisted by the development of the thermal manikin.*

Apart the thermal manikin in the experimental part of the study was used different measurement equipment. In our study we used state of the art equipment in order to measure and characterize the flow patterns inside the cabin. *This is the first time at our acknowledgement when such a detailed characterization of the flow rates discharging from the dashboard of a real car is proposed in the literature.*

The flow patterns and their effect on thermal sensation are not completely considered by manufacturers or by users, given that flow trajectory might substantially differ from the direction imposed by the guiding vanes of the air vents. This is related on one hand to these previously mentioned convective effects but might be also an intrinsic characteristic of the air vent itself. No studies combining passive induction control via the conception of air diffusers were found in the literature. The proposal of some innovative designs of air vents for the present studies was based on the previous findings of the French and Romanian research teams where the doctoral project was developed. *A part of the manuscript is dealing with the development of an innovative thermal manikin and of new concepts of air diffusers. The approach is based on both experimental and numerical approach.*

This is the first time when a very large number of human subjects, resulting in a large sample of questionnaires (almost 300) and is the only study from the literature combining the three methods of investigation: thermal manikin, comfort meter, human subjects.

A complex numerical model has been developed. This model includes a passenger with

anatomic shape and takes into consideration to types of air diffusers: one which is the reference – the classic air grilles that were originally designed in the cabin and one innovative set of air diffusers that we wanted to test. The validation of the chosen approach for introducing the effect of the flows generated by the two types of diffusers is also presented in this manuscript.

The doctoral research has been disseminated through articles published in journals, proceedings and communications in international conferences. This work is listed hereafter:

Articles in proceedings indexed in Web of Science

1. **Danca, P.**, Bode, F., Nastase, I., and Meslem, A., *CFD simulation of a cabin thermal environment with and without human body – thermal comfort evaluation*, Advances in Heat and Transfer in Built Environment, Bucharest, E3S Web Conf., 32 (2018) 01022, pp 111-118, ISBN: 978-1-5108-5878-7, DOI: 10.1051/e3sconf/20183201018;
2. Horobet, T., **Danca, P.**, Nastase, I., and Bode, F., *Preliminary research on virtual thermal comfort of automobile occupants*, Advances in Heat and Transfer in Built Environment, Bucharest, E3S Web Conf., 32 (2018) 01022, pp136-140, ISBN: 978-1-5108-5878-7, DOI: 10.1051/e3sconf/20183201022;
3. Sandu, M., Bode, F., **Danca, P.**, and Voicu, I., *Water flow structure optimization between the screenings and grit removals in a wastewater plant*, Proceedings of the 8th International Conference on ENERGY and ENVIRONMENT (CIEM), Bucharest, 2017, pp 101-104, ISBN:978-1-5386-3943-6, DOI: 10.1109/CIEM.2017.8720839, WOS:000427610300022;
4. Bode, F., Nastase, I., **Danca, P.**, and Meslem, A., *The influence of the inlet angle of vehicle air diffuser on the thermal comfort of passengers*, Proceedings of the 8th International Conference on ENERGY and ENVIRONMENT (CIEM), Bucharest, 2017, pp 442-446, ISBN:978-1-5386-3943-6, DOI: 0.1109/CIEM.2017.8720839, WOS:000427610300094;
5. **Danca, P.**, Bode, F., Nastase, I., and Meslem, A., *On the possibility of CFD modeling of the indoor environment in a vehicle*, Energy Procedia 112 (2017), pp 656-663, ISSN: 1876-6102, DOI: 10.1016/j.egypro.2017.03.1086, WOS:000404848300081;
6. **Danca, P.**, Vartires, A., and Dogeanu, A., *An overview of current methods for thermal comfort assessment in vehicle cabin*, Energy Procedia 85 (2016), pp 162-169, ISSN: 1876-6102, DOI: 10.1016/j.egypro.2015.12.322, WOS:000377911100020;
7. Vartires, A., Dogeanu, A., and **Danca, P.**, *The human thermal comfort evaluation inside the passenger compartment*, Proceedings of the 15th International Multidisciplinary Scientific Geoconference (SGEM), Bulgaria, 2015, pp 1113-1120, ISSN: 1314-2704, ISBN:978-619-7105-38-4, DOI:10.5593/SGEM2015/B41/S19, WOS:000371056000143;

Articles indexed in B+ and BDI

1. Ouhimi, P., Lechartier, T., **Danca, P.**, and Fabian, C., *Thermal comfort evaluation inside vehicles with classical indices - experimental approach*, Romanian Journal of Civil Engineering Volume 7 (2016), Nr. 2, ISSN 2068-3987, eISSN 2559-748;

2. Dan, M., **Danca, P.**, Ursu, I., Nastase, I., *Advanced thermal manikin with neuro-fuzzy control*, Romanian Journal of Civil Engineering Volume 8 (2017), Nr. 4, ISSN 2068-3987, eISSN 2559-748;

Proceedings of international conferences

1. **Danca, P.**, Bode, F., Nastase, I., Croitoru, C., and Meslem, A., *Experimental and numerical study of the air distribution inside a car cabin*, Proceedings of the 1st Conference of the UTCB Doctoral School (2018), Bucharest, pp 1-6;
2. Ursu, I., Guță, D., Croitoru, C., **Danca, P.**, Nastase, I., *Advanced Thermal Manikin Prototype with Neuro-fuzzy Control System*, Proceedings of the 4th International Conference On Building Energy & Environment 2018, pp 542-546, ISBN 978-0-646-98213-7;
3. Bode, F., **Danca, P.**, Nastase, I., Meslem, A., Croitoru, C., and Dogeanu, A., *Developing a realistic CFD model of the air distribution inside a vehicle cockpit*, Proceedings — Roomvent & PROCEEDINGS — Roomvent & Ventilation 2018, Helsinki, Finland, pp1109-1114 , ISBN 978-952-5236-48-4;
4. **Danca, P.**, and Vartires, A, *Thermal comfort assessment using human subjects*, Scientific Proceedings of XXIII International Scientific-Technical Concerence "trans & MOTAUTO '15", Bulgaria, 2015, vol. 3 Section III, pp 22-26, ISSN:1310-3946;
5. **Danca, P.**, and Vartires, A - *Thermal comfort assessment using human subjects*; Machines, Technologies, Materials International Journal, International Journal for Science, technics and innovations for the industry, Bulgaria, 2015, ISSN:1313-0226, Year IX, Issue 9/2015, pag. 20-24

Participation at international conferences

1. **Danca, P.**, Bode, F., Nastase, I., Croitoru, C., and Meslem, A., *Experimental and numerical study of the air distribution inside a car cabin*, 1st Conference of the UTCB Doctoral School, DSC 2018, 26 October 2018, Bucharest, Romania, oral presenattion;
2. Bode, F., **Danca, P.**, Nastase, I., Meslem, A., Croitoru, C., and Dogeanu, A., *Developing a realistic CFD model of the air distribution inside a vehicle cockpit*, Roomvent & Ventilation 2018 Conference, ROOM VENTILATION 2018, 2-5 June 2018, Espoo, Finland – poster presentation;
3. **Danca, P.**, Meslem, A., Nastase, I., and Bode, F., *Influence of the driver presence and of velocity profile of ventilation jet over airflow distribution and thermal comfort in a vehicle cabin*, Thermique Recherche Internationale Industrie, TR2i 2018, 24&25 May 2018, Saint Malo, France – oral presentation;
4. Ursu, I., Guță, D., Croitoru, C., **Danca, P.**, Nastase, I., *Advanced Thermal Manikin Prototype with Neuro-fuzzy Control System*, 4th International Conference On Building Energy & Environment, COBEE 2018, 5 – 9 February 2018 , Melbourne, Australia– oral presentation;
5. **Danca, P.**, Bode, F., Nastase, I., and Meslem, A., *On the possibility of CFD modeling of the indoor environment in a vehicle*, Advances in Heat and Transfer in Built

- Environment EENVIRO 2017, 24 November 2017, Bucharest, Romania – oral presentation;
6. Bode, F., Nastase, I., **Danca, P.**, and Meslem, A., *The influence of the inlet angle of vehicle air diffuser on the thermal comfort of passengers*, 8th International Conference on ENERGY and ENVIRONMENT CIEM 2017, 19 – 20 October 2017, Bucharest, Romania – oral presentation;
 7. **Danca, P.**, Vartires, A., and Dogeanu, A., *An overview of current methods for thermal comfort assessment in vehicle cabi*, International Conference of Sustainable Solution for Energy and Environment, EENVIRO 2016, 26-28 October 2016, Bucharest, Romania – oral presentation;
 8. **Danca, P.**, Vartires, A., and Dogeanu, A., *An overview of current methods for thermal comfort assessment in vehicle cabin*, , International Conference of Sustainable Solution for Energy and Environment, EENVIRO - YRC 2015, 18-20 November 2015, Bucharest, Romania – oral presentation;
 9. **Danca, P.**, Vartires, A., Croitoru, C., and Nastase, I., - *Evaluation of thermal environments in vehicles*, 17èmes Journées Internationales de Thermique JITH 2015, 28 - 30 Octobre 2015 Marseille, France
 10. Vartires, A., Dogeanu, A., and **Danca, P.**, *The human thermal comfort evaluation inside the passenger compartment*, 15th International Multidisciplinary Scientific Geoconference, SGEM 2015, 18-24 June 2015, Varna, Bulgaria – oral presentation;
 11. **Danca, P.**, and Vartires, A., - *Thermal comfort assessment using human subjects*, 23rd International Scientific and Technical Conference on Transport, Road-building, Agricultural, Hoisting & Hauling and Military Technisc and Technologies, trans&MOTAUTO 2015, 24-27 June 2015, Varna, Bulgaria – oral presentation;

CHAPTER 7 – CONCLUSIONS AND PERSPECTIVES

Designers in the automotive field started to be focused on comfortable mobility only over the last decades given the lowering of production costs and the increasing safety of vehicles. Their approach was mainly based on methods used in the field of building systems. In the same time, the thermal comfort of vehicular occupants and globally the Indoor Environment Quality achieved more importance mostly due to the fact that the time that people spend in vehicles (private or public transport) has grown substantially. Researchers focused their attention in direction of thermal comfort of car passengers in last decades due to increasing of personal and public number of cars.

Thermal comfort in vehicular spaces acquired more importance due to the growing of the distances between home and workplace [1] with a direct impact on the time that people spend in vehicles [2]. During each trip, thermal comfort must to be ensured for a good psychological and physical state of the passengers. Certainly, comfortable vehicular climate control in many cases not only help to reduce the driver stress but also guarantee good visibility by avoiding the fogging phenomenon, and thus contributing to a safer driving. In addition, today's demand for more efficient vehicular energy exploitation has led to an increased interest in investigating and analyzing the system and the design requirements [3, 4].

An uncomfortable environment may be unhealthy and of course, can affect the physical and psychological condition of the passengers. Comfortable thermal environment can alleviate fatigue and improve the mood of irritability and driving safety. For example, according to the study of Tsutsumi et al. [5], uncomfortable cabin environment affects driver's comfort, performance and fatigue. Danen et al. [6] also found that driving performance was affected by the cold and hot ambient conditions. It can be pointed out that the improved climate within vehicles is critical not only to passenger comfort but also to their safety. Therefore, thermal comfort has become one of the most important criteria for evaluating vehicle performance.

Today's demand for better vehicular energy utilization and more efficient performance, have led to an increased interest in investigating and analyzing the system and design requirements for good indoor and vehicle environments. The need to reduce the heat loads that enter passenger compartments has become an important for the vehicle design, also attaining an enhanced thermal comfort system will lead to substantial cost reductions. The tightening fuel economy constraints and the use of environmentally safe refrigerant [278] as a result to reduce the greenhouse gasses and other pollutants emissions with direct impact on the urban air quality,

are among the major problems in the current geopolitical context. European directives [7] aimed at reducing energy consumption and pollutant emissions up to 2020.

This cost can be reduced only by improving HVAC systems design. Techniques of air flow diffusions are not simultaneously enhanced for these two inseparable goals: thermal comfort and energy savings. This contradiction is due on one hand to non-efficient diffusion of cold air, and on the other hand, to feebleness of the design of these systems. The use of flow models (concepts) and simplified air distribution schemes that are not entirely adapted to real conditions found inside buildings and all other interior spaces are still used by the conceptors. This issue could receive a theoretical response to the adaptation of existing theoretical models for different indoor (building or other enclosures) conditions, in terms of human thermal comfort. Now the researchers may take all the possible advantage of the sophisticated methods and devices that are available both in terms of computing capabilities and experimental techniques. Thermal comfort models are all built with simplified hypothesis, often limited because of available resources when they were conceived – over three decades ago for the most used of them. With the evolution of techniques we have today the opportunity to validate easier these models, we also have the opportunity to correct them and to propose new models. On the other hand, a technical answer may come from the design itself of the air diffusion terminal units which have to be improved and optimized for enhancing mixing between supplied flows and their ambient in order to achieve thermal comfort. Still, this direction of research has to be preceded by the theoretical advances in improving the existing comfort models which seem to be inappropriate in many situations [37, 40, 279, 280].

Thermal comfort is usually defined as the state of a person that would express a feeling of wellbeing regarding the thermal conditions in an occupied space. But, for the same environment, different individuals can give different feedback regarding their thermal sensation. This difficulty is directly related to the presence of the two inseparable human components: the physical and mental condition. Nevertheless, it is the tangible interest of engineering applications that motivated a continuous exploration of quantitative models for estimating, predicting or classifying the state of thermal comfort in occupied spaces. The great majority of these trials are focusing on the physiological component. Most of them are relying on the assumption that the state of thermal comfort might be obtained when the human body can maintain constant body temperature (about 36.7°C) without a big intervention of its thermo-regulatory mechanisms. Its mechanisms are important because when the body produces for any reason, too much heat, it must be evacuated so that the body temperature remains constant. Fanger [11] showed that "the

human thermo-regulatory system is quite efficient and tends primarily to ensure thermal equilibrium without an explicit effort and then adjust their reaction to external stimuli". Also it is universally accepted nowadays that an environment is considered comfortable from the thermal point of view, when 80% to 90% of people from that environment do not express thermally dissatisfaction [1-4].

The prediction or the design of comfortable thermal parameters inside a vehicular space cabin is still a challenge due to the transient behavior of this environment. The understanding of flow patterns is still a complicated for the researchers due to the interior cabin complex geometry and also to the ventilation system complexity (flow rate, location and geometry of all the involved air diffusers) [8]. Additionally, the strong thermal gradients on the surfaces directly affect the air flow patterns through the convective effects. Flows and their effect on thermal sensation are not completely accounted by the car designers and manufacturers or by the users themselves, given that flow trajectory might substantially differ from the direction imposed by the guiding vanes of the air vents. This is related on one hand to these previously mentioned convective effects but might be also an intrinsic characteristic of the air vent itself. The grilles design and fan characteristics are not taken into consideration by the manufacturers when designing the air conditioning system, these being a source of noise [12] with impact on passenger's state of mind.

The currently available standard intended for evaluation of vehicle thermal environment, EN ISO 14505 [13-15], propose buildings evaluation models, which do not meet the demands of for cabin environment evaluation. Unlike the indoor environment from buildings, the vehicular cabin climate is dominated by thermal transient conditions: the strongly non-uniform thermal environment associated with the high localized air speeds with high turbulence and that could be characterized also by low frequency fluctuations when an automatically controlled air conditioning system is presented, the higher levels of relative humidity, the solar radiation intensity, and the radiative heat flux from the interior surfaces, the solar intensity and its scattering over the different material and surfaces in the vehicle, the angles of incidence of the solar radiation etc. [5], [6]. Added to all these parameters arise the physiological differences between the passengers in terms of age, sex, state of health for instance. The psychological component represents in this case even a greater supplementary challenge knowing that drivers' concentration could be associated with different thermal sensations between different subjects or compared to other passengers [7]. In the absence of evaluation models adapted to this environment, the available literature is dispersed around those papers dealing with environmental

conditions inside the vehicle that might affect the human thermal comfort and those concerning the human's response and perception of its interaction with the environment. The available literature is equally divided within experimental and numerical approaches. Due to complexity of this environment and due to unadapted models of evaluation from standards, this process experimental and numerical is divided in three subcategories of studies. The first category is represented by studies that deal with the idea of thermal environment assessment without considering any comfort assessment. The second subcategory include those studies where thermal comfort assessment models proposed by standards are used. The third subcategory covers the articles using or proposing new thermal comfort assessment methods.

Starting with the previous idea of a real need of developing models for the human body for studying IEQ in vehicles and after a survey of the specialized literature we identified several problems: (1) There is a lack of knowledge regarding consequences of using the existing, non-adapted, comfort models for vehicular cabins. (2) Few studies regarding the influence on ventilation strategies on thermal comfort and on the passengers' behavior are available. (3) Studies focused on improving HVAC system strategies of control are rarely connected with thermal comfort studies.

In this context, we decided to orient the subject of the thesis around the complex problematic of cabin thermal environment and its effect on driver's and passenger's thermal state. Thermal comfort has been widely studied in build environments, while thermal comfort in vehicles is a relatively new subject, there have been relatively few studies. In the manuscript are presented numerical and experimental studies of the effects of different passive grills over passengers' thermal comfort. Thus, the general objectives of the doctoral research project could be summarized as following: (1) The first general objective of this thesis was **to deepen the knowledge and to understand thermal phenomena that occur in cabin thermal environment**. (2) The second general objective of this doctoral study was **to develop an advanced thermal manikin able to evaluate cabin thermal comfort** knowing that thermal manikins are the most proper measurement tool in the case of non-uniform and transient environments. (3) The third general objective was **to develop and validate a complex numerical model in order to get insight into the complex phenomena previously evoked**.

These three general objectives were intended to sustain the main goal of the doctoral research that is: **improvement of thermal sensation of vehicle occupants, by implementation of innovative air diffusers**. To this end we oriented our research towards diffusers with a special geometry that allows flow control mechanisms resulting in the improvement of mixing

between air supply by the ventilation system and the ambient air in the cabin.

During the complex quest represented by the doctoral project we could have the opportunity to become familiar to the intricate thermal phenomena governing the thermal comfort in general, to analyze the real role played by transient environment parameters (such as radiant temperature of surfaces, air velocity pulsation, local air turbulence for instance) air flow turbulence in perceiving thermal comfort and in its estimation.

During all this quest we tried to stay on a line that would ultimately allow to respond to a set of fundamental questions, namely: *To what extent this kind of parameters can affect the perceiving of comfort, and also the consequences of an "incomplete" assessment proposed by the existing evaluation models? How is in this context affected the ventilation and air conditioning design due to the use of current models for pre-evaluating a good functioning of the HVAC systems – in particular for vehicles - and an acceptable environment for their users?*

This manuscript is divided in five chapters of results each representing a distinct phase of the current of thesis preparation. In the first part, the thesis is organized around the study of current research, mainly aiming two directions: methods, models and indicators for prediction of vehicular thermal comfort and numerical simulation techniques for turbulent flows. Thus Chapter 1, offers an overview of the main concepts and results of numerous studies from literature for numerical and experimental research in the field of thermal comfort. This chapter is the summary of our initial search of landmarks in the literature that allowed us to get directions to a study and to choose a specific numerical and experimental validation, based on existing results and the available means. This chapter is a bibliographical one, proposing an extensive and exhaustive introduction in the thermal comfort research field with focus on cabin thermal environment, a synthesis of theoretical aspects concerning thermal comfort, vehicle environments and related environmental factors, that have a major effect on the vehicular space mainly aiming two directions: methods, models and indicators for the prediction of indoor thermal comfort and numerical simulation techniques for the turbulent flows used for the study of air flow in the cabin environment. It represents the summary of our initial extensive search of milestones in the existing literature. It allowed us to set the main directions for our research and to define specific numerical and experimental validation based on the existing data and on the available methods.

Modeling the comfort response itself is the ultimate goal in using heat balance models. Indeed, all of the rational models make the inherent assumption that there is some predictable comfort response for a given physiological state of the body. Still, it is not clear if there is such a

relationship and how it could be expressed in a universal, applicable way. The state of comfort is inherently a psychological response, not a physiological response and we should expect many nonphysical factors to affect comfort perceptions (e.g. expectations). We have to note that *there is absolutely no consensus amongst the models as how comfort should be related to the physiological variables or even which are the variables that have to be considered as important parameters.*

Even if the adaptive thermal comfort concept has been discussed only for buildings, in our opinion a viable direction for taking into account the psychological component in the case of the thermal state evaluation in vehicles and would be to orient some studies towards this direction. The head load is strictly depending on the climate conditions. The second context is the cabin itself, especially the features and the level of ergonomics that it offers to its occupants. The third context is the time, the human activity taking place in the time unit and comfort temperature being variable in time.

Even if in this study we didn't have the time to extend our researches to the adaptive approach, our belief is that a future perspective of study in the field of thermal comfort studies dedicated to vehicles is to combine the quest for a new comfort equation adapted to these enclosures, taking into account the rapid climate changes and physical and psychological adaptation of the human occupants. This is crucial in our opinion given that all presented evaluation methods based on environmental physical parameter measurement cannot capture the inherent mental capabilities of humans.

Nevertheless, *the importance of the thermal manikins and of the concept of equivalent temperature cannot be denied.* However, the presented standardized methods are either difficult to interpret, either impossible to apply, either use expensive approaches. There are few articles using standardized methods for evaluating thermal comfort in the literature and even less the ones that are combining air distribution strategies with thermal comfort.

On the other hand, there are many papers dealing with the observation of the environmental conditions inside the vehicle that might affect the human thermal comfort and those concerning the human's response and perception of its interaction with the environment. Part of them stops only on the study of the effect of a certain parameter (the air temperature and the mean radiant, the relative humidity, the solar radiation including the effect of the glass transmittance, the outdoor temperature, etc.) on the thermal environment of the vehicle without considering any thermal comfort assessment using comfort models. Different methods are used to measure these different equivalent temperatures, besides the use of individual sensors dedicated to all the intervenient variables, e. g. thermal comfort meters with heated sensor, local discomfort meters, plane surface sensors and thermal mannequins. These last are considered as the reference method

with which other methods are compared. Significant differences were found in the values of equivalent temperatures arising from different methods in tests performed in uniform environments inside a climatic chamber, which are attributed to different characteristics of the measuring devices, such as size, geometry, posture, number and type of sensors, control method, etc. The scientific research reality, shows nowadays, only rare solitary set-ups to assess the thermal comfort in vehicles using the equivalent temperatures experimentally. These are either very expensive or suitable for punctual measurements only. However, data acquisition at different locations in the interior space of a vehicle is highly desired, generating the need for cost-effective and accurate systems that are supposed to provide access to the local equivalent temperatures and further, especially if strong thermal gradients are present if the real ventilation systems are considered, to simulate the heat impact of real passengers as well. *This is the motivation of developing thermal manikins in our research group and thus one of the most important objectives of the thesis was consisted by the development of the thermal manikin that is presented in Chapter 2.*

No studies combining passive induction control via the conception of air diffusers were found in the literature. The proposal of some innovative designs of air vents for the present studies was based on the previous findings of the French and Romanian research teams were the doctoral project was developed. The following parts of the manuscript are dealing with the development of an innovative thermal manikin and of new concepts of air diffusers. The approach is based on both experimental and numerical approach.

The second chapter is dedicated to the design and development of an advanced thermal manikin with 79 independent zones and neuro-fuzzy control. The concept and the development are presented step by step as well as the preliminary tests of this prototype. I was directly involved in designing and manufacturing of this particular thermal manikin that was conceived and developed with the help of the Systems and Mechatronics department from the National Institute of Research Aerospace Elie Carafoli (INCAS) from Bucharest.

Apart the thermal manikin in the experimental part of the study was used different measurement equipment. This way, the third chapter is dedicated in a first part to the measuring principles of all used measuring instruments and in a second part to the three main experimental set-ups used during the entire study. All the experimental tests were made with the car was kept inside a hall. The main reason for this choice was related to our desire to maintain constant values of external factors, to decouple the in-cabin conditions from the solar radiation effect and to protect measurement equipment from the outdoor meteorological conditions. As a result,

indoor thermal conditions varied much slower than outside. The objective of the experimental campaign was multiple:

- to record in different conditions, like previously, the evolutions of the temperatures on the surfaces inside the cabin and in different points in the air;
- to test the effect on different flow rates and cold air temperatures on the air distribution inside the cabin;
- to « measure » thermal comfort indices using the Comfort Sense system and the thermal manikin previously developed for different flow rates and two geometries of air diffusers in cooling conditions, and thus to provide data for validation purposes of the numerical models developed in Chapter 4;
- to perform subjective thermal comfort evaluations for the same flow rates and the two geometries of air diffusers in cooling conditions allowing a direct comparison between the subjective response and the dedicated measurement systems;
- to provide data recording air speed values and temperatures in different points inside the car cabin for validation purposes of the numerical models developed in Chapter 4.

In the introduction of the fourth chapter we propose to pass briefly through the current developments related to Computational Fluid Dynamics applied to air distribution and thermal comfort. In the bibliographical chapter we put in evidence all numerical studies that we found in literature relevant for our subject. Still, the great majority of these studies lacks details and explanations of modeling choices, this way we decided to rely on the knowledge gained in the much more studied field of air distribution and thermal comfort in buildings. In the following parts of the chapter we present the steps employed in our numerical approach. In a first time a simple car-cabin numerical model was designed and in our quest of methods of calibration of the correct boundary conditions, we used temperature and air flow measurements in a real car-cabin. In a second time, a complex numerical model has been developed. This model includes a passenger with anatomic shape and takes into consideration to types of air diffusers: one which is the reference – the classic air grilles that were originally designed in the cabin and one innovative set of air diffusers that we wanted to test. The validation of the chosen approach for introducing the effect of the flows generated by the two types of diffusers is also presented in this chapter.

With the previously elaborated complex numerical models we can proceed in the fifth chapter to our final quest: finding which is the influence of the inlet conditions determined by the two types of air diffusers. This way, we wanted to check first what is happening with the global

distribution of the flow inside the cabin in non-isothermal conditions. Next, we wanted to gain a deeper perspective in the thermal comfort aspects. To this end we compared thermal indexes from the numerical data with the measured values of the parameters characterizing the thermal environment from the car such as described in the experimental set-up from Chapter 3.

We finish the last chapter dedicated to our study with a comparison between the numerical study and the experimental results obtained in the real car cabin from measurements and from the subjective studies.

Given the originality of this research study, a first stage of analysis that opens interesting study perspectives for the continuation of several research directions. First of all, with regard to the experimental part, a short-term perspective is to continue the experimental studies in winter conditions using both the developed thermal manikin and human subjects. Also, other geometries of diffusers that we already adapted to the real studied car, will be tested in the near future.



Figure 200: Other geometries of diffusers to be explored....

From a numerical point of view, first of all we would like to implement a LES model to capture the temporal and spatial dynamics of convective natural current and the influence of scale and frequency of vortices present in airflows. We also want to connect the RANS with a nodal model for body thermoregulation and adaptive comfort simulations. We would like to modify the geometrical models in order to resolve the flows through the grilles. A long-term perspective is given by the coupling of these researches with numerical and experimental studies related to the quality of indoor air and especially to the particular dispersion inside the vehicle.

REFERENCES

1. Bertolini, J.C.L., *Measuring urban job accessibility with distance decay, competition and diversity*. Journal of Transport geography, 2013. **30**(1): p. 100-109.
2. Cristiana CROITORU, et al., *Thermal comfort models for indoor spaces and vehicles - current capabilities and future perspectives*. Renewable & Sustainable Energy Reviews, accepted for publication, 2015.
3. Chen, A. and V.W.C. Chang, *Human health and thermal comfort of office workers in Singapore*. Building and Environment, 2012. **58**(Supplement C): p. 172-178.
4. Ormandy, D. and V. Ezzratty, *Health and thermal comfort: From WHO guidance to housing strategies*. Energy Policy, 2012. **49**(0301-4215): p. 116-121.
5. Tsutsumi, H., et al., *Effect of Car Cabin Environment on Driver's Comfort and Fatigue*. 2007, SAE International.
6. Daanen, H.A.M., E. van de Vliert, and X. Huang, *Driving performance in cold, warm, and thermoneutral environments*. Applied Ergonomics, 2003. **34**(6): p. 597-602.
7. Fang L., C.G.a.F.P.O., *Impact of temperature and humidity on the perception of indoor air quality*. Ind. Air, 1998. **8**: p. 80–90.
8. Rugh, J. and V. Hovland. *National and world fuel savings and CO2 emission reductions by increasing vehicle air conditioning COP*. in *Proceedings from the 2003 Alternate Refrigerant Systems Symposium in Phoenix*. 2003.
9. Nastase, I., *Analyse des jets lobés en vue de leur intégration dans les Unités Terminales de Diffusion d'air*. 2007, Université de La Rochelle: Ph.D. Thesis.
10. Nastase, I., et al., *Lobed grilles for high mixing ventilation - An experimental analysis in a full scale model room*. Building and Environment, 2011. **46**(3): p. 547-555.
11. Fanger, P.O., ed. *Thermal Comfort-Analysis and Applications in Environmental Engineering*. ed. C.D.T. Press. 1970.
12. Lee, M.-J.P.D.-J., *Sources of broadband noise of an automotive cooling fan*. Applied Acoustics, 2017. **118**(2017): p. 66-75.
13. ISO, *Ergonomics of the thermal environment -Evaluation of thermal environments in vehicles Part 3: Evaluation of thermal comfort using human subjects*, in *ISO 14505-3:2006*. 2006.
14. ISO, *Ergonomics of the thermal environment - Evaluation of thermal environments in vehicles - Part 2: Determination of equivalent temperature in ISO 14505-2:2006*. 2006.
15. ISO, *Ergonomics of the thermal environment - Evaluation of thermal environments in vehicles Part 1: Principles and methods for assessment of thermal stress*, in *ISO 14505-1:2007*. 2007.
16. Hensel, H., *Thermoreception and Temperature Regulation*
ed. L. Academic Press. 1981.
17. Nakamura, M., et al., *Regional differences in temperature sensation and thermal comfort in humans*. Journal of Applied Physiology, 2008. **105**(6): p. 1897-1906.
18. Slater, K., *Human Comfort*. Vol. 1. 1985.
19. ISO, E., *ISO 7730 - Ergonomics of the thermal environment—Analytical determination and interpretation of thermal comfort using calculation of the PMV and PPD indices and local thermal comfort criteria*. 2005.
20. Humphreys, M.A. and J.F. Nicol, *Understanding the adaptive approach to thermal comfort*. ASHRAE Transactions, 1998. **104**.
21. De Dear, R.J. and G.S. Brager, *Developing an adaptive model of thermal comfort and preference*. ASHRAE Transactions, 1998. **104**(1A): p. 145-167.
22. Gagge, A.P., J.A.J. Stolwijk, and Y. Nishi, *An effective temperature scale based on a simple model of human physiological regulatory response*. ASHRAE Transactions, 1970. **77**(1): p. 247-262.
23. Haldane, J.S., *The Influence of High Air Temperatures*. The Journal of Hygiene, 1905. **5**: p. 494-513.

24. F.C. Houghten, C.P.Y., *Determining lines of equal comfort*. ASHVE. Transactions, 1923. **29**: p. 163-175.
25. Gagge, A.P., A.P. Fobelets, and L.G. Berglund, *A standard predictive index of human response to the thermal environment*. ASHRAE Transactions, 1986. **92**(2B): p. pp. 709-731.
26. ASHRAE, "*Thermal environmental conditions for human occupancy*," ANSI/ASHRAE Standard 55-2013, American Society of Heating, Refrigerating and Air-Conditioning Engineers, Atlanta, GA. 2013.
27. Havenith, G. and D. Fiala, *Thermal Indices and Thermophysiological Modeling for Heat Stress* Comprehensive physiology, 2015. **6**(1): p. 255-302.
28. ISO, *Moderate thermal environments -- Determination of the PMV and PPD indices and specification of the conditions for thermal comfort*, in ISO 7730:1984. 1984.
29. Paulke, S., et al., *Thermal simulation of a complete vehicle including manikins*, in SIMVEC – Simulation und Erprobung in der Fahrzeugentwicklung November 18th -19th, 2014, Baden-Baden, Germany. 2014.
30. Psikuta, A., et al., *Thermal manikins controlled by human thermoregulation models for energy efficiency and thermal comfort research – A review*. Renewable and Sustainable Energy Reviews, 2017. **78**: p. 1315-1330.
31. Melikov, A., *Breathing thermal manikins for indoor environment assessment: important characteristics and requirements*. European Journal of Applied Physiology, 2004. **92**(6): p. 710-713.
32. Grundstein, A., V. Meentemeyer, and J. Dowd, *Maximum vehicle cabin temperatures under different meteorological conditions*. Int J Biometeorol 2009. **53**: p. 255–261.
33. Shin, Y., et al., *Experimental study on the change in driver's physiological signals in automobile HVAC system under Full load condition*. Applied Thermal Engineering, 2017. **112**: p. 1213-1222.
34. *International Encyclopedia of Ergonomics and Human Factors, Vol I*, ed. W. Karwowski. 2001: Taylor & Francis.
35. Feher, S., *Thermoelectric Air Conditioned Variable Temperature Seat (VTS) and Effect Upon Vehicle Occupant Comfort, Vehicle Energy Efficiency, and Vehicle Environmental Compatibility*. 1993, SAE International.
36. Walgama, C., et al., *Passenger Thermal Comfort in Vehicles - A Review*. Proceedings of the Institution of Mechanical Engineers, Part D: Journal of Automobile Engineering, 2006. **220**(5): p. 543-562.
37. Alahmer, A., et al., *Vehicular thermal comfort models; a comprehensive review*. Applied Thermal Engineering, 2011. **31**(6–7): p. 995-1002.
38. Hensen, J.L.M., *Literature review on thermal comfort in transient conditions*. Building and Environment, 1990. **25**(4): p. 309-316.
39. Djongyang, N., R. Tchinda, and D. Njomo, *Thermal comfort : A review paper*. Renewable and Sustainable Energy REviews, 2010. **14**: p. 2626-2640.
40. Cheng, Y., J. Niu, and N. Gao, *Thermal comfort models: A review and numerical investigation*. Building and Environment, 2012. **47**(Supplement C): p. 13-22.
41. Croitoru, C., et al., *Thermal comfort models for indoor spaces and vehicles—Current capabilities and future perspectives*. Renewable and Sustainable Energy Reviews, 2015. **44**(Supplement C): p. 304-318.
42. Walgama, C., et al., Proc. IMechE Part D: Automobile Engineering, 2006. **220**.
43. Fanger, P.O.a.P., C.J.K. . *Discomfort due to air velocities in spaces*. in *Proceedings of the Meeting of Commissions B1, B2, E1 and the IIR, 4, Belgrade*. 1977.
44. Fanger, P.O. and N.K. Christensen, *Perception of draught in ventilated spaces*. Ergonomics, 1986. **29**(2): p. 215 - 235.
45. Van Hoof, J., *Forty years of Fanger's model of thermal comfort: comfort for all?* Indoor Air, 2008. **18**(3): p. 182-201.

46. ISO 7730 - *Ergonomics of the thermal environment —Analytical determination and interpretation of thermal comfort using calculation of the PMV and PPD indices and local thermal comfort criteria*. 2005.
47. ASHRAE, “*Thermal environmental conditions for human occupancy,*” ANSI/ASHRAE Standard 55-2004, American Society of Heating, Refrigerating and Air-Conditioning Engineers, Atlanta, GA. 2004.
48. Koestel, A. and G.L. Tuve, *Performance and evaluation of room air distribution systems*. ASHRAE Transactions, 1955. **61**: p. 533.
49. Organisation, I.S., *ISO 7243 Hot environments – estimation of the heat stress on working man, based on the WBGT-index (wet bulb globe temperature)*. 1989: Geneva.
50. Rydberg, J. and P. Norback, *Air distribution and draft*. ASHVE Transactions, 1949. **55** p. 225.
51. Straub, H.E. and M.M. Chen, *Distribution of air within a room for year-round air conditioning- Part II*. . University of Illinois Engineering Experiment Station Bulletin, 1957: p. 442.
52. Madsen, T.L., *Thermal comfort measurements*. ASHRAE Trans., 1976. **82**(1).
53. Fiala, D., *Ph.D dissertation: Dynamic simulation of human heat transfer and thermal comfort*. 1998, De Montfort University: England.
54. Fiala, D., K.J. Lomas, and M. Stohrer, *A computer model of human thermoregulation for a wide range of environmental conditions: The passive system*. Journal of Applied Physiology, 1999. **87**(5): p. 1957-1972.
55. Fiala, D., K.J. Lomas, and M. Stohrer, *Computer prediction of human thermoregulatory and temperature responses to a wide range of environmental conditions*. International Journal of Biometeorology, 2001. **45**(3): p. 143-159.
56. Fiala, D., et al., *UTCI-Fiala multi-node model of human heat transfer and temperature regulation*. International Journal of Biometeorology, 2012. **56**(3): p. 429-441.
57. Nagano, K. and T. Horikoshi, *New index indicating the universal and separate effects on human comfort under outdoor and non-uniform thermal conditions*. Energy and Buildings, 2011. **43**(7): p. 1694-1701.
58. Jendritzky, G., R. de Dear, and G. Havenith, *UTCI-Why another thermal index?* International Journal of Biometeorology, 2012. **56**(3): p. 421-428.
59. Standards, I.O.f., *Ergonomics of the thermal environment -- Analytical determination and interpretation of heat stress using calculation of the predicted heat strain*, in ISO 7933:2004. 2004.
60. Standards, I.O.f., *Ergonomics of the thermal environment -- Methods for the assessment of human responses to contact with surfaces -- Part 3: Cold surfaces*, in ISO 13732-3:2005. 2005. p. 21.
61. Standards, I.O.f., *Ergonomics of the thermal environment -- Determination and interpretation of cold stress when using required clothing insulation (IREQ) and local cooling effects*, in ISO 11079:2007. 2007. p. 34.
62. Budd, G.M., *Wet-bulb globe temperature (WBGT)-its history and its limitations*. J Sci Med Sport., 2008. **11**(1): p. 20-32.
63. d'Ambrosio Alfano, F.R., et al., *Ann Occup Hyg*, 2014 **58**(8): p. 955-970.
64. ISO, *Ergonomics of the thermal environment -Evaluation of thermal environments in vehicles Part 2: Determination of Equivalent Temperature*, in ISO 14505-3:2006. 2006.
65. Holmer, I., *Evaluation of vehicle climate in Environmental Ergonomics*, Y.T.a.T. Ohnaka, Editor. 2005, Elsevier Ltd.
66. Nilsson, H., *Comfort Climate Evaluation with Thermal Manikin Methods and Computer Simulation Models*, in Department of Civil and Architectural Engineering Royal Institute of Technology, Sweden; Department of Technology and Built Environment University of Gävle, Sweden. 2004.

67. Nilsson, H., et al. *Equivalent temperature and thermal sensation - Comparison with subjective responses*. in *Comfort in the automotive industry- Recent development and achievements*. 1997. Bologna, Italy.
68. Nilsson, H., et al. *Thermal climate assessment in office environment - CFD calculations and thermal manikin measurements*. in *ROOMVENT*. 2000. Reading, UK.
69. Nilsson, H.O., *Thermal comfort evaluation with virtual manikin methods*. *Building and Environment*, 2007. **42**(12): p. 4000-4005.
70. Nilsson, H.O. and I. Holmér, *Definitions and Measurements of Equivalent Temperature, European commission cost contract no smt4-ct95-2017 Development of standard test methods for evaluation of thermal climate in vehicles*. 2002.
71. ISO, *Ergonomics of the thermal environment - Assessment of the influence of the thermal environment using subjective judgement scales, ISO 10551*. 1995.
72. Givoni B., G.R.F., *Predicting rectal temperature response to work, environment, and clothing*. *J. Appl. Physiol*, 1972. **32**: p. 812-821.
73. Huizenga, C., Z. Hui, and E. Arens, *A model of human physiology and comfort for assessing complex thermal environments*. *Building and Environment* 2001. **36**: p. 691-699.
74. Gao, N.P., H. Zhang, and J.L. Niu, *Investigating indoor air quality and thermal comfort using a numerical thermal manikin*. *Indoor and Built Environment*, 2007
75. Schminder, J., et al. *Development of a Cockpit-Pilot Model for Thermal Comfort Optimization During Long-Mission Flight*. in *AIAA Modeling and Simulation Technologies Conference*. 2016.
76. Azer, N.Z., Hsu, S., *The prediction of Thermal Sensation from Simple model of Human Physiological Regulatory Response*. *ASHRAE Trans.*, 1977. **83**(1).
77. Stolwijk, J.A.J., *A mathematical model of physiological temperature regulation in man*. NASA CR-1855, Washington DC, 1971.
78. Tanabe, S., et al., *Evaluation of thermal comfort using combined multi-node thermoregulation (65MN) and radiation models and computational fluid dynamics (CFD)*. *Energy and Buildings*, 2002. **34**: p. 637-646.
79. Alahmer, A., M. Abdelhamid, and M. Omar, *Design for thermal sensation and comfort states in vehicles cabins*. *Applied Thermal Engineering*, 2012. **36**(0): p. 126-140.
80. Yi, L., et al., *An integrated model for simulating interactive thermal processes in human–clothing system*. *Journal of Thermal Biology*, 2004. **29**(7–8): p. 567-575.
81. Gao, N.P. and J.L. Niu, *Indoor and Built Environment*. CFD study of thermal environment around a human body: A review, 2005. **14**: p. 5-16.
82. Huizenga, C., Z. Hui, and E. Arens, *A model of human physiology and comfort for assessing complex thermal environments*. *Building and Environment*, 2001. **36**: p. 691-699.
83. Gwak, J., M. Shino, and M. Kamata, *Interaction between Thermal Comfort and Arousal Level of Drivers in Relation to the Changes in Indoor Temperature*. *International Journal of Automotive Engineering*, 2018. **9**(2): p. 86-91.
84. Lv, B., et al., *Effects of stimulus mode and ambient temperature on cerebral responses to local thermal stimulation: An EEG study*. *International Journal of Psychophysiology*, 2017. **113**: p. 17-22.
85. Farrell, M.J., et al., *Brain activation associated with ratings of the hedonic component of thermal sensation during whole-body warming and cooling*. *Journal of Thermal Biology*, 2011. **36**(1): p. 57-63.
86. Yao, Y., et al., *Experimental study on physiological responses and thermal comfort under various ambient temperatures*. *Physiology & Behavior*, 2008. **93**(1): p. 310-321.
87. Bulcao, C.F., et al., *Relative contribution of core and skin temperatures to thermal comfort in humans*. *Journal of Thermal Biology*, 2000. **25**(1): p. 147-150.
88. Dowman, R., D. Rissacher, and S. Schuckers, *EEG indices of tonic pain-related activity in the somatosensory cortices*. *Clinical Neurophysiology*, 2008. **119**(5): p. 1201-1212.

89. Chang, P.F., L. Arendt-Nielsen, and A.C.N. Chen, *Comparative cerebral responses to non-painful warm vs. cold stimuli in man: EEG power spectra and coherence*. International Journal of Psychophysiology, 2005. **55**(1): p. 73-83.
90. Burch, S., V. Hassani, and T. Penney. *Use of infra-red thermography for automotive climate control analysis*. in *Proceedings of the SAE World Congress, SAE (1993) - 921136*.
91. Korukçu, M.Ö. and M. Kilic, *The usage of IR thermography for the temperature measurements inside an automobile cabin*. International Communications in Heat and Mass Transfer, 2009. **36**(8): p. 872-877.
92. Kang, J.H. and S.J. Lee, *Investigation on the flow characteristics inside an automotive HVAC system with varying ventilation mode*. Journal of Visualization, 2009. **12**(4): p. 375-382.
93. Chien, C.-H., et al., *3-D numerical and experimental analysis for airflow within a passenger compartment*. International Journal of Automotive Technology, 2008. **9**(4): p. 437-445.
94. Ležovič, T., et al., *HVAC automotive vents evaluation and their performance*. HVAC&R Research, 2013. **19**(8): p. 1073-1082.
95. Fojtlín, M., et al., *Airflow Measurement of the Car HVAC Unit Using Hot-wire Anemometry*. EPJ Web of Conferences, 2016. **114**: p. 02023.
96. Jonsson, J., *Including Solar Load in CFD Analysis of Temperature Distribution in a Car Passenger Compartment*. 2007, Lulea University of Technology: Sweden.
97. Alahmer, A., et al., *Effect of relative humidity and temperature control on in-cabin thermal comfort state: Thermodynamic and psychometric analyses*. Applied Thermal Engineering, 2011. **31**(14-15): p. 2636-2644.
98. Alahmer, A., et al., *Analysis of vehicular cabins' thermal sensation and comfort state, under relative humidity and temperature control, using Berkeley and Fanger models*. Building and Environment, 2012. **48**(0): p. 146-163.
99. Fountain, M.E., *Laboratory studies of the effect of air movement on thermal comfort: A comparison and discussion of methods*. ASHRAE Transactions, 1991. **97**(1): p. 863-873.
100. Alahmer, A., et al., *Effect of relative humidity and temperature control on in-cabin thermal comfort state: Thermodynamic and psychometric analyses*. Applied Thermal Engineering, 2011. **31**(14-15): p. 2636-2644.
101. Holmer, L., et al. *Equivalent temperature in vehicles-conclusions and recommendations for standard*. in *6th ATA International Conference, Florence, Italy, EQUIV. Seminar II*. 1999.
102. Bohm, M., et al. *Comparison of methods to determine the equivalent temperature in a cab in a climatic chamber*. in *6th ATA International Conference, Florence, Italy, 17-19 November*. 1999.
103. Martinho, N.A.G., M.C.G. Silva, and J.A.E. Ramos. *Evaluation of thermal comfort in a vehicle cabin* in *Proceedings of the Institution of Mechanical Engineers: Journal of Automobile Engineering, Part D; London Vol. 218, Iss. 2, 159-166*. 2004.
104. Pascal Lange, A.W., Daniel Schmeling, Johannes Bosbach. *Cost-effective human comfort manikin with realistic thermal load for convection-driven ventilation systems*. in *Roomvent 2018*. 2018. Espoo, Finland.
105. Chun, H.J.L.Y.R.C.C.Y., *Effect of indoor air temperature on the occupants' attention ability based on the electroencephalogram analysis*. J. Archi. Inst. Korea Plan. Des., 2012. **28**(3): p. 217-225.
106. Kim, J.S.K.D.G.K.H.C., *A study of physiology signal change by air conditioner temperature change*. J. Fish. Mar. Sci. Edu., 2007. **19**(3): p. 502-509.
107. Kim, D. and K. Kang. *Design and Implementation of Integrated Information System for Monitoring Resources in Grid Computing*. in *2006 10th International Conference on Computer Supported Cooperative Work in Design*. 2006.
108. Kim, D.J.K.H.H., *Comfortableness evaluation method using EEGs of the frontopolar and the parietal lobes*. Trans. KIEE, 2004. **53D**(5): p. 374-379.

109. Kang, K.N. and S.D. Song, *Study on the evaluation of amenity and physical characteristic of air-conditioning systems applying fluctuation characteristic on natural wind*. J. Archit. Inst. Korea Plan. Des., 2013. **29**(12): p. 267-275.
110. Lan, L., et al., *Experimental study on thermal comfort of sleeping people at different air temperatures*. Building and Environment, 2014. **73**: p. 24-31.
111. Liu, Y., et al., *A study of human skin and surface temperatures in stable and unstable thermal environments*. Journal of Thermal Biology, 2013. **38**(7): p. 440-448.
112. Nguyen, A.T., M.K. Singh, and S. Reiter, *An adaptive thermal comfort model for hot humid South-East Asia*. Building and Environment, 2012. **56**: p. 291-300.
113. Yao, Y., et al., *Experimental study on physiological responses and thermal comfort under various ambient temperatures*. Physiology and Behavior, 2008. **93**(1-2): p. 310-321.
114. Seo, J.W., J.H. Park, and Y.H. Choi, *Evaluation of thermal comfort and cooldown performance inside automotive cabin according to air-conditioning vent location*. KSAE, 2012. **20**(5): p. 120-129.
115. Kobayashi, Y.T.K., et al. *Thermal comfort in car cabin with cooling individual body parts*, in: *10th International Conference on Healthy Buildings*, vol. 2 of 3. 2012.
116. Murakami, S., S. Kato, and J. Zeng, *CFD analysis of thermal environment around human body*. 1996. **2**: p. 479-484.
117. Dunnett, S.J., *A numerical study of the factors affecting worker exposure to contaminant*. Aerosol Science and Technology, 1994. **25**(1): p. 481-482.
118. Niwa, K., et al. *Numerical analysis of flow and temperature field with local air conditioning by supply jets from the seats in hall*. in *ROOMVENT*. 1996.
119. Heinsohn, R.J., *Industrial ventilation: engineering principle*. 1991, New-York: John Wiley & Sons.
120. Tjelflaat, P.O. and R. Knott. *A simulation model for thermal comfort of a person in a large enclosure*. in *INDOOR AIR*. 1996.
121. Iwamoto, S. *A study on numerical prediction methods of thermal environment around occupants*. in *Indoor Air*. 1996.
122. Bluysen, P.M. and T. Lemaire. *The distribution of perceived air quality in an office space-computer simulations and sensory evaluations*. in *ROOMVENT*. 1992.
123. Gan, G., *Numerical method for full assessment of indoor thermal comfort*. Indoor Air, 1994. **4**: p. 154-168.
124. Brohus, H. and P.V. Nielsen. *Personal exposure to contaminant sources in uniform velocity field in Healthy Buildings*. 1995.
125. Brohus, H. and P.V. Nielsen. *CFD models of persons evaluated by full-scale wind channel experiments*. in *ROOMVENT*. 1996.
126. Kiliç, M. and G. Sevilgen, *The effects of using different type of inlet vents on the thermal characteristics of the automobile cabin and the human body during cooling period*. The International Journal of Advanced Manufacturing Technology, 2012. **60**(5): p. 799-809.
127. Limaye, V.M., et al., *Design of Dynamic Airvents and Airflow Analysis in a Passenger Car Cabin*. SASTECH, 2012. **11**(1): p. 41-48.
128. Konstantinov, M. and C. Wagner, *Numerical Simulation of the Thermal Comfort in a Model of a Passenger Car Cabin*, in *New Results in Numerical and Experimental Fluid Mechanics X: Contributions to the 19th STAB/DGLR Symposium Munich, Germany, 2014*, A. Dillmann, et al., Editors. 2016, Springer International Publishing: Cham. p. 383-393.
129. Ahirrao, A.K., et al., *Effect of Vent Shape on Thermal Comfort of Passengers in a Car*. SASTECH 2011. **10**(2): p. 21-28.
130. Hodder, S.G. and K. Parsons, *The effects of solar radiation on thermal comfort*. International Journal of Biometeorology, 2007. **51**(3): p. 233-250.
131. Mezrhab, A. and M. Bouzidi, *Computation of thermal comfort inside a passenger car compartment*. Applied Thermal Engineering, 2006. **26**(14-15): p. 1697-1704.

132. SEVILGEN, G. and M. KILIC, *Investigation of transient cooling of an automobile cabin with a virtual manikin under solar radiation*. Thermal Science, 2013. **17**: p. 397-406.
133. Zhang, H., et al., *Studies of air-flow and temperature fields inside a passenger compartment for improving thermal comfort and saving energy. Part II: Simulation results and discussion*. Applied Thermal Engineering, 2009. **29**(10): p. 2028-2036.
134. Zhang, H., et al., *Studies of air-flow and temperature fields inside a passenger compartment for improving thermal comfort and saving energy. Part I: Test/numerical model and validation*. Applied Thermal Engineering, 2009. **29**(10): p. 2022-2027.
135. Srisilpsophon, T., J. Tiansuwan, and T. Kiatsiriroat, *Effect of anti-solar glass film on heat transfer and mean radiant temperature inside cabin of air-conditioned vehicle*. International Journal of Ambient Energy, 2007. **28**(1): p. 39-50.
136. Stoecker, W.F. and J.W. Jones, *Refrigeration & Air Conditioning*. 1987: McGraw-Hill Science/Engineering/Math.
137. Moon, J.H., et al., *Thermal comfort analysis in a passenger compartment considering the solar radiation effect*. International Journal of Thermal Sciences, 2016. **107**: p. 77-88.
138. Bode, F., et al. *The influence of the Inlet angle of vehicle air diffuser on the thermal comfort of passengers*. in *2017 International Conference on ENERGY and ENVIRONMENT (CIEM)*. 2017.
139. Han, T., et al., *Virtual thermal comfort engineering*. 2001.
140. J., T., et al., *Coupling of Human Thermoregulation and URANS Computation for Investigation of Local Heat Transfer and Flow Structures in a Generic Car Cabin*. Flow, Turbulence and Combustion, 2016. **97**(4): p. 1281-1296.
141. Zhang, H., et al., *Thermal sensation and comfort models for non-uniform and transient environments, part II: Local comfort of individual body parts*. Building and Environment, 2010. **45**(2): p. 389-398.
142. Zhang, H., et al., *Thermal sensation and comfort models for non-uniform and transient environments: Part I: Local sensation of individual body parts*. Building and Environment, 2010. **45**(2): p. 380-388.
143. American Society of Heating, R. and A.-C. Engineers, *2001 ASHRAE Handbook: Fundamentals*. 2001: ASHRAE.
144. Kader, M.F., M.A. Jinnah, and K.-B. Lee, *The effect of solar radiation on automobile environment through natural convection and mixed convection*. Journal of Engineering Science and Technology, 2012. **7**: p. 589 - 600.
145. Nilsson, H.O., *Comfort Climate Evaluation with Thermal Manikin Methods and Computer Simulation Models*. National Institut for Working Life, 2004.
146. Oh, M.S., et al., *Thermal comfort and energy saving in a vehicle compartment using a localized air-conditioning system*. Applied Energy, 2014. **133**: p. 14-21.
147. Neacsu, C.A. and M. Ivanescu, *The Development of a New Thermal Comfort Indexes*, in *Proceedings of the European Automotive Congress EAEC-ESFA 2015*, C. Andreescu and A. Clenci, Editors. 2016, Springer International Publishing: Cham. p. 703-714.
148. Nastase, I. and A. Meslem, *Vortex dynamics and entrainment mechanisms in lobed jets*. Bulletin of the American Physical Society, 2007. **52** (12).
149. Nastase, I. and A. Meslem, *Passive control of jet flows using lobed nozzle geometries*. Mécanique & Industries, 2007. **8**(2): p. 101-109.
150. Nastase, I. and A. Meslem. *Lobed jets for improving air diffusion performance in buildings*. in *The 29th AIVC Conference*. 2008. Kyoto, Japon.
151. Nastase, I. and A. Meslem, *Vortex dynamics and entrainment mechanisms in low Reynolds orifice jets*. Journal of Visualization, 2008. **11**(4).
152. Nastase, I. and A. Meslem, *Vortex Dynamics and mass entrainment in turbulent lobed jets with and without lobe deflection angles*. Experiments in Fluids, 2010. **48**(4): p. 693-714.

153. Nastase, I., A. Meslem, and T. Bowmans, *Vortical structures analysis in jet flows using a classical 2D-PIV system and time resolved visualization image processing*. Journal of Flow Visualization and Image Processing, 2008. **15**(4): p. 275-300.
154. Nastase, I., A. Meslem, and I. Colda. *Innovative passive mixing devices for better air diffusion performance in buildings*. in *43-th National Conference, Building services for the beginning of the third millennia*. 2008. Sinaia, Roumanie.
155. Meslem, A. and I. Nastase. *Analysis of free or twin-jets for innovative air diffusion terminal units*. in *Roomvent 2009*. 2009. Busan, South Korea.
156. Meslem, A., I. Nastase, and K. Abed-Meraim, *Experimental investigation of a lobed jet flow mixing performance*. Journal of Engineering Physics and Thermophysics, 2007. **81**(1).
157. Meslem, A., I. Nastase, and F. Allard, *Passive mixing control for innovative air diffusion terminal devices for buildings*. Building and Environment, 2010. **45** (2679-2688).
158. Nastase, I., A. Meslem, and P. Gervais, *Primary and secondary vortical structures contribution in the entrainment of low Reynolds number jet flows*. Experiments in Fluids, 2008. **44**(6): p. 1027-1033.
159. Nastase, I. and A. Meslem, *Vortex Dynamics and Entrainment Mechanisms in Low Reynolds Orifice Jets*. Journal of Visualisation, 2008. **11**(4): p. 309-318.
160. Nastase, I. and A. Meslem, *Vortex dynamics and mass entrainment in turbulent lobed jets with and without lobe deflection angles*. Experiments in Fluids, 2010. **48**(4): p. 693-714.
161. Nastase, I., et al., *Lobed grilles for high mixing ventilation - An experimental analysis in a full scale model room*. Building and Environment, 2010.
162. Meslem, A., M. El-Hassan, and I. Nastase, *Analysis of jet entrainment mechanism in the transitional regime by time-resolved PIV*. Journal of Visualization, 2010. **online first**: p. 1-12.
163. El-Hassan, M. and A. Meslem, *Time-resolved stereoscopic PIV investigation of the entrainment in the near-field of circular and daisy-shaped orifice jets*. Physics of Fluids, 2010. **22**(3).
164. Nastase, I., *Terminal inovative devices for HVAC air diffusion– research project PNII RP cod CNCSIS 6, 2008- 2010*.
165. Nastase, I. and A. Meslem, *Passive control of jet flows using lobed nozzle geometries*. Mécanique et Industries, 2007. **8**: p. 101-109.
166. Bolashikov, Z., et al., *Improved inhaled air quality at reduced ventilation rate by control of airflow interaction at the breathing zone with lobed jets*. Hvac&R Research, 2014. **20**(2): p. 238-250.
167. Meslem, A., M. El-Hassan, and I. Nastase, *Analysis of jet entrainment mechanism in the transitional regime by time-resolved PIV*. Journal of Visualization, 2011. **14**(1): p. 41-52.
168. Meslem, A., et al., *Optimization of a Lobed Perforated Panel Diffuser - A Numerical Study of Orifice Arrangement*. International Journal of Ventilation, 2012. **11**(3): p. 255-270.
169. Nastase, I., *INADEVA: INtelligent Air Diffusion for healthy environments: advanced strategies and EVALuation methods - research project PN-II-ID-2011-3-0835*. 2011, UEFISCDI.
170. Nicol, J.F. and M.A. Humphreys, *Adaptive thermal comfort and sustainable thermal standards for buildings*. Energy and Buildings, 2002. **34**(6): p. 563-572.
171. Leaman, A., L. Thomas, and M. Vandenberg, *Green buildings: what Australian users are saying?* EcoLibrium, 2007. **6**(10): p. 22-30.
172. Nicol, F. and M. Humphreys, *Maximum temperatures in European office buildings to avoid heat discomfort*. Solar Energy, 2007. **81**(3): p. 295-304.
173. Baron, J., *Thinking and deciding*. Cambridge University Press, 2008. **4**.
174. Baron, J., *Against bioethics*. Cambridge, MA, 2006. **2006**.
175. Baron, J., *Norm-endorsement utilitarianism and the nature of utility*. Economics and Philosophy, 1996. **12**(1): p. 165-182.
176. Burke, R., J. Rugh, and R. Farrington. *ADAM - The Advanced Automotive Manikin*. in *International meeting on thermal manikins and modelling*. 2003. Strasbourg, France.

177. Lebbin, P., M. Hosni, and T. Gielda. *Design and manufacturing of two thermal observation manikins for automobile applications*. in *International meeting on thermal manikins and modelling*. 2003. Strasbourg, France.
178. A. DOGEANU, et al., *Conception of a real human shaped thermal manikin for comfort assesment*, in *PhD & DLA Symposium Pesc, Hungary*. 2012.
179. A. DOGEANU, et al., *Conception of a simplified seated thermal manikin for CFD validation purposes*. *Revista Romana de Inginerie Civila*, 2013. **5**.
180. Lee, Y.Y., et al., *Surrogate human sensor for human skin surface temperature measurement in evaluating the impacts of thermal behaviour at outdoor environment*. *Measurement*, 2018. **118**: p. 61-72.
181. Shi, S., Y. Li, and B. Zhao, *Deposition velocity of fine and ultrafine particles onto manikin surfaces in indoor environment of different facial air speeds*. *Building and Environment*, 2014. **81**: p. 388-395.
182. Holmér, I., *Thermal manikin history and applications*. *European Journal of Applied Physiology*, 2004. **92** p. 614-618.
183. Nayak, R. and S. Houshyar, *7 - Comparison of manikin tests with wearer trials*, in *Manikins for Textile Evaluation*. 2017, Woodhead Publishing. p. 159-171.
184. Jambunathan, K., et al., *A review of heat transfer data for single circular jet impingement*. *International Journal of Heat and Fluid Flow*, 1992. **13**: p. 106-115.
185. I. Ursu, D.G., C. Croitoru, P. Danca, I. Nastase. *Advanced Thermal Manikin Prototype with Neuro-fuzzy Control System*. in *COBEE 2018*. 2018. Melbourne 2018.
186. Sakoi, T., et al., *Thermal comfort, skin temperature distribution, and sensible heat loss distribution in the sitting posture in various asymmetric radiant fields*. *Building and Environment*, 2007. **42**(12): p. 3984-3999.
187. Bjorn, E. and P.V. Nielsen, *Dispersal of exhaled air and personal exposure in displacement ventilated rooms*. *Indoor Air*, 2002. **12**(2): p. 147-164.
188. Melikov, A.K., et al. *Impact of airflow interaction on inhaled air quality and transport of contaminants in rooms with personalized and total volume ventilation*. in *Healthy Buildings*. 2003. Singapore.
189. Fan, J. *New Functions and Applications of "Walter"-Sweating Fabric Manikin*. . in *International meeting on thermal manikins and modelling*. 2003. Strasbourg, France.
190. Topp, C., et al. *Influence of geometry of Thermal Manikins on concentration distribution and personal exposure*. in *Healthy Buildings*. 2003a. Singapore.
191. Topp, C., et al. *Influence of geometry of Thermal Manikins on room airflow*. in *Healthy Buildings* 2003b. Singapore.
192. Tamura, T., *Development of a two-layer movable sweating thermal manikin*. *Industrial Health*, 2006 **44**(3): p. 441-444.
193. Damjana, C., M. Harriet, and G. Jelka, *A study of the influence of different clothing materials on heat and moisture transmission through clothing materials, evaluated using a sweating cylinder*. *International Journal of Clothing Science and Technology*, 2008. **20**(2): p. 119-130.
194. McCullough, E.A., *The use of thermal manikins to evaluate clothing and environmental factors*, in *Elsevier Ergonomics Book Series*, Y. Tochihara and T. Ohnaka, Editors. 2005, Elsevier. p. 403-407.
195. Tanabe, S., et al., *Evaluating thermal environments by using a thermal manikin with controlled skin surface temperature*. *ASHRAE Transactions*, 1994. **100**: p. 39-48.
196. Croitoru, C., *Studii teoretice și experimentale referitoare la influența turbulenței aerului din încăperile climatizate asupra confortului termic*, in *UTCB*. 2011.
197. Lund Madsen, T., *Thermal effects of ventilated car seats*. *International Journal of Industrial Ergonomics*, 1994. **13**(3): p. 253-258.
198. Karimi, G., et al., *Thermal Comfort Analysis of an Automobile Driver with Heated and Ventilated Seat*. 2002, SAE International.

199. Preusser, L., *Development of a thermal model for a heated steering wheel to compensate defective feedback variables*. 2017, SAE Technical Paper.
200. Mao, Y., J. Wang, and J. Li, *Experimental and numerical study of air flow and temperature variations in an electric vehicle cabin during cooling and heating*. Applied Thermal Engineering, 2018. **137**: p. 356-367.
201. Baur, D.G. and N. Todorova, *Automobile Manufacturers, Electric Vehicles and the Price of Oil*. Energy Economics.
202. De Dear, R.J., J.W. Ring, *Human subjective experience of ambient temperature step-changes: experimental results compared to the predictions of a numerical model*. Indoor Air, 1990.
203. Jeong, K., Z. Zhai, and M. Krarti, *Experimental and Numerical Investigation on Cooling Characteristics of Partition Air Supply System*. ASHRAE Transactions 2006. **112**(2006): p. 6.
204. Kilic, M. and S.M. Akyol, *Experimental investigation of thermal comfort and air quality in an automobile cabin during cooling period*. Heat Mass Transfer, 2012. **48** p. 1375-1384.
205. Chen, C.-P., et al., *Effects of temperature steps on human skin physiology and thermal sensation response*. Building and Environment, 2011. **46**(11): p. 2387-2397.
206. Oi, H., et al., *Effects of heated seats in vehicles on thermal comfort during the initial warm-up period*. Applied Ergonomics, 2012. **43**(2): p. 360-367.
207. Hepokoski, M., et al., *Simulating Physiological Response with a Passive Sensor Manikin and an Adaptive Thermal Manikin to Predict Thermal Sensation and Comfort*. 2015, SAE International.
208. Krajčič, M., A. Simone, and B.W. Olesen, *Air distribution and ventilation effectiveness in an occupied room heated by warm air*. Energy and Buildings, 2012. **55**: p. 94-101.
209. Xing, H., A. Hatton, and H.B. Awbi, *A study of the air quality in the breathing zone in a room with displacement ventilation*. Building and Environment, 2001. **36**(7): p. 809-820.
210. Wu, W. and Z. Lin, *Experimental study of the influence of a moving manikin on temperature profile and carbon dioxide distribution under three air distribution methods*. Building and Environment, 2015. **87**: p. 142-153.
211. Dogeanu, A., *Cercetari privind realizarea unor proceduri performante de evaluare si clasificare a microclimatului interior, Teza de doctorat*. 2015.
212. Gardon, R. and J.C. Akfirat, *The role of turbulence in determining the heat-transfer characteristics of impinging jets*. International Journal of Heat and Mass Transfer, 1965. **8**: p. 1261-1272.
213. Ursu, D.G., C Croitoru, P Danca, I Nastase. *Advanced Thermal Manikin Prototype with Neuro-fuzzy Control System* in COBEE 2018. 2018.
214. Ursu, I., et al., *Switching neuro-fuzzy control with antisaturating logic. Experimental results for hydrostatic servoactuators*. Proceedings of the Romanian Academy, Series A, Mathematics, Physics, Technical Sciences, Information Science, 2011. **12**(3): p. 231-238.
215. Ioan, U., U. Felicia, and I. Lucian, *Neuro-fuzzy synthesis of flight control electrohydraulic servo*. Aircraft Engineering and Aerospace Technology, 2001. **73**(5): p. 465-472.
216. Li-Xin, W. *Combining mathematical model and heuristics into controllers: an adaptive fuzzy control approach*. in *Proceedings of 1994 33rd IEEE Conference on Decision and Control*. 1994.
217. Ursu, I. and F. Ursu, *Airplane ABS control synthesis using fuzzy logic*. Journal of Intelligent & Fuzzy Systems, 2005. **16**(1): p. 23-32.
218. Ursu, I., F. Ursu, and L. Iorga, *Neuro-fuzzy synthesis of flight controls electrohydraulic servo*. Aircraft Engineering and Aerospace Technology, 2001(73): p. 465-471.
219. Adrian, R.J., *Laser Velocimetry*, in *Fluid Mechanics Measurements*, R.J. Goldstein, Editor. 1983, Springer-Verlag. p. 155-240.
220. Boutier, A., *L'ensemencement en vélocimétrie laser*. AFVL Ecole d'automne: Vélocimétrie et granulométrie laser. 2003, St-Pierre d'Oléron.

221. Kähler, C., B. Sammler, and J. Kompenhans, *Generation and control of tracer particles for optical flow investigations in air*. Experiments in Fluids, 2002. **33**(6): p. 736-742.
222. Echols, W.H. and J.A. Young, *Studies of portable air-operated aerosol generators*. 1963.
223. Dantec Dynamics, A.S. *ComfortSense*. 2017 [cited 2017 23.02.]; Available from: <https://www.dantecdynamics.com/comfortsense>.
224. Wang, L.-X., *Combining mathematical model and heuristics into controllers: An adaptive fuzzy control approach*. Fuzzy Sets and Systems, 1997. **89**(2): p. 151-156.
225. Nastase, I., C. Croitoru, and C. Lungu, *A Questioning of the Thermal Sensation Vote Index Based on Questionnaire Survey for Real Working Environments*. Energy Procedia, 2016. **85**(Supplement C): p. 366-374.
226. ISO, *Ergonomics of the thermal environment. Assessment of the influence of the thermal environment using subjective judgement scales in EN ISO 10551:2001*. 2001.
227. Garcia, C.M., P.R. Jackson, and M.H. Garcia, *Confidence Intervals in the Determination of Turbulence Parameters*. Experiments in Fluids, 2006. **40**(4): p. 514-522.
228. Petrie, H.L., M. Samimy, and A.L. Addy, *Laser Doppler velocity bias in separated flows*. Experiments in Fluids, 1988. **6**(1): p. 80-88.
229. Barnett, D.O. and H.T. Bentley. *Statistical bias of individual realization laser velocimeters*. in *Proceedings of the Second International Workshop on Laser Velocimetry*. 1974.
230. Bendat, J.S. and A.G. Piersol, *Random Data. Analysis and Measurement Procedures*. Second Edition ed. 1986: Wiley-Interscience Publication. 566.
231. Haertig, J., *Traitement de données en Vélocimétrie Laser Doppler*. AFVL Ecole d'automne: Vélocimétrie et granulométrie laser. 2003, St-Pierre d'Oléron.
232. Danaila, S. and C. Berbente, *Metode numerice în dinamica fluidelor*, ed. E. Academiei. 2003.
233. Tenekes, H. and J. Lumley, *First course in turbulence* ed. M. Press. 1975.
234. Launder, B.E., W.C. Reynolds, and W. Rodi, *La simulation des modeles de turbulence et leurs applications*. 1984.
235. Meslem, A., et al., *A comparison of three turbulence models for the prediction of parallel lobed jets in perforated panel optimization*. Building and Environment, 2011. **46**(11): p. 2203-2219.
236. Nielsen, P.V., *Berechnung der Luftbewegung in einem zwangsbelüfteten Raum*. Gesundheits-Ingenieur, 1973. **94**: p. 299-302.
237. Nielsen, P.V., et al., *Benchmarks test for a computer simulated person Indoor Air*, 2003. **14**(7): p. 144-156.
238. Murakami, S., S. Kato, and J. Zeng, *Numerical simulation of contaminant distribution around a modeled human body: CFD study on computational thermal manikin Part II*. ASHRAE Transactions, 1998. **104**: p. 226-233.
239. Hayashi, T., et al., *CFD analysis on rising stream around a human body and its effect on inhalation air quality*. ASHRAE Transactions, 2002. **108**(2): p. 1173-1178.
240. Sorensen, D.N., *Radiation between segments of the seated human body in ROOMVENT*. 2002. p. 317-320.
241. Murakami, S., S. Kato, and J. Zeng, *Combined simulation of airflow, radiation and moisture transport for heat release from a human body*. Building and Environment, 2000. **35**(6): p. 489-500.
242. Sorensen, D.N. and L.K. Voigt, *Modeling airflow and heat transfer around a seated human body by computational dynamics*. Building and Environment, 2003. **38**(6): p. 753-762.
243. Topp, C., P.V. Nielsen, and D.N. Sorensen, *Application of computer simulated persons in indoor environmental modeling*. ASHRAE Transactions, 2002. **108**(2): p. 1084-1089.
244. Yang, T., et al. *A new simulation system to predict human-environment thermal interactions in naturally ventilated buildings*. in *Building Simulation*. 2007. Beijing, China.
245. Zhang, Y. and T. Yang. *Simulation of human thermal responses in a confined space*. in *Indoor Air*. 2008. Copenhagen, Denmark.

246. Voigt, L.K., *Navier-Stokes simulations of airflow in rooms and around a human body*. 2001, Technical University of Denmark.
247. Chen, Q. and W. Xu, *A zero-equation turbulence model for indoor airflow simulation*. *Energy and Buildings*, 1998. **28**(2): p. 137-144.
248. Torano, J., R. Rodríguez, and I. Diego, *Computational Fluid Dynamics (CFD) use in the simulation of the death end ventilation in tunnels and galleries*. *WIT Transactions on Engineering Sciences*, 2006. **52**.
249. Gadgil, A.J., et al., *Indoor pollutant mixing time in an isothermal closed room: an investigation using CFD*. *Atmospheric Environment* 2003. **37** (39-40): p. 5577-5586.
250. Zhang, Z. and Q. Chen, *Experimental measurements and numerical simulations of particle transport and distribution in ventilated rooms*. *Atmospheric Environment*, 2006. **40**(18): p. 3396-3408.
251. Bosbacha, J., et al. *Experimental and numerical simulations of turbulent ventilation in aircraft cabins*. in *The Second ASME-ZSIS International Thermal Science Seminar (ITSS II)*. 2006.
252. Posner, J.D., C.R. Buchanan, and D. Dunn-Rankin, *Measurement and prediction of indoor air flow in a model room*. *Energy and Buildings*, 2003. **35**(5): p. 515-526.
253. Wilcox, D.C., *Reassessment of the scale-determining equation for advanced turbulence models*. *AIAA Journal*, 1988. **26**: p. 1299-1310.
254. Stamou, A. and I. Katsiris, *Verification of a CFD model for indoor airflow and heat transfer*. *Building and Environment*, 2006. **41**(9): p. 2171-1181.
255. Kuznik, F., G. Rusaouën, and J. Brau, *Experimental and numerical study of a full scale ventilated enclosure: Comparison of four two equations closure turbulence models* *Building and Environment*, 2007. **42**(3): p. 1043-1053
256. Musser, A. and K. McGrattan, *Evaluation of a fast Large-Eddy-Simulation model for indoor airflows*. *J. Arch. Engrg*, 2002. **8**(1): p. 10-18.
257. Sevilgen, G. and M. Kilic, *Numerical analysis of airflow, heat transfer, moisture transport and thermal comfort in a room heated by two-panel radiators*. *Energy and Buildings*, 2011. **43**(1): p. 137-146.
258. Bode, F., *Cercetari privind procesele termo-fluidodinamice din arzatoare si focare la arderea turbionara*, in *Facultatea de Mecanica, Universitatea Tehnica din Cluj-Napoca*. 2010.
259. Homma, H. and M. Yakiama, *Examination of free convection around occupant's body caused by metabolic heat*. *ASHRAE Transactions*, 1988. **94**(1): p. 104-124.
260. Fountain, M.E., *Laboratory studies of the effect of air movement on thermal comfort: A comparison and discussion of methods*. *ASHRAE Transactions*, 1991. **97**(1): p. 863-873.
261. Humphreys, M.A., *Field studies and climate chamber experiments in thermal comfort research*, in *Thermal Comfort : Past Present and Future*, N.A.O.M.A. Humphreys, Editor. 1994, Building Research Establishment: Garston. p. 52-72.
262. Oseland, N.A. and M.A. Humphreys, *Trends in Thermal Comfort Research 1994*, Building Research Establishment: Garston, Watford, UK.
263. Humphreys, M.A. and J.F. Nicol, *The validity of ISO-PMV for predicting comfort votes in everyday thermal environments*. *Energy and Buildings*, 2002. **34**(6): p. 667-684.
264. Al-Mogbel, A. *A coupled model for predicting heat and mass transfer from a human body to its surroundings*. in *36th AIAA Thermophysics Conference*. 2003. Florida, USA.
265. Omori, T., et al. *Coupled simulation of convection and radiation on thermal environment around an accurately shaped human body*. in *ROOMVENT*. 2004. Portugal.
266. Srebric, J., et al., *CFD boundary conditions for contaminant dispersion, heat transfer and airflow simulations around human occupants in indoor environments*. *Building and Environment*, 2008. **43**.
267. Kilic, M. and G. Sevilgen, *Modelling airflow, heat transfer and moisture transport around a standing human body by computational fluid dynamics*. *Int. Journal Heat Mass Transfer*, 2008. **33**(2008): p. 1159-1164.

268. Ansys Inc, *Fluent 19.0 User Guide*.
269. Chen, Q.Y., Z. Zhang, and W. Zuo. *Computational fluid dynamics for indoor environment modeling: past, present and future*. in *XXV UIT National Heat Transfer Conference*. 2007. Trieste, Italy.
270. Zhang, Z., J.Z. Zhai, and Q. Chen. *Evaluation of various CFD models in predicting room airflow and turbulence*. in *ROOMVENT*. 2007. Helsinki, Finland.
271. Jaramillo, J.E., et al., *Numerical Study of Plane and Round Impinging Jets using RANS Models*. Numerical Heat Transfer, Part B: Fundamentals, 2008. **54**(3): p. 213-237.
272. Danca, P., et al., *On the Possibility of CFD Modeling of the Indoor Environment in a Vehicle*. Energy Procedia, 2017. **112**: p. 656-663.
273. Fanger, P.O., et al., *Air turbulence and sensation of draught*. Energy and Buildings, 1988. **12**(1): p. 21-39.
274. Fanger, P.O., *The new comfort equation for indoor air quality*. Ashrae Journal, 1989. **31**(10): p. 33-38.
275. Awbi, H.B., *Ventilation of Buildings*. 2003, London, U.K.: E&FN SPON. 313.
276. Yan, W.M., et al., *Measurement of detailed heat transfer on a surface under arrays of impinging elliptic jets by a transient liquid crystal technique*. International Journal of Heat and Mass Transfer, 2004. **47**: p. 5235–5245.
277. Buratti C, R.P., *Adaptive analysis of thermal comfort in university classrooms: correlation between experimental data and mathematical models*. Build Environ, 2009. **44**: p. 674-87.
278. Jungwoo Lee, J.K., Jungseo Park, *Effect of the air-conditioning system on the fuel economy in a gasoline engine vehicle*. Institution of mechanical engineers, 2012. **227**(1): p. 66-77.
279. Croitoru, C., et al. *Numerical and experimental modeling of airflow and heat transfer of a human body*. in *Roomvent 2011*. 2011. Trondheim, Norway.
280. Croitoru, C., et al., *Inlet turbulence intensity influence on the thermal comfort in the case of a mixing ventilation system* submitted to Building and Environment, 2011.

Titre : Stratégies de ventilation pour l'amélioration de la qualité de l'environnement intérieur dans les véhicules

Mots clés : confort thermique; environnement thermique du véhicule; mannequin thermique; sujets humains; CFD; diffuseurs d'air innovants

Résumé: La prédiction des conditions thermiques confortables à l'intérieur d'une cabine de véhicule reste un défi en raison du comportement transitoire de cet environnement. Le développement des modèles d'écoulement reste toujours un défi pour les chercheurs en raison de la géométrie complexe de la cabine et de la complexité du système de ventilation (débit, emplacement et géométrie des diffuseurs d'air).

Le confort thermique a été largement étudié dans le bâtiment, alors que le confort thermique dans les véhicules est un sujet relativement nouveau, avec peu d'études qui y sont dédiées. La norme actuellement disponible destinée à l'évaluation de l'environnement thermique du véhicule, EN ISO 14505, propose des modèles d'évaluation des bâtiments, qui ne répondent pas aux exigences de l'évaluation de l'environnement cabine. Contrairement à l'environnement intérieur des bâtiments, le climat de la cabine de véhicule est dominé par des conditions transitoires thermiques: environnement thermique fortement non uniforme associé aux vitesses élevées de l'air localisé, des niveaux plus élevés d'humidité relative, le flux de chaleur solaire et le flux de chaleur radiatif des surfaces intérieures, l'intensité solaire et sa diffusion sur les différents types de matériaux et niches de surface de la cabine, les angles d'incidence du rayonnement solaire, etc.

En l'absence de modèles d'évaluation adaptés à cet environnement, la littérature disponible est dispersée autour des articles traitant des conditions environnementales dans le véhicule susceptible d'affecter le confort thermique de l'homme ainsi que de celles concernant la réaction de l'homme et la perception de son interaction avec l'environnement. Dans ce contexte, nous avons décidé d'orienter le sujet de la thèse autour de la problématique complexe de l'environnement thermique de la cabine et de ses effets sur l'état thermique du conducteur et du passager. Le manuscrit présente des études numériques et expérimentales des effets de différentes grilles passives sur le confort thermique des passagers;

Ainsi, les objectifs généraux du projet de recherche doctorale pourraient être résumés comme suit: approfondir les connaissances et comprendre les phénomènes thermiques qui se produisent dans l'environnement thermique de la cabine; développer un mannequin thermique avancé capable d'évaluer le confort thermique de la cabine développer un mannequin thermique avancé capable d'évaluer le confort thermique de la cabine; développer et valider un modèle numérique complexe afin de mieux comprendre les phénomènes complexes précédemment évoqués. Ces trois objectifs généraux visaient à soutenir l'objectif principal de la recherche doctorale, à savoir: l'amélioration de la sensation thermique des occupants du véhicule, par la mise en œuvre de diffuseurs d'air innovants. À cette fin, nous avons orienté nos recherches vers des diffuseurs à géométrie spéciale permettant des mécanismes de contrôle du débit et permettant d'améliorer le mélange entre l'alimentation en air par le système de ventilation et l'air ambiant dans la cabine.

Au cours de la quête complexe, nous pourrions avoir l'opportunité de nous familiariser avec les phénomènes thermiques, afin d'analyser le rôle réel joué par les paramètres d'environnement transitoires, dans la perception du confort thermique et dans son estimation. Pendant toute cette quête, nous avons essayé de rester sur une ligne qui permettrait finalement de répondre à un ensemble de questions fondamentales, à savoir: *dans quelle mesure ce type de paramètres peut affecter la perception du confort, ainsi que les conséquences d'une évaluation "incomplète" proposée par les modèles existants? Dans ce contexte, comment la conception de la ventilation et de la climatisation est-elle affectée par l'utilisation des modèles actuels pour pré-évaluer le bon fonctionnement des systèmes CVC - en particulier pour les véhicules - et un environnement acceptable pour ses utilisateurs?*

Title : Ventilation strategies for improving the indoor environment quality in vehicles

Keywords : thermal comfort; vehicle thermal environment; thermal manikin; human subjects; CFD; innovative diffusers

Abstract: Prediction of comfortable thermal conditions inside a vehicle cabin is still a challenge due to the transient behavior of this environment. Understanding flow patterns is still difficult nowadays for researchers due to the complexity of the interior cabin geometry and of the ventilation system (flow rate, location and geometry of the air diffusers). Thermal comfort has been widely studied in build environments, while thermal comfort in vehicles is a relatively new subject, with fairly few extensive studies that are exploring all possibilities of investigation in this direction. The currently available standard intended for the evaluation of vehicle thermal environment, EN ISO 14505, propose models extensively used for buildings, which do not seem to be entirely adapted for the vehicular space. Unlike the indoor environment from buildings, the vehicular cabin climate is dominated by thermal transient conditions: the strongly non-uniform temperature distributions, both in air and on the surfaces, associated with the high localized air speeds, the relatively higher levels of relative humidity compared to the buildings, the solar radiation intensity, and the radiative heat exchange from the interior surfaces, the angles of incidence of the solar radiation etc. In the absence of the evaluation models adapted to this environment, the available literature is dispersed around those papers dealing with environmental conditions inside the vehicle that might affect the human thermal comfort and those concerning the human's response and perception of its interaction with the environment. In this context, we decided to orient the research work in this thesis around the complex problematic of cabin thermal environment and its effect on driver's and passenger's thermal state. The thesis presents numerical and experimental studies of the effects of an improved set of dashboard air diffusers over passengers' thermal comfort

The general objectives of the doctoral research project could be summarized as following: to deepen the knowledge and to understand thermal phenomena that occur in cabin thermal environment; to develop and validate a complex numerical model in order to get insight into the complex phenomena previously evoked. These three general objectives were intended to sustain the main goal of the doctoral research that is: improvement of thermal sensation of vehicle occupants, by implementation of innovative air diffusers. To this end we oriented our research towards diffusers with a special geometry that allows flow control mechanisms resulting in the improvement of mixing between air supply by the ventilation system and the ambient air in the cabin. During the complex quest, we could have the opportunity to become familiar to the intricate thermal phenomena, to analyze the real role played by transient environment parameters perceiving thermal comfort and in its estimation. During all this quest we tried to stay on a line that would ultimately allow to respond to a set of fundamental questions, namely: *To what extent this kind of parameters can affect the perceiving of comfort, and also the consequences of an "incomplete" assessment proposed by the existing evaluation models? How is, in this context, affected the ventilation and air conditioning design due to the use of current models for pre-evaluating a good functioning of the HVAC systems – in particular for vehicles - and an acceptable environment for their users?*